THESIS

Colliding branes and its application to string cosmology

ブレイン衝突とストリング宇宙論への応用

Department of Physics, Waseda University

Yu-ichi Takamizu

高水　裕一

A doctoral dissertation submitted to
Department of Physics,
Waseda University

July, 2007

Contents

Chapter 1

Introduction

Cosmology

Cosmology represents a fundamental study on the large scale physics in the whole Universe, to investigate its origin and evolution. Here, the word, "Universe" is all existing matter and space considered as a whole, in other words, where the law of nature exits. Then cosmology is also a study of its all components, existing in which the universe, how they formed, how they have evolved [1]. It has a long history to understand the Universe as the world around humanity's place including of course science, philosophy, and religion. Cosmology firstly started as a simple questions in early history of humankind about 100 thousands years ago, such as "What's going on around me?" or "How does the Universe (God) work?" It was based on local pray as respecting God of Nature who creates phenomena around the world. The earliest scientific observations for understanding the Universe were related to the epoch of four big civilizations in 5000 years ago, Egypt, Mesopotamia, India and China. Actually in the ancient cosmology of Egypt, the sun god, Ra, was seen to control the annual solar motion along the horizon.

Modern cosmology as a study of science is usually known as a beginning with Albert Einstein who found the Special and General Relativity. The general relativity not only gives a precise description of gravitational force but also has completely changed the idea of space and time. Gravity is described as a geometrical object, and energy and momentum densities of matter fields deform a spacetime. As a result, a spacetime becomes a dynamical object, which allows us to study the universe as a whole. Therefore, the cosmology was born as one of physical science by this theory. Alexander Friedmann derived the Friedmann equations describing expansion of the universe in 1921. In 1927 Georges Lemaitre proposed the big bang theory and Edwin Hubble discovered the red shift by expanding of the universe in 1929 (the so-called Hubble law) [212, 211]. In 1964 Arno Penzias and Robert Woodrow Wilson detected the cosmic microwave background radiation [355, 466] as a consequence of Big bang theory.

Thus cosmology has long history as old as human beings and may be perhaps one kind of thinking ourself as their birth? or, their history? or themselves? We don't say it clearly, but the universe is of course, the largest special "nature" existing around us, which works as a *some kind of "mirror" to human being*, attracting humankind for a long time. Recently, the idea of Anthropic Principle seems to be related to such direction of discussion. All the physical laws of Nature involves particular physical constants such as the gravitational constant, the speed of light, the electric charge and Planck's constant etc. Some are derived from physical laws, however, for most, their values are arbitrary. If all above constants take critical values in a possible narrow range, life like a humankind could be created, otherwise no life comes who understands the universe. The Anthropic Principle may be not scientific, but is one approach to explain the above fundamental question; what our world, the universe takes special values of physical constants? This idea is interesting to think in the point of view of landscape existing in String theory as you will see later, where there exist other different universes and this principle may give a necessary condition for the existence of our universe. In this sense, based on the Anthropic principle, the universe

[1] The word "Cosmology" is from the Greek: *cosmologia*, (*cosmos*) the universe seen as a well-ordered whole + (*logos*) word, reason, plan.

is just *a mirror to face ourselves.*

Cosmological hierarchy structures

The cosmology is also studying of large scale structures, such as galaxy and cluster. Here, let us introduce briefly cosmological structures by looking up to large scales from the our planet, Earth. This is interesting in the view point of an ancient study, "Cosmology", which ancient man asked, "What's going on around me?" The Earth is the planet whose radius is $R \sim 6378$km and circuit $2\pi R \sim 40.08$ thousand km [2]. The galaxy which the Sun and we live in, of course, is called the Milky Way or the Galaxy [3]. Our Galaxy is made of a *bulge* of old stars, whose size is totally about 100,000 light-years($\sim$ 30kpc). The sun system is located at about 2/3($\sim$ 9kpc, see also 'parsec' in (2.31)) from the center. Almost all galaxies can be classified into three classes as ellipticals, spirals, and irregulars. The smallest aggregates of galaxies are called *groups of galaxy*. The Andromeda galaxy is most closed to the Milky Way about 700kpc($\sim 2.1 \times 10^6$lyr), belonging to a local group of galaxies. The next class is *cluster of galaxies*, where *groups* and *clusters* may contain from ten (group) to thousands of galaxies (cluster) and they form the densest part of the large scale structure of the Universe. The clusters themselves are often associated with larger groups called *superclusters*. Superclusters are usually consist of chains of about a dozen clusters which have a mass of about 10^{16} solar masses. Our own Local Supercluster is centered on Virgo located at 20Mpc from the Earth, and is relatively poor having a size of 15Mpc. The largest superclusters, like that associated with Coma, are up to 100Mpc in extent. The structures of *filaments* which consists of galaxies, are the largest known structures in the Universe, thread-like structures with a typical length of 70 to 150 Mpc that form the boundaries between large *voids* in the universe.

Modern scientific cosmology

Recently, the standard cosmological scenario is the so-called the *Big Bang theory*, proposed by George Gamow et al in 1948 [11], which is based on General Relativity and *"Cosmological Principle"* in which, if one consider physics on large efficient scales, one believe our universe is homogeneous and isotropic. It leads to an expandng universe, which started from a hot dense state in around ten billion years ago, called *"the Big Bang"* [165, 166]. This scenario can explain the evolution of both of the spacetime and its components (matter) from nucleosynthesis at three minutes after starting, to the present time 13.7 billion years, consistent with the several observational data. The observational evidences are mainly three: 1. confirmation of cosmic expansion, 2. consistent abundances of the light element and 3. existence of cosmic microwave background radiation (CMB). The first can be seen as Hubble law and the second on the theory of nucleosynthesis. The last one, CMB is the most strongest confirmation that the Big Bang theory received. It was detected by Arno Penzias and Robert Wilson in 1964 [355, 466]. However, the big bang theory has key theoretical problems which are called the flatness, the horizon problems and related to the origin of the structure formation [289, 259]. In order to resolve these problems at the same time, there exists *Inflationary scenario* where before the big bang universe, there was a period that the universe expands quasi-exponentially [289, 259, 280]. So far, only the idea of inflation provides a resolution of those problems. Not only does it give some picture of the earlier stage of the universe before the big bang but also it seems to be supported by some recent observational data on CMB. On the other hand, in the inflationary scenario, the temperature of the universe has fallen to zero and the universe has become very cold after the inflation, because of its exponential expansion. This state of the universe, however, is not consistent with the initial condition of the universe at the big bang beginning since it was huge hot, so the mechanism to connect smoothly the inflationary scenario with the big bang theory would be needed, the so-called *Reheating*. Recent observations of CMB radition detected by the COsmic Background Explorer (COBE) [40] and Wilkinson Microwave Anisotropy Probe (WMAP) satellites [41, 264, 359, 427] are consistent with predictions by *standard cosmological scenario* including the big bang scenario, Inflation and Reheating mechanism as described above (see also Fig. 1.1). Furthermore, combined with the new observational data such as the astronomical instruments like the Sloan Digital Sky Survey (SDSS) [440] and the Two Degree Field system (2dF) [100], supernovae data and Lyman α forest data, the WMAP

[2] This value is very close to 40 thousand km because the distance of "meters" was originally defined by 1/40000 of the circuit of Earth. The light can travel to 7.5 circles around Earth in one second, whose speed is 3×10^5 km/s, and then we can roughly estimate $R = 300/7.5 \times 10^3 = 4 \times 10^4$ km.

[3] The name capitals "Galaxy" comes from the Greek "Gala" meaning milky.

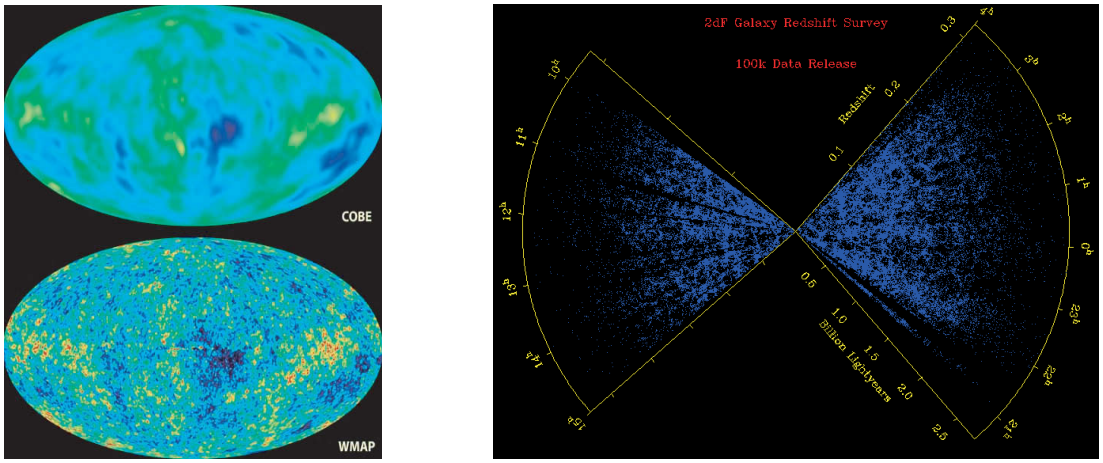

(a) The tempeature maps of CMB

(b) Distribution of galaxies in 2dF

Figure 1.1: (a): The difference between the temperature anisotropy of cosmic microwave background radiation detected by COBE [40] and WMAP satellite [427]. The upper map is COBE and lower WMAP. The recent observational data of CMB can give us more information of the universe. (b) Distribution of galaxies in the 2dF (Colless et al 2001 [100]). By the end of the survey, redshifts for 250, 000 galaxies will have been obtained. As shown here, they probe structure in the universe out to $z = 0.3$, corresponding to distance up to $1000h^{-1}$ Mpc away from us (we are located at the center).

data can give us more accurate information about our universe (see 2dF in Fig. 1.1).

It is known from the modern accurate observations, surprising us greatly, that the current universe is mainly about 90 percents fulfilled with the unknown components, the so-called dark energy and dark matter. The recent universe estimated by WMAP observational data is composed of dark energy(72%), dark matter(25%), and ordinary matter(4%) including baryon [427]. Dark energy leads to accelerated expansion of the universe and then the accelerated expansion is recent found to start form about 4 billion years, slightly after the Solar system formation. Dark matter is non-baryonic matter, interacting only through the gravitational force, and is necessary to explain the large-scale structure of the universe. In the modern cosmology, they can not be explained naturally, however, their existences are confirmed, which account for almost of the total energy of the universe. This becomes the most difficult remaining question which the modern cosmology must reply. According to the Friedmann equations and interpreted as the matter term, dark energy is a fluid which has a negative pressure, as the cosmological constant or the energy density of vacuum does. It implies the existence of curious matter, conversely, it may demand us the alteration of the theory itself, or is a "window" to see a new physics of fundamental theory. Moreover, if dark energy is a vacuum energy of the universe, it is seen that the special value of this constant energy has been chosen in the early universe, a long 13.7 billion years ago. It is unnatural and strange to explain, and by some possibility, it may be related to a fundamental physics in the early stage of the universe. These high energy physics so far has not been understood yet beyond the nucleosynthesis. Physics in this stage, in the point view of unification of fundamental forces, is very attractive us. On the other hand, dark matter needs to have concentrated the origin of large scale structures in order to build efficiently large scale structures of the universe such as clusters, because the origins of these structures are considered of quantum fluctuations generated by inflation. It also implies the possibility of testing the relation between dark matter and high energy physics. Thus *the dark components of the universe may be not independent of the unified theory of all forces existing in nature*.

For the recent studies of the unified theory (or the so-called *theory of everything*), one of most promising approaches is a it superstring theory, or *M-theory*, considered as a quantization of fields including gravitational interaction [366]. Such unified theories are usually formulated in higher dimensions than four. These extra dimensions can solve the hierarchy problem because they can lower the value of the

Planck mass. This problem can be stated that why is the gauge symmetry group of the field theory that is supposed to describe all the phenomena of nature broken not at one, but at two completely different energy levels? The cosmological implications of string theory are receiving a lot of attention, the so-called *String cosmology*. It was inspired by the recent advances of string theory. The goal of string cosmology is to examine the dynamical evolution at the early stage of the universe, and re-examine cosmological origins in order to understand a convincing link between string theory and unknown problems e.g., what dark energy and dark matter are ? String theory has a much richer set of fundamental degree of freedom, consisting—in addition to fundamental strings—of *D-branes* [365] of various dimensionalities. This fundamental objects, D-branes denote non–perturbative effects of string theory as "soliton" of strings, while string theory has been only described in perturbative form. Inspired by such speculation, recently a new paradigm on the early universe has been proposed, the so-called *brane-world* [206, 365], where ordinary matter fields are confined to hypersurface in higher dimensional spacetime, while only gravitational fields propagate throughout all of spacetime. In the brane-world, Randall and Sundrum [373] proposed a new model where four-dimensional Newtonian gravity is recovered at low energies even without compact extra dimensions. This models can give us the new picture of the early universe. Furthermore, brane-world shows a possibility of the unification scale within reach of our near-future experiments. It implies an important possibility that black hole can be produced in an accelerator such as the CERN Large Hadron Collider [92]. Moreover the recent accurate observations give rich information of the universe and especially detection of the gravitational wave background arising due to the early universe, is a challenging future task for the Laser Interferometer Space Antenna (LISA) [294] or the Deci-hertz Interferometer Gravitational Wave Observatory (DECIGO) [416]. The future data has rich information on the early universe, and hence provide us with powerful tools to probe fundamental physics. Based on such a new world picture, many cosmological scenarios have been studied. In such a brane-world scenario, for resolving the above-mentioned key theoretical problems in the big bang theory, a new idea of the early universe has been proposed, which is called the *Ekpyrotic universe* or the *Cyclic universe* scenario [246, 248, 432]. It is based on a collision of two cold branes. The universe starts with a cold, empty, and nearly ground state [52], which contains two parallel branes at rest. The two branes approach each other and then collide. The energy is dissipated on the brane and the big bang universe starts. Since this scenario is not only motivated by the fundamental unified theory but also may resolve the key theoretical problems, such as the flatness and horizon problems, therefore, it could provide an alternative to an inflationary scenario and would be very attractive. While for the inflationary scenario, it is still unclear what the origin of inflaton is. So far, there has been no convincing link with the fundamental unified theory, that is string/M-theory. Furthermore, these brane models can give us the possibility of resolving the above mentioned key cosmological problems, such as dark energy and dark matter. *Colliding branes would be a fundamental phenomena in the string cosmology* since there exist many branes of various dimensionalities produced in the string theory and they dynamically move and continue to collide each other. The colliding branes not only leads to the ekpyrotic universe scenario, alternative to inflation, but also another scenario, the so-called *String (brane) gas cosmology* [64], resolving the dimensionality problem, which is described as the fundamental question; why the space we live in has three dimensions ? In this thesis, we pay attention to a phenomena of colliding branes and study several applications of colliding branes to string cosmology.

The thesis is organized as follows. In Chapter 2, we review the big bang theory as a standard cosmological scenario. Then the inflationary scenario and reheating mechanism are introduced as the remedy of them in Sec. 2.2. So far, we have studied the homogeneous universe, however, we can find hierarchy of structure scales in the universe, such as galaxy and cluster of galaxies. In Sec. 2.3, we pay attention to such inhomogeneity of the universe and discuss the large-scale structures. In Sec. 2.4, we shall review the modern problem of the universe, dark energy and dark matter and summarize a modern cosmological standard picture. In Chapter 3, we briefly review string theory and a brane-world scenario. In Chapter 4, we briefly explain two scenarios based on colliding branes.

We study several applications of colliding branes to string cosmology, where we formally classify two cases: Minkowski spacetime (Chapter 5) and curved spacetime (Chapter 6). In Chapter 5, we would like to show our works studying reheating mechanism in the ekpyrotic scenario (Sec. 5.2 and based on [436])

and evolution of fermions confined on the brane (Sec. 5.3 and based on [184]). In Chapter 6, taking account of effects from background spacetime, we are planning to study collision of anti de sitter (AdS) branes (Sec. 6.1 and based on [437]), production of black brane by colliding AdS branes (Sec. 6.2 and based on [439]) and resolution of the dimensionality problem by string gas cosmology (Sec. 6.3 and based on [438]). Chapter 7 is devoted to conclusions and remarks.

Chapter 2

Standard cosmological scenario

2.1 Big bang scenario

2.1.1 Big bang scenario

Investigating the general relativity (GR) plays important role to study an evolution of the universe because GR is the most plausible theory which describes the most fundamental force on large scale physics, that is gravitational interaction. It was proposed by Einstein in 1915 and Einstein equations are expressed as [466]

$$G_{\mu\nu} = \kappa^2 T_{\mu\nu} - \Lambda g_{\mu\nu}\,, \tag{2.1}$$

where we define $\kappa^2 \equiv 8\pi G = M_{\rm pl}^{-2} = 8\pi m_{\rm pl}^{-2}$ and $G_{\mu\nu}$, $T_{\mu\nu}$, G and $m_{\rm pl}$ are Einstein tensor, energy-momentum tensor, Newton's constant and Plank mass, respectively. Λ is a cosmological constant, which Einstein firstly introduced to keep the universe static. When we consider a dynamics of the universe itself, the basic assumption is that the universe can be found to be homogeneous and isotropic over some efficient large scale (*The Cosmological Principle*). The assumption of isotropy is strongly supported by the observational evidence of CMB radiation [1]. In fact, the universe is homogeneous and isotropic on 100Mpc scale supported by Redshift surveys [100, 440]. Mathematically, satisfying the cosmological principle, the candidates of the three-dimensional space are limited to 3 cases. The corresponding metric is obtained by [466] (see also the reviews of standard cosmology, big bang theory [280, 259, 355], recent reviews [332, 123])

$$\mathrm{d}s^2 = -\mathrm{d}t^2 + a^2(t)\left[\frac{\mathrm{d}r^2}{1-Kr^2} + r^2(\mathrm{d}\theta^2 + \sin^2\theta \mathrm{d}\varphi^2)\right]. \tag{2.2}$$

Here t and $a(t)$ denote a cosmic time, and a scale factor, which means a scale of the universe. The constant K represents a normalized spatial curvature. The case of $K = 1$, 0, and -1 represents a closed, flat, and open universe, respectively, which is related to the spatial shape (or geometry) of our universes (see Fig. 2.1). The metric form of (2.2) is called Friedmann-Robertson-Walker metric (FRW metric)[2]. By using it, we can characterize an evolution of the homogeneous and isotropic universe in terms of $a(t)$.

The evolution of the universe changes depending on matter components. We will consider a perfect fluid[3], whose form is often used as,

$$T^{\mu\nu} = (\rho + P)u^\mu u^\nu + P g^{\mu\nu}\,, \tag{2.3}$$

[1] It is natural to consider the assumption of homogeneity is also supported by CMB [41, 264, 359, 427]. However, there are some works [233, 261, 333] which claim that this assumption may be broken since the present cosmological structure, i.e., galaxies and clusters form $z \simeq 1$. Usually, Cosmology is based on the cosmological principle and then Friedmann equations is the basic equations for analysis of its dynamics. They think present dark energy component comes from the inhomogeneity near $z \sim 1$. In thesis, however, the homogeneity is assumed as first step of analysis.

[2] Another form of this metric is given by (2.23).

[3] The perfect fluid is equivalent to a fluid whose entropy is conserved along their flow. This assumption satisfy the cosmological principle. We can treat the equation of motion as $P = P(\rho, s_0) = P(\rho)$ with constant entropy s_0.

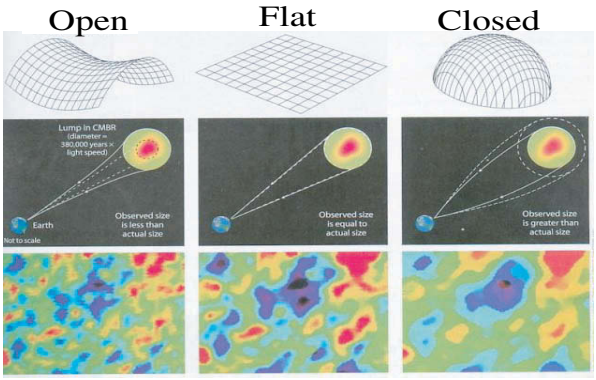

Figure 2.1: Sketches of geometry of the universe. In the flat universe, observed size is equal to actual size, however, it is less (greater) than actual size for the open (closed) universe. This figure is from the website: http://universe-review.ca

where ρ, P and u^μ are an energy density, pressure and a four velocity of fluid, respectively. Considering the FRW metric Eq. (2.2) and the perfect fluid as matter component, the Einstein equation can be reduced to

$$H^2 = \frac{\kappa^2}{3}\rho - \frac{K}{a^2} + \frac{\Lambda}{3}\,, \quad \text{and} \quad \dot{\rho} + 3H(\rho + P) = 0\,, \tag{2.4}$$

where $H \equiv \dot{a}/a$ is called a Hubble expansion rate. The first equation in (2.4) is termed as the *Friedmann equation* and the second one represents *the energy conservation law* in general relativity. Combining these relations, it gives the following acceleration equation (or *Raychaudhuri equation*),

$$\frac{\ddot{a}}{a} = -\frac{\kappa^2}{6}(\rho + 3P) + \frac{\Lambda}{3}\,. \quad \text{or} \quad \dot{H} = -\frac{\kappa^2}{2}(\rho + P) + \frac{K}{a^2}\,. \tag{2.5}$$

From the Friedmann equation, we see there is a particular density, that is known as a critical density $\rho_{\rm cr}$ corresponding to the spatial flat Universe ($K = 0$) in the absence of a cosmological constant ($\Lambda = 0$). This is given by $\rho_{\rm cr} = 3H^2/\kappa^2$ and is a function of time obtained by a given value of the Hubble parameter. Using it, the Friedmann equation can be simplified as

$$\Omega - 1 = \frac{K}{a^2 H^2}\,. \tag{2.6}$$

where $\Omega = \rho_/\rho_{\rm cr}$ is the dimensionless density parameter. One also can include a contribution $\Omega_\Lambda = \Lambda/3H^2$ corresponding to the cosmological constant, so that we use $\Omega_{\rm total} = \Omega + \Omega_\Lambda$ instead of Ω. The case of $\Omega > 1$, $\Omega = 1$ and $\Omega < 1$ corresponds to a closed, flat and open universe, respectively. The recent observations shows that the current universe becomes almost spatial flat ($\Omega \simeq 1$). As an other forms, by defining $\Omega_{\rm K} \equiv \frac{-K}{a^2H^2}$, it can become a simple form $\Omega_{\rm total} + \Omega_{\rm K} = 1$.

In order to close the system, we can provide another information in terms of the equation of state (EOS) of matter

$$P = P(\rho)\,, \tag{2.7}$$

which is generally characterized by micro physics. As typical EOS of matter in Cosmology, 111111 we give two examples; relativistic species ($E \gg mc^2$) and nonrelativistic ones ($E \ll mc^2$). The energy density and pressure are obtained by using a phase distribution function $f(p) = [\exp((E-\mu)/T) \pm 1]^{-1}$ where $+1$ pertains to Fermi-Dirac and -1 to Bose-Einstein particles under thermal equilibrium is realized [4].

[4] We stress that the universe can evolve dynamically, therefore it cannot be treated as a usual thermal equilibrium. Here we define this equilibrium state by *local equilibrium*, in which the characteristic time scale of some reaction $t_c \simeq 1/\sigma n v$ becomes smaller than the cosmic time $t_H \sim 1/H$; $t_c \ll t_H$, where σ denotes an effective cross-section, n is a number density and H is the Hubble parameter. See the further article of Temperature.

To describe relativistic particles, energy density and pressure are obtained as follows [259],

$$\rho = \frac{\pi^2}{30} g_*(T) T^4 \,, \quad P = \frac{1}{3} g_*(T) T^4 \,, \tag{2.8}$$

with $g_*(T) = \sum_{\rm boson} g_i + \frac{7}{8} \sum_{\rm fermion} g_i$ is internal degree of freedom, especially $g_* = 2$ corresponds to photon. Then total EOS of all relativistic spices can be simplified by

$$P = \frac{1}{3}\rho \qquad ({\rm radiation}) \,, \tag{2.9}$$

independent of their spins and chemical potentials. Another important example is an ordinary matter. Its rest mass is much greater than its kinetic energy. So the EOS is approximated by

$$\rho \simeq mnc^2 + \frac{3}{2} nT \,. \quad P \simeq nT \ll \rho \,, \tag{2.10}$$

and then we can treat them as

$$P = 0 \qquad ({\rm matter}) \,. \tag{2.11}$$

If one take the cosmological constant as an one kind of matter $\rho_{\rm vac} = \Lambda/\kappa^2$, the vacuum energy is given by the equation, $\rho_{\rm vac} = {\rm const}$. Then combed with the energy conservation law (2.4), its EOS is obtained as,

$$P = -\rho \qquad ({\rm cosmological\ constant}) \,. \tag{2.12}$$

Here we can show a simple description for three examples described above. The form of EOS is given using an adiabatic index $\gamma (= \omega - 1)$ as

$$P = (\gamma - 1)\rho = \omega \rho \,. \tag{2.13}$$

Combined with the energy conservation law, equivalently, $(a^{3\dot{\gamma}}\rho) = 0$, we obtain

$$\rho \propto a^{-3(\omega+1)} \,. \tag{2.14}$$

We can see the energy density ρ decreases when the scale factor a becomes large. If one would consider radiation and matter, the energy density of radiation $\rho_{\rm r}$ (matter $\rho_{\rm m}$) varies as a^{-4} (a^{-3}). This means that energy loss of radiation is bigger than of matter, therefore, as the universe becomes large, matter becomes more dominant than radiation. It is consistent with the current observational data $\Omega_{\rm m,0} \simeq 3500 \Omega_{\rm r,0}$ (see, where $\Omega_{\rm m}$ includes dark matter). As one go back to the early time of the universe, we can estimate the time when energy density of matter is equal to that of radiation (*Matter-Radiation equality time*) as $a_{\rm eq} = \Omega_{\rm r,0}/\Omega_{\rm m,0} \sim 1/3500$. Here the present scale factor is normalized as $a_0 = 1$. The cosmological constant is characterized as $\omega = -1$ and that is clearly understood from a constant energy density in Eq.(2.14). In the following discussion, it is shown as an important component of the recent universe; dark energy $\Omega_{\rm de,0} \simeq 0.7$, if we consider it as the cosmological constant, we similarly obtain the time when the dark energy begins to dominate as $a|_{\rm (de=matter)} = (\Omega_{\rm m,0}/\Omega_{\rm de,0})^{1/3} \sim 1/0.75$. That is when the universe was about 0.75 times of the present scale.

Next, let us see the evolution of the universe $a(t)$. Putting $\Lambda = 0$, when we consider the geometry as a spatial flat ($K = 0$), we easily find the solution for Eqs. (2.4) as

$$a \propto t^{\frac{2}{3(1+\omega)}} \,, \quad H = \frac{2}{3(1+\omega)t} \,, \quad H \propto a^{-\frac{3(1+\omega)}{2}} \,, \tag{2.15}$$

therefore, we find $a \propto t^{2/3}$ and $a \propto t^{1/2}$, for matter dominant era for radiation dominant era, respectively. This universe expands forever, but its speed is decreasing. i.e., *deaccelerated expansion* with $\ddot{a} < 0$ for the both cases. For other simple cases, where we consider matter ($P = 0$) is filled in the open universe ($K = -1$), the universe expands forever as well as flat case and in the closed universe ($K = 1$), after

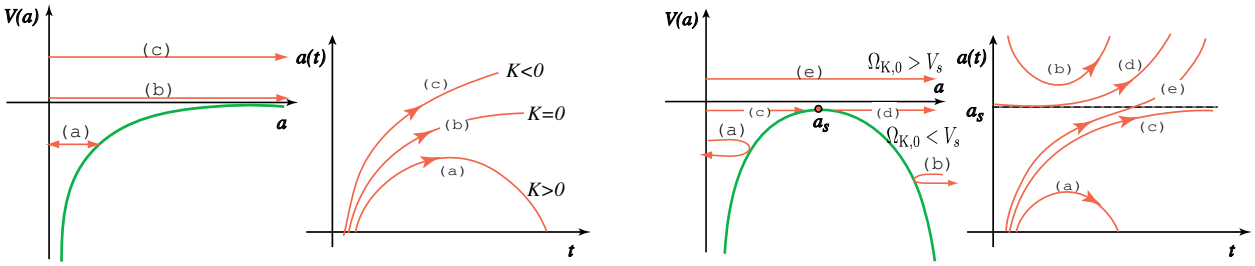

(a) Potenial $-1/3 < \omega$ (b) Scale factor $-1/3 < \omega$ (c) $-1 < \omega < -1/3$ (d) $-1 < \omega < -1/3$

Figure 2.2: The potentials are plotted in (a) and (c) for $-1/3 < \omega$ and $-1 < \omega < -1/3$, respectively and typical evolutions of scale factor corresponding to their potentials are also plotted in (b) and (d). In fig (c), we define $V_s \equiv -\frac{3\omega}{1+3\omega}\frac{\Omega_{\mathrm{m},0}}{a_s}$ and $a_s \equiv \left(\frac{-(1+3\omega)\Omega_{\mathrm{de},0}}{\Omega_{\mathrm{m},0}}\right)^{1/(3\omega)}$.

some period of the expansion, the universe begins to contract, which implies that the final scale factor a becomes 0. On the other hand, the case of vacuum energy ($\omega = -1$) is, for the flat universe, the time evolution of scale factor is obtained as *accelerated expansion*; $a \propto e^{H\,t}$, with the constant Hubble H, from the Friedmann equation. Similarly, both the open and closed universe asymptotically behave as exponential expansion. If the dark energy is the vacuum energy itself, the recent universe evolves as accelerated expansion: $a \propto e^{H_0 t}$. The condition for EOS which distinguishes a deaccelerated expansion from an accelerated is given by the Eq. (2.5) as $\omega < -1/3$, and thereby, the cosmological constant (or vacuum energy) is a typical example of ω satisfying this condition.

Newtonian picture and Potential problem: The Friedmann and Raychauhdhuri equations are partially obtained in the ordinary Newton theory as follows. We consider the expansion of the universe, characterized by the hubble expansion rate as $\vec{v} = d\vec{r}/dt = H(t,\vec{r})\vec{r}$. Assuming the hubble expansion rate is homogeneous and isotropic $H(t,\vec{r}) \to H(t)$, consistent with the observational evidence *Hubble law* seen later, leads to the distance characterized by the scale factor $\vec{r} = a(t)\vec{\chi}$, where χ denotes the Lagrangian coordinate $d\vec{\chi}/dt = 0$, (basically which is the *comoving distance* seen later). Substituting $\vec{r} = a(t)\vec{\chi}$, the conservation law of mass can be rewritten as

$$\frac{dM}{dt} = \frac{d}{dt}\left(\frac{4\pi}{3}r^3\rho\right) = 0 \implies \dot{\rho} = -3H\rho\,. \tag{2.16}$$

The Newton equation $\vec{F} = m\frac{d^2\vec{r}}{dt^2}$ also can be rewritten as

$$m\frac{d^2\vec{r}}{dt^2} = -\frac{GmM}{r^3}\vec{r} = -\frac{Gm}{r^3}\left(\frac{4\pi r^3\rho}{3}\right)\vec{r} \implies \frac{\ddot{a}}{a} = -\frac{4\pi G}{3}\rho\,. \tag{2.17}$$

The equation of motion (EOM) for the scale factor (2.17) implies that the the universe can not be static in the existence of matter. (2.16) and (2.17) are related to the second one of (2.4) and (2.5), however, it is just correspondence, and hence the differences between Newtoninan and general relativistic equations are seen as additional terms of pressure: $\rho \to \rho + P$ and $\rho \to \rho + P/3$ for (2.16) and (2.17), respectively. Furthermore, as a additional correction term, the cosmological constant of $\Lambda/3$ needs to the right hand side of (2.17). Including this term, integrating (2.17) by time, we obtain $\dot{a}^2 - \frac{8\pi G}{3}\rho a^2 - \frac{\Lambda}{3}a^2 \equiv -K$, where K is a integration constant and related to the spatial curvature. The first term denotes kinetic energy and the second gravitational energy and related to the Friedmann equation, the first one of (2.4). It can give us interpretation of evolution of the universe as a potential problem as follows. In the absence of Λ term and considering the matter ($P = 0$) and the dark energy ($P = \omega\rho$), (2.4) can be rewritten in the

following form:

$$\frac{\dot{a}^2}{H_0^2} + V(a) = \Omega_{\mathrm{K},0}\,, \quad V(a) = -\frac{\Omega_{\mathrm{m},0}}{a} - \Omega_{\mathrm{de},0}\, a^{-(1+3\omega)}\,. \tag{2.18}$$

Notice that as a correspondence with Newton gravity, the mass and the energy are given by $m = 2/\dot{H}_0^2$ and $E = \Omega_{\mathrm{K},0} = -K/a^2H_0^2$, respectively. For the potential problem, the negative energy $E < 0$ leads to binding state and hence the closed universe expands and begins to contract after some period as discussed above. The potential types are divided into two cases: 1. $\omega > -1/3$ and 2. $-1/3 > \omega > -1$, as shown in figs (a) and (c) in Fig. 2.2 and we show the corresponding typical evolution of the universe in figs (b) and (d). The first case has been pointed out in the above discussion. Types named (b), (d) and (e) seen in the second case (fig 2.2(d)), evolve asymptotically as exponential expansion $a \propto e^{H_0 t}$. The type e is seen to be just the case denoting the evolution of the current universe, which deaccelerates and then begins to accelerate around the present time. The case of $\omega < -1$ will be seen to correspond to a *phantom* (ghost) dark energy in the further section of 2.4.

If the universe is sufficiently small at its early stage, the previous discussion implies that the most dominant component is radiation in the universe. By comparing with phenomena occurred at that corresponding temperature in the nuclear physics, we can understand the scenario at the early stage of the universe as effects of the cooling because of the cosmic expansion. For an important physics at this stage, we will evaluate the abundances of the light element. It is consistent with the observational data (Helium-4 constitutes about 25%, which will be shown in the following section). The other important observation to support the big bang scenario is Cosmic Microwave Background (CMB), that is the radiation (photon) decoupled at about $T = 4000K$. The current temperature of CMB radiation is about $T \sim 3K$, which has been firstly detected by Penzias and Wilson in 1965. Now we can understand the big bang scenario as a standard cosmology supported by many observational results. In the next subsection, we shall explain three observational evidences supporting the big bang scenario. Before that, we will introduce important definitions and concepts to discuss the cosmology through the thesis.

• Redshift

Redshift is an useful quantity to measure an expansion of the universe because a redshift of the photon wavelength emitted by a stellar object when the universe expands. Using a wavelength λ and a scale factor a, the redshift z can be obtained

$$1 + z = \frac{\lambda_0}{\lambda} = \frac{a_0}{a}\,,. \tag{2.19}$$

Here the subscript zero represents a present value. It is useful to introduce the following relation:

$$\dot{H} = -\frac{H}{a} = -H(1+z)\,, \quad \text{equivalently,} \quad \int \frac{dz}{H(z)} = -\int \frac{dt}{a}\,, \tag{2.20}$$

where $H(z)$ is given explicitly as (2.33).

• Horizon

In GR, there exists a causality as a connected region since the speed of light gives a maximum for traveling information. In particular the boundary between causal connected and disconnected region is called the *(particle) horizon*. Actually, the particle horizon d_p in a flat geometry can be obtained by

$$d_p = \int_0^r \sqrt{|g_{rr}|}dr \;=\; a(t)\int_0^r dr \;=\; a(t)\int_0^t \frac{dt}{a(t)} \;\simeq\; \frac{a}{\dot{a}}\,. \tag{2.21}$$

Notice that the horizon is approximately given by H^{-1}, which is the so-called *Hubble radius* defined as $d_H \equiv H^{-1}$. Consequently, the terms "Hubble scale" and "particle horizon" are sometimes used interchangeably $d_p \simeq d_H$ because they are of similar magnitude for some models[5]. The *comoving* particle

[5]They can differ by a large factor when a strong energy condition is violated as $\rho + 3P < 0$, where the size of the causally connected region d_p grows exponentially fast, whereas the Hubble radius d_H is constant as you will see in Inflationary scenario.

horizon is defined and then the relation between the *physical* distance and *comoving* distance is given as

$$d_p{}^{\rm com} = \int_0^t dt/a(t)\,, \quad d_p{}^{\rm phy} = a(t)\, d_p{}^{\rm com}\,. \tag{2.22}$$

If the Hubble parameter can be estimated, we can find the corresponding physical horizon scale ($d_p{}^{\rm phy} \sim H^{-1}$), and the comoving horizon, roughly given by $d_p{}^{\rm com} \simeq 1/(aH)$, respectively. Notice that in the perturbation theory (see Sec. 2.3), one usually compare the comoving wavelength $\lambda = 1/k$ with $d_p{}^{\rm com}$, i.e., which is larger k or aH (equivalently, a/k or H^{-1} for the physical wavelength). At the preset time, the scale factor is usually normalized $a_0 = 1$ and yields $d_p{}^{\rm phy} = d_p{}^{\rm com}|_{t=t_0}$. Using the evolution of scale factor (2.15), we find $d_p{}^{\rm phy} = 3t$ in the matter-dominant era and $d_p{}^{\rm phy} = 2t$ in the radiation-dominant era, respectively. As for a typical value of Hubble parameter, it is known that the present Hubble scale H_0^{-1} is about 3000Mpc, i.e., 10^{10} (a ten billion) light years (1pc $\sim 3\,$ly).

• Cosmological distances

We introduce concepts of a definition of distance in order to observe it in an expanding background. Let us introduce two useful definitions of distance; a comoving distance and a physical distance. We can write the FRW metric (2.2) in the following form:

$$ds^2 = -dt^2 + a^2(t)\left[d\chi^2 + f_K^2(\chi)(d\theta^2 + \sin^2\theta d\phi^2)\right]\,, \quad \text{where} \quad f_K(\chi) = \begin{cases} \sin\chi\,, & K = +1\,, \\ \chi\,, & K = 0\,, \\ \sinh\chi\,, & K = -1\,. \end{cases} \tag{2.23}$$

The distance $\chi_s = \int d\chi = \int \frac{dt}{a(t)}$ is the so-called the *comoving distance*. The light traveling along the χ direction follows the geodesic equation $ds^2 = -dt^2 + a^2(t)d\chi^2 = 0$. As for other example, we will introduce a Luminosity distance.

Luminosity distance: is defined by a luminosity of a stellar object. Using an absolute luminosity L_s [6] and an energy flux $\mathcal{F}$ obeying $\mathcal{F} = L_s/(4\pi d^2)$, the luminosity distance d_L can be defined as

$$d_L^2 \equiv \frac{L_s}{4\pi\mathcal{F}}\,. \tag{2.24}$$

One can get a relation between two luminosities L_s and L_0 as

$$L_s = L_0(1+z)^2\,. \tag{2.25}$$

Using an area of sphere as $S = 4\pi(a_0 f_K(\chi_s))^2$, we obtain an observed energy flux as

$$\mathcal{F} = \frac{L_0}{4\pi(a_0 f_K(\chi_s))^2}\,. \tag{2.26}$$

Then we can get a luminosity distance in an expanding universe by

$$d_L = a_0 f_K(\chi_s)(1+z)\,, \tag{2.27}$$

where $f_K(\chi) = \chi$ for a flat FRW spacetime. We estimate

$$d_L = \frac{1+z}{H_0}\int_0^z \frac{dz'}{h(z')}\,, \tag{2.28}$$

and hence rewrite $H(z)$ in terms of $d_L(z)$:

$$H(z) = \left\{\frac{d}{dz}\left(\frac{d_L(z)}{1+z}\right)\right\}^{-1}\,. \tag{2.29}$$

[6] The difficult problem is to determine the absolute luminosity L_s. There is a "ladder" of distance determinations [466], with five distinct rungs, dependent on cosmological interesting distances: 1. Kinematic method, using trigonometric parallaxes ($d < 30$pc), 2. Main-Sequence method, using HR(Hertzsprug-Russell) relation (< 100kpc), 3. Cepheids method, using the period of photons emitted from such stars (< 1Mpc), 4. Tully-Fisher method, using Tully-Fisher relation (< 100Mpc), and 5. Supernovae Ia ($z \lesssim 1$), using their spectral features with declining light, as seen in dark energy.

In cosmology (astronomy), distances are usually measured in parsecs instead of meters. One year is written in terms of seconds as 1yr $\simeq 3\times 10^7$sec. Recalling the light speed having the value of $c \simeq 3\times 10^8$m/s, the light years are related to meters

$$1\,\text{light year} \simeq 3\times 3\times 10^{7+8} \simeq 10^{16}\text{m}\,. \tag{2.30}$$

Therefore, parsecs are related to meters via

$$1\,\text{pc} = 3.26\text{ light years} \simeq 3\times 10^{16}\text{m}\,. \tag{2.31}$$

Angular diameter distance: In a static Euclidean space, the angle which an object with a given transverse size subtends on the sky is inversely proportional to the distance to this object. The angular diameter distance is defined by the apparent angular separation $\Delta\theta$ and the proper size l of object as $d_A = l/\Delta\theta$. In an expanding universe, $\Delta\theta$ can be written in terms of the comoving distance between χ_s and $\chi = 0$ as $\Delta\theta = l/(a\chi_s) = l/(a\int_{t_1}^{t_0}\frac{\mathrm{d}t}{a})$. In the non-zero curvature case $K \neq 0$, it needs to interchange $\chi_s(z)$ with $f_K(z)$. Therefore, the angular diameter distance is given by

$$d_A = a_0(1+z)^{-1}f_K(z) \simeq a_0(1+z)^{-1}\int_{t_1}^{t_0}\frac{\mathrm{d}t}{a} = \frac{1}{H_0(1+z)}\int_0^z\frac{\mathrm{d}z'}{h(z')}\,, \tag{2.32}$$

where we have used a relation $\chi = f_K(\chi)$ for a flat geometry on the second equation and (2.20) on the last equation. Note that the diameter angular distance also depend on the hubble parameter as similar to the luminosity distance (2.28).

• **Age**

Let us consider the age of the universe. The Hubble is a function of the redshift z as

$$H^2(z) = H_0^2[\Omega_{\rm r}^{(0)}(1+z)^4 + \Omega_{\rm m}^{(0)}(1+z)^3 + \Omega_\Lambda^{(0)} + \Omega_{\rm K}(1+z)^2]\,, \tag{2.33}$$

rewritten from the Friedmann equation (2.4), where we consider the three material contributions to ρ; radiation ($\omega_{\rm r} = 1/3$), dust ($\omega_{\rm m} = 0$) and a cosmological constant ($\omega_\Lambda = -1$) plus the spatial curvature ($\Omega_{\rm K} \equiv -K/(a_0^2H_0^2)$). If one generally consider a dark energy contribution, the term of $\Omega_{\rm de}^{(0)}(a/a_0)^{2/3(1+\omega)}$ needs in stead of the cosmological constant. Using (2.20), the age of the universe can be estimated by

$$t = \int_0^{t_0} dt = \int_0^\infty \frac{dz}{H(1+z)} = \int_1^\infty \frac{dx}{H_0 x[\Omega_{\rm r}^{(0)}x^4 + \Omega_{\rm m}^{(0)}x^3 + \Omega_\Lambda^{(0)} + \Omega_{\rm K}x^2]^{1/2}}\,, \tag{2.34}$$

where $x(z) \equiv 1+z$. It implies that the age of the universe is determined by its including components Ω_i. In a simple situation, when we only consider dust $\Omega_{\rm m} \simeq 1$ with $\Omega_{\rm K} = \Omega_\Lambda = \Omega_{\rm r} \simeq 0$ (*Einstein-de Sitter*), it follows the age of the universe $t_0 \simeq \frac{2}{3}\frac{1}{H_0} \sim 9$Gyr (or billion years). It is interesting to compare it with the age of the oldest stellar. For example, the age of globular clusters can be estimated as $t_1 = 13.5\pm 2$Gyr. It gives us the lower bound which the age of the universe needs to satisfy, obtained as $t_0 \gtrsim 13$Gyr. From the above estimation it is difficult for a flat universe to satisfy this condition with a normal form of matter. However the age problem can be easily solved in a flat universe if one re-consider a cosmological constant $\Omega_\Lambda^{(0)}$. If the parameters can be taken as $\Omega_\Lambda^{(0)} \simeq 0.7$ and $\Omega_{\rm m}^{(0)} \simeq 0.3$, the age becomes $t_0 \sim 0.96/H_0$ and accordingly, the age becomes larger by a factor of about 3/2: $t_0 \sim 13.5$Gyr. As a result, the age of the universe can be roughly estimated as $t_0 \simeq 1/H_0$ and it corresponds to the horizon of the universe is $d_H \simeq c/H_0$ since the light emitted at the onset of big bang, travels during the age of the universe. The spatial geometry also changes the age. For an open universe model, the age is larger than the flat case, because the amount of matter decreases and then it takes longer. Conversely, the closed case makes it become shorter.

• **Temperature**

The entropy density of the proton is given by $s = \frac{4}{45}\pi^2 T^3$ and it reads a conservation of s as $T^3 a^3 =$const, that is,

$$T \propto \frac{1}{a} \simeq (2.73K) \times z\,, \tag{2.35}$$

normalized by a current "temperature" of a Planck distribution $T_0 = 2.73K$. If a radiation can interact with ordinal matter and be thermalized, this temperature denotes the temperature of the universe[7]. After thermal decoupling of radiation from other matter at $z \sim 1100$ or $T \sim 3000K$ (see a heading of CMB), it denotes temperature of a planck distribution of freely streaming photon and it does not represent a thermal equilibrium of the universe. As the universe expands, the "temperature" also decreases. Conversely, the temperature at the early stage of the universe became very high. That is the idea of the big bang universe. At this hot stage of the universe (where a radiation dominated), it is useful to estimate a relation its time scale and its temperature as

$$t \propto T^{-2} \implies t_{\rm sec} \simeq \frac{O(1)}{T^2_{\rm MeV}}\,. \tag{2.36}$$

It is also useful to estimate a energy scale corresponding to a temperature by using the relation

$$1{\rm eV} \simeq 10^4 K\,. \tag{2.37}$$

For a few order of eV, its corresponding events are the equality time at $T_{\rm eq} \sim 10^4 K \sim 1{\rm eV}(z \sim 3500)$ and the recombination at $T_{\rm dec} \sim 3000K \sim 0.3{\rm eV}(z \sim 1100)$.

2.1.2 Observational evidences

The standard cosmological scenario is the so-called the *Big Bang theory*, proposed by George Gamow et al in 1948, where the universe started from a hot dense state around ten billion years ago, as a high density Egg, "the Big Bang" [165, 166, 11]. We will explain the three observational evidences confirming the big bang theory.

(1) Hubble law

This fact that the universe is now expanding is discovered by E. Hubble in 1929 [212, 211]. He observed and estimated a relation between distances (r) and radial velocities (v) of twenty four extra-galaxies as

$$v = H_0 r\,. \tag{2.38}$$

The value of the Hubble parameter, H_0 at his estimation, is about 53km/s/Mpc [211] (compared with the current value; $71 \pm 4{\rm km\,s^{-1}\,Mpc^{-1}}$ [158], see Fig. 2.3)[8], because the errors of distance determined from the Cepheid variables, were very large. It shows that the faraway galaxies are receding more rapidly from our galaxy. This fact can be explained from the homogeneous and isotropic expanding of the universe. That is $H(t, \vec{r})$ is reduced to the function of only time $H(t)$, equivalently, $\vec{r} = a(t)\vec{\chi}$ with Lagrange coordinate $d\vec{\chi}/dt = 0$. In GR, a receding velocity is related to the redshift $z = a_0/a(t) - 1$ of the wavelengths of emission lines as $v = cz$ (2.38). Notice that it can interpret v as a receding velocity only for a low redshift $z \ll 1$, however, one usually by using it, extensively define a redshift as a distance $r = cz/H_0$. Cosmologist can usually use a dimensionless Hubble parameter $h \equiv H/100$. The current value of Hubble constant also has other three meanings *1. Age, 2. Size 3. Energy scale.* The first and second meanings are related each other by multiplying c. The current universe is mainly characterized by the present value of the Hubble H_0 and so we summarize its several physical meanings as follows: **1. Expansion rate** $H_0 = 100h$km/s/Mpc, **2. Age** $H_0^{-1} \simeq 13.7$Gyr, **3. Horizon** $H_0^{-1} \simeq 13.7$Glr $\simeq 4200$Mpc, and **4. Vacuum energy** $H_0 \simeq 10^{-42}$GeV.

[7] It is not thermal equilibrium. Thermal equilibrium can not be realized at $1 + z \sim 5 \times 10^4$, but the isothermal effect occurs after that, and then, as a result, black body keeps until $1 + z \sim 1100$. Moreover, after that, even though both thermal equilibrium and isothermal effect break, when one compare it with a black body, "temperature" is obtained.

[8] It means the velocity of galaxy existing at 1Mpc is 71km/s, compared with a velocity to escape from the gravity of earth is 11.2km/s.

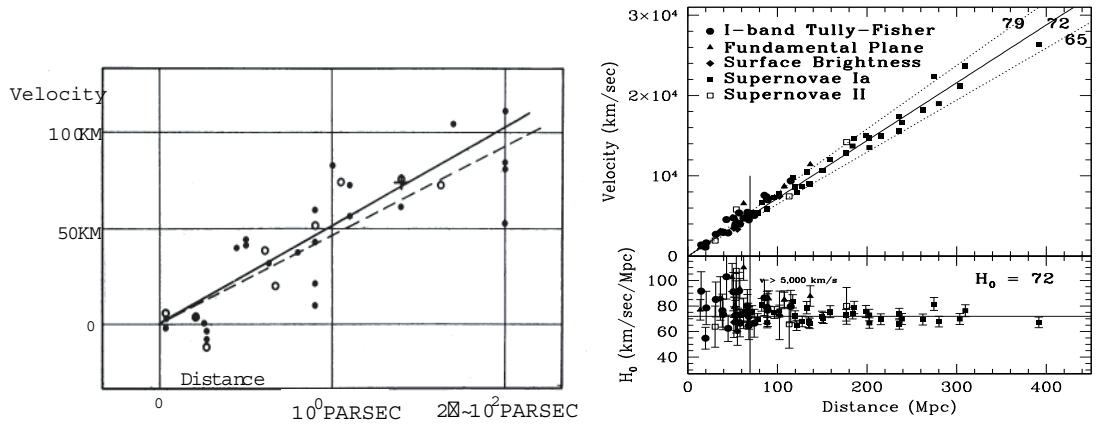

(a) The original Hubble diagram (1929) (b) Hubble Space Telescope Key Project (2001)

Figure 2.3: (a): This figure is in Hubble (1929) [211]. Velocities of distant galaxies (units should be km $\sec^{-1}$) are plotted vs distance (units should be Mpc). Solid (dashed) line is the best fit to the filled (open) points which are corrected (uncorrected) for the sun's motion. In this early work, $H_0 \simeq 53$km/s/Mpc. (b) The Hubble diagram from the Hubble Space Telescope Key Project (Freedman et al., 2001 [158]) using five different measures of distance. Bottom panel shows H_0 vs distance with the horizontal line equal to the best fit value of 72km $\sec^{-1}$ Mpc^{-1}.

(2) Nucleosynthesis

The most widespread chemical element in the universe is hydrogen, constituting nearly 75% of all baryonic matter. Helium-4 (He-4) constitutes about 25%. The other light elements and metals have only very small abundance. Simple arguments lead to the conclusion that the large amount of ^{4}He could not have been produced in stars, that is, if the luminosity of baryonic matter in the past was not much larger than at present, less than 0.5% of ^{4}He can be fused in stars. It can not explain that one quarter of all baryons has been fused into ^{4}He in stars. The big bang theory explain the light elements [11, 203], H, He, Li and Be, are produced in the early stage of the universe, at nearly $T \sim 10^9 K \sim 0.1$MeV, that is, *a few minutes after the big bang starts*. We will explain the amount of produced helium hereafter (see the review book [332]). This amount depends on the availability of neutrons at this time, since the neutron-to-proton ration freezes out. This ratio is roughly determined by their mass difference $\Delta m \sim 1.2$MeV as

$$\frac{n_p}{n_n} \propto e^{\Delta mc^2/k_B T} . \tag{2.39}$$

Therefore, the neutron decreases as cooling of the universe. This ratio *freezes out* at $T \sim 0.8\,MeV$ where $n_p/n_n \sim 5.3$. After freeze-out, the neutron (beta) decay is the sole remaining cause for a change in the number of neutrons. Then the neutron concentration decreases as $X_n \equiv n_n/n_N \propto e^{-t/\tau_n}$ where τ_n is a lifetime of a free neutron $\tau_n \approx 886$s and $n_N = n_n + n_p$ is the total number of nucleons (baryons). He-4 could, in principle, be built directly in the four-body collision: $p + p + n + n \rightarrow {}^4He$, however, actually, the He-4 are formed as a result of complex nuclear interactions. In these interactions, the most important process is a deuterium (D) production $p + n \rightleftharpoons D + \gamma$. Then two interactions convert deuterium into heavier elements helium-3 (^3He) and tritium (T) and finally produce He-4. The deuterium can constitute a significant fraction of baryonic matter only if the temperature is about 0.08MeV. The equilibrium concentration $X_D = 2n_D/n_N$ increases from 10^{-4} to 10^{-2} as the temperature drops from 0.08MeV to 0.07 MeV. This increasing of deuterium makes nucleosynthesis, to produce more heavy atoms, begin quickly. When the deuterium concentration reaches its maximal value $X_D \simeq 10^{-2}$, the final He-4 abundance is completely determined by the number density of free neutrons at this time. The abundance

of He-4 is determined as $n_n/2$, and accordingly the abundance ratio by weight $X_{^4He} = 4n_{^4He}/n_N$ is given as

$$X_{^4He} = \frac{4 \times \frac{n_n}{2}}{(n_n + n_p)} = \frac{2}{1 + \frac{n_p}{n_n}} \,. \tag{2.40}$$

When X_D is of order 10^{-2} at temperature $T \sim 0.07$MeV, the neutron-to-proton ratio is estimated as nearly $\frac{n_p}{n_n} \sim 7$ or $X_n \sim 0.12$. Therefore one finally obtains $X_{^4He} \sim \frac{2}{(1+7)} \sim 0.25$. Recent observational data shows $He = 24.72 \pm 0.12\%$ for Ref. [220] and $He = 24.74 \pm 0.28\%$ for Ref. [358]. The nucleosynthesis produces $^4He, D, ^3He, T$, lithium-7 ($7Li$) and beryllium (^7Be) at most. Other elements such as ^6Li, ^8Be etc. are produced in much smaller amounts and will be ignored. Final abundances of these light elements are obtained as $D \lesssim 10^{-4}$ ^4He, T, $^3He \lesssim 10^{-1} D$ and ^7Li, $^6Be \lesssim 10^{-5} D$ for $\eta_{10} = 3$ where η_{10} is the baryon-to-photon ratio $\eta_{10} \equiv 10^{10} \times n_N/n_\gamma$. From the recent observational data [220, 357, 358], one can constraint them as $1.0 \times 10^{-4} < D/He < 1.2 \times 10^{-4}$ and $4.0 \times 10^{-6} < {}^7Li/D < 1.2 \times 10^{-5}$ and it is consistent with the result abundances obtained from the big-bang nucleosynthesis, which occurs at the temperature dropping form $0.1MeV$ to $10keV$.

(3) CMB

CMB is the most powerful tool to look into the early image of the universe, which is a isotropic emission of radiation from a hydrogen recombination (or simply, *Recombination*)[9]; $p + e^- \rightleftharpoons H + \gamma$ where H is a neutral hydrogen atom. For the ground ($1S$) state, the binding energy of neutral hydrogen, $\Delta E = m_p + m_e - m_H = 13.6$eV corresponds to a temperature of about $10^5 K$ and then the recombination appears to occur at this temperature. However, a real temperature is different from this one. The Saha formula ($\mu_e + \mu_p = \mu_H$) can be derived as

$$\frac{n_e n_p}{n_H} = \Big(\frac{T m_e}{2\pi}\Big)^{3/2} \exp\Big(-\frac{\Delta E}{k_B T}\Big) \tag{2.41}$$

We introduce the ionization fraction $X_e = \frac{n_e}{n_B}$, according to a neutrality $n_p = n_e$ and the baryon number density: $n_B \simeq n_p + n_H \simeq 10^{-7}(1+z)^3 \mathrm{cm}^{-3}$, Eq. (2.41) becomes

$$\frac{n_p n_e}{n_H n_B} = \frac{X_e^2}{1 - X_e} \simeq 2.2 \times 10^{23} \Big(\frac{T}{1K}\Big)^{-3/2} e^{-\Delta E/k_B T} \,. \tag{2.42}$$

The factor of 10^{23} shown in the above equation is a big value and so even if the temperature reaches $k_B T \sim \Delta E \sim 10^5 K$, X_e does not decrease readily. In fact, when the ionization fraction is $X_e = 0.5$, the temperature is obtained as $T_{\rm rec} \sim 3750K (z \sim 1370)$. So far we have assumed thermal equilibrium of ground state, however, if we do not assume it, it takes a lower value as $T_{\rm rec} \sim 3400K (z \sim 1220)$ [10]. After that, a radiation decoupled from other elements begin to stream freely through the universe and then an observer today detects the photons that last interacted with matter. It is the so-called *decoupling* (or *last scattering*), which occurs at $T_{\rm dec} \sim 2500K (z_{\rm dec} \sim 900)$ obtained by estimating $t_{\rm dec} \lesssim H^{-1}$. A. Penzias and R. Wilson casually discovered the CMB as isotropic weak radio signals in 1965. That stretched wavelength is same as a planck distribution at $T \sim 3K$. After that, The COBE satellite (COsmic Background Explorer) [40] detects the CMB and can estimate more accurate value of this "temperature", as $2.725 \pm 0.002K$ in 1992. So the redshift is obtained as $1 + z = 3000K/2.73K \simeq 1100$. On the other

[9] There also exists Helium recombination, where capture of one electron giving He^+ occurs at $T \sim 12000K$ and the neutral Helium becomes at $T \sim 5000K$. However even complete recombination of helium reduces the number of free electrons by 12% at most and the universe is still opaque to radiation. As a result, hydrogen recombination is a more interesting and dramatic event from an observational point of view.

[10] To be accurate, under thermal equilibrium, the redshift is obtained as $z \sim 1370$ for $X_e \sim 0.5$ and $z \sim 1200$ for $X_e \sim 0.1$, while considering deviation from thermal equilibrium (nonthermal effects of radiation in excited sates $2S$ and $2P$ etc seen in [332]), $z \sim 1220$ for $X_e \sim 0.5$ and $z \sim 1100$ for $X_e \sim 0.1$. Therefore, recombination occurs at about $z \sim 1100 - 1200$ ($T_{\rm rec} \sim 3000K$)

hand, not a radiation but a neutrino decouples from other elements at $T \sim 1.5MeV$ and yields a *cosmic background neutrino* having a planck distribution with temperature as $T_\nu = (4/11)^{1/3}T_\gamma \sim 2.7K/1.4 \sim 1.95K$. The neutrino temperature is lower by a factor of $(4/11)^{1/3}$ since photons are heated by the *annihilation of electron and positron* when the temperature drops below their rest mass $T \sim m_e \sim 500\text{keV}(0.5MeV)$. If one will detect them in the future, it is perfect evidence of the big bang theory. (see the article of "history" in summary of this chapter). BOOMERanG (Balloon Observations of Millimetric Extragalactic Radiation and Geophysics) [53] has flown around Antarctica in two separate flight (the first in 1998, the second in 2003) to map the CMB. The recent CMB data are obtained by WMAP satellite (Wilkinson Microwave Anisotropy Probe) [41, 264, 359, 427] and it can estimate several cosmological parameters as Table 2.2. In the following, we shall explain the relation between cosmological parameter Ω_i and the CMB spectrum in the section 2.3.

2.1.3 Problems in Big bang scenario

The big bang cosmology has been shown as a successful scenario, however it contains some unexplained theoretical problem by its own. Let us clarify what the problems are (see the review of inflation [36, 280, 289, 332]).

• Flatness problem

The density parameter Ω today (see (2.6)) is constrained by the recent observational data as

$$\Omega_0 = 1.02 \pm 0.02\,. \tag{2.43}$$

The curvature term (K/a^2) becomes effective at the early stage of the universe since its decay rate is slower than other components: matter($\rho_{\rm m} \propto a^{-3}$) and radiation($\rho_{\rm r} \propto a^{-4}$). So Ω must be very close to unity in the early universe. It is also seen from (2.6) that the $a^2H^2(=\dot{a}^2)$ term always decreases since the standard big-bang theory implies a decelerating of the universe $\ddot{a} < 0$. We can evaluate the parameter Ω in the stage at which the temperature is T_i,

$$\Omega_i \sim 1 + \Big(\frac{\Omega_0 - 1}{\Omega_0}\Big)\Big(\frac{T_0 T_{\rm eq}}{T_i^2}\Big)\,, \tag{2.44}$$

where $T_{\rm eq} \sim 10^4K$, $T_0 \sim 3K$ are the temperature at the (*Matter-Radiation equality time*) and at present, respectively. For example, the density parameter can be evaluated as $|\Omega_i - 1| \leq 10^{-16}$ at the epoch of nucleosynthesis ($T \sim 1$MeV) and $|\Omega_i - 1| \leq 10^{-60}$ at the Planck epoch ($T \sim 10^{19}$GeV). It was an extreme fine-tuning of initial conditions. Why the universe is so close to flat as the initial condition is the so-called *flatness problem*.

• Horizon problem

The CMB radiation temperature is the same across the entire sky to an accuracy of a few parts in one million. Then it leads to that the universe had to be in thermodynamic equilibrium at some past before CMB radiation was emitted, since the radiation has been effectively non-interacting after that point in time. As noted in the above article of Horizon, the present value of the Hubble radius is about $H_0^{-1} \sim 10^{10}$lyr($\simeq$ 3000Mpc) and the corresponding physical hubble radius at the decoupling ($T_{\rm dec} \sim 3000K$) can be estimated as,

$$l_{\rm dec}{}^{\rm phy} \sim H_0^{-1}(a_{\rm dec}/a_0) \sim H_0^{-1}(T_0/T_{\rm dec}) \sim 10^7 \text{ light years}\,. \quad (t_{\rm dec} < t < t_0) \tag{2.45}$$

On the other hand, noting that the universe at the decoupling is dominated by the matter, the horizon scale at decoupling is obtained from Eq. (2.21) as,

$$d_p{}^{\rm phy}(t_{\rm dec}) \simeq 3t_{\rm dec} \sim (T_{\rm dec}/T_0)^{-3/2}\, H_0^{-1} \sim 10^5 \text{ light years}\,. \quad (0 < t < t_{\rm dec}) \tag{2.46}$$

The volume ratio of $d_p{}^{\rm phy}(t_d)$ to the particle horizon today at decoupling $l_{\rm dec}{}^{\rm phy}$, is estimated as

$$\frac{d_p{}^{\rm phy}(t_{\rm dec})}{l_{\rm dec}{}^{\rm phy}} \sim 10^{-2}(\times 360/(2\pi) \simeq 1^\circ)\,. \tag{2.47}$$

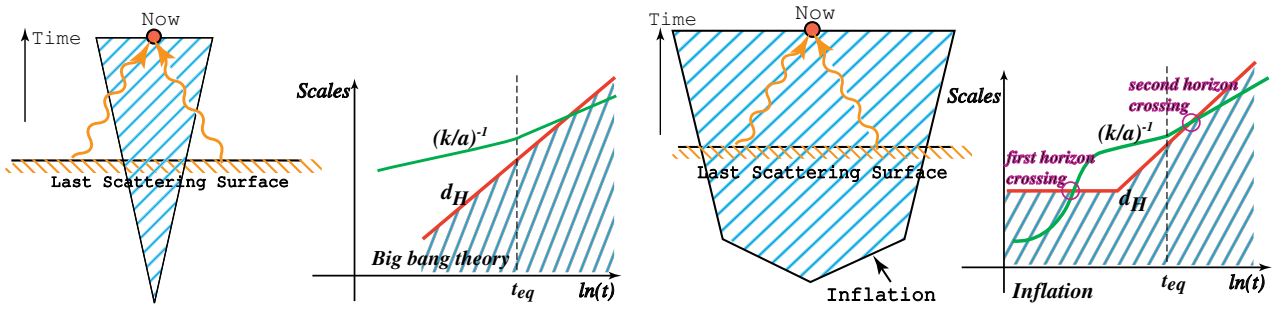

(a) Big bang theory (b) Big bang theory (c) Inflation (d) Inflation

Figure 2.4: Sketches of the horizon problem and the formation of the structure problem in the big bang theory. The region inside the cone at any time is causally connected to us (at the center) (a). Photons emitted from the last scattering surface (at redshift ~ 1100) started outside of this region. Therefore, at the last scattering surface, they were not in causal contact with us and certainly not with each other. In this universe, similarly, the fluctuations ($(k/a)^{-1}$) is not causally connected (b). Inflation gives us solutions to these problems seen in (c) and (d). (same sketches in the book [123])

These causally regions corresponds to an angle of order 1°. This result is also obtained from estimating the ratio of the comoving particle horizon $d_p{}^{\rm com} = (1+z)d_p{}^{\rm phy} \propto (1+z)^{-1/2}$ to the present as $d_p{}^{\rm com}(z = 1100)/d_p{}^{\rm com}(z = 0) = 1/\sqrt{1101} = 1.7^\circ$ [11]. On the other hand we have observed photons which are thermalized as a same temperature at all regions in the CMB sky. The observed temperature from the different region can be evaluated as $\Delta T/T \sim 10^{-5}$. Why these causally disconnected regions have same temperature is the so-called *horizon problem* (see Fig 2.4).

• Origin of large-scale structure

The COBE satellite shows the anisotropies of temperature has a nearly scale-invariant spectrum, the so-called *Harrison-Zel'dovich spectrum*. In a theory describing a structure formation (the perturbation theory of the FRW metric, seen the section of inhomogeneity in more detail), it may be possible to obtain the present structure if one would use observational results at the last scattering as initial conditions. However, it needs to consider some physical mechanism providing such small perturbations. Moreover it is difficult to generate large scale fluctuations through causal process in a FRW metric, which is related to a resolution of horizon problem in the view point of causality. The big bang theory alone cannot explain this problem.

• Relic density problem

In modern particle physics, it has been known that many unwanted objects can be produced due to symmetry breaking. For example, topological defects, such as Monopole, cosmic strings, and domain walls can be formed by phase transitions. It is natural that some relic remains in a general situation at the early universe. In particular, it is known that the monopole energy density is bigger than the critical density, i.e., $\rho_{\rm mon} \geq 10^{10}\rho_{\rm cr}$. It is clearly inconsistent with the present universe. Why the amount of monopole is so small? This problem is known as the relic density problem.

2.2 Inflation cosmology and Reheating mechanism

Inflationary cosmology [408, 195] played an important role. Inflation can give us prediction about a theoretical origin of structure formation in the universe. Moreover this scenario has also a possibility to

[11] The comoving horizon size at decoupling is $d_p{}^{\rm com}(t_{\rm dec}) \simeq 400$Mpc, similar order of typical supercluster's scale. The equality time locates before the decoupling, which corresponds to the comoving horizon scale $d_p{}^{\rm com}(t_{\rm eq}) \simeq 90 - 100$Mpc, similar order of cluster's scale.

investigate a fundamental physics as a new window. The idea is very simple. We can show the review, e.g., [289, 259, 280, 51, 344, 62, 279, 282, 36] for some early review and [303] found for a model building in the context of supersymmetric models.

2.2.1 Basic Idea

We assume the universe would be in an accelerated expansion at its early stage,

$$\ddot{a} > 0\,. \tag{2.48}$$

This corresponds to the following two cases by the relation (2.5): one is, in the absence of Λ,

$$\rho + 3P < 0\,, \tag{2.49}$$

and another is a positive Λ only. For the typical example, we show the vacuum energy (or the cosmological constant) dominates the accelerated expansion of the universe, characterized as $\omega = -1$. It is obvious this EOS satisfies the above condition (2.49) and from the Friedmann equation (2.4), we obtain the following solutions in $K = 0$, which behaves as exponential expansion,

$$a(t) = a_0\, e^{Ht}\,, \quad \text{with} \quad H = \sqrt{\rho_{\rm vac}\kappa^2/3} \tag{2.50}$$

where a_0 is the integral constant, corresponding the scale factor at $t = 0$. Even if we consider the spatial curvature K, it is easy to see that every solutions behave as exponential expansion in the epoch $t \gg 1/H$. It is also seen that the Hubble parameter is constant during this epoch. We shall show how an accelerated expansion of the universe solves the cosmological puzzles in the standard big bang theory.

• Flatness problem

Eq. (2.4) of the Friedmann equation is reduced to (2.6):

$$\Omega - 1 = \frac{K}{a^2H^2}\,. \tag{2.51}$$

During inflation, the a^2H^2 term in the above equation increases, that shows a decreasing of comoving Hubble radius $(aH)^{-1}$. Ω rapidly approaches unity by this increase. Once inflationary expansion efficiently occurs Ω becomes close to one and the present universe also shows Ω is of order unity.

• Horizon problem

In order to resolve the horizon problem, the comoving particle horizon needs to satisfy

$$\int_0^{t_{\rm dec}} \frac{dt}{a(t)} \gg \int_{t_{\rm dec}}^{t_0} \frac{dt}{a(t)}\,, \tag{2.52}$$

where $t_{\rm dec}$ and t_0 are the decoupling and present time, respectively. It means that a comoving distance before decoupling is larger than one after decoupling (see Fig 2.4). If the universe expands about $e^{60-70} \sim 10^{28-30}$ times during inflation, the horizon problem can be resolved. This amount of inflation is fairly easily achieved in the usual inflationary scenario.

• Origin of large-scale structure

It is an important point to introduce inflation that it can provide primordial density perturbations through causal mechanism, which describe origin of galaxies and clusters. Fig 2.4 shows a sketch of the evolution of perturbation. In the early stage of inflation, all perturbations within the Hubble radius become small because in which causal physics works well. When a scale of perturbation is stretched over the Hubble, which is known as constant (i.e., the *first horizon-crossing*), a longer perturbation than Horizon can 'frozen' since causality is violated. Later such longer perturbations go inside the Hubble horizon again (the *second horizon-crossing*), (see also the evolution of the fluctuations of the structure formation in Fig. 2.4(d)). After the second horizon crossing, the initial small perturbations generated during inflation becomes large scale perturbation. It is possible to generate perturbations in a causal mechanism. Note

that perturbations are generated by a causal microphysical process, which will be shown in the next section.

• Relic density problem

When inflation occurs, the energy density of the universe decreases as a^{-2} or slower. For example, an energy density of supersymmetry particles decreases faster as a^{-3} and they can be cleared away via a red-shift. Reheating process can also resolve an unwanted particles as graviton after inflation. It is known that a reheating temperature needs to be lower than 10^9GeV, in order not to overproduce an unwanted relic object such as gravitinos and to make nucleosynthesis succeed [404].

2.2.2 Dynamics of inflation

The energy density and pressure of inflaton (scalar field) can be characterised by

$$\rho = \frac{1}{2}\dot{\phi}^2 + V(\phi)\,, \quad P = \frac{1}{2}\dot{\phi}^2 - V(\phi)\,. \tag{2.53}$$

There has been not presently a regard well established fundamental theory, so we have to consider $V(\phi)$ as a different function corresponding to different models of inflation. Some examples of potentials are (1): Higgs potential, $V(\phi) = \lambda(\phi^2 - M^2)^2$ (2): Massive scalar field, $V(\phi) = m^2\phi^2/2$ and (3): Self-interacting scalar field, $V(\phi) = \lambda\phi^4$. The basic equations for a homogeneous scalar field are obtained by substituting Eqs. (2.53) into the Friedmann equations, Eqs. (2.4) as

$$H^2 = \frac{\kappa^2}{3}\Big[\frac{1}{2}\dot{\phi}^2 + V(\phi)\Big] \quad \ddot{\phi} + 3H\dot{\phi} + V'(\phi) = 0\,, \tag{2.54}$$

where prime represents $d/d\phi$. During inflation, the relation (2.5) yields

$$\ddot{a} > 0 \iff P < -\frac{\rho}{3} \iff \dot{\phi}^2 < V(\phi) \tag{2.55}$$

which means that the potential energy $V(\phi)$ dominated than the kinetic energy $\dot{\phi}^2/2$. Namely, in order to achieve a sufficient inflation, we require a flat potential along which inflaton rolls down slowly. This is related to the so-called slow-roll condition, which is the condition to take place during inflation. We can find this condition as

$$\frac{\ddot{a}}{a} = \dot{H} + H^2 > 0 \iff -\frac{\dot{H}}{H^2} < 1 \iff \frac{M_{\rm pl}^2}{2}\left(\frac{V'}{V}\right)^2 < 1\,, \tag{2.56}$$

where the last manipulation uses the slow-roll approximation ($\dot{\phi}^2/2 \ll V(\phi)$ and $|\ddot{\phi}| \ll 3H|\dot{\phi}|$). One can define the so-called slow roll parameters

$$\epsilon(\phi) = \frac{1}{2\kappa^2}\left(\frac{V_\phi}{V}\right)^2, \quad \eta(\phi) = \frac{1}{\kappa^2}\frac{V_{\phi\phi}}{V}\,, \quad \xi^2 = \frac{1}{\kappa^4}\frac{V_\phi V_{\phi\phi\phi}}{V^2}\,, \tag{2.57}$$

where $V_\phi \equiv dV/d\phi$. The final condition in Eq. (2.56) is just slow-roll condition $\epsilon < 1$. The first term ϵ denotes the slope of potential and the second η denotes its curvature and the condition $\eta < 1$, roughly speaking, relates to prolonged period of inflation. The necessary conditions is $\epsilon \ll 1$ and $|\eta| \ll 1$, the so-called slow-roll approximation.

Imposing these conditions, EOMs are approximately given as

$$H^2 \approx \frac{\kappa^2}{3}V(\phi)\,, \quad 3H\dot{\phi} \approx -V'(\phi)\,, \quad \text{and hence} \quad \dot{H} \approx -\frac{\kappa^2}{2}\dot{\phi}^2\,. \tag{2.58}$$

If the potential is flat and constant at this time, the above equation leads an exponential expansion of the universe $a \sim e^H \sim e^V$. The inflation ends once ϵ and $|\eta|$ become of order unity. The number of e-foldings N is a useful quantity measuring an inflationary expansion, which is given by

$$N \equiv \ln\frac{a(t_{\rm final})}{a(t_{\rm initial})} = -\frac{\kappa^2}{2}\int_{\phi_i}^{\phi_f}\frac{H}{H'(\phi)}\,d\phi \simeq \kappa^2\int_{\phi_f}^{\phi_i}\frac{V}{V_\phi}\,d\phi\,, \tag{2.59}$$

where the slow-roll approximation is used at the final step. If one take $|\Omega_f - 1| \lesssim 10^{-60}$ after inflation, the flatness problem can be solved. The ratio $|\Omega - 1|$ between the initial and final can be estimated as

$$\frac{|\Omega_f - 1|}{|\Omega_i - 1|} \simeq \left(\frac{a_i}{a_f}\right)^2 = e^{-2N}\,. \tag{2.60}$$

In order to resolve the flatness problem, the number of e-foldings needs to be $N \gtrsim 60$. The condition $N > 60$ represents a minimum e-folding number for any model of inflation to solve the flatness and horizon problem. If we take the potential form as $V \propto \phi^{2q}$, Eq. (2.59) is reduced to

$$N(\phi) = \frac{\kappa^2}{2q}\int_{\phi_f}^{\phi_i} \phi d\phi = \frac{\kappa^2}{4q}(\phi_i^2 - \phi_f^2) \sim \frac{2\pi}{q}\Big(\frac{\phi_i}{m_{\rm pl}}\Big)^2\,. \tag{2.61}$$

and then the sufficient e-folding condition leads to

$$N \gtrsim 60 \;\Rightarrow\; \phi_i \gtrsim 3\sqrt{q} m_{\rm pl}\,. \tag{2.62}$$

On the other hand, breaking down of slow roll condition gives

$$1 \approx \frac{\dot\phi^2}{V} \approx \Big(-\frac{V'}{3H}\Big)^2 \frac{1}{V} = \frac{V'^2}{3\kappa^2 V^2} = \frac{q^2 m_{\rm pl}^2}{6\pi\phi^2} \quad\Longrightarrow\quad \frac{\phi_f}{m_{\rm pl}} \approx 0.2q\,. \tag{2.63}$$

Quadratic potential $V(\phi) = m_\phi^2\phi^2/2$
As a typical example, let us consider the massive potential. We get the exact solutions as

$$\phi \simeq \phi_i - \frac{m_\phi m_{\rm pl}}{2\sqrt{3\pi}}t\,,\quad a \simeq a_i \exp\left[2\sqrt{\frac{\pi}{3}}\frac{m_\phi}{m_{\rm pl}}\left(\phi_i t - \frac{m_\phi m_{\rm pl}}{4\sqrt{3\pi}}t^2\right)\right], \tag{2.64}$$

where ϕ_i denotes an initial value of inflaton. Eq. (2.64) shows an exponential expansion of the universe. It is also important that these solutions are attractor solutions since using the phase diagram method, they relate to a fixed point $d\dot\phi/d\phi = 0$. It implies inflation naturally occurs along these trajectories in phase space. From Eqs. (2.62) and (2.63), we find that the scalar field (*inflaton*) takes its value during inflation as

$$\phi_i \gtrsim 3m_{\rm pl}:\ \text{(initial)}\,,\quad \phi_f \simeq 0.2m_{\rm pl}:\ \text{(final)}\,. \tag{2.65}$$

Moreover, in this simple potential case, the value of Hubble during inflation is approximately equal to a mass of scalar field i.e., $H^2 \sim V/m_{\rm pl}^2 \sim m_\phi^2$. On the other hand the normalization of the CMB on large scales, which will be obtained in the farther section as $P_{\mathcal R}^{1/2} \sim H^2/(2\pi\dot\phi) \sim H/(\sqrt{\pi\,\epsilon} m_{\rm pl})$ (see (2.192)), must be smaller than order 10^{-5}. It implies that $H \lesssim 10^{-6} m_{\rm pl}$ (2.92) and combing it with $H \sim m_\phi$ gives a constraint equation to a mass of scalar field

$$m_\phi \lesssim 10^{-6} m_{\rm pl}\ (=\ 10^{13}\text{GeV})\,. \tag{2.66}$$

This constraint equation is well used.

2.2.3 Reheating mechanism

At the end of inflation the universe is in a non-thermal state and becomes a very cold. It also make the universe at effectively zero temperature and model of inflation must explain the process the universe was reheated to the high temperatures as an initial state of Big Bang. We call this mechanism *Reheating*, which involves both baryogenesis and nucleosynthesis. Baryogenesis usually needs greater energy than the electroweak 100 GeV and nucleosynthesis requires temperature around 1 MeV. We now review reheating mechanism as follows (see [36, 332]).

• **Elementary reheating theory**

The "old" type of reheating [1, 125] was achieved by a decay of inflaton. Inflaton field ϕ has a finite probability of decay via coupling to other scalar (χ) or fermion (ψ) fields representing the terms $g\phi\chi^2$ and $h\phi\bar{\psi}\psi$, where g and h have a dimension of mass and dimensionless coupling, respectively. We can estimate decay rates (Γ) by dimensional analysis. Since $[\Gamma] = t^{-1} = m_\phi$, if $m_\phi \gg m_\chi, m_\psi$, the decay rates are obtained [125, 289]

$$\Gamma_{\phi\to\chi\chi} = \frac{g^2}{8\pi m_\phi}\,, \quad \Gamma_{\phi\to\psi\bar{\psi}} = \frac{h^2 m_\phi}{8\pi}\,. \tag{2.67}$$

One can show that quantum corrections do not significantly modify the interactions only if $g < m_\phi$ and $h < m_\phi^{1/2}$. Therefore, for $m_\phi \ll m_{\rm pl}$ (2.66), the highest decay rate into χ particles, $\Gamma_\chi \sim m_\phi$, is much larger than the highest possible rate for the decay into fermions, $\Gamma_\psi \sim m_\phi^2$. It implies that *decaying into scalar field more thermalizes the universe than into fermions*. The condition of thermal equilibrium of the universe reads $\Gamma > H$. By solving a relation for a total decay rate as $\Gamma_{\rm tot} \equiv \Gamma_{\phi\to\chi\chi} + \Gamma_{\phi\to\psi\bar{\psi}} = H = (8\pi\rho/3m_{\rm pl}^2)^{1/2}$, the reheating temperature $T_{\rm R}$ can be estimated by

$$T_{\rm R} \simeq 0.2 \left(\frac{100}{g_*}\right)^{1/4} \sqrt{\Gamma_{\rm tot} m_{\rm pl}}\,. \tag{2.68}$$

Imposing the constraint $\Gamma < m_\phi \sim 10^{-6} m_{\rm pl}$, the reheat temperature is limited to be below the GUT scale, $T_{\rm R} < 10^{16}$GeV. However, such model of inflation may overproduce gravitinos. In order to resolve the gravitino problem, the reheating temperature must be below 10^6 GeV for a general situation ([140, 236, 238, 239, 328]). This value gives a most rigid upper limit of reheating temperature. On the other hand, the lower limit is determined by a successful nucleosynthesis around MeV scale [237]. So the reheating temperature needs in the following range

$$\text{MeV} \lesssim T_{\rm R} \lesssim 10^6 \text{GeV}\,. \tag{2.69}$$

We study the background evolution during reheating by adopting a polynomial potential $V \propto \phi^{2q}$. Using the Virial theory, we find

$$a(t) \propto t^{(q+1)/3q}\,, \quad H \propto \frac{q+1}{3q}\frac{1}{t}\,. \tag{2.70}$$

When $q = 1$ ($V \propto \phi^2$) and $q = 2$ ($V \propto \phi^4$), the universe at the reheating phase expands as matter-dominant ($a \propto t^{2/3}$) and radiation-dominant ($a \propto t^{1/2}$), respectively.

Quadratic potential $V(\phi) = m_\phi^2\phi^2/2$
In this simple case, the evolution is described by decreasing oscillation

$$\phi(t) = \bar{\phi}(t)\sin(m_\phi t)\,, \quad \bar{\phi}(t) = \frac{m_{\rm pl}}{\sqrt{3\pi} m_\phi t}\,. \tag{2.71}$$

The initial amplitude is given by $0.2 m_{\rm pl}$. The energy density of inflaton decreases following $\rho = \dot{\phi}^2/2 + V(\phi) \approx m_\phi^2\bar{\phi}^2/2 \propto a^{-3}$ and these decaying energy transfers to coupled other particles as the above elementary theory shows [259]. However, the domain of applicability of this elementary reheating theory is limited. The reason is why (1): no Bose condensation effects (related to *narrow resonance*) and (2): non-adiabatic process (*broad resonance*) do not be considered. These effects become important very soon after the beginning of the inflaton decay. This stage is the so-called *preheating*, where the inflaton decays into other coupled scalar field (see [256, 257] and also Ref. [448, 420]). The most of the energy density in the inflation field may be available for conversion into thermalized form. We shall review this preheating in the following (see also other processes: gravitational particle production [154, 428], and instant preheating [148, 149], but we omit them in this thesis).

• Preheating
If the inflaton couples with other fields, their effective masses change very rapidly via a time-dependence

of inflation. Then it results in non-adiabatic excitation of the field fluctuations by parametric resonance. This is the essence of preheating [448, 126, 420, 256] (see also Refs. [243, 244, 245, 475, 56, 57, 368, 426, 22, 257]). Let us simply consider a coupling to one scalar χ only, via $g^2\phi^2\chi^2/2$. The Klein-Gordon equation in terms of Fourier modes of χ field follows

$$\ddot{\chi}_k + 3H\dot{\chi}_k + \left[\frac{k^2}{a^2} + g^2\phi^2(t)\right]\chi_k = 0\,, \tag{2.72}$$

leading to the momentum k of produced χ particle as $k = \sqrt{\left(\frac{m_\phi}{2}\right)^2 - m_\chi^2 - 2g\phi(t)}$. The oscillating term $g\phi \simeq g\bar{\phi}\cos(m_\phi t)$ leads to a "scattering" in the momenta space. If $g\bar{\phi} \ll m_\phi^2/8$ (called a weak coupling regime), particles are created within a width

$$\Delta k \simeq m_\phi\left(\frac{4g\bar{\phi}}{m_\phi^2}\right) \ll m_\phi \tag{2.73}$$

located near the radius $k_0 \simeq m_\phi/2$, called a **narrow parametric resonance** (see Fig. 2.5). Narrow parametric resonance is related to Bose condensation. Depending on the narrow regime Δk located on the radius $k \sim m_\phi/2$, the number density n_k is calculated as

$$n_{k=m_\phi/2} \simeq \frac{n_\chi}{4\pi k_0^2 \Delta k/(2\pi)^3} \simeq \frac{\pi^2\bar{\phi}}{g}\frac{n_\chi}{n_\phi}\,. \tag{2.74}$$

The occupation numbers n_k exceed unity i.e., $n_k \gg 1$ and this case is not applicable in the above "old"

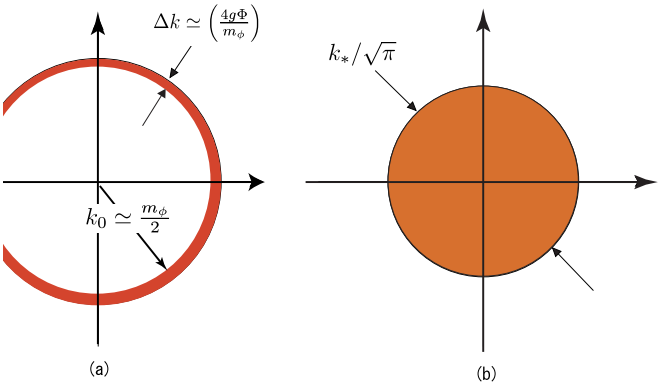

Figure 2.5: The sketches for (a) narrow and (b) broad resonances.

reheating. Then substituting the effective decay rate with the above Bose factor n_k into the evolution equation of number density, we obtain $\frac{1}{a^3}\frac{d(a^3 n_\chi)}{dN} = \frac{g^2}{2m_\phi^2}\left(1 + \frac{2\pi^2\bar{\phi}}{g}\frac{n_\chi}{n_\phi}\right)n_\phi$, where $N = m_\phi t/2\pi$ is the number of inflaton oscillations. In the case $\bar{\phi}$ =const and for $n_k \gg 1$ this can be integrated as

$$n_\chi \propto \exp\left(\frac{\pi^2 g\bar{\phi}}{m_\phi^2}N\right) \propto \exp\Big(2\pi\mu N\Big)\,, \quad \text{with} \;\; \mu = \pi g\bar{\phi}/2m_\phi^2\,, \tag{2.75}$$

where is the parameter of instability. This result is also obtained by the so-called *Mathieu equation*,

$$\frac{d^2X_k}{dz^2} + (A_k - 2q\cos 2z)X_k = 0\,. \tag{2.76}$$

Compared with (2.72), the above variables are given as $X_k = a^{3/2}\chi_k$, $z = m_\phi t$ and

$$A_k = 2q + \frac{k^2}{m_\phi^2 a^2}\,, \quad q = \frac{g^2\bar{\phi}^2(t)}{4m_\phi^2}\,. \tag{2.77}$$

From Eq. (2.77) the parameters A_k and q are allowed in the range of $A_k \geq 2q$. The variables A_k and q lead to instability condition of the Mathieu equation [271, 256]. When they take values in an instability band, the perturbation X_k grows exponentially $X_k \propto \exp(\mu_k z)$. If one take a $q(\lesssim 1)$ (weak coupling), the instability band has a small width $\mu_k = \sqrt{(q/2)^2 - (2k/m_\phi - 1)^2}$ which takes the maximal value $\mu_k \simeq q/2$ near $k \sim m_\phi/2$. It gives a same order of instability $\mu_k \sim 4\pi g\bar{\phi}/m_\phi^2$ as (2.75).

If one take a q ($\gg 1$), it leads to broad resonance with a wide range for parameters. This regime is equivalent to $|g\bar{\phi}| \gg m^2$, where a coupling constant is strong. We see that this particle production occurs by non-adiabatic process in the following discussion. In order to see it, for simplify, we can neglect the expansion of the universe. For a strong coupling regime, the mode equation is $\ddot{\chi}_k + \omega^2(t)\chi_k = 0$ with $\omega(t) = \sqrt{k^2 + g^2\bar{\phi}^2\cos^2(m_\phi t)}$. Every time the oscillating inflaton vanishes at $t_j = m_\phi^{-1}(j + 1/2)\pi$, the effective mass of the χ field, proportional to $|\cos(m_\phi t)|$, vanishes. It is shortly before and after t_j that the adiabatic condition is strongly violated:

$$\frac{|\dot{\omega}|}{\omega^2} = \frac{m_\phi g^2\phi^2|\cos(m_\phi t)\sin(m_\phi t)|}{(k^2 + g^2\bar{\phi}^2\cos^2(m_\phi t))^{3/2}} \geq 1\,. \tag{2.78}$$

Considering a small time interval $\Delta t \ll 1/m_\phi$ in the vicinity of t_j, we can rewrite this condition as $\Delta t/\Delta t_* \geq (k^2\Delta t_*^2 + (\Delta t/\Delta t_*)^2)^{3/2}$ where $\Delta t_* \simeq 1/\sqrt{g\bar{\phi}m_\phi} \ll 1$. It follows that the adiabatic condition is broken only within short time intervals $\Delta t \sim \Delta t_*$ nears t_j and only for the modes with

$$k \;<\; k_* \simeq \Delta t_*^{-1} \simeq m_\phi(g\bar{\phi}/m_\phi)^{1/2}\,. \tag{2.79}$$

It is worth nothing that the momentum of the created particle can be larger than the inflaton mass by the ratio $\sqrt{g\bar{\phi}/m_\phi} > 1$, which is called **broad resonance** [257] (see Fig 2.5). The adiabatic violation is largest for $k = 0$ and so the created particle grows from one oscillation to the next by $(n^{j+1}/n^j)_{k=0} = \exp(2\pi\mu_{k=0})$ as similar as narrow resonance, where the number density increases exponentially. The parameter of instability μ_k is obtained by using WKB solution in the adiabatic regime $\dot{\omega} \ll \omega^2$ and solving "scattering" problem in the parabolic potential for the non-adiabatic regime $\dot{\omega} \gg \omega^2$. As a result, the instability parameter is given by

$$\mu_k \simeq \frac{1}{2\pi}\ln\left[1 + 2e^{-\pi\kappa^2} + 2\cos\theta e^{-\frac{\pi}{2}\kappa^2}\sqrt{1 + e^{-\pi\kappa^2}}\right]\,, \tag{2.80}$$

where $\kappa^2 = k/k_*$ is the dimensionless wavenumber defined by Eq. (2.79) and θ denotes the phase of the wavefunction which changes quantum mechanically at each scattering. This parameter takes its maximal value $\mu_k^{\max} = \pi^{-1}\ln(1 + \sqrt{2}) \simeq 0.28$ for $k = 0$ and $\theta = 0$. Assuming random θ, we conclude that the particle number in every mode changes stochastically, which is called *stochastic resonance*. Skipping the $\cos\theta$ term, we obtain

$$\bar{\mu}_k \simeq \frac{1}{2\pi}\ln(1 + 2e^{-\pi\kappa^2})\,. \tag{2.81}$$

It also takes its maximal values at the center $k = 0$ as $\bar{\mu}_{k=0} = (\ln 3)/2\pi \simeq 0.175$. Therefore the broad resonance is more effective particle production characterised as exponential growth $n_k \propto e^{2\pi\mu_k N}$ with $\mu_k \sim O(0.1)$ than the narrow resonance as small instability parameter $\mu_k \sim O(0.01)$. These processes, preheatings occur before single-body decay (see elementary reheating theory) as described above and it leads the universe to be thermalized.

2.2.4 Theoretical models and Observational constraints

• Models of inflation

Here we shall overview several generic inflationary models. The original "old inflation" scenario [195, 408] is based on the idea of a metastable false vacuum which will be transited to a true vacuum. Although there have existed many inflation models, a single-field inflation can be basically classified into three classes: "large-field", "small-field", and "hybrid". Typical example for Large-field models is a chaotic inflation where the field rolls toward the potential minimum. Small-field models would be expected as an inflaton shown by consequence of spontaneous symmetry breaking. New inflation [286, 7] and natural inflation [159] are the examples of this type. One can classify these two classes as large field models ($V''(\phi) > 0$) and small field ($V''(\phi) < 0$). A third class of models is "hybrid" inflation where inflation can be ended by a second scalar field. Hybrid inflation only predicts a "blue" spectrum, $n_{\mathcal{R}} > 1$. As a simple example in such model Double inflation models exist which have two stages of inflation by two scalar fields [363]. We show the typical potential forms of the three types in Fig **??**.

(1) Large-field models

Let us show the simplest example of large field model, which is characterized by the monomial potential

$$V(\phi) = V_0 \phi^n \,. \tag{2.82}$$

Note that Chaotic inflation often uses this form of potential [287]. In order to compare these models with the observational data, we need to estimate a primordial power spectrum $\mathcal{P}_{\mathcal{R}_c}$ produced by quantum mechanism of inflaton's fluctuations (see the more details in Sec 2.3). It is characterized by its scale dependencies $n_{\mathcal{R}} - 1 \equiv d\ln\mathcal{P}_{\mathcal{R}_c}/d\ln k$ (2.194) and the tensor to scalar ratio $r \equiv \mathcal{P}_{\rm T}/\mathcal{P}_{\mathcal{R}_c}$ (2.202). Using the slow-roll parameters written in terms of scalar field $\epsilon(\phi)$ and $\eta(\phi)$, it is easily shown that these quantities is given by

$$n_{\mathcal{R}} = 1 - \frac{2n+4}{n+200}\,; \quad r \simeq 13.7\frac{n}{n+200}\,. \tag{2.83}$$

Note that the spectrum is red $n_{\mathcal{R}} \simeq 0.97(0.94)$ and the tensor mode is suppressed $r \simeq 0.14(0.27)$ for the quadratic(quartic) potential.

Exponential potentials: $V = V_0 \exp\Big(-\sqrt{\frac{16\pi}{\alpha}}\frac{\phi}{m_{\rm pl}}\Big)$, equivalent to $n \to \infty$ limit of the large field models in (2.82) and hence the border between large-field and hybrid models. Exponential potentials lead to a power-law expansion of the scale factor, usually called *power-law inflation* [297]. Exponential potentials are motivated by the effective low-energy description of extra spatial dimensions such as dilatons and moduli fields in superstring theory. This model yields an useful relation: $\epsilon = 2\eta = 2/\alpha$. Thus, if inflation starts, i.e., when $\epsilon < 1$, it will never end. We obtain a useful relationship between the index $n_{\mathcal{R}}$ and the ratio r as

$$r = 8(1 - n_{\mathcal{R}})\,. \tag{2.84}$$

Using it, we can classify the inflationary models in the $n_{\mathcal{R}} - r$ plane as seen below.

(2) Small-field models

The typical form of potential is

$$V(\phi) = V_0\left[1 - \left(\frac{\phi}{\mu}\right)^n\right], \tag{2.85}$$

which may arise from a phase transition. Eq. (2.85) is equivalent to a Taylor expansion around $\phi = 0$. The Coleman-Weinberg potential [98] used as the potential of New inflation models [286, 7] corresponds to $n = 4$. Similarly to th large-field models, the parameters r and $n_{\mathcal{R}}$ are obtained by

$$n_{\mathcal{R}} = 1 - \frac{n-1}{25(n-2)}\,, \quad r \simeq 0\,. \tag{2.86}$$

It gives the red spectrum ($n_{\mathcal{R}} \lesssim 1$) and negligibly small tenser mode ($r \simeq 0$).

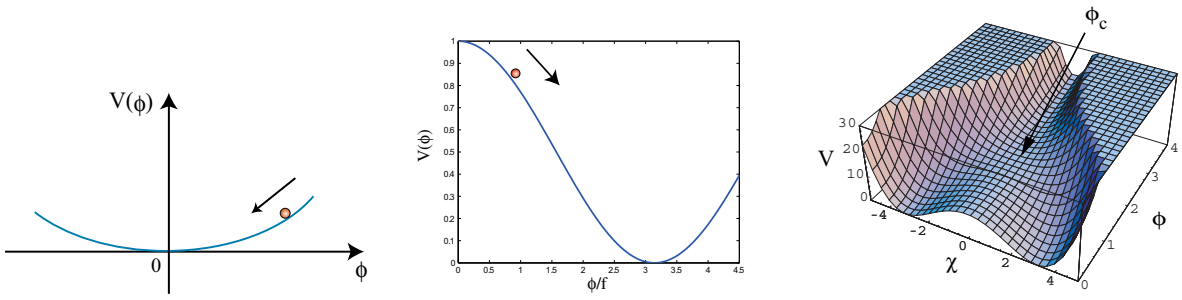

(a) Large-field models (b) Small-field models (c) Hybrid modes

Figure 2.6: Schematic illustration of the potential of (a) large-field, (b) small-field and (c) hybrid (these figures in Ref [36]).

Linear potentials: $V(\phi) = V_0\phi$ is the border of large and small-field models. In this case, $\epsilon = -\eta$ =const is independent of ϕ. We also obtain the border line characterized by

$$r = \frac{8}{3}(1 - n_{\mathcal{R}})\,. \tag{2.87}$$

(3) Hybrid inflation

In this class, the field rolls toward a minimum with a nonzero vacuum energy [290, 291, 102], which is motivated from the viewpoint of particle physics [102, 303, 292]. Hybrid inflation models involve more than one scalar field. The second scalar field plays a role of trigger of instability as a "waterfall" transition towards a true minimum (see Fig. **??**). The typical form of potential is given by

$$V(\phi) = V_0\left[1 + \left(\frac{\phi}{\mu}\right)^n\right]. \tag{2.88}$$

Let us consider the Linde hybrid inflation model with potential [291]

$$V = \frac{\lambda}{4}\left(\chi^2 - \frac{M^2}{\lambda}\right)^2 + \frac{1}{2}g^2\phi^2\chi^2 + \frac{1}{2}m^2\phi^2\,. \tag{2.89}$$

When the field rolls down toward $\chi = 0$, it reduces to

$$V \simeq \frac{M^4}{4\lambda} + \frac{1}{2}m^2\phi^2\,. \tag{2.90}$$

For $\phi < \phi_c \equiv M/g$, the field rolls toward a true minima at $\phi = 0$ and $\chi = \pm M/\sqrt{\lambda}$. For generally, $\epsilon(\phi)$ and $\eta(\phi)$ cannot be fixed outside the context of a particular model. However, we obtain in the limit of ϕ/μ to be less than unity

$$\frac{\eta}{\epsilon} \simeq \frac{2(n-1)}{n}\left(\frac{\mu}{\phi}\right)^n. \tag{2.91}$$

In this case, recalling that $n_{\mathcal{R}} = 1 - 4\epsilon + 2\eta$, we can find the spectrum of hybrid models $n_{\mathcal{R}} > 1$, shows blue, due to $\eta > 2\epsilon$. The fact of a "blue" scalar spectrum is one typical prediction by hybrid inflation.

• Observational constraints

As we will see in the further section, quantum fluctuations during inflation can become temperature

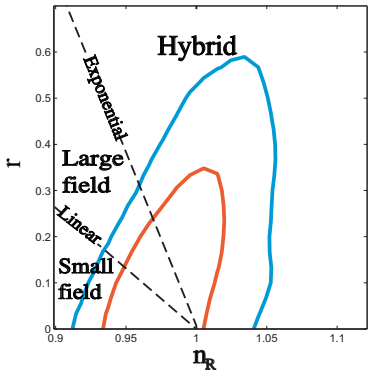

Figure 2.7: The $n_{\mathcal{R}}$-r parameter space allows us to classify inflationary models. The line of $r = (8/3)(1 - n_{\mathcal{R}})$ shows the border between large and small field models given by Eq. (2.87), and $r = 8(1 - n_{\mathcal{R}})$ is the one of large-field and hybrid models Eq. (2.84) (see [31, 36]).

anisotropies of CMB radiation. The CMB observations can give constraints to classify many models [122]. The observational data from the WMAP can give constraint on many models [31, 359, 250, 276]. Fig. 2.7 shows the $n_{\mathcal{R}} - r$ plane classifying three classes: the small-field, large-field and hybrid models [250]. With the WMAP data, precisions of inflationary scenarios can be established [359]. This paper shows that WMAP observation gives us constraint to the parameter space of inflationary models and for example, a minimally-coupled inflation with $\lambda\phi^4$ can be excluded as in Fig. 2.7.

The amplitude of scalar perturbations by CMB observational data is given by $A^2_{\mathcal{R}} \simeq 2.4 \times 10^{-9}$, that is the COBE normalization (2.163). On the other hand the amplitude of scalar perturbations can be written as $A^2_{\mathcal{R}} = \frac{1}{\pi\epsilon}\left(\frac{H}{m_{\rm pl}}\right)^2$ (2.192). Hence using them with $\epsilon < 0.032$ we can give an upper limit on the energy scale of inflation:

$$\frac{H}{m_{\rm pl}} < 1.55 \times 10^{-5}\,. \tag{2.92}$$

Note that the case of just $n_{\mathcal{R}} = 1$, that is pure Harrison-Zel'dovich value (corresponding to $\epsilon = 0$), is still consistent with the data.

2.3 Cosmological inhomogeneity

Measurements of the cosmic microwave background tell us how homogeneous and isotropic the universe is at the time of recombination. Today, however, the universe has a well developed nonlinear structure. This structure takes the form of galaxies (their scales is $10 - 100$kpc), cluster $(1 - 10$Mpc$)$[12] and superclusters of galaxies (which is a group of clusters ~ 100Mpc), and, on larger scales, of *voids*, *sheets* and *filaments* of galaxies. Deep redshift surveys show, however, that when averaged over $O(100$Mpc$)$, the inhomogeneities in the density distribution remain small. The simple explanation as to how nonlinear structure could develop from small initial perturbations is based on the fact of gravitational instability. In this section, we consider this gravitational instability and study formation and evolution of large scale structure. Here we pay attention to a linear order in a perturbation theory[13]. This instability is easily understood in terms of Jeans theory, which is treated in the Newtonian gravity. In the Newtonian gravitational theory, the physical interpretations are easily obtained, however, the Newtonian analysis of gravitational instability

[12]Here, "Cluster" of galaxies is divided into (1): a galaxy group, which is made of about ten galaxies and its scale is about 1Mpc (2): a galaxy cluster, which is made of one hundred galaxies and about 10Mpc.

[13]It is obvious that when the perturbation amplitude δ reaches unity ($\delta \sim 1$), the neglected nonlinear terms $\sim \delta^2$ etc., become important, which corresponds to $k_{\rm nonlinear} \simeq 0.1{\rm Mpc}^{-1}$ (~ 10Mpc). It is roughly given by a redshift time, $z \sim 20$.

has limitations. We have to use General Relativity (GR) for both short-wavelength and long-wavelength perturbations. This theory gives us a unified description for any matter on all scales. Unfortunately, the physical interpretation of the results obtained is less transparent in GR than in Newtonian theory. The main problem is the freedom in the choice of coordinate used to describe the perturbations. In contrast to the homogeneous and isotropic universe, where the preferable coordinate system is fixed by the symmetry properties of the background, there are no obvious preferable coordinates for analyzing perturbations. The freedom in the coordinate choice, or gauge freedom, leads to the appearance of fictitious perturbation modes. These fictitious modes do not describe any real inhomogeneities, but reflects only the properties of the coordinate system used. In order to be independent of gauge choices, one can use a gauge invariant perturbation theory. First, let us review this cosmological perturbation theory.

2.3.1 Cosmological perturbation theory

We will follow Ref. [330] in terms of our notation here. (See also [27, 60, 128, 141, 216, 255, 302, 398] for other approaches). In the linear approximation different types of perturbations evolve independently and therefore can be analyzed separately. We first classify metric perturbations as follows. Let start from spatial flat FRW metric with inhomogeneous metric perturbations around it. The line element of perturbed FRW spacetime can be expressed as

$$ds^2 = a^2(\tau)\Big[-(1+2A)d\tau^2 - 2B_i d\tau dx^i + (\delta_{ij}+2C_{ij})dx^i dx^j\Big]\,, \tag{2.93}$$

where we define the conformal time

$$\tau = \int_0^t \frac{dt}{a}\,. \tag{2.94}$$

It is also convenient to define new conventions in order to go forward the following discussion.

$$(\cdots)' = \frac{d}{d\tau}(\cdots) = a\frac{d}{dt}(\cdots)\,,\quad \mathcal{H} = a'/a = aH\,,\quad X_{j_1 j_2 \ldots |i} = \nabla_i X_{j_1 j_2 \ldots}\,,\quad X_{(i|j)} = \frac{1}{2}(X_{i|j} + X_{j|i})\,. \tag{2.95}$$

Note that horizon-crossing ($k = aH$) is equivalent to $k = \mathcal{H}$. All metric perturbations can be classified into three modes: scalar, vector and tensor parts, that are determined by their dependences for transformation on spatial hypersurfaces. Therefore we can decompose the above components B_i and C_{ij} into scalar, vector and tensor, respectively as

$$B_i = B_{|i} + S_i\,,\quad C_{ij} = -\delta_{ij}\psi + E_{|ij} + F_{(i|j)} + h_{ij}\,, \tag{2.96}$$

where scalar parts are A, B, ψ and E [14], vector parts are S_i and $F_{(i|j)}$, which are additionally constrained by $S_i^{|i} = 0$ (divergenceless/transverse condition), and tensor parts are h_{ij} with the constraint $h_{ij}^{|j} = 0$ and $h_i^i = 0$ (transverse-traceless condition). The Einstein equations for the scalar, vector and tensor parts can be decoupled each other at linear order. We do not consider second-order cosmological perturbations shown as [2].

Scalar perturbations: the metric takes the form

$$ds^2 = a^2(\tau)\Big[-(1+2A)d\tau^2 - 2B_{,i} d\tau dx^i + ((1-2\psi)\delta_{ij} + 2E_{|ij})dx^i dx^j\Big]\,. \tag{2.97}$$

Considering a scalar gauge transformation

$$\tau \to \tilde{\tau} + T\,,\quad x^i \to \tilde{x}^i + L_{,i}\,, \tag{2.98}$$

[14] This metric perturbations follow the notation of Ref [330], but we use A rather than ϕ as perturbation of the lapse function.

we have

$$A \to A - T' - \mathcal{H}T\,,\ B \to B + L' - T\,,\ \psi \to \psi + \mathcal{H}T\,,\ E \to E - L\,. \tag{2.99}$$

There exist many combinations made of scalar metric perturbations as a gauge-invariant variable, however the simplest gauge-invariant linear combinations of these functions, which span the two-dimensional space of the physical perturbation, are

$$\Phi \equiv A + \frac{1}{a}\left[a(B - E')\right]'\,,\quad \Psi \equiv \psi + \mathcal{H}(E' - B)\,. \tag{2.100}$$

These gauge invariant variables give a good physical interpretation in the *longitudinal/Newtonian gauge*. The Newtonian gauge is a specific gauge-transformation choice, where the new frame becomes zero-shear $E = B = 0$ and it leads to the simple form as $\Phi_N = A$ and $\Psi_N = \psi$. Matter perturbations are also gauge-dependent variables. Energy-momentum tensor is obtained in the terms of 4-velocity u^μ as

$$T^\mu_\nu = (\rho + P)u^\mu u_\nu + P\delta^\mu_\nu + \Sigma^\mu_\nu\,, \tag{2.101}$$

where Σ is an anisotropic stress and it is traceless. For scalar field, the above components are described as density, pressure and velocity perturbations in the limit of first order perturbations

$$T^0_0 = -\bar{\rho}(1 + \delta)\,,\quad T^0_i = (\bar{\rho} + \bar{P})v_{|i}\,,\quad T^i_j = (\bar{P} + \delta P)\delta^i_j + \Sigma^i_j\,, \tag{2.102}$$

where the variables characterised by bar $\bar{\rho}$ take their background values and note that the variables $\delta\rho = \delta\bar{\rho}$ and Π defined as $\Sigma^i_j = \bar{P}(\partial^i\partial_j - \delta^i_j\Delta/3)\Pi$ are often useful. Π represents the gauge-invariant variable itself. The adiabatic pressure perturbation can be described as

$$\delta P_{\rm ad} \equiv \frac{\dot{P}}{\dot{\rho}}\delta\rho = c_s^2\delta\rho\,, \tag{2.103}$$

where we also define the sound velocity $c_s = \dot{P}/\dot{\rho}$ and a non-adiabatic part of pressure perturbation, or *entropy perturbation*, is a gauge-invariant perturbation

$$\delta P_{\rm nad} = \delta P - c_s^2\delta\rho\,.\ \text{ or }\ \Gamma \equiv \frac{\delta P}{\bar{P}} - \frac{c_s^2}{w}\delta\,. \tag{2.104}$$

Since Γ vanishes for adiabatic perturbations $\delta P/\delta\rho = \dot{P}/\dot{\rho} = c_s^2$, Γ represents the amplitude of an entropy perturbation. The scalar part of the 3-momentum v can be related to a gauge-invariant velocity V

$$V \equiv v - k^{-1}E'\,, \tag{2.105}$$

where k is frequency. In contrast to the velocity, there exists no unique natural definition of a gauge invariant quantity corresponding to the density perturbation [15]. One convenient choice is defined by the following combinations,

$$\Delta_c \equiv \delta + 3(1 + \omega)\mathcal{H}k^{-1}(v - B)\,. \tag{2.106}$$

The variable Δ_c represents a comoving density perturbation [27, 255], which is the density contrast in the slicing such that the material 4-velocity is orthogonal to constant time hypersurfaces as $v = B$, called *Comoving gauge*. The Δ_c and V are the fundamental variables to write the perturbed Einstein equation in the terms of which [255].

Vector perturbations: characterised by the metric form of

$$ds^2 = a^2(\tau)\Big(-d\tau^2 - 2S_i d\tau dx^i + (\delta_{ij} + 2F_{(i|j)})dx^i dx^j\Big)\,, \tag{2.107}$$

[15] for examples, $\Delta_s \equiv \delta + 3(1+\omega)\mathcal{H}k^{-1}(E'/k - B)$ for Newtonian gauge and $\Delta_g \equiv \delta + 3(1+\omega)(\psi + E/3)$ for Flat gauge, which are seen more detail in [255].

and these variables change as

$$S_i \to S_i + L_i' \,, \quad F_i \to F_i - L_i \,, \tag{2.108}$$

and then $F_i' + S_i$ becomes the gauge-invariant vector shear perturbation. In contrast to a scalar perturbation, there exist two natural gauge-invariant combinations corresponding to a velocity perturbation $V_s = v - F'/k$ and $V = v - S$ represent the amplitudes of the shear and the vorticity of the matter velocity field, respectively.

Tensor perturbations: the metric is

$$ds^2 = a^2(\tau)\Big[-d\tau^2 + (\delta_{ij} + h_{ij})dx^i dx^j\Big] \,, \tag{2.109}$$

and h_{ij} does not change under coordinate transformations. It already describes the gravitational waves in a gauge invariant manner. We can decompose any tensor perturbations by using eigenmodes of an equation $\nabla^2 e_{ij} = -k^2 e_{ij}$, which is given as

$$h_{ij} = h(t) e_{ij}^{(+,\times)}(x) \,, \tag{2.110}$$

with two possible polarisation states, + and ×.

Curvature perturbations
We can construct two gauge-invariant variables commonly used. One is curvature perturbation on uniform-density obtained by

$$-\zeta \equiv \psi + \frac{H}{\dot\rho}\delta\rho \,, \tag{2.111}$$

which was first defined by Bardeen, Steinhardt and Turner [28] (see also Refs. [30, 317, 461]) [16]. The comoving curvature perturbation can be defined by [17]

$$\mathcal{R}_c \equiv \psi - \frac{H}{\rho + P}\delta q \,, \tag{2.112}$$

where δq is a momentum potential relating to a 3-momentum given by $\partial_i(\delta q)$. It has been used in [300, 302, 330]. The variables $\mathcal{R}_c$ is related to $-\zeta$ and the difference is proportional to Δ_c as

$$-\zeta = \mathcal{R}_c + \frac{H}{\dot\rho}\Delta_c \,. \tag{2.113}$$

Moreover the relationships between the previous defined gauge-invariant variables (Bardeen's variables [28]) Φ, Ψ and them is obtained as

$$-\zeta \equiv \frac{2}{3}\frac{\mathcal{H}^{-1}\Phi' + \Phi}{1+\omega} + \Phi \,. \tag{2.114}$$

To see more their relationships, let us consider the perturbed Einstein equations $\delta G_{\mu\nu} = \kappa^2 \delta T_{\mu\nu}$. As an important result, we find the gauge-invariant equation

$$k^2\Psi = -4\pi G a^2 \bar\rho \Delta_c \,. \tag{2.115}$$

[16] This curvature perturbation is equivalent to a perturbed expansion to uniform-density hypersurfaces δN as $\zeta = \delta N$, that is so-called the δN formalism. It is a powerful tool to investigate nonlinear evolution of perturbation of inflation including multi-field inflation [406, 407, 461, 305, 383, 306]. It is based on a similar idea used in separate universe approach [406, 407, 461, 383].

[17] See Kodama-Sasaki [255], the curvature perturbation is given by the amplitude $\mathcal{R} = \psi + E/3$ of the spatial scalar curvature perturbation of the constant time hypersurface $\delta R^{(3)} = 4k^2/a^2\mathcal{R}$. In order to distinguish this notation, we added a index c. $\mathcal{R}$ is not gauge-invariant and it exactly becomes the Newtonian potential in the Newtonian gauge $\mathcal{R}_N = \Phi$.

It shows that the Newtonian gauge metric perturbation is related to the comoving density perturbation and corresponding to generalization of the Poisson equation $k^2\psi = -4\pi G\delta\rho$ in the Newtonian perturbation theory. With the help of it, the Eq. (2.113) reduces to

$$\mathcal{R}_c = -\zeta - \frac{2\bar{\rho}}{9(\bar{\rho}+\bar{P})}\Big(\frac{k}{aH}\Big)^2\Psi\,, \tag{2.116}$$

and hence two commonly used curvature perturbations coincide each other on the large scale,

$$\mathcal{R}_c = -\zeta \quad \text{on the large scale} \tag{2.117}$$

where their comoving scales are larger than the comoving Hubble horizon $1/(aH) \ll 1/k$. It is also important to see the traceless part of Einstein equation yields

$$\Psi - \Phi = \kappa^2 k^{-2} a^2 \bar{P}\Pi \tag{2.118}$$

and hence we have $\Psi = \Phi$ in the absence of anisotropic stress $\Pi = 0$. Finally, we summary three gauge coordinates, (1): *Newtonian/Longitudinal gauge* ($E = B = 0$), (2): *Flat gauge* ($\psi = 0$) and (3): *Comoving gauge* ($v = B$). (1) is equivalent to zero-shear condition, $\sigma_g = 0$, where $\sigma_g = E'/k - B$ is the shear of the unit vector normal to the constant time hypersurface. In this gauge, Bardeen variables are reduced to generalization of the Newtonian potential as $\Phi = A$ and $\Psi = \psi$. There is no extra coordinate freedom which preserves this condition. (2) is useful to quantize the inflaton during inflation as shown the further section. It is related to the fact that the mass term of perturbed inflation field can be neglected under the slow-roll condition and hence we can use the result obtained by neglecting metric perturbation $\psi = 0$. In that time, the Mukhonov variable can be directly reduced to the perturbed inflaton, $v = a\delta\phi$. (3) is equivalent to the condition $\delta\phi = 0$ during inflation. In this gauge, the gauge-invariant curvature perturbation $\mathcal{R}_c$ is equivalent to Newtonian potential $\mathcal{R}_c = \psi$. Moreover, the comoving curvature perturbation $\mathcal{R}_c$ is proportional to Φ as

$$\Phi = \frac{3+3\omega}{5+3\omega}\mathcal{R}_c\,, \tag{2.119}$$

and yields

$$\Phi = \frac{2}{3}\mathcal{R}_c \text{ (radiation dominant)}\,, \qquad \Phi = \frac{3}{5}\mathcal{R}_c \text{ (matter dominant)}\,. \tag{2.120}$$

This equation is shown by the conservation of $-\zeta = \mathcal{R}_c$ on large scales as shown in the following subsection. From this equation, if Φ is constant, we can obtain the simplest relation between $\mathcal{R}_c$ and Φ and hence Φ becomes times 9/10 through radiation and matter dominant epoch, $\Phi_m = (9/10)\Phi_r$. In this gauge, Δ_c can be reduced to density perturbation, $\Delta_c = \delta$.

2.3.2 Evolution of perturbations

We will see classical evolutions of perturbations. First, we briefly summarize vector and tensor modes and mainly discuss scalar perturbations in this subsection.

Vector perturbations

Let us consider a 3-momentum as a divergence-free, that obeys a following equation

$$\dot{\delta q}_i + 3H\delta q_i = k^2\delta\Pi_i\,, \tag{2.121}$$

where $\delta\Pi_{ij} = \partial_{(i}\Pi_{j)}$ represents anisotropic stress. The gauge-invariant of vector metric perturbation satisfies a following constraint equation

$$k^2\left(\dot{F}_i + S_i/a\right) = 16\pi G\delta q_i\,. \tag{2.122}$$

It is shown that the gauge-invariant vector metric perturbation vanishes if only scalar fields, exist since a divergence-free momentum needs to vanish. Eq. (2.121) shows that vector perturbations vanish without anisotropic stress.

Tensor perturbations

Tensor perturbations have no constraint equation since gravitational degrees of freedom is free, corresponding to gravitational waves. Tensor metric perturbations obey an equation

$$\ddot{h} + 3H\dot{h} + \frac{k^2}{a^2}h = 0\,. \tag{2.123}$$

Note that it is same form of equation describing evolution of a massless scalar field in a FRW background.

Scalar perturbations

We will consider scalar perturbations for single perfect fluid in the simple situation where $K = \Lambda = 0$ and $\Pi = 0$. In this case, we have seen $\Phi = \Psi$ and the perturbed Einstein equations can be reduced to the closed form equation for the gravitational potential

$$\Phi'' + 3\mathcal{H}(1 + c_s^2)\Phi' - c_s^2\Delta\Phi + 8\pi G a^2\bar{\rho}(c_s^2 - \omega)\Phi = 4\pi G a^2\bar{\rho}\omega\Gamma\,. \tag{2.124}$$

Note that entropy perturbation Γ is the source term for this equation. Once we solve this equation, it follows the density and velocity as

$$\delta = \frac{2\Delta\Phi}{3\mathcal{H}^2} - 2\Big(\Phi + \frac{\Phi'}{\mathcal{H}}\Big)\,, \qquad v = -\frac{2(\Phi + \Phi'/\mathcal{H})}{3\mathcal{H}(1+\omega)}\,, \tag{2.125}$$

where Δ denotes Laplacian of spatial derivatives. For the other approach to analyze the system, Kodama-Sasaki [255] write the continuous and Euler equations for the matter perturbations Δ_c and V. This formulation is useful to compare the Newtonian perturbation/Jeans theory and easy to interpret physical meanings. The Euler equation for the gauge-invariant velocity V is obtained as

$$V' + \mathcal{H}V = ik\Big[\frac{c_s^2}{1+\omega}\Delta + \frac{\omega}{1+\omega}\Gamma\Big] + ik\Psi - \frac{2}{3}\frac{\omega}{1+\omega}ik\Pi\,. \tag{2.126}$$

The second term on the left-hand side represents the adiabatic slowing-down of velocity via a cosmic expansion. The first term comes from pressure gradient and the third term shows a generalized term appearing in the Newtonian perturbation theory. The terms proportional to Γ and Π appear as GR corrections. Eliminating V from the continuous equation $\Delta_c' - 3\omega\mathcal{H}\Delta_c = \ldots$ and the Euler equation, we obtain the second-order form of the evolution equation for the comoving gauge-invariant density perturbation Δ_c (see it in the [255]). We omit to write and discuss them and solve the equation for Φ in the first approach. For simplify, we neglect the source term $\Gamma = 0$ (considering the adiabatic perturbation). The background solutions are obtained as a function of the conformal time τ as

$$a \propto \tau^{\nu}\,, \quad \bar{\rho} = \tau^{-2(\nu+1)}\,, \quad \Big(\nu \equiv \frac{2}{1+3\omega}\Big)\,. \tag{2.127}$$

From this equation, we find the relation between the conformal and physical time as

$$t \propto \tau^{\frac{3(1+\omega)}{3\omega+1}}\,. \tag{2.128}$$

The typical examples are matter-dominant $\omega = 0$ and radiation $\omega = 1/3$. For each epoch, $\nu = 2$ (matter) and $\nu = 1$ (rad) yield $a \propto \tau^2, t \propto \tau^3$ (matter) and $a \propto \tau, t \propto \tau^2$ (rad), respectively. The growing solutions for Φ are generally described as the Bessel function of order ν by

$$\Phi \propto x^{-\nu} j_\nu(c_s x) \simeq \begin{cases} 1 & (c_s x \ll 1) \\ x^{-\nu-1}\cos[c_s x - \frac{\pi}{2}(\nu+1)] & (c_s x \gg 1) \end{cases} \tag{2.129}$$

where we define $x = k\tau$, representing the ratio of the horizon size to the wavelength of perturbation, since $k/aH = k/\mathcal{H} = x/\nu$ from (2.127) and spherical Bessel function $f(x) = j_\nu(x)$, satisfying $f''(x) + 2f'(x)/x + [1 - \nu(\nu+1)/x^2]f(x) = 0$.

• Subhorizon scale

We consider the shortwave perturbations with $k\tau(= x) \gg 1$. In the radiation dominant era, the solutions oscillate as

$$\Phi = -\frac{\Phi_0}{k^2\tau^2}\cos\Big(\frac{k\tau}{\sqrt{3}}\Big)\,, \quad \delta = \frac{2\Phi_0}{3}\cos\Big(\frac{k\tau}{\sqrt{3}}\Big)\,, \quad v = \frac{\Phi_0}{2\sqrt{3}k}\sin\Big(\frac{k\tau}{\sqrt{3}}\Big)\,. \tag{2.130}$$

The physical interpretation for oscillation is that the gravitational forces make radiation perturbations contracted, while radiations have the pressure expanding themselves and hence the competing two forces gives the oscillations for their evolutions. We also find that the Newtonian potential Φ decays as τ^{-2} in this stage, which is shown as the power spectrum of CDM for the large wavenumber $k_{\rm eq} < k$. In matter dominant era, we obtain the solutions as

$$\Phi = \text{const} \equiv \Phi_{\rm m0}\,, \quad \delta = -\frac{k^2\tau^2}{6}\Phi_{\rm m0}\,, \quad v = -\frac{\tau}{3}\Phi_{\rm m0}\,, \tag{2.131}$$

where the constant amplitude $\Phi_{m0} = \frac{9}{10}\Phi_0$. We find that the density perturbation δ is proportional to $\tau^2 \propto a \propto t^{2/3}$. This result is in agreement with the Newtonian result. In the matter-dominated universe, Φ obeys $\Phi'' + 6/\tau\Phi' = 0$ and yields the same solutions $\Phi = C_1 + C_2/\tau^5$ and $\delta \simeq -k^2/6(C_1\tau^2 + C_2\tau^{-3}) = \tilde{C}_1 t^{2/3} + \tilde{C}_2 t^{-1}$. In order to compare the above obtained results with the Newtonian theory, let us shortly review the Newtoninan/Jeans theory.

Jeans theory: is reduced to the continuous and Euler equations as

$$\dot\rho + 3H\rho + \frac{1}{a}\boldsymbol{\nabla}\cdot\rho\boldsymbol{v} = 0\,, \quad \dot{\boldsymbol{v}} + \frac{1}{a}(\boldsymbol{v}\cdot\boldsymbol{\nabla})\boldsymbol{v} + H\boldsymbol{v} = -\frac{1}{\rho a}\nabla P - \frac{1}{a}\boldsymbol{\nabla}\psi\,, \tag{2.132}$$

with the Newtonian potential ψ, obeying the Poisson equation $\Delta\psi = -4\pi G\bar\rho$. Considering linear perturbation as $\rho = \bar\rho(1+\delta)$ and fourier transformation $\delta = \delta_k e^{i\mathbf{k}\cdot\mathbf{x}}$, we can obtain the second-order equation for δ_k as

$$\ddot\delta_k + 2H\dot\delta_k + \left[\Big(\frac{c_s}{a}\Big)^2 k^2 - 4\pi G\bar\rho\right]\delta_k = 0\,. \tag{2.133}$$

This equation can be interpreted as $\ddot\delta + [\text{Expansion rate}]\dot\delta + [\text{Pressure} - \text{Gravity}]\delta = 0$, that is, gravitational instability occurs, if gravity wins in the regions, where mass near overdense region is attracted to the center by gravity but repelled by pressure. The last term determines the typical scale (the so-called *Jeans length*), on large scales than which, gravity dominates and density perturbation can grow. The critical frequency is $k_J = \frac{a}{c_s}\sqrt{4\pi G\bar\rho}$ and its corresponding Jeans length $\lambda_J^{\rm ph} = 2\pi/k_J \times a$ is given by

$$\lambda_J = c_s\sqrt{\frac{\pi}{G\bar\rho}} \quad \text{(Jeans length)}\,. \tag{2.134}$$

Using Hubble equation $H^2 \simeq G\bar\rho$, the time scale (free fall time) $t_{\rm ff} = 1/\sqrt{G\bar\rho}$ is equivalent to the cosmological time scale $1/H$. So the Jeans length is of order the sound horizon (or "sound communication" scale) $\lambda_J \sim c_s t_{\rm ff}$, where sound can maximally contacts during cosmological time scale. In order to see the typical evolutions of perturbation, neglecting the cosmological expansion $H = 0$, Eq. (2.133) becomes $\ddot\delta_k + \omega^2(k)\delta_k = 0$ with $\omega(k) = \sqrt{k^2 - k_J^2}$ and we can find the solution $\delta_k \propto \exp(\pm i\omega(k)t)$. If we consider the smaller length $\lambda < \lambda_J$, the solution describes oscillation $\delta_k \propto \sin(wt)$, while the larger length $\lambda > \lambda_J$, the gravitational instability grows exponentially $\delta_k \propto e^{|\omega|t}$. We interpret it as that Jeans length $\lambda_J \sim c_s t_{\rm ff}$ is the sound communication scale over which the pressure can still react to changes in the energy density due to gravitational instability. Including the cosmological expansion, even though this growth rate

becomes smaller, the main result is obtained similarly. On much smaller scale than the Jeans scale ($\lambda \ll \lambda_J$), if c_s changes adiabatically, then the solution oscillates as WKB solution by

$$\delta_k \propto \frac{1}{\sqrt{c_s a}} \exp\Big(\pm ik \int \frac{c_s dt}{a}\Big) . \tag{2.135}$$

If c_s is constant, it is reduced to the Jeans oscillation $\delta_k \propto e^{ikc_s\tau}$. It is consistent with the above obtained result (2.130) due to $c_s = 1/\sqrt{3}$. On scales much larger than the Jeans scale ($\lambda \gg \lambda_J$), gravity dominates and in the matter-dominated universe, the solutions can be given by

$$\delta_k \propto t^{2/3} \propto a \quad \text{(growing mode)} , \qquad \delta_k \propto t^{-1} \quad \text{(decaying mode)} . \tag{2.136}$$

Contrast this relatively slow growth rate with the exponential Jeans instability $\delta_k \propto \exp|\omega|t$ due to cosmic expansion. This result is consistent with the above obtained solutions in GR perturbation theory. It is important result to explain the existence of dark matter in the universe. Since the growing mode is proportional to the scale factor, if we want to obtain the large inhomogeneities ($\delta \gtrsim 1$) today, the inhomogeneities were already substantial ($\delta \gtrsim 10^{-3}$), which evolved from a primordial density perturbation at redshift $z \simeq 1000$. However, this conclusion is inconsistent with the observational quantity $\delta \approx 10^{-4}$ as favored by the observed CMB fluctuations, therefore, *dark matter* has been need to grow density perturbation before the recombination, in the radiation-dominated universe (see the details in Sec 2.4).

In order to see evolution of (cold) dark matter in the presence of other components in the universe (radiation or dark energy), (2.133) can be applied. The total energy density is $\rho_{\rm tot} = \frac{\rho_{\rm eq}}{2}(y^{-3} + y^{-3(1+\omega)})$ with $y \equiv a/a_{\rm eq}$ and this equation can be written in terms of y by [332]

$$y^2(1 + y^{-3\omega})\frac{d^2\delta}{dy^2} + \frac{3}{2}y\Big(1 + (1-\omega)y^{-3\omega}\Big)\frac{d\delta}{dy} - \frac{3}{2}\delta = 0 , \tag{2.137}$$

where we have skipped the term proportional to c_s^2 because it is determined only by the pressure of cold dark matter and hence it is negligible. For radiation background ($\omega = 1/3$), we find the general solutions

$$\delta(y) = C_1\Big(1 + \frac{3}{2}y\Big) + C_2\left[\Big(1 + \frac{3}{2}y\Big)\ln\frac{\sqrt{1+y}+1}{\sqrt{1+y}-1} - 3\sqrt{1+y}\right] . \tag{2.138}$$

At early times, during the radiation-dominated stage ($y \ll 1$), the amplitude of perturbations grows as

$$\text{CDM in rad dominated :} \qquad \delta(y) = (C_1 - 3C_2) - C_2\ln(y/4) + O(y) \;\propto\; \ln(a_{\rm eq}/a) \propto \ln k , \tag{2.139}$$

that is, *logarithmically at most*. Thus, the radiation suppress the growth of inhomogeneities in the cold component. When one consider the case of dark energy $\omega = -1$, a general solution of (2.137) can be obtained

$$\delta(y) = C_1\sqrt{1+y^{-3}} + C_2\sqrt{1+y^{-3}}\int_0^y \Big(\frac{x}{1+x^3}\Big)^{3/2} dx . \tag{2.140}$$

At early times when the cold matter dominates ($y \ll 1$), the perturbation grows as $\delta \simeq C_1 y^{-3/2} + 2/5 C_2 y$ in complete agreement with our previous result, Subsequently the cosmological constant becomes dominant and in the limit $y \gg 1$ we have

$$\text{CDM in DE dominated :} \qquad \delta(y) = (C_1 + IC_2) - \frac{1}{2}C_2 y^{-2} + O(y^{-3}) \;\simeq\; \text{const} , \tag{2.141}$$

where $I = \int_0^\infty (x/(1+x^3))^{3/2} dx \simeq 0.57$. Thus, when the cosmological constant overtakes the matter density the growth ceases and the amplitude of the perturbation is frozen.

• Superhorizon scale

We consider the larger wavelength than the horizon size $x \gg 1$. In the radiation-dominated universe, the solutions become

$$\Phi = \Phi_0 \text{ (constant)} \equiv \Phi_{\rm r0} , \quad \delta = -2\Phi_0 , \quad v = -\frac{\tau}{2}\Phi_0 , \tag{2.142}$$

and while matter-dominated,

$$\Phi = \Phi_0 \text{ (constant)} \equiv \Phi_{\rm m0}\,, \quad \delta = -2\Phi_0\,, \quad v = -\frac{\tau}{2}\Phi_0\,. \tag{2.143}$$

In the both stages, we find that the gravitational potential is constant and the relation between the energy density fluctuations and the gravitational potential on superhorizon scales becomes $\delta\rho/\bar{\rho} = -2\Phi$. As you seen, the gravitational potential decays on subhorizon scale only for the radiation dominated universe like (2.130), otherwise, it is constant.

In general speaking, for the general case where the EOS is arbitrary $P(\rho)$, it is convenient to recast the equation in a slightly different from. To do this, introducing the new variable, which can eliminate a friction term proportional to Φ',

$$u \equiv \frac{\Phi}{(\bar{\rho}+\bar{P})^{1/2}}\,, \tag{2.144}$$

a generalisation of Eq. (2.124) takes the simple form [330]

$$u'' - c_s^2\Delta u - \frac{\theta''}{\theta}u = a^2(\bar{\rho}+\bar{P})^{-1/2}\bar{P}\Gamma\,, \quad \text{where } \theta \equiv \frac{1}{a}\Big(1+\frac{\bar{P}}{\bar{\rho}}\Big)^{-1/2}. \tag{2.145}$$

The obtained solutions are of course agreement with our previous results (see them in [332]). When long wavelength adiabatic perturbations $c_s k\tau \ll 1$ and $\Gamma = 0$, omitting the spatial derivative term and applying the scale factor $a(\tau) = a_{eq}(\xi^2+2\xi)$ with $\xi \equiv \frac{\tau}{\tau_{eq}}(\sqrt{2}-1)$, we obtain

$$\Phi = \frac{\xi+1}{(\xi+2)^3}\Big[A\Big(\frac{3}{5}\xi^2+3\xi+\frac{1}{\xi+1}+\frac{13}{3}\Big)+B\frac{1}{\xi^3}\Big]\,, \tag{2.146}$$

where A and B are integration constants representing nondecaying and decaying modes respectively. For two asymptotical regions ($\xi \ll 1$ and $\xi \gg 1$), it is easy to see $\Phi \sim 1/8\times 16/3 = 2/3$ and $\Phi \sim 3/5$, respectively. Therefore, it shows that the amplitude of Φ decreases by a factor of $9/10$ after the transition. If one calculate the energy density fluctuations from this solution, it also shown that the amplitude of δ is always equal to -2Φ on superhorizon scales. The change in the amplitude of Φ can also be inferred from a widely used "conservation law" for the quantity ζ as

$$\dot{\zeta} = O((k\tau)^2)H\zeta\,, \quad \zeta \equiv \frac{2}{3}\Big(\frac{8\pi G}{3}\Big)^{-1/2}\theta^2\Big(\frac{u}{\theta}\Big)'\,. \tag{2.147}$$

For long wavelength $k\tau \ll 1$, it implies that ζ is constant ($\dot{\zeta}=0$). From (2.117), $\mathcal{R}_c$ is also constant on superhoziron. It is also seen directly from the evolution equation $\mathcal{R}_c'' + 2z/z'\mathcal{R}_c' \approx 0$ on large scale (see (2.188)), which is satisfied for the solution $\mathcal{R}_c$ =const. This conservation is obtained under the assumption of no entropy perturbations $\Gamma = 0$. If we consider entropy perturbation, the above equation is reduced to $\dot{\zeta} \propto \bar{P}\Gamma$ and hence entropy perturbation can grow curvature perturbation on superhorizon scale. Recalling the definition of ζ (2.114), the constant ζ follows that, in the case where the initial and final values of Φ are also constants, Φ changes only when ω changes from an initial into a final value as

$$\Phi_f = \Big(\frac{1+\omega_f}{1+\omega_i}\Big)\Big(\frac{5+3\omega_i}{5+3\omega_f}\Big)\Phi_i\,. \tag{2.148}$$

For a matter-radiation universe, $\omega_i = 1/3$ and $\omega_f = 0$, and we obtain the familiar result $\Phi_f = (9/10)\Phi_i$.

Entropy perturbation

Until now we have been considering adiabatic perturbations in an isotropic fluid where the pressure depends only on the energy density. In a multi-component media both adiabatic and entropy perturbations can arise. For entropy perturbations, the source terms of the evolution equations for Φ or equivalently u, (2.124) and (2.145), respectively. The source term is proportional to $\bar{P}\Gamma$ and it can consist of two

parts; a part coming from the intrinsic entropy perturbation Γ_α of each component and the relativistic part as $\bar{P}\Gamma = \bar{P}\Gamma_{\rm int} + \bar{P}\Gamma_{\rm rel}$, where $\bar{P}\Gamma_{\rm int} = \sum_\alpha P_\alpha \Gamma_\alpha$. Since Γ and Γ_α are gauge-invariant, $\Gamma_{\rm rel}$ is also gauge-invariant by itself. Here after, we do not consider the intrinsic entropy perturbation $\Gamma_\alpha = 0$. In order to see the physical meaning of $\Gamma_{\rm rel}$, it is more convenient to rewrite it as [255]

$$\bar{P}\Gamma_{\rm rel} = \Big(\frac{\delta P}{\delta\rho} - c_s^2\Big)\delta\rho = \sum_{\alpha,\beta}\frac{h_\alpha h_\beta}{h}(c_\alpha^2 - c_\beta^2)S_{\alpha\beta}\,, \quad \text{with} \;\; S_{\alpha\beta} \equiv \frac{\Delta_{c\alpha}}{1+\omega_\alpha} - \frac{\Delta_{c\beta}}{1+\omega_\beta}\,, \tag{2.149}$$

where we define $h_\alpha = \rho_\alpha + P_\alpha$. We can see this part comes from the difference of the dynamical behavior of components $c_\alpha^2 \neq c_\beta^2$, proportional to $S_{\alpha\beta}$ [18]. One important interpretation of the quantity $S_{\alpha\beta}$ is obtained from the radiation and matter fluid (for other examples, multi-components mixed dark matter and baryon-radiation plasma). In this special case, we find

$$S_{\alpha\beta} = \Delta_{\rm m} - \frac{3}{4}\Delta_{\rm r} = \delta_{\rm m} - \frac{3}{4}\delta_{\rm r}\,, \tag{2.150}$$

and hence the adiabatic perturbation is equivalent to the condition $\delta_{\rm m} = \frac{3}{4}\delta_{\rm r}$. Then the source term for (2.124) becomes $\Phi'' + 3\mathcal{H}(1+c_s^2)\Phi' + \ldots = \frac{16\pi G a^2}{3}\frac{\bar{\rho}_{\rm m}\bar{\rho}_{\rm r}}{(4\bar{\rho}_{\rm r}+4\bar{\rho}_{\rm m})}S_{\rm mr}$. In order to solve this equation, we shall assume there are no adiabatic perturbations at the initial time. Then, to define the entropy perturbations, we impose the initial time condition $\Phi \to 0$ as $t \to 0$. This is called *isocurvature perturbations*, since the curvature perturbation vanishes at the initial time, i.e., that the gauge-invariant curvature perturbation ζ also vanishes. If the initial time is taken to be 0, then this definition coincides with the definition of entropy perturbations. If the initial time is finite, then the two definitions might differ by a term proportional to the decaying mode of Φ. So we will consider they describes the same one. Isocurvature perturbation sometimes coincides *isothermal perturbation* in the radiation dominated stage because if we impose the isocurvature condition as $k^2\Phi \propto (\rho_{\rm r}\delta_{\rm r} + \rho_{\rm m}\delta_{\rm m}) \propto (\delta_{\rm r} + a\delta_{\rm m}) \simeq 0$, which comes from the Poisson equation (2.115), we find $\delta_{\rm m} = S_{\rm mr}$ and $\delta_{\rm r} = -aS_{\rm mr} \ll 1$ in the limit of $a \to 0$. It implies that isocurvature perturbation is mainly composed of a small amount of matter densities, whose perturbations are enlarged and radiation perturbation is vanishingly small $\delta_{\rm r} \ll \delta_{\rm m}$ at the initial time, i.e., no thermal perturbation $\theta_0 = \delta_{\rm r}/4 \ll 1$. Entropy perturbations may well be important for structure formation on superhorizon scales, for examples, generated by cosmic strings stretching over the size of the universe. Causality constraints forbid the formation of adiabatic perturbations on scales larger than the Hubble horizon. Hence only perturbations which can be formed on these scales are entropy (isocurvature) perturbations. If $S_{\rm mr}$ is constant, the equation for Φ has the particular solution $\Phi = S_{\rm mr}$. Obviously, the above particular solution does not satisfy the required initial condition. The solution is obtained by adding it to a general solution of the homogeneous equation and choosing the coefficients such that the initial conditions are satisfied, and hence the result is

$$\Phi = \frac{1}{5}\xi\frac{\xi^2 + 6\xi + 10}{(\xi+2)^3}S_{\rm mr}\,, \tag{2.151}$$

where $\xi = \frac{\tau}{\tau_{eq}}(\sqrt{2}-1)$. The important conclusion is that the gauge-invariant amplitude for this type of entropy perturbations increases linearly in conformal time until τ_{eq}, whereas it is constant for adiabatic perturbations. From increasing Φ, the energy density also increases on superhorizon scale. Generally, the analysis of entropy perturbation in several cases is rather complicated, however, the main result is that produced density perturbation is about of order entropy perturbation itself and it can be evaluated to be much smaller than standard one produced by adiabatic perturbation $|\Delta_c| \sim O(|\Gamma|) \ll 10^{-5}$ [255]. Then the entropy perturbation is usually considered to be inefficient. The other reason for disfavoring this type of perturbation is why it is inconsistent with the observational data of CMB anisotropy. Similar to non-adiabatic perturbations, the anisotropic stress Π acts inefficiently for enhancing the density perturbations

[18] Strictly speaking, when the energy-momentum tensor of each component is not conserved $T^{\nu}_{(\alpha)\,\mu;\nu} = Q_{(\alpha)\mu}$, if we consider the energy and momentum transfer quantities Q_α is not equal to the other Q_β, $\Gamma_{\rm rel}$ is also proportional to $\bar{P}\Gamma_{\rm rel} \propto \sum_{\alpha,\beta}(c_\beta^2 - c_\alpha^2)(Q_\beta - Q_\alpha)$ as shown in [255].

as $|\Delta| \sim O(\Pi)$ [255].

Boltzmann equations for each components

If we consider the situation that the universe is filled with multi-components, the evolutions for each components needs. Until now, we have dealt with the quantities $\bar{\rho}, \bar{P}$ etc, as total quantities $\bar{\rho} = \sum_\alpha \bar{\rho}_\alpha$. The evolutions of each components are described as Boltzmann equations $\mathrm{d}f(x^\mu, p^\nu)/\mathrm{d}\lambda = C[f]$, where the distribution function f and the collision term $C[f]$. Using the geodesic equation, it can be rewritten as

$$p^\mu \frac{\partial f}{\partial x^\mu} - \Gamma^\mu_{\nu\lambda} p^\nu p^\lambda = C[f]\,. \tag{2.152}$$

If we consider each f for several components, we obtain the evolution equations. For another approach, considering each energy-momentum tensor $T^\nu_{(\alpha)\,\mu;\nu} = Q_{(\alpha)\mu}$ with energy momentum transfer term, which is relating to the interaction term between them $Q^\mu_{(\alpha)} = 2\int d\Pi p^\mu C[f]$ where $d\Pi$ is an invariant volume element on momentum space, gives the same result, however, here we shall go further discussion about the linearized Boltzmann equations. In the Newtonian gauge $ds^2 = a^2[-(1+2\Phi)d\tau^2 + \eta_{ij}(1-2\Psi)dx^i dx^j]$, we define the new variables, where a momentum $q^i = a(1-\Psi)p^i$ and its amplitude $q = \sqrt{p^i p_i}$ and the direction cosine $\gamma^i = q^i/q$ and expand the perturbation δf as the Fourier and Legendre series

$$\delta f(\boldsymbol{x}, q, \boldsymbol{\gamma}, \tau) = \int \frac{d^3k}{(2\pi)^3} e^{i\mathbf{k}\cdot\mathbf{x}} \sum_{l=0}^{\infty} (-i)^l (2l+1) P_l(\mu) F_l(q, \mathbf{k}, \tau)\,. \tag{2.153}$$

The quantities F_l are related to each perturbation of hydrodynamical variables $\delta\rho, \delta P, v$ and Π by integration in momentum space q as [255]

$$\begin{aligned} \delta\rho &= \int \frac{q^2 dq}{2\pi^2\hbar^3} \sqrt{q^2+m^2} F_0\,, \quad \delta P = \frac{1}{3}\int \frac{q^2 dq}{2\pi^2\hbar^3} \frac{q^2}{\sqrt{q^2+m^2}} F_0\,, \\ (\bar{\rho}+\bar{P})v &= -\frac{1}{k}\int \frac{q^2 dq}{2\pi^2\hbar^3} q F_1\,, \quad \bar{P}\Pi = \frac{1}{k^2}\int \frac{q^2 dq}{2\pi^2\hbar^3} \frac{q^2}{\sqrt{q^2+m^2}} F_2\,. \end{aligned} \tag{2.154}$$

From the above equations, we find a rough relationship $\delta\rho, \delta P \Leftrightarrow F_0$, $v \Leftrightarrow F_1$ and $v\Pi \Leftrightarrow F_2$. For the distribution functions, let us consider dark matter, baryon and radiation. The Boltzmann equations for each component are obtained by calculation of the collision term, which becomes vanishing for dark matter due to no interaction except for gravitational force and becomes equivalent to Thomson scattering and Coulomb interaction, for radiation-electron system and for electron-baryon system. As a result, we can deal with both electrons and baryons as one fluid and hence the *baryon* we call means both them. The continuous and Euler equations are given by [123]

$$\begin{array}{lll} \delta'_{\rm dm} + ikv_{\rm dm} - 3\Psi' = 0\,, & v'_{\rm dm} + \mathcal{H}v_{\rm dm} - ik\Phi = 0\,, & \text{for dark matter} \\ \delta'_{\rm b} + ikv_{\rm b} - 3\Psi' = 0\,, & v'_{\rm b} + \mathcal{H}v_{\rm b} - ik\Phi = -\frac{4}{3}\frac{\rho_{\rm r}}{\rho_{\rm b}} a n_e \sigma_T (v_{\rm b} - v_{\rm r})\,, & \text{for baryon(+electron)} \\ \delta'_{\rm r} + \frac{4}{3}ikv_{\rm r} - 4\Psi' = 0\,, & v'_{\rm r} - \frac{1}{4}ik\delta_{\rm r} + \frac{ik}{6}\Pi_{\rm r} - ik\Phi = a n_e \sigma_T (v_{\rm b} - v_{\rm r})\,, & \text{for radiation} \end{array} \tag{2.155}$$

where σ_T is Thomson cross section $\sigma_T = 0.665 \times 10^{-24}\mathrm{cm}^2$ and n_e, $\Pi_{\rm r}$ represent the number density of free electron and the anisotropic stress of radiation, respectively. There exists momentum transfer term in right hand side of Euler equations for baryon and radiation. This term comes from Thomson collision term and it is related to momentum conservation between baryon and radiation as $(\rho_{\rm r} + P_{\rm r})\delta v_{\rm r} + \rho_{\rm b}\delta v_{\rm b} = 0$, yielding momentum transfer $\delta v_{\rm b} = -R\delta v_{\rm r}$ and sound velocity of baryon-radiation fluid $c_s^2 = \frac{1}{3(1+R)}$ where $R = 3\rho_{\rm b}/(4\rho_{\rm r})$. For photon (radiation), we introduce a *brightness function* Θ, which is convenient to describe temperature fluctuations as

$$\Theta(\boldsymbol{x}, \boldsymbol{\gamma}, \tau) = \frac{1}{4}\frac{\int dpp^3\delta f}{\int dpp^3 \bar{f}} = \frac{\delta T}{T}\,. \tag{2.156}$$

Expanding it as the Fourier and Legendre series,

$$\Theta(\boldsymbol{x},\boldsymbol{\gamma},\tau)=\int\frac{d^3k}{(2\pi)^3}e^{i\mathbf{k}\cdot\mathbf{x}}\sum_{l=0}^{\infty}(-i)^l(2l+1)P_l(\mu)\Theta_l(\mathbf{k},\tau)\,, \tag{2.157}$$

we find the relationships

$$\Theta_0=\frac{1}{4}\delta_{\rm r}\,,\quad \Theta_1=-kv_{\rm r}\,,\quad \Theta_2=\frac{20k^2}{3}\Pi_{\rm r}\,. \tag{2.158}$$

and the evolution equations of them become

$$\begin{aligned}&\Theta_0'=-\frac{ik}{3}\Theta_1+\Psi'\ \text{ for } l=0\,,\quad \Theta_1'=ik(\Theta_0+\Phi-\frac{2}{5}\Theta_2)-an_e\sigma_T(\Theta_1-v_b)\ \text{ for } l=1\,,\\ &\Theta_2'=ik\Big(\frac{2}{3}\Theta_1-\frac{3}{7}\Theta_3\Big)-\frac{9}{10}an_e\sigma_T\Theta_2\ \text{ for } l=2\,,\ \Theta_l'=ik\Big(\frac{l}{2l-1}\Theta_{l-1}-\frac{l+1}{2l+3}\Theta_{l+1}\Big)-an_e\sigma_T\Theta_l\ \text{ for } l>2\,.\end{aligned} \tag{2.159}$$

These equations continue infinitely, however, if the universe is optically thick (for example, before recombination), i.e., that photon's free streaming scale is much smaller $\lambda_T=1/an_e\sigma_T\ll 1$ (the so-called *tight coupling limit*), we can neglect $l\geq 3$ modes due to $\Theta_l=e^{-\lambda_T}$ obtained from $\Theta_l\approx-\lambda_T\Theta_l$ in this situation. Then we consider only Θ_0,Θ_1 and Θ_2 hereafter. These equations will be used for the analysis of CMB photons.

Power spectrum: is defined by square of some quantity with given wavenumber as

$$\langle\Phi^*(\mathbf{k})\Phi(\mathbf{k}')\rangle=(2\pi)^3\delta^3(\mathbf{k}-\mathbf{k}')P_\Phi(k)\,. \tag{2.160}$$

It is convenient to introduce the dimensionless power spectrum by the k-space weighted, which is

$$\mathcal{P}_\Phi(k)=4\pi k^3P_\Phi(k)=\frac{4\pi k^3}{(2\pi)^3}\langle|\Phi|^2\rangle\,. \tag{2.161}$$

Equivalently, it implies the logarithmic spectrum $\langle\Phi^2\rangle=\int\frac{dk}{k}\mathcal{P}_\Phi(k)$. Similarly, the power spectrum for adiabatic perturbations is $\mathcal{P}_{\mathcal{R}_c}\equiv\frac{4\pi k^3}{(2\pi)^3}|\mathcal{R}_c^2|$. The tensor power spectrum is also written as

$$\mathcal{P}_{\rm T}\equiv 2\frac{4\pi k^3}{(2\pi)^3}|h^2|\,, \tag{2.162}$$

where additional factor of 2 shows two independent modes as polarisations of the graviton. Another commonly used quantities describing the amplitudes of scalar and tensor power spectrum are

$$A_{\mathcal{R}}^2\equiv\frac{4}{25}\mathcal{P}_{\mathcal{R}_c}\,,\quad A_{\rm GW}^2\equiv\frac{1}{100}\mathcal{P}_{\rm T} \tag{2.163}$$

The scale dependencies of the scalar and tensor power spectrums are given by logarithmic derivative of power spectrum

$$n_{\mathcal{R}}-1\equiv\left.\frac{{\rm d}\ln\mathcal{P}_{\mathcal{R}_c}}{{\rm d}\ln k}\right|_{k=aH}\,,\quad n_{\rm T}\equiv\left.\frac{{\rm d}\ln\mathcal{P}_{\rm T}}{{\rm d}\ln k}\right|_{k=aH}\,, \tag{2.164}$$

where we have to evaluate it at Hubble-crossing $k=aH$. Obviously, it implies $\mathcal{P}_{\mathcal{R}_c}=Ak^{n_{\mathcal{R}}-1}$ and $\mathcal{P}_{\rm T}=Ak^{n_{\rm T}}$. The cases of $n_{\mathcal{R}}=1$ and $n_{\rm T}=0$ represent scale-invariant spectrums. Finally, we introduce the *transfer function*, which connects the initial value to the current value, defined by

$$T(k)=\sqrt{\frac{\mathcal{P}_\Phi(k)}{\mathcal{P}_{\Phi_{m0}}(k)}}\,. \tag{2.165}$$

Using the transfer function, the CDM power spectrum is obtained by

$$P(k) = P_{\Delta_c}(k) = AkT^2(k)\mathcal{P}_{\Phi_{m0}}(k)\,. \tag{2.166}$$

CDM-type spectra have the following approximate form of the transfer function [390, 431, 391]

$$T(k) = \left(1 + \frac{Ak^2}{\log(1+Bk)}\right)^{-1}\,. \tag{2.167}$$

It behaves as $T(k) \sim$const for the small wavenumbers k (i.e., large scales), while $T(k) \propto k^{-2}\ln k$ for the large wavenumbers (small scales). See the CDM spectrum in Fig. 2.11 and the details in Sec 2.4. Equations (2.166) and (2.167) illustrate the 'turn around' of the power spectrum from its primordial scale invariant form as

$$P(k) \propto k \;\text{ on the largest scales}\,, \quad P(k) \propto k^{-3}\log^2 k \;\text{ on small scales}\,. \tag{2.168}$$

Notice that on large scales, power spectrum proportional to k, implies that a scale-invariant spectrum, while on small scales, one proportional to k^{-3} comes from (2.130). Here a growth factor of $\log k$ has been obtained in the evolution of CDM perturbations in the radiation dominated universe seen as (2.139). The location of the turn-around is close to the wavenumber at the equality time $k_{\rm eq} \simeq 0.01 \sim (80{\rm Mpc})^{-1}$.

2.3.3 Origin of cosmological structure on large scale

In this section, let us discuss the origin of the large-scale structure, which gives initial conditions for the previous perturbed quantities. Even if there exists the fluctuations of radiation and inflaton in the inflationary universe, one can see conclusion that the amplitude of the scalar field perturbation induced from the radiation perturbation is of order Φ of radiation, and it decreases monotonically. Hence we conclude that the perturbation of radiation existing before the inflationary stage has negligible influence on the present structure of the universe. In other words, we must seek for sources of perturbations either in the inflationary stage itself, such as quantum fluctuations. Therefore, in the standard cosmology, it is considered that the primordial fluctuations are generated by quantum fluctuations of inflaton. Let us consider a single-field inflation model. In this case we can get a comoving curvature perturbation (2.112)

$$\mathcal{R}_c = \psi + \frac{\mathcal{H}}{\phi'}\delta\phi\,. \tag{2.169}$$

As seen in the previous discussion, it is constant on superhorizon size from crossing outside of Hubble radius to going inside of Hubble radius again. So this quantity is useful in order to describe the evolution of perturbations. We introduce another variable which is commonly used to describe scalar perturbations υ (called *Mukhonov-Sasaki variable*), which is rescaled of $\mathcal{R}_c$ by $z = a\phi'/\mathcal{H}$. It is also important that this variable is reduced to the one describing the quantum fluctuations. In order to see this, we consider the perturbed EOM for a single scalar field. It becomes simplest form in a flat slicing (where $\psi = 0$). Using constraint equations, we can obtain one master equation

$$\ddot{\delta\phi} + 3H\dot{\delta\phi} + \left[\frac{k^2}{a^2} + V_{\phi\phi} - \frac{8\pi G}{a^3}\frac{\mathrm{d}}{\mathrm{d}t}\left(\frac{a^3\dot{\phi}^2}{H}\right)\right]\delta\phi = 0, \tag{2.170}$$

Introducing new variables, $\upsilon = a\delta\phi$, Eq. (2.170) reduces to

$$\upsilon'' + \left(k^2 - \frac{z''}{z}\right)\upsilon = 0\,. \tag{2.171}$$

It is easy to see that this variable becomes a gauge-invariant due to proportional to the gauge-invariant $\mathcal{R}_c$ as

$$\upsilon \equiv a\left[\delta\phi + \frac{\phi'}{\mathcal{H}}\psi\right] = \mathcal{R}_c z\,, \quad z \equiv \frac{a\phi'}{\mathcal{H}}\,. \tag{2.172}$$

It is easy to see that the flat gauge condition ($\psi = 0$) gives the $\mathcal{R}_c = H\delta\phi/\dot{\phi}$ and it is equivalent to the definition of curvature perturbation as $\zeta = H\delta\tau$ where $\delta\tau = -\delta\phi/\dot{\phi}$ is a time delay in the time delay formalism by Guth [196, 197]. The evolution of the perturbations is determined by the Einstein action. The first-order perturbation equations of motion are given by a second-order action. Mukhanov et al [330] showed that the full action for linear scalar perturbations is given by $S_2 = \int d\tau d^3x(\upsilon'^2 - (\nabla\upsilon)^2 + z''/z\ \upsilon^2)/2$ and varying this action is consistent with the above obtained equation. It is important to fix the proportional factor and define the momentum π canonically conjugated to υ in order to need in a canonical quantizing as $\pi \equiv \partial\mathcal{L}/\partial\upsilon' = \upsilon'$. Let us briefly summarize how the primordial density perturbation is generated below. Inside the Hubble horizon, quantum vacuum fluctuations can be generated by inflaton, and then these small perturbations can stretch over the Hubble by the accelerated expansion (*first horizon-crossing* or *Hubble-exit*) (see Fig. 2.4(d)). Since in this region, the causality breaks, these longer fluctuations freeze and become classical fluctuations. After that, the scale of the fluctuations are constant and they will enter the Hubble radius. They can lead to classical fluctuations. When the fluctuations enter the Hubble radius again (*second horizon-crossing*), they evolve according to the classical theory and form the large scale structure such as cluster of galaxies (see Fig. 2.4(d)). In quantum theory, the variables υ and π become operators $\hat{\upsilon}$ and $\hat{\pi}$, which at any moment of time τ satisfy the standard communication relations: and the theory is then quantized by promoting υ and its conjugate momentum to operators that satisfy the following commutation relations on the τ =constant hypersurfaces:

$$[\hat{\upsilon}(\tau,\mathbf{x}),\hat{\upsilon}(\tau,\mathbf{y})] = [\hat{\pi}(\tau,\mathbf{x}),\hat{\pi}(\tau,\mathbf{y})] = 0\,, \quad [\hat{\upsilon}(\tau,\mathbf{x}),\hat{\pi}(\tau,\mathbf{y})] = i\delta^{(3)}(\mathbf{x}-\mathbf{y})\,. \tag{2.173}$$

We express $\hat{\upsilon}(\tau,\mathbf{x})$ in terms of plane waves

$$\hat{\upsilon}(\tau,\mathbf{x}) = \int \frac{d^3\mathbf{k}}{(2\pi)^{3/2}}[\upsilon k(\tau)\hat{a}_k e^{i\mathbf{kx}} + \upsilon_{\mathbf{k}^*}(\tau)\hat{a}_k^\dagger e^{-i\mathbf{kx}}]\,, \tag{2.174}$$

and these modes are normalized yielding Wronskian condition $\upsilon_{\mathbf{k}^*}\upsilon'_{\mathbf{k}} - \upsilon_{\mathbf{k}}\upsilon_{\mathbf{k}^*}{}' = -i$ and satisfy (2.171). This condition ensures that creation and annihilation operators $\hat{a}_k^\dagger$ and $\hat{a}_k$ satisfy following relations for bosons:

$$[\hat{a}_{\mathbf{k}},\hat{a}_{\mathbf{l}}] = [\hat{a}_{\mathbf{k}}^\dagger,\hat{a}_{\mathbf{l}}^\dagger] = 0\,, \quad [\hat{a}_{\mathbf{k}},\hat{a}_{\mathbf{l}}^\dagger] = \delta^{(3)}(\mathbf{k}-\mathbf{l})\,. \tag{2.175}$$

We then define a vacuum state by $\hat{a}_{\mathbf{k}}$ as

$$\hat{a}_{\mathbf{k}}|0>=0\,, \quad \forall k\,. \tag{2.176}$$

We need to determine the initial vacuum state. The vacuum state is usually called *Banch-Davies vacuum* [48], since there are not any particles at the initial time (see e.g. [61]). The Bunch-Davies state corresponds to a attractor solution for initial values in an expanding background (see e.g. [63]). Recalling the basic equation (2.171), the effective mass term, z''/z, can be written as [434, 282, 217]

$$\frac{z''}{z} = (aH)^2\left[2 + 5\epsilon - 3\eta + 9\epsilon^2 - 7\epsilon\eta + \eta^2 + \xi^2\right]\,, \tag{2.177}$$

where

$$\epsilon \equiv -\frac{\dot{H}}{H^2}\,, \quad \eta \equiv 2\epsilon - \frac{\dot{\epsilon}}{2H\epsilon}\,, \quad \xi^2 \equiv \left(2\epsilon - \frac{\dot{\eta}}{H\eta}\right)\eta\,. \tag{2.178}$$

These definitions of the slow-roll parameters coincide with our earlier definitions in Eq. (2.57) at leading order in a slow-roll expansion. If we do not consider a time-dependence of ϵ and η, we can get

$$\tau \simeq -\frac{1}{(1-\epsilon)aH}\,, \tag{2.179}$$

and

$$\frac{z''}{z} = \frac{\nu_{\mathcal{R}}^2 - (1/4)}{\tau^2}\,, \quad \text{with} \quad \nu_{\mathcal{R}} \simeq \frac{3}{2} + 3\epsilon - \eta\,. \tag{2.180}$$

The conformal time $\tau \simeq (aH)^{-1}$ in the dS background denotes the comoving hubble radius as noted in (2.21). The index $\nu_{\mathcal{R}}$ is so important because it gives a scale dependence of the power spectrum. If we include the mass term of Inflaton m_ϕ in de Sitter background, it becomes $\nu_{\mathcal{R}}^2 = \frac{9}{4} - \frac{m_\phi^2}{H^2}$ and in the massless limit, $\nu_{\mathcal{R}} = 3/2$ corresponds to the scale invariant $n_{\mathcal{R}} = 1$ as seen in the further discussion. Then the general solution to Eq. (2.171) can be obtained in terms of a combination of Hankel functions

$$v_{\mathbf{k}} \simeq \frac{\sqrt{\pi|\tau|}}{2} e^{i(1+2\nu_{\mathcal{R}})\pi/4} \left[c_1 H^{(1)}_{\nu_{\mathcal{R}}}(k|\tau|) + c_2 H^{(2)}_{\nu_{\mathcal{R}}}(k|\tau|) \right] , \tag{2.181}$$

where the Hankel functions $f(k,\tau) = \sqrt{\tau} H_\nu^{(1),(2)}(k\tau)$ satisfies a Bessel equation of the form $(\frac{d^2}{d\tau^2} + k^2 - \frac{\nu^2 - 1/4}{\tau^2}) f(k,\tau) = 0$ and the additional factors are need for satisfying the normalized condition of $v_{\mathbf{k}}$, using the relation $H_\nu^{(1)}(z) H_\nu^{(2)'}(z) - H_\nu^{(1)'}(z) H_\nu^{(2)}(z) = -4i/\pi z$. Note that $\tau = 0$ is the point corresponding to the asymptotic future. The power spectrum for the scalar field perturbations is written by

$$\mathcal{P}_{\delta\phi} = \frac{1}{a^2} \mathcal{P}_v \equiv \frac{4\pi k^3}{(2\pi)^3} \left| \frac{v}{a} \right|^2 . \tag{2.182}$$

Imposing the usual positive frequency in the Minkowski vacuum, in the limit of small scale, i.e., $k \to \infty$,

$$v_{\mathbf{k}} \to \frac{e^{-ik\tau}}{\sqrt{2k}} . \tag{2.183}$$

The case $c_1 = 1$ and $c_2 = 0$ in Eq. (2.181) is equivalent to this choice. This vacuum state is the so-called *Banch-Davies vacuum* (BD vacuum). Actually, in the asymptotic past $k\tau \to -\infty$, $H_\nu^{(1)}(k|\tau|) \to \sqrt{\frac{2}{\pi k|\tau|}} e^{-ik\tau} e^{-i(\nu+1/2)\pi/2}$ satisfying this condition. In the simple situation, purely de Sitter spacetime where slow-roll parameters vanish, the basic equation and its solutions become

$$v_{\mathbf{k}}'' + \Big(k^2 - \frac{2}{\tau^2} \Big) v_{\mathbf{k}} = 0 , \quad v_{\mathbf{k}} = \frac{1}{\sqrt{2k}} \Big(1 \pm \frac{i}{k\tau} \Big) e^{\pm ik\tau} , \tag{2.184}$$

and the choice of BD vacuum corresponds to

$$v_{\mathbf{k}} = \frac{1}{\sqrt{2k}} \Big(1 - \frac{i}{k\tau} \Big) e^{-ik\tau} \quad : \text{BD vacuum} . \tag{2.185}$$

The power spectrum on small scales ($k \gg aH$) is given by $\mathcal{P}_{\delta\phi} \simeq \left(\frac{k}{2\pi a} \right)^2$, and on the large scales ($k \ll aH$) we have

$$\mathcal{P}_{\delta\phi} \simeq \left((1-\epsilon) \frac{\Gamma(\nu_{\mathcal{R}})}{\Gamma(3/2)} \frac{H}{2\pi} \right)^2 \left(\frac{|k\tau|}{2} \right)^{3-2\nu_{\mathcal{R}}} , \tag{2.186}$$

where we have used the relation $H_\nu^{(1)}(k|\tau|) \to -(i/\pi)\Gamma(\nu)(k|\tau|/2)^{-\nu}$ for $k\tau \to 0$ and $\Gamma(3/2) = \sqrt{\pi}/2$. In particular when we consider a massless field in de Sitter ($\nu_{\mathcal{R}} = 3/2$) a well-known result can be recovered

$$\mathcal{P}_{\delta\phi} \to \left(\frac{H}{2\pi} \right)^2 \quad \text{for} \quad \frac{k}{aH} \to 0 . \tag{2.187}$$

The comoving curvature perturbation $\mathcal{R}_c$ obeys an evolution equation as

$$\mathcal{R}_c'' + 2 \frac{z'}{z} \mathcal{R}_c' + k^2 \mathcal{R}_c = 0 , \tag{2.188}$$

and the large-scale limit ($k \to 0$) leads to a general solution

$$\mathcal{R}_c = C_1 + C_2 \int \frac{\mathrm{d}t}{a^3 \epsilon} , \tag{2.189}$$

In most single-field inflationary scenarios, a second term corresponds to a decaying mode and can be negligible after Hubble-exit. Therefore one can conclude that a curvature perturbation remains constant on superhorizon scales. Using Eq. (2.186) we obtain power spectrum

$$\mathcal{P}_{\mathcal{R}_c}(k) = \frac{1}{|z|^2}\mathcal{P}_v(k) = \left(\frac{H}{\dot\phi}\right)^2 \mathcal{P}_{\delta\phi}(k) \simeq \left(\frac{H^2}{2\pi\dot\phi}\right)^2_{k=aH}, \tag{2.190}$$

which is valid up to leading order in slow-roll parameters. It is useful to find the relationships the power spectrum of Φ and $\mathcal{R}_c$ by using (2.120),

$$\mathcal{P}_\Phi(k) = \mathcal{P}_{\mathcal{R}_c} \times \begin{cases} 4/9 & (k \gg k_{eq}) \\ 9/25 & (k \ll k_{eq}) \end{cases} \tag{2.191}$$

(2.190) can be written in terms of the only Hubble variables (using (2.58) and $\epsilon \sim \frac{4\pi}{m_{\rm pl}^2}(\dot\phi/H)^2$) or the value of the potential energy as

$$\mathcal{P}_{\mathcal{R}_c} \simeq \left.\frac{H^2}{\pi\,\epsilon m_{\rm pl}^2}\right|_{k=aH}, \quad \mathcal{P}_{\mathcal{R}_c} \simeq \left(\frac{128\pi}{3m_{\rm pl}^6}\frac{V^3}{V_\phi^2}\right)_{k=aH}. \tag{2.192}$$

The COBE normalization [78] is $\mathcal{P}_{\mathcal{R}_c} \simeq 2\times 10^{-9}$ corresponding to about 60 e-folds. It allows us to determine an inflation energy scale. For example let us consider the quadratic potential $V(\phi) = \frac{1}{2}m_\phi^2\phi^2$. Substituting the previous result of (2.65) to the latter equation in Eq. (2.192), the inflaton mass m_ϕ can be $m_\phi \simeq 10^{-6}m_{\rm pl}$. The same result is roughly obtained by the first equation in (2.192) with $H \simeq m_\phi$. The spectral index, $n_{\mathcal{R}}$, is obtained from (2.186)

$$n_{\mathcal{R}} - 1 = 3 - 2\nu_{\mathcal{R}}\,. \tag{2.193}$$

Obviously, $\nu_{\mathcal{R}} = 3/2$ gives the scale-invariant and it corresponds to the coefficient 2 of $1/\tau^2$ term appearing in the EOM (2.184). To leading order in the slow-roll parameters we can evaluate up to a leading order

$$n_{\mathcal{R}} = 1 - 6\epsilon + 2\eta\,. \tag{2.194}$$

Since $\epsilon \ll 1$ and $\eta \ll 1$, it gives that scalar perturbations shows nearly scale-invariant ($n_{\mathcal{R}} \simeq 1$). The case of $n_{\mathcal{R}} < 1$ ($n_{\mathcal{R}} > 1$) leads to a red (blue) tilted spectrum. For example a chaotic inflation: $V = V_0\phi^q$ gives

$$n_{\mathcal{R}} = 1 - \frac{q(q+2)}{8\pi}\left(\frac{m_{\rm pl}}{\phi}\right)^2, \tag{2.195}$$

which is a red spectrum. The CMB data from WMAP3rd [427] gives $n_{\mathcal{R}} = 0.96 \pm 0.017$.

Gravitational wave : As noted in the previous subsection, in a scalar field universe any linear vector perturbation vanishes, but tensor perturbations propagate as gravitational waves. Let us show gravitational waves in an accelerating universe [191]. Introducing $\mu \equiv ah$, a basic equation of tensor perturbations (2.123) can be reexpressed as

$$\mu_k'' + (k^2 - \frac{a''}{a})\mu_k = 0\,, \tag{2.196}$$

with

$$\frac{a''}{a} = (aH)^2(2-\epsilon)\,. \tag{2.197}$$

In the slow-roll approximation, it results in

$$\frac{a''}{a} \simeq \frac{\nu_{\rm T}^2 - (1/4)}{\tau^2}, \quad \text{with} \quad \nu \simeq \epsilon\,. \tag{2.198}$$

We obtain a tensor power spectrum as

$$\mathcal{P}_{\rm T} \simeq \frac{64\pi}{m_{\rm pl}^2}\left((1-\epsilon)\frac{\Gamma(\nu_T)}{\Gamma(3/2)}\frac{H}{2\pi}\right)^2\left(\frac{|k\tau|}{2}\right)^{3-2\nu_T} . \tag{2.199}$$

To leading order in slow-roll we have

$$\mathcal{P}_{\rm T} \simeq \frac{64\pi}{m_{\rm pl}^2}\left(\frac{H}{2\pi}\right)^2_{k=aH} \simeq \frac{128}{3}\left(\frac{V}{m_{\rm pl}^4}\right)_{k=aH} . \tag{2.200}$$

The spectral index of tensor perturbations, $n_{\rm T}$, is given by

$$n_{\rm T} = -2\epsilon\,, \tag{2.201}$$

which is a red spectrum. A tensor to scalar ratio is an important observational quantity, defined by

$$r \equiv \frac{\mathcal{P}_{\rm T}}{\mathcal{P}_{\mathcal{R}_c}} \simeq 16\epsilon\,. \tag{2.202}$$

From Eqs. (2.201) and (2.202) a relation between r and $n_{\rm T}$ can be obtained by

$$r = -8n_{\rm T}\,, \tag{2.203}$$

so-called *consistency relation* [282] for single-field slow-roll inflation. It is important to investigate how observational data such that CMB constrains a single-field slow-roll inflation. As you seen, inflation also predicts the gravitational wave background arising due to the quantum fluctuations and the detection of such gravitational wave of inflationary origin is a challenging future task for the Laser Interferometer Space Antenna (LISA) [294] or the Deci-hertz Interferometer Gravitational Wave Observatory (DECIGO) [416].

2.3.4 CMB anisotropy

In the case of the anisotropic stress of radiation vanishing $\Pi_{\rm r} = \Theta_2 = 0$ [19], the basic equations (2.159) for the brightness functions $\Theta_{0,1}$ can be reduced to one equation for Θ_0, with the help of the equation for $v_{\rm b}'$ in (2.155),

$$\Theta_0'' + \mathcal{H}\frac{R}{1+R}\Theta_0' + k^2c_s^2\Theta_0 = \Psi'' + \frac{R}{1+R}\mathcal{H}\Psi - \frac{k^2}{3}\Phi\,. \tag{2.204}$$

where $R = 3\rho_{\rm b}/(4\rho_{\rm r})$ and we have expanded the baryon velocity as $v_{\rm b} = v_{\rm r}(=\Theta_1) + \lambda_T f$ by the first order of the tight coupling limit, equivalently, the small free streaming scale $\lambda_T = an_e\sigma_T \ll 1/k$. This is a master equation for CMB during a baryon-photon fluid and it is basically interpreted as Jeans equation (2.133), where the pressure denotes $k^2c_s^2\Theta_0$ term and the gravity denotes term proportional to Φ. The other terms are relativistic effects. If we consider the derivative terms Ψ'', Ψ' and Φ' neglect, we obtain the solution as

$$\begin{aligned}\Theta_0 &= [\Theta_0(0) + (1+R)\Phi]\cos(kr_s) + \frac{1}{kc_s}\Theta_0'(0)\sin(kr_s) - (1+R)\Phi\,,\\ \text{with}\quad r_s &\equiv \int_0^\tau c_s d\tau \quad \text{(Sound comoving horizon)}\,.\end{aligned} \tag{2.205}$$

[19] In the thesis, we do not consider the anisotropic stress of photon $\Pi_{\rm r}$, which is related to the quadrupole Θ_2, however, if the recombination has a finite duration, non zero quadrupole gives a *polarization of CMB* [123, 332]. The polarization has more information about the our universe. In particular, polarization can be decomposed into E and B-modes, dependent on their parity even and odd, respectively and B-modes is not generated by scalar perturbations. Hence detecting B-modes of polarization may give us an information about a gravitational wave generated by inflation for future observations.

It shows the so-called *acoustic oscillation*, as seen in the Jeans oscillation. The amplitude of this oscillation is determined by the initial value of $\Theta_0 + (1+R)\Phi$. For the initial condition, the *adiabatic perturbation* gives $\Theta_0'(0) = 0$, while the *entropy perturbation* gives $\Theta_0'(0) \propto S$. Therefore, we see that *a phase of an acoustic oscillation changes by* $\pi/2$. The term $\Theta_0 + \Phi$ is related to the *Sachs-Wolfe* (SW) effect [389] and the amplitude is also dependent on the baryon density as $R \propto \Omega_{\rm b} h^2$. The SW effect is shown in the original Boltzmann equation for $\Theta = \delta T/T$ given by $\Big(\frac{\partial}{\partial\tau} + \gamma^i \frac{\partial}{\partial x^i}\Big)\Big(\Theta + \Phi\Big) = 2\frac{\partial\Phi}{\partial\tau}$. If we consider the matter dominated epoch, from Eqs. (2.131) and (2.143), the gravitational potential Φ is constant and yields

$$\Theta + \Phi = \frac{\delta T}{T} + \Phi = \text{const}\,. \quad \text{(SW effect)} \tag{2.206}$$

Similar to (2.205), the general solution for Θ_l (2.133) is written in terms of spherical Bessel function of order l j_l as

$$\Theta_l(\tau) = [\Theta_0 + \Phi](\tau_{\rm dec})(2l+1)j_l(k\Delta\tau) + \Theta_1(\tau_{\rm dec})[l j_{l-1}(k\Delta\tau) - (l+1)j_{l+1}(k\Delta\tau)] + (2l+1)\int_{\tau_{\rm dec}}^{\tau} (\Phi' + \Phi')j_l(k(\tau-\tau_1))d\tau_1\,, \tag{2.207}$$

where $\Delta\tau = \tau - \tau_{\rm dec}$. It also shows the amplitude of oscillation is determined by the SW effects at the decoupling $[\Theta_0 + \Phi](\tau_{\rm dec})$. Let us estimate this term. From the perturbation theory, $\Theta_0 = \delta_{\rm r}/4$ is related to Φ as $\Theta_0 = -\frac{1}{2}\Phi$, which comes form Eq. (2.143) $\delta_{\rm r} = -2\Phi$. The initial condition of Φ_0 has been given by quantizing the inflaton fluctuations in the inflationary scenario and the generated primordial perturbation stretched out the horizon (first horizon-crossing) and then enter into the horizon (second horizon-crossing), leading to a CMB temperature fluctuation Θ at the decoupling time. On the other hand, the evolution equation for Θ_0 (2.159) in the superhorizon limit, becomes $\Theta_0' - \Psi' \approx 0$ and hence $\Theta_0 - \Psi =$const. At the radiation dominated epoch, $\Theta_0 = -\frac{1}{2}\Phi_0$, yielding const$= -\frac{3}{2}\Phi_0$ due to vanishing anisotropic stress $\Phi = \Psi$. Therefore, at the matter dominated epoch, Θ_0 is estimated as $\Theta_0 = \text{const} + \Psi_{\rm m0} = -\frac{3}{2}\Phi_0 + \Psi_{\rm m0} = -\frac{3}{2}\frac{10}{9}\Phi_{\rm m0} + \Psi_{\rm m0} = -\frac{2}{3}\Phi_{\rm m0}$ where we use the fact that Φ changes by factor of 10/9 through these epochs seen (2.148). The decoupling occurs at the matter dominated epoch, at which Φ is constant, and hence we can estimate the SW term $[\Theta_0 + \Phi](\tau_{\rm dec})$ as

$$[\Theta_0 + \Phi](\tau_{\rm dec}) = -\frac{2}{3}\Phi_{\rm m0} + \Phi_{\rm m0} = \frac{1}{3}\Phi_{m0}\,. \quad \text{(SW effect at decouping)} \tag{2.208}$$

This result comes from the analysis for adiabatic modes. For the entropy perturbation, $\Theta_0(\tau_{\rm dec})$ becomes $\Phi_{\rm m0}$ and yields the corresponding SW term $2\Phi_{\rm m0}$, larger than the adiabatic mode by a factor of 6. On the other hand, the second term in (2.207) denotes Doppler effects proportional to velocity $\Theta_1 \propto v_r$ and the last term denotes the Integrated Sachs-Wolfe (ISW) effect [378]. ISW effect is seen on the very large scale $l \lesssim 20$. This effect occurs by the changing of the gravitational potential Φ' or Ψ' and it is useful to see directly the effect of the cosmological constant Λ or dark energy. Next, we consider the second order of the tight coupling limit $O((k\lambda_T)^2)$ for (2.204), we obtain the so-called *Silk damping* scale in the WKB solution [422]:

$$\Theta_0 \propto e^{\pm ikr_s} e^{-k^2/k_D^2}\,, \quad \text{with} \quad k_D^{-2} = \frac{1}{6}\int \frac{\lambda_T}{1+R}\Big(\frac{8}{9} + \frac{R^2}{1+R}\Big)d\tau \quad \text{(Silk damping)}\,. \tag{2.209}$$

It shows that the acoustic oscillation $e^{\pm kr_s}$ decays as exponentially damping e^{-k^2/k_D^2} since photons defuse the baryon perturbation which they are coupled with (see also a sketch of Fig. 2.8(b)).

Power spectrum of CMB

A sky map of the CMB temperature fluctuations can be fully characterized in terms of an infinite sequence of correlation functions. If the spectrum of fluctuations is Gaussian, as predicted by inflation and as current data suggest, then only the even order correlation functions are nonzero and all of them can be directly expressed through the two-point correlation function (also known as the temperature

power spectrum):

$$C(\theta) \equiv \left\langle \frac{\delta T}{T}(\gamma_1)\frac{\delta T}{T}(\gamma_2)\right\rangle , \tag{2.210}$$

where the brackets denote averaging over all directions γ_1 and γ_2, satisfying the condition $\gamma_1\cdot\gamma_2=\cos(\theta)$. The three-point function is a sensitive test for a non-Gaussian contribution, however, we here does not discuss it [20]. The power spectrum of temperature perturbation Expanding the temperature fluctuation $\delta T/T=\Theta$ in terms of spherical harmonics $\delta T/T=\sum_l\sum_m a_{lm}Y_l^m(\theta,\phi)$ and also expanding C as Legendre series $C=\sum_l C_l\frac{2l+1}{4\pi}P_l(\cos\theta)$, we obtain the multipole moment C_l of the power spectrum as

$$\langle a_{lm}, a^*_{l',m'}\rangle = \delta_{ll'}\delta_{mm'}C_l \;\Rightarrow\; C_l=\frac{1}{2l+1}\sum_{m=-l}^{l}|a_{lm}|^2 . \tag{2.211}$$

It is related to the above obtained function Θ_l as

$$\frac{2l+1}{4\pi}C_l=\frac{1}{2\pi^2}\int\frac{dk}{k}\frac{k^3|\Theta_l|^2}{2l+1} . \tag{2.212}$$

Notice that the dimensionless power spectrum is given by $\frac{l(2l+1)}{4\pi}C_l$ driven from the relation $C=\int\frac{dl}{l}\frac{l(2l+1)}{4\pi}C_lP_l(\cos\theta)$. For a small $l<20$, there exist the so-called *cosmic variance*, which limits the information about statistical properties of the primordial spectrum gathered from a single vantage point. This indeterminate variance is $\Delta C_l/C_l\simeq(2l+1)^{-1/2}$, and hence about 50% for the quadrupole ($l=2$) and 15% for $l\sim 20$. Therefore, only considering $l>20$, let us concentrate only the contribution from the SW term. In this case, using (2.208) for the adiabatic modes, the power spectrum (2.212) can be estimated as

$$\frac{2l+1}{4\pi}C_l=\frac{1}{2\pi^2}\int\frac{dk}{k}k^3\left|\frac{1}{3}\Phi_{\rm m0}\right|^2 j_l^2(k\Delta\tau)(2l+1)=A\frac{\Gamma(3-n)\Gamma(\frac{n+2l-1}{2})(2l+1)}{(\Delta\tau)^{n-1}2^{3-n}\Gamma(2-\frac{n}{2})\Gamma(2-\frac{n}{2})\Gamma(l+\frac{5}{2}-\frac{n}{2})} , \tag{2.213}$$

where we have assumed the power spectrum is written in terms of the index $n_{\mathcal R}$ as $k^3|\Phi_k|^2\propto k^{n_{\mathcal R}-1}$. As you seen, $n_{\mathcal R}=1$ is predicted by inflation, the so-called scale invariant (Harrison-Zel'dovich) spectrum. In this case, the above equation shows on the large scale $l\lesssim 100$,

$$\frac{2l+1}{4\pi}C_l\propto\frac{2l+1}{(l+1)l}\;\Longrightarrow\; l(l+1)C_l=\text{const} . \tag{2.214}$$

Therefore it is commonly convenient to use the spectrum $\frac{l(l+1)}{2\pi}C_l$ in which it becomes a plateau on the large scale (see Fig. 2.8(a)). This is a *flat curve* of CMB spectrum. The angular size θ on today's sky is related to l as $\theta\sim\pi/l$(rad) and then $l\lesssim 100$ is $\theta>1.8^\circ$. For the more small scale $l\gtrsim 100$, the acoustic oscillation works, which can be decomposed into "oscillating"(O) and "nonoscillating" (N) [332]:

$$l(l+1)C_l\simeq\frac{B}{\pi}(O+N_1+N_2+N_3) , \tag{2.215}$$

where

$$\begin{aligned} &O\propto A_1\cos(l\varrho+\pi/4)+A_2\cos(2l\varrho+\pi/4) , \quad N_1\propto\xi^2[P-0.22(l/l_f)^{0.3}-2.6]^2e^{-(l/l_f)^2} ,\\ &N_2\propto\frac{e^{-(l/l_S)^2}}{(1+\xi)^{1/2}}[P-0.22(l/l_f)^{0.3}+1.7]^2 , \quad N_3\propto\frac{e^{-(l/l_S)^2}}{(1+\xi)^{3/2}}[P-0.5(l/l_f)^{0.55}+2.2]^2 . \end{aligned} \tag{2.216}$$

[20] Non-Gaussianity is important for distinguishing many inflation models by future observational data. It is characterized by $f_{\rm NL}$ from the decomposition of the gravitational potential as $\Phi=\Phi_{\rm Gaussian}+f_{\rm NL}\Phi^2_{\rm Gaussian}$ [263, 264, 34]. The recent constraint to non-Gaussianity is obtained $-58<f_{\rm NL}<134$ and the future observation Planck can detect non-Gaussianity for $f_{\rm NL}\gtrsim 5$.

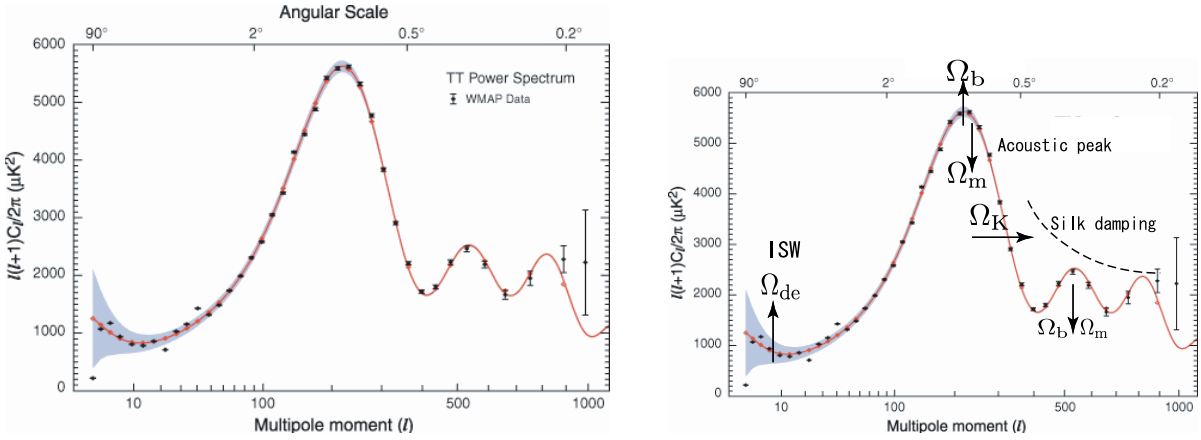

(a) (b)

Figure 2.8: (a): Anisotropies in the CMB predicted by the theory of inflation compared with observations [427]. (b): Schematic illustration shows the typical dependencies of the cosmological parameters. The arrow represents the direction of shift of the spectrum with increasing of parameter. Here we define $\Omega_{\rm K} = -K/(a_0^2 H_0^2)$ and increasing this denotes the open universe, which makes us look the lights traveling from smaller angular $\theta \searrow$ (larger multipole $l \nearrow$) (see also Fig. 2.1).

Here we defined the several variables dependent on the cosmological parameters and two important damping scales: the finite thickness l_f and Silk dissipation l_S effects, which are given by

$$\varrho = 0.014(1+0.13\xi)^{-1}(\Omega_{\rm m}h_{75}^{3.1})^{0.16}\,,\quad \xi = R|_{\tau_{\rm rec}} \simeq 17(\Omega_{\rm b}h_{75}^2)\,,\quad P = \ln\Big(\frac{I_\Lambda l_{200}}{\sqrt{\Omega_{\rm m}h_{75}^2}}\Big)\,,\quad I_\Lambda \simeq (1-\Omega_\Lambda)^{-0.09}$$
$$l_f^{-2} = 2\sigma^2\Big(\frac{\tau_{\rm rec}}{\tau_0}\Big)^2\,,\quad l_S^{-2} = 2\Big(\sigma^2 + (k_D\tau)_{\rm rec}^{-2}\Big)\Big(\frac{\tau_{\rm rec}}{\tau_0}\Big)^2\,,\quad \sigma = \frac{1}{\sqrt{6}(14400\mathcal{H}\tau/z)_{\rm rec}}\,. \tag{2.217}$$

where $h_{75} = (h/0.75)$ and $l_{200} = (l/200)$. σ denotes the finite duration of recombination and then l_f denotes this effect directly, while l_S denotes a combination this thickness with Silk damping $1/k_D$. The oscillation peaks are determined by the O term, where the two cosine terms are $A_1 < 0$ and $A_2 > 0$. Therefore the term proportional to A_1 interferes constructively for the odd peaks and destructively for the even peaks. As a result, the location of peaks are at $l_n \simeq \pi\varrho^{-1}(n-1/8)$. The standard cosmological parameter gives $l_1 \simeq 230$ ($d \sim 210$Mpc) and $l_2 \simeq 460$ ($d \sim 103$Mpc), where d is the corresponding length scales obtained by $d \approx \theta d_H(z=0) = \frac{\pi}{l} d_H(z=0)$. The locations of these peaks also directly obtained by the acoustic oscillation (2.205) as $kr_s = n\pi$. On the other hand, angular diameter distance d_A relates to multipole l as $l \sim kd_A/a$ obtained from combining $\Delta\theta = \lambda/d_A = \pi/l$ (see diameter distance in Sec. 2.1) with $\lambda = \pi a/k$. Then the location of acoustic peak is determined by

$$l_n \simeq \frac{n\pi(1+z)d_A}{r_s}\,, \tag{2.218}$$

and its shift to a cosmological parameter is roughly determined by $\sqrt{\Omega_{\rm m}^{(0)}}d_A(z)$. $d_A(z)$ is dependent on a cosmological parameter through a hubble parameter$H(z)$ as seen in (2.32).

Let us see the dependencies of the cosmological parameters on the CMB spectrum in more details. *The location of first peak is sensitive to* $l_1 \propto \Omega_{\rm tot}^{-1/2}$, that is, to *the spatial curvature* $\Omega_{\rm K}$. *The baryon density* $\Omega_{\rm b}$ *increases the height of this peak while the matter density decrease the height* (see the first peak in Fig. 2.8(b)). It is seen easily from (2.216) and (2.217) as follows. If we increase $\Omega_{\rm b}h^2$, both ξ and N_1,

which is proportional to ξ^2 increases for fixed $\Omega_{\rm m}h^2$. An increase of the cold matter density for fixed ξ suppresses the height since P decreases as $\Omega_{\rm m}h^2$ increases. On the other hand, for the height of second peak, baryonic matter work in opposite direction in terms of their effect on the first peak, that is, the second peak decreases as the baryon density increases. Hence *the baryon density and the dark matter density work in the same direction* in terms of how they alter the *height of the second peak* (see second peak in Fig. 2.8(b)). Using both peak heights enables us to resolve the degeneracy in the determination of $\Omega_{\rm m}h_{75}^2$ and $\Omega_{\rm b}h_{75}^2$. Moreover (2.217) show that the different combinations of $\Omega_{\rm m}$ and h_{75} gives the more information; namely, we can determine the Hubble constant since the heights of the peaks P depend on $\Omega_{\rm m}h_{75}^2$ and their location ϱ on $\Omega_{\rm m}h_{75}^{3.1}$.

The CMB observational data by COBE in 1992 [40] and by WMAP in 2003 [41, 264, 359, 427] found spectrum of primordial perturbations is nearly scale-invariant, that is consistent with a prediction of inflation. WMAP data [427] gives a spectral index is $n_{\mathcal{R}} = 0.951^{+0.015}_{-0.019}$, that is good agreement with a flat ΛCDM model. WMAP data also tells us that the universe is very close to be flat $|1-\Omega_{\rm total}| = 0.030^{+0.026}_{-0.025} \ll 1$ [350] as predicted by inflationary cosmology. In a flat cosmological models ($\Omega_{\rm tot} = 1$), using the observational value of the hubble parameter $h = 0.71 \pm 0.076$, we can conclude the constraint on cosmological constant as $\Omega_\Lambda = 0.69 \pm^{0.03}_{0.06}$. See Table 2.2 in the details for several cosmological parameters.

2.4 Dark energy and dark matter

We shall review unknown components in the modern cosmology, called dark energy and dark matter. First, main observational data will be introduced and we will mention the existences of these dark components. See recent reviews [105, 394].

2.4.1 Observational evidences for dark energy

The observations of Type Ia Supernova in 1998 pointed out the accelerated expansion of the universe [360, 381]. First, we will explain the observational evidences for dark energy from the supernovae Ia.

• Constraints from Supernovae Ia

The Hubble parameter can be written as a convenient form, from Eq. (2.33)

$$H^2 = H_0^2 \sum_i \Omega_i^{(0)} (1+z)^{3(1+\omega_i)} \,, \tag{2.219}$$

where $\Omega_i^{(0)} = \rho_i^{(0)}/\rho_{\rm cr}^{(0)}$ seen in (2.6), and ω_i and $\rho_i^{(0)}$ correspond to the EOS and the present energy density, respectively. The luminosity distance in a flat space (2.28) can be rewritten as

$$d_L = \frac{(1+z)}{H_0} \int_0^z \frac{{\rm d}z'}{\sqrt{\sum_i \Omega_i^{(0)} (1+z')^{3(1+\omega_i)}}} \,. \tag{2.220}$$

Therefore the luminosity distance depends on how each component exists in the universe. Fig. 2.9(a) shows a luminosity distance (2.220) for a non-relativistic matter $\omega_{\rm m} = 0$ and a cosmological constant $\omega_\Lambda = -1$ in a flat FRW universe. They satisfy $\Omega_{\rm m}^{(0)} + \Omega_\Lambda^{(0)} = 1$. One can know that $d_L \simeq z/H_0$ when z takes a small value. It shows the hubble law as $v = cz = H_0 d_L$. The observation of luminosity distances of high redshift supernovae can give us the direct evidence for the current acceleration of the universe [360, 381]. The apparent magnitude m and absolute M obey the following equation, using a luminosity distance d_L [392, 348]

$$m - M = 5 \log_{10} \left(\frac{d_L}{\rm Mpc} \right) + 25 \,. \tag{2.221}$$

It comes from taking the logarithm of Eq. (2.24) and the numerical factors are commonly used in astronomy. One can observe a Type Ia supernova (SN Ia) as an explosion of white dwarf stars reaching its maximum mass called *Chandrasekhar mass limit* $\sim 1.4 M_\odot$. Since the explosion of SN Ia is achieved in the same way, the observation of SN can become a "standard candle" for a high redshift. Once we observe

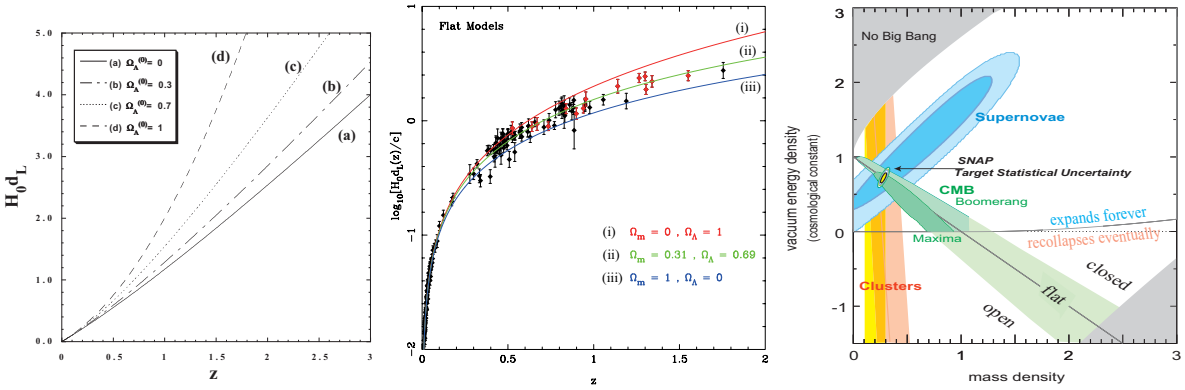

(a) (b) (c)

Figure 2.9: The figures from Ref. [8]. (a): Plot of $H_0 d_L$ versus z for two components in a flat universe. (b): Log plot of luminosity distance $H_0 d_L$ for a flat cosmological model. Three curves correspond to (i) $\Omega_{\rm m}^{(0)} = 0$, $\Omega_\Lambda^{(0)} = 1$, (ii) $\Omega_{\rm m}^{(0)} = 0.31$, $\Omega_\Lambda^{(0)} = 0.69$ and (iii) $\Omega_{\rm m}^{(0)} = 1$, $\Omega_\Lambda^{(0)} = 0$. (c): The constrained region in a parameter space of $\Omega_{\rm m}^{(0)}$-$\Omega_\Lambda^{(0)}$ plane, using SN, CMB and galaxy counting.

the apparent magnitude m, it gives us the luminosity distance d_L from the above equation (2.221) due to the well-known absolute magnitude M. On the other hand, the redshift can be obtained as their shifted wavelength of emission lines as $L_s = L_0(1+z)^2$ (2.25). Therefore, combining the luminosity distance d_L from m with the redshift z leads to the information about the components in the universe through the Eq. (2.220). As for one typical example of data, we get relation

$$H_0 d_L \simeq 1.16\,, \quad \text{for} \quad z = 0.83\,. \tag{2.222}$$

On the other hand, from Eq. (2.220) the theoretical estimation of the luminosity distance for two components

$$H_0 d_L \simeq 0.95, \ \text{for} \ \ \Omega_{\rm m}^{(0)} \simeq 1\,, \qquad H_0 d_L \simeq 1.23, \ \text{for} \ \ (\Omega_{\rm m}^{(0)} \simeq 0.3, \ \Omega_\Lambda^{(0)} \simeq 0.7)\,. \tag{2.223}$$

It shows the case $H_0 d_L = 1.23$ is more close to the above observational data $H_0 d_L = 1.16$ and yields the dark energy dominated universe. This estimation shows clearly the existence of a dark energy. When we assume a flat universe, it can be found as $\Omega_{\rm m}^{(0)} = 0.28^{+0.09}_{-0.08}$ (1σ statistical). It shows that the present universe has *about 70 % of its current energy density as dark energy.*

• Constraints by CMB and LSS

The observations by CMB [427] and large-scale structure (LSS) [440, 411] can give us information of a dark energy. Using the most recent WMAP data [427] with a constant equation of state $\omega_{\rm de} = -1$, and combined with SN legacy Survey, we can get $\Omega_{\rm K}^{(0)} = -0.015^{+0.02}_{-0,016}$, implying a flat universe. We caution that the CMB alone does not strongly constrain $\Omega_\Lambda^{(0)}$ without putting any prior for the other cosmological parameters. However if a flat universe is assumed with a hubble $h = 0.71 \pm 0.076$, the CMB data gives $\Omega_\Lambda^{(0)} = 0.69^{+0.03}_{-0.06}$ [421]. In Fig. 2.9(c) we plot an allowed region constrained from SN Ia, CMB and large-scale galaxy clustering [8]. All data strongly shows a density parameter of each component in the current universe as a dark energy $\Omega_\Lambda^{(0)} \simeq 0.7$, $\Omega_{\rm m}^{(0)} \simeq 0.3$ and a baryonic matter only 4 %. Thus the rest of the matter (26 %) denotes a non-baryonic matter with a dust EOS ($\omega = 0$) known as Cold Dark Matter (CDM). We can summarize main three components in the present universe as [427]

$$\Omega_\Lambda^{(0)} \simeq 0.72\,, \quad \Omega_{\rm DM}^{(0)} \simeq 0.25\,, \quad \Omega_{\rm baryon}^{(0)} \simeq 0.04\,. \tag{2.224}$$

In addition to SN, there are other candidates of standard candles: **1. Baryon oscillation** for future observations at $z \sim 3$, **2. Weak lensing** for future $z \sim 4-6$ and **3. Gamma ray bursts** for future $z \sim 6$. Baryon oscillation appears an oscillation in the CDM power spectrum (seen in Fig. 2.11(b)), corresponding to the so-called acoustic oscillation of photon emitted from baryon-radiation fluid existing before recombination (see review papers Eisenstein et al [138, 415]). This phenomena, baryon acoustic oscillation (BAO) is also observed as acoustic peaks in the CMB spectrum (see Fig. 2.8(b) and compared with Fig. 2.11(b)). For a representative measurement, BAO will be detected by the measurements e.g. the Canada-France-Hawaii Telescope Legacy Survey (CFHTLS) [93]. Weak lensing effect is based on photon bending (see reviews [253, 204, 379, 123]). The cosmological gravitational field distorts the paths travels by light from distant sources to us, the so-called *Lensing*. This effect can be quantified with a two-by-two symmetric matrix, named the *distortion tensor*, encoding information about image distortion. Gamma Ray Bursts (GRB) is the measurement observing to the most high redshift.

2.4.2 Dark energy

• Cosmological constant problem

The cosmological constant Λ was firstly introduced by Einstein in 1917. Using it, he wanted to make a universe static. The cosmological constant corresponds to an energy density of the vacuum, but such energy scale is naturally much larger than that of the present Hubble. This is the so-called "cosmological constant problem" [468].

There have been many ways to solve this problem. For examples we can show attempts as adjustment mechanisms [124, 72], anthropic considerations [288, 32, 467, 228, 171, 172, 173, 316], modified gravity [457], quantum gravity [98], degenerate vacua [474], higher-dimensional gravity [17, 223, 456], supergravity [157, 5], string theory [55, 424, 150, 225, 80]. In this section we will explain a fine-tuning problem and discuss several origins of Λ. The cosmological constant leads to an accelerating of the universe by a some kind of *repulsive force* as $\ddot{a}/a = \Lambda/3$ seen in (2.4) with a negative pressure (2.12), while ordinary matters does attractive forces $\ddot{a}/a < 0$. The Poisson equation for gravitational potential Φ including the cosmological constant Λ yields

$$\Delta\Phi = 4\pi G\rho - \Lambda\,. \tag{2.225}$$

Since Λ has dimensions of $[\text{Length}]^{-2}$, it can be estimated by using the present Hubble parameter H_0, yielding

$$\Lambda \approx H_0^2 = (2.13h \times 10^{-42}\,\text{GeV})^2\,. \tag{2.226}$$

It can read a critical density ρ_Λ [21],

$$\rho_\Lambda = \frac{\Lambda m_{\rm pl}^2}{8\pi} \approx 10^{-47}\,\text{GeV}^4 \sim (10^{-3}\text{eV})^4\,. \tag{2.227}$$

On the other hand, we can evaluate a sum of zero-point energies with mass m as a vacuum energy, which is given by

$$\rho_{\rm vac} = \frac{1}{2}\int_0^\infty \frac{\mathrm{d}^3\mathbf{k}}{(2\pi)^3}\sqrt{k^2+m^2} = \frac{1}{4\pi^2}\int_0^\infty \mathrm{d}k\,k^2\sqrt{k^2+m^2}\,. \tag{2.228}$$

It shows an ultraviolet divergence: $\rho_{\rm vac} \propto k^4$. However it is usually known that there exists some cut-off scale $k_{\rm max}$ inwhich quantum field theory is valid. It makes the integral (2.228) finite $\rho_{\rm vac} \approx \frac{k_{\rm max}^4}{16\pi^2}$. For an example case of General Relativity, we expect it to be the Planck scale: $m_{\rm pl} = 1.22 \times 10^{19}\,\text{GeV}$, one get

$$\rho_{\rm vac} \approx 10^{74}\,\text{GeV}^4\,, \tag{2.229}$$

[21] Notice that a mass scale of critical density $m_{\rm cr} \sim 10^{-3}$eV may be of the same order of magnitude as neutrino mass $m_{\nu_e} < 2.2$eV. In this point, there is recent idea of dark energy as neutrino mixing [88].

which means that vacuum energy scale is 10^{121} orders of magnitude larger than the present Hubble constant Eq. (2.227).

Another cosmological constant problem is described as the so-called **coincidence problem**. It implies that why each energy densities have now the same order as

$$O(\rho_\Lambda^{(0)}) \sim O(\rho_{\rm DM}^{(0)})\,. \tag{2.230}$$

The coincidence problem implies that we appear to live during *a special epoch when the densities in dark energy and in dark matter are almost equal*. Since the cosmological constant does not evolve while both matter and radiation evolve rapidly ($\rho_{\rm m} \propto a^{-3}$, $\rho_{\rm r} \propto a^{-4}$), it follows that the small current value $\rho_\Lambda \simeq 10^{-47}$ GeV^4 implies $\rho_\Lambda/\rho_{\rm r} \simeq 10^{-123}$ at the Planck time (when the temperature of the universe was $T \sim 10^{19}$ GeV), or $\rho_\Lambda/\rho_{\rm r} \simeq 10^{-55}$ at the time of the electroweak phase transition ($T \sim 100$ GeV). Thus an extreme fine-tuning needs in order to ensure that $\rho_\Lambda/\rho_{\rm m} \sim 1$ today.

Moreover Kallosh claims to add more one problem: Why *positive value* the cosmological constant takes? In the string theory, AdS vacuum is naturally obtained due to satisfy SUSY. It has been also seen in a complex setup of KKLT model in order to get a dS vacuum in string theory. As summary, the cosmological constant problem is the following three statements: *(1) Why small?*, related to the fine-tuning problem, *(2) Why now?*, related to the coincidence problem and *(3) Why positive?*, related to the fact that AdS vacuum is naturally obtained in the string theory.

• **Quintessence**

The cosmological constant remains a constant as $\omega = -1$, but in general the time evolution of ω can be allowed to consider with a time-dependent EOS $\omega(t)$. Scalar fields naturally arise in particle physics, they can play role of a dark energy and known as scenarios, quintessence, phantoms, K-essence, tachyon and ghost condensates. Let us firstly explain quintessence [376, 83]. Quintessence is described by an ordinary scalar field ϕ minimally coupled to gravity, but as we will see with particular potentials that lead to late time inflation. The action for Quintessence is given by $S = \int {\rm d}^4x\sqrt{-g}\left[-\frac{1}{2}(\nabla\phi)^2 - V(\phi)\right]$, where $(\nabla\phi)^2 = g^{\mu\nu}\partial_\mu\phi\partial_\nu\phi$. The EOS for ϕ is characterised by

$$\omega_\phi(t) = \frac{p}{\rho} = \frac{\dot\phi^2 - 2V(\phi)}{\dot\phi^2 + 2V(\phi)}\,. \tag{2.231}$$

It is obvious to see the EOS change with time. In order to see this changing of EOS from observations, one often use a linear fitting formula of the EOS as $\omega(t) = \omega_0 + \omega_1 z$ for a small redshift $z \ll 1$. The energy density is obtained by

$$\rho = \rho_0 \exp\left[-\int 3(1+\omega_\phi)\frac{{\rm d}a}{a}\right]\,. \tag{2.232}$$

This gives us a general definition of the energy density of dark energy. Using it, the Hubble (2.33) for the universe made up matters and dark energy becomes

$$H^2 = H_0^2\left\{\Omega_{\rm m,0}/a^3 + \Omega_{\rm de,0}\exp\left[-\int_a^{a_0} 3(1+\omega(t))\frac{{\rm d}a}{a}\right]\right\}. \tag{2.233}$$

The specific EOS $\omega < -1$ is called a *phantom* (ghost) dark energy. It leads to another expanding solution given by

$$a = (t_{\rm rip} - t)^{\frac{2}{3(1+\omega)}}\,,\quad H = -\frac{2}{3(1+\omega)(t_{\rm rip}-t)}\,,\quad \text{with}\ \ t_{\rm rip} \simeq t_0 + \frac{2}{3H_0\sqrt{\Omega_{\rm de,0}}|1+\omega|}\,. \tag{2.234}$$

The scale factor and Hubble diverge when $t \to t_{\rm rip}$, which corresponds to divergence, the so-called *Big Rip singularity*. If $\omega = -3/2$, the big rip time $t_{\rm rip} \sim 36$Gyr, i.e. after 22 billion years.

It is interesting case where powerlaw expansion $a(t) \propto t^p$ achieves by a scalar-field potential, which results in

$$V(\phi) = V_0\exp\left(-\sqrt{\frac{16\pi}{p}}\frac{\phi}{m_{\rm pl}}\right)\,, \tag{2.235}$$

where the accelerated expansion occurs for $p > 1$. The ϕ field evolves as $\phi \propto \ln t$. The original quintessence models [376, 83] used a following power-law potential

$$V(\phi) = \frac{M^{4+\alpha}}{\phi^\alpha}\,, \tag{2.236}$$

and the potential of quintessence is used as an exponential type (2.235) $V \propto e^{-\phi}$ or the inverse power-law potential (2.236) $V \propto 1/\phi^\alpha$. For other scalar field models giving a dynamical EOS, **K-essence** models are characterized by the following extended general action [20, 21]

$$S = \int \mathrm{d}^4x\sqrt{-g}P(\Phi, X)\,, \quad \text{where} \quad X \equiv -(1/2)(\nabla\phi)^2\,, \qquad (\mathrm{K-essence}) \tag{2.237}$$

and the Lagrangian density $P(\phi, X)$ equates to a pressure density. It can be applied to a kinetic driven inflation, called K-inflation [19] and a dark energy [95].

The another dark energy model is **Tachyon field**. Sen [414] used a pressureless gas as dark energy, which is generated by a decay of D-branes (see also Refs. [413, 168, 43]). It is called tachyon [321, 146, 147, 399, 400] and is characterized by the action

$$S = -\int \mathrm{d}^4x V(\phi)\sqrt{-\det(g_{ab} + \partial_a\phi\partial_b\phi)}\,. \qquad (\text{Tachyon field}) \tag{2.238}$$

Note that it is exactly a Dirac-Born-Infeld action, describing D-3 brane, seen in Chapter 3.

2.4.3 Observational evidences for dark matter

• Flat rotation curves

Though the observational evidence favoring a flat Universe with $\Omega_{\rm total} \simeq 1$ is fairly recent, the nature of the 'unseen' component of the universe (which dominates its mass density), is a long-standing issue in modern cosmology. Indeed, the need for dark matter was originally pointed out by Zwicky (1933) [477] who realized that the velocities of individual galaxies located within the Coma cluster were quite large, and that this cluster would be gravitationally bound only if its total mass substantially exceeded the sum of the masses of its component galaxies. For clusters which have relaxed to dynamical equilibrium the mean kinetic and potential energies are related by the virial theorem [99]

$$K + \frac{U}{2} = 0\,, \tag{2.239}$$

where $U \simeq -GM^2/R$ is the potential energy of a cluster of radius R, $K \simeq 3M\langle v_r^2\rangle/2$ is the kinetic energy and $\langle v_r^2\rangle^{1/2}$ is the dispersion in the line-of-sight velocity of cluster galaxies. This relation allows us to infer the mean gravitational potential energy if the kinetic energy is accurately known. In individual galaxies the presence of dark matter has been convincingly established through the use of Kepler's third law

$$v(r) = \sqrt{\frac{GM(r)}{r}} \tag{2.240}$$

to determine the 'rotation curve' $v(r)$ at a given radial distance from the galactic center. Observations of galaxies taken at distances large enough for there to be no luminous galactic component indicate that, instead of declining at the expected rate $v \propto r^{-1/2}$ true if $M \simeq$ constant, the velocity curves flattened out to $v \simeq$ constant implying $M(r) \propto r$ (see fig 2.10). This observation suggests that the mass of galaxies continues to grow even when there is no luminous component to account for this increase. Velocity curves have been compiled for over 1000 spiral galaxies usually by measuring the 21 cm emission line from neutral hydrogen (HI) [361, 425]. It is interesting that the total mass of an individual galaxy is still somewhat of an unknown quantity since a turn around to the $v \propto r^{-1/2}$ law at large radii has not been convincingly observed. This is the so-called *flat rotation curve problem in galaxies*. An important difference between

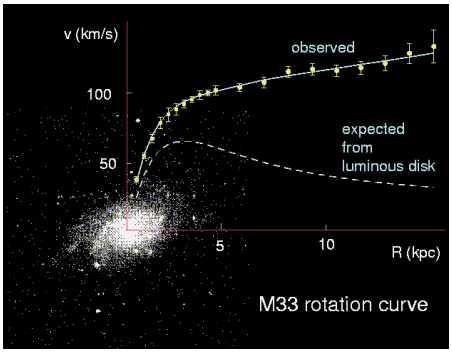

Figure 2.10: The observed rotation curve of the dwarf spiral galaxy M33 extends considerably beyond its optical image (shown superimposed); from Roy [386]. (This figure is Fig1 in Sahni [394].)

the distribution of dark matter in galaxies and clusters needs to be emphasised: whereas dark matter appears to *increase* with distance in galaxies, in clusters exactly the reverse is true, the dark matter distribution actually *decreases* with distance. Indeed, for certain dwarfs (such as DD0154) the rotation curve has been measured to almost 15 optical length scales indicating that the dark matter surrounding this object is extremely spread out (see also figure 2.10). A foreground cluster, on the other hand, acts as a gravitational lens which focuses the light from background objects such as galaxies and QSO's (Quasi-Stellar Object) thereby allowing us to determine the depth of the cluster potential well. Observations of strong lensing by clusters indicate that dark matter is strongly concentrated in central regions with a projected mass of $10^{13} - 10^{14} M_{\odot}$ being contained within 0.2 - 0.3 Mpc of the central region. This observation may prove to be problematic for alternatives to the dark matter hypothesis such as the Modified Newtonian Dynamics (MOND) approach of Milgrom [325]. As the name suggests, MOND is a modification of Newtonian physics which proposes to explain the flat rotation curves of galaxies without invoking any assumptions about dark matter. Briefly, MOND assumes that Newtons law of inertia ($F = ma$) is modified at sufficiently low accelerations ($a < a_0$) to $\mathbf{F} = m\mathbf{a}\mu(a/a_0)$ where $\mu(x) = x$ ($\mu(x) = 1$) for $x \ll 1$ ($x \gg 1$) [325, 403].

• The constraint from baryon density

As discussed earlier, the fact that the cosmic density is made of baryonic as only 4% can read that the dark matter which we are observing could well be non-baryonic in origin. This fact is related to nucleosynthesis. In a successful nucleosynthesis, the baryon-photon ratio $\eta_{10} \equiv 10^{10} \times n_N/n_\gamma$ is constrained as $\eta_{10} = 5.5 \pm 0.5$. This is still constant even if the universe expands. Therefore the energy density of the baryon can be estimated by the present number density of radiation $n_\gamma \approx 412\text{cm}^{-3}$ as

$$\Omega_{\rm b} = \frac{\rho_{\rm b}}{\rho_{\rm cr}} = \frac{m_N n_N}{\rho_{\rm cr}} = \frac{m_N \eta_{10} n_\gamma 10^{10}}{\rho_{\rm cr}} \approx 0.0224 h^{-2} \approx 0.04 \quad \text{for } h = 0.7\,. \tag{2.241}$$

For candidates for dark matter, if we pay attention to baryonic objects, one can consider white dwarfs, neutron stars and black holes etc. These are candidates for dark matter, the so-called, MAssive Compact Halo Objects (MACHO) [345].

• The constraint from structure formation

The need for non-baryonic forms of dark matter gets indirect support from the fact it difficult to obtain current large-scale structure by only baryon hence to reconcile the existence of a well developed cosmic web of filaments, sheets and clusters at the present epoch with the exceedingly small amplitude of density perturbations ($\delta\rho/\rho \sim 10^{-5}$ at $z \simeq 1100$) inferred from COBE measurements and more recent CMB experiments [427]. Indeed, it is well known that, if the effects of pressure are ignored, linearized density perturbations in a spatially flat matter dominated universe grow at the rate (see the result of (2.136))

$$\delta \propto t^{2/3} \propto (1+z)^{-1}\,, \tag{2.242}$$

where $1+z = a_0/a(t)$ is the cosmological redshift. In a baryonic universe, due to large radiation pressure density perturbations of baryons can grow only after recombination at $z \simeq 1100$ at which point of time baryons and radiation decouple. Requiring $\delta > 1$ today implies $\delta > 10^{-3}$ at recombination, which contradicts CMB observations by over an order of magnitude. In non-baryonic models on the other hand, a structure can begin to grow much earlier since there is no coupling between dark matter and radiation, significantly before recombination. Hence a universe with a non-baryonic matter can allow us to restudy a structure formation. Moreover a recent CMB data independently shows the existence of dark matter, obtained by fitting the CMB spectrum derived from several cosmological models.

2.4.4 Dark matter

• Cold dark matter

The structure can grow by gravitational instability and it depends both on whether primordial perturbations is adiabatic or isocurvature and whether dark matter is hot or cold. Non-baryonic *Hot Dark Matter* (HDM) is considered to be relativistic when it had decoupled from the other matter and it has a large velocity dispersion (hence called 'hot'). While *Cold Dark Matter* (CDM) has a small velocity dispersion and decoupled at its non-relativistic stage. The free-streaming (collisionless phase mixing) of non-baryonic particles as they travel from high density to low density regions (and vice versa) introduces an important length scale called the 'free-streaming distance' $\lambda_{\rm fs}$ – which is the mean distance traveled by a relativistic particle species until its momentum becomes non-relativistic. In both HDM and CDM the processed *final* spectrum of density perturbations differs from its initial form. In the case of HDM this difference arises because fluctuations on scales smaller than $\lambda_{\rm fs}$ are wiped out due to free streaming with the result that the processed final spectrum has a well defined cutoff on scales smaller than $\lambda \sim \lambda_{\rm fs}$. Perhaps the best example of HDM is provided by a light neutrino of mass about 30 eV. In this case $\lambda_{\rm fs} \simeq 41(30{\rm eV}/m_\nu)$ Mpc with the result that large proto-pancakes having masses comparable to those of rich clusters of galaxies $M \sim 10^{15} M_\odot$ are the first objects to form in HDM. Smaller objects (galaxies) are formed by the fragmentation of the proto-pancake. This *top-down* scenario for structure formation was originally suggested by Zeldovich and coworkers in connection with adiabatic baryonic models and subsequently applied to HDM. It has since fallen out of favour mainly due to the strong observational constraints on the mass of the neutrino $\sum_{\nu_i} m_{\nu_i} < 0.7$ eV and on the relic neutrino density $10^{-3} \lesssim \Omega_\nu h^2 \lesssim 10^{-1}$ [139, 143, 326, 427]. It also faces considerable difficulty in forming structure sufficiently early to explain the existence of galaxies and QSO's at high redshifts. In contrast to HDM, constituents of CDM have a much smaller free-streaming distance. Because of this small scales are the first to go non-linear and gravitational clustering proceeds in a *bottom up* fashion in this scenario.

• Power spectrum of CDM

A key quantity defining gravitational clustering is the power spectrum of density perturbations $P(k)$ (2.166) and (2.168). The relevant cosmological quantity is the shape of the power spectrum of density perturbations, which for CDM-like models, can be characterised by the 'shape parameter' $\Gamma = \Omega_{\rm m} h$. The exact solution for the transfer function is the fitting form of Bardeen, Bond, Kaiser and Szalay (1986) [29, 123]:

$$T(q) = \frac{\ln[1+2.34q]}{2.34q}\Big[1+3.89q+(16.2q)^2+(5.47q)^3+(6.71q)^4\Big]^{-0.25}, \quad q \equiv k/\Gamma h{\rm Mpc}^{-1}\,. \qquad (2.243)$$

The 'standard' cold dark matter (SCDM) models with $\Omega_{\rm m} = 1$ and the HST-determined value $h \simeq 0.7$ predict $\Gamma \simeq 0.5$ which is much larger than the observed value $\Gamma = 0.207 \pm 0.030$ inferred from observations of galaxy clustering in the sloan digital sky survey (SDSS) [367]. A modification of SCDM called LCDM assumes that, in addition to CDM the universe consists of a smoothly distributed component called a cosmological constant or a Lambda-term. LCDM models with $h \simeq 0.7$ and $\Omega_{\rm m} = 0.3$ predict a smaller value for the shape parameter, $\Gamma \simeq 0.2$, and the resulting amplitude and shape of the power spectrum is in excellent agreement with several different sets of observations as demonstrated in figure 2.11.

• Candidates for DM

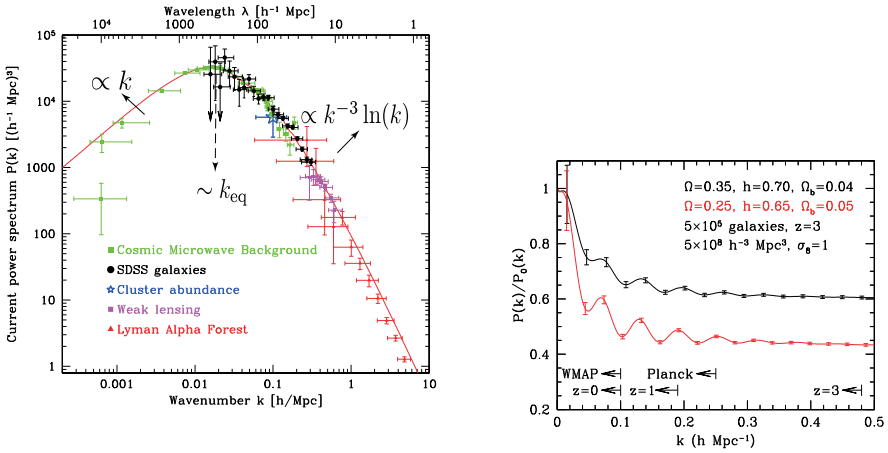

(a) (b)

Figure 2.11: (a): The power spectrum inferred from LSS, Lymanα forest, gravitational lensing and CMB. The solid line shows the power spectrum prediction for a flat scale-invariant LCDM model with $\Omega_{\rm m} = 0.28$, $\Omega_{\rm b}/\Omega_{\rm m} = 0.16$, $h = 0.72$; from Tegmark et al [440]. It also shows asymptotic k dependencies seen in (2.168), where the location of turn-around is closed to the wavenumber at the equality time $k_{\rm eq} \simeq 0.01 \sim (80{\rm Mpc})^{-1}$. (b): Plot of baryon acoustic oscillation. We enlarge the CDM power spectrum of Fig. 2.11(a) at $0.01 < k < 0.5$, where oscillation can be seen due to tight coupling of baryons with photons. Two different lines denotes the cases of $\Omega_{\rm m} = 0.35$, $h = 0.70, \Omega_{\rm b} = 0.04$ and $\Omega_{\rm m} = 0.25$, $h = 0.65, \Omega_{\rm b} = 0.05$. This figure is from [415].

Promising candidates for cold dark matter include a $100 - 1000$ GeV particle called a **neutralino**. The neutralino is a weakly interacting massive particle (WIMP) and is seen to be consider SUSY partner of neutrino. It is believed that the lightest supersymmetric particle will be stable due to R-parity which makes the neutralino an excellent candidate for cold dark matter (see [385, 222] for reviews of particle dark matter). A radically different particle candidate for cold dark matter is an ultra-light pseudo-Goldstone boson called an **axion** with a mass of only $m_a \sim 10^{-5\pm1}$ eV. Although ultralight, the axion is 'cold' because it was created as a zero-momentum condensate. Its existence is a by-product of an attempt to resolve QCD of what is commonly called the *'strong CP problem'* [259]. This problem is described as why a theoretical parameter is so unnaturally small $\theta < 10^{-9}$, which required by the CP invariant consistent with the observational data. This parameter is given in the Lagrangian of the form: $L \sim L_0 + \Theta\pi^2 F_{\mu\nu}F^{\mu\nu}/32$ where the last term works CP violation, however, it needs to explain the mass constraint for the π and η mesons as $m_\eta < \sqrt{3}m_\pi$. The most compelling solution is the one proposed by Peccei and Quinn in 1977 [354]. The crux of their idea is to make Θ a dynamical variable, which is driven to zero by the action of its classical potential. This feat is accomplished by introducing an additional global, chiral symmetry, now known as PQ (Peccei-Quinn) symmetry. Weinberg and Wilczek pointed out that because this symmetry is a spontaneously broken global symmetry, there must be a Nambu-Goldstone boson, which is just the axion. Other candidates for non-baryonic cold dark matter include string theory motivated modulii fields [76]; non-thermally produced super-heavy particles having a mass $\sim 10^{14}$ GeV and dubbed Wimpzillas [260]; as well as axino's and gravitino's – superpartners of the axion and graviton respectively [385]. There has been many models for dark matter, however, their theoretical origins are still unknown. We shall summarize the features of dark matter as follows: (1) *dark* (non-luminous), (2) *non-baryonic*, (3) *long-lived* and (4) *cold* (non-relativistic) dust.

2.5 Summary

2.5.1 The modern imaging of the universe

We summarize the modern imaging of the universe. Especially, based on the ancient questions about Cosmology, the simple answers are noted as follows.
(i) Age: for *13.7 billion years*, the universe keeps to expand from an initial dense and hot state.
(ii) Shape(geometry): There are three types of the universe, closed, flat and open related to spatial curvature K. The universe is seen to be *close to spatially flat* as seen in Table. 2.2. Even though the question such as "Is there the end in the universe?" is difficult to answer, one response is a causal particle horizon, where the light can reach during the age of the universe. This observational patch of the universe is of order 3000Mpc$\sim$ 10 billion years$\times c$. Moreover, the standard cosmological theory, inflation suggests that this may be the end of the story. According to inflationary theory, the universe becomes homogeneous and isotropic over larger distance than the horizon.
(iii) Matter compositions: we know that

1. CMB radiation has $T \simeq 2.73K$;
2. baryonic matter with no amount of antimatter;
3. where baryonic matter is composed of *about 75 % hydrogen, 25 % helium, plus heavier elements*;
4. *baryons contribute a small percentage (0.04 %) in the universe; the rest is a cold dark matter ($\sim$ 25 %) and dark energy ($\sim$ 70 %).*

(iv) History(evolution): See Table. 2.1 in the details. The main flow of the theory is that: Superstring or Quantum gravity $\rightarrow$ Inflation $\rightarrow$ Reheating $\rightarrow$ Big bang theory (radiation dominated $\rightarrow$ matter dominated universe). Let us pay attention to the sequence of main events constituting the history of our universe as follows [332].

- $\sim \mathbf{10^{-43} - 10^{-14}}$s ($10^{19}$GeV-10TeV) This energy range will probably not be reached at accelerators in the near future. Instead, the very early universe gives us the possibility to deal with the universe as "experiment" in order to study the high energy fundamental physics such as quantum gravity, unified theory.
- $\sim \mathbf{10^{-14} - 10^{-10}}$s (10TeV-100GeV) This range of energy scales can still be probed by accelerators. The Standard Model of electroweak and strong interaction appears to be applicable here.
- $\sim \mathbf{10^{-5}}$s (200MeV) The quark-hadron transition takes place: free quarks and gluons become confined within hadron (baryons and mesons).
- $\sim \mathbf{0.2}$s ($1 - 2$MeV) Two important events take place during this period. First, the primordial neutrinos decouple from the other particles and propagate without further scattering ($T \sim 1.5$MeV). Second, the ratio of neutrons to protons "freezes out" because the interactions that keep neutrons and protons in chemical equilibrium become inefficient ($T \sim 0.8$MeV).
- $\sim \mathbf{1}$s (0.5MeV) The typical energy at this time is of order the electron mass. The numerous electron-positron paris begin to annihilate when the temperature drops below this energy scale. After annihilation, the neutrino temperature is lower by a factor of $(4/11)^{1/3}$ since photons are heated by the annihilation.
- $\sim \mathbf{200 - 300}$s (0.05MeV) The abundances of the light elements resulting from primordial *nucleosynthesis* are in very good agreement with available observation data. The number density of free neutrons at $T \sim 0.07$MeV gives the abundance of Helium-4, about 25%.
- $\sim \mathbf{10^{11}}$s **($\sim$ eV)** This time corresponds to matter-radiation equality which separates the radiation-dominated epoch from the matter-dominated epoch.
- $\sim \mathbf{10^{12} - 10^{13}}$s At this time nearly all free electrons and protons recombine as neutral hydrogen (*recombination*). The universe becomes transparent to the background radiation (*decoupling*).
- $\sim \mathbf{10^{16} - 10^{17}}$s Galaxies and their clusters are formed from small initial inhomogeneities as a result of gravitational instability.

Event	Temperature (T)	Time (t)	Redshift (z)
Birth of Universe	∞ (?)	0sec	
Superstring(?) Quantum gravity(?)	$\sim 10^{19}$GeV	10^{-42}sec	
Inflation	$\sim 10^{13}$GeV	10^{-34}sec	
Matter-antimatter asymmetry	$\sim 10^{13}$GeV		
Reheating	10^6GeV $\gtrsim T \gtrsim$ MeV	10^{-34}sec	
Maximum energy of accelerator	10TeV	10^{-14}sec	
SUSY breaking	$\sim$ 1TeV	10^{-11}sec	
Dark matter production (?)	$\sim$ 1TeV	10^{-11}sec (?)	
Electroweak sym breaking	100GeV	10^{-10}sec	
Quark-hadron transition	200MeV	10^{-5}sec	
Neutrons decoupling	1.5MeV	$\sim$ 0.1sec	
$n-p$ ratio freezes out	0.8MeV	$\sim$ 0.2sec	
$e-e^+$ annihilation	0.5MeV	$\sim$ 1sec	
Nucleosynthesis	0.1MeV $> T >$ 10keV	$200-300$sec ($\sim$ 3 min)	
Helium recombination	~ 1.2eV(=$12000K$) (He^+)	10^{11}sec ($\sim$ 3kyr)	~ 4395
	$\sim 5000K$(He)	10^{12}sec ($\sim$ 30kyr)	~ 1832
Matter-radiation equality	$\sim 9450K$(= 1eV)	10^{11}sec	~ 3500
H recombination	$\sim 3400K(X_e = 0.5)$		~ 1200
	$\sim 3000K(X_e = 0.1)$		~ 1100
Photons decoupling (CMB)	$\sim 2700K$	378kyr	~ 1000
Primordial galaxy formation		200 million yr	~ 20
Reionization		500 million yr	~ 10
Current most distant galaxy		800 million yr	7
Solar system formation		$\sim$ 9 billion yr	~ 1 ($a = a_0/2$)
Birth of Earth		9.2 billion yr	~ 0.43
		(4.5 billion yr ago)	
Birth of life		10 billion yr	~ 0.35
Dark energy domination (?)		10 billion yr	~ 0.3
Typical distance in SDSS of galaxies		11.3 billion yr	~ 0.2
Dinosaur era		220 million yr ago	~ 0.016
Disappearance of dinosaur		65 million yr ago	~ 0.0047
Appearance of Humankind		4.5 million yr ago	~ 0.00033
Now	$2.73K$	13.7 billion yr	0

Table 2.1: Summary of the sequence of main events constituting the history of our universe. This is just a rough estimation denoting the thermal history. It is useful to estimate two relations: year and second as 1yr $\simeq 3 \times 10^7$sec and temperature and energy as 1eV $\simeq 10^4 K$.

(v) Future: The answer to the question such as "What the universe will be in the future?" is depend on the EOS of dark energy. We have known that the universe is now in the stage of slowly accelerated expansion, and hence dark energy will continues to be dominant in the future, leading to an almost empty universe. If the dark energy is phantom $\omega_{\rm de} < -1$ (see Sec. 2.4), the evolution changes drastically, and the universe will begin to contract at a finite time ($\sim$ after 22 billion years) in the future, towards to the Big Rip. Contracting phase in the future is also seen in the case of the closed universe $K > 0$, however, the observations suggest the flat universe. In the further chapter, we will show the *cyclic universe* scenario. This implies that the universe will continue to accelerating expand and contract forever.

Finally, we summarize the current best values of the cosmological parameters obtained by the WMAP data [427] in Table 2.2.

2.5.2 Problems in the standard cosmology

• Dark matter, Dark energy and Inflaton

Description	Symbol	Value
Total density	$\Omega_{\rm tot}$	1.014 ± 0.017
Baryon density	$\Omega_{\rm b}$	$0.041^{+0.0013}_{-0.0017}$
Dark matter density	$\Omega_{\rm m}$	$0.235^{+0.013}_{-0.018}$
Dark energy density	$\Omega_{\rm de}$	0.716 ± 0.055
EOS of dark energy	$\omega_{\rm de}$	-0.967 ± 0.073(with SN)
		-1.08 ± 0.017(with LSS)
Hubble constant	h	$0.734^{+0.028}_{-0.038}$
Age of universe	t_0	$13.73^{+0.13}_{-0.17}$Gyr
Baryon-to-photon ratio	η	$(5.5 \pm 0.5) \times 10^{-10}$
CMB temperature	T_0	$2.725 \pm 0.002K$
Redshift of decoupling	$z_{\rm dec}$	1089 ± 1
Age at decoupling	$t_{\rm dec}$	379^{+8}_{-7}kyr
Thickness of decoupling	$\Delta z_{\rm dec}$	195 ± 2
Decoupling time interval	$\Delta t_{\rm dec}$	118^{+3}_{-2}kyr
Redshift of matter-radiation equality	$z_{\rm eq}$	3233^{+194}_{-210}
Redshift of reionization	$z_{\rm re}$	11 ± 4.3
Power spectrum normalization	A	$0.833^{+0.086}_{-0.083}$
Scalar spectral index	$n_{\mathcal{R}}$	0.961 ± 0.017
Tensor-to-scalar ratio	r	< 0.65
		< 0.3(with Lensing+LSS)
Sound horizon at decoupling	r_s	147 ± 2Mpc
Acoustic scale	$l_A = \pi d_A / r_s$	301 ± 1

Table 2.2: The best fit values of the cosmological parameters by WMAP [427]. The critical density $\rho_{\rm cr}$ is obtained from the hubble parameter as $\rho_{\rm cr} \equiv 3H_0^2/(8\pi G) = 1.88h^2 \times 10^{-29}{\rm g/cm^3}$. In the case of $h = 0.73$, it becomes $\rho_{\rm cr} = 1.0 \times 10^{-29}{\rm g/cm^3} = 4.3 \times 10^{-47}{\rm GeV}^4$.

Observations of the cosmic microwave background (CMB) and the deuterium abundance in the Universe suggest that $\Omega_{\rm baryon} \simeq 0.04$ if the current Hubble expansion rate is $h = H_0/100{\rm km/sec/Mpc} = 0.7$. Although $\Omega_{\rm baryon}$ is much larger than the observed mass in stars, $\Omega_{\rm stars} \simeq 0.005$, it is nevertheless very much smaller than the total energy density in the universe inferred from the observed anisotropy in the cosmic microwave background [427]

$$\Omega_{\rm total} \equiv \frac{8\pi G \rho_{\rm total}}{3H^2} = 1.014 \pm 0.017. \tag{2.244}$$

Both dark matter (DM) and dark energy (DE) are considered essential missing pieces in the cosmic jigsaw puzzle. There is strong evidence of these two unknown components having their contributions as

$$\Omega_m \simeq 1/3, \quad \Omega_{\rm DE} \simeq 2/3 \ . \tag{2.245}$$

We summarize their features based on the three contexts, (1) *When*, (2)*Duration* and (3)*Energy scale* in the followings: *Dark energy*: is characterised that (1) 10 billion years, (2) a few billion years and (3) 10^{-42} GeV, *Dark matter*: (1) 10^{-11}sec, (2) almost history of the universe, (3) of same order dark energy, and *Inflation*: (1) 10^{-32}sec, (2) 10^{-30}sec and (3) 10^{13}GeV.

• Baryogenesis/Baryon asymmetry

The universe is asymmetric: there are more baryons than antibaryons. While antibaryons are produced in accelerator or in cosmic rays, "antigalaxies" are not observed. The relative excess of the baryons

$$B \equiv \frac{(n_{\rm b} - n_{\bar{\rm b}})}{s} \sim 10^{-10} \, , \tag{2.246}$$

is exactly what we need to explain the abundance of light elements and the observations of CMB fluctuations. Any particular model for baryogenesis should possess three ingredients which are independent of the details of the actual theory. These conditions are the so-called *Sakharov's three conditions* as *(1) violation of baryon number*, *(2) C/CP violation* and *(3) non-equilibrium*. First condition is obvious and does not require a long explanation. If baryon number is conserved and is equal to zero at the beginning, it will remain zero forever. If baryon number does not satisfy any conservation law, it vanishes in the state of thermal equilibrium. Therefore we need the third condition. The second condition is less trivia: it is a prerequisite for ensuring a different reaction (decay) rate for particles and antiparticles. If this condition is not met, the numbers of baryons and antibaryons produced are equal and no net baryon charge is generated even if the other two conditions are fulfilled. The Standard Model possesses all the ingredients necessary for the generation of baryon asymmetry. In fact, baryon number is not conserved in topological transitions (the so-called sphaleron process), CP is violated in weak interactions, related to the non zero phase in Cabibbo-Kobayashi-Maskawa (CKM) matrix [254], and the departure from thermal equilibrium naturally occurs in the expanding universe. It would be remarkable if the baryon number could be explained within the Standard Model itself. Unfortunately this seems not to work. The main obstacle is the third condition. For realistic values of the Higgs mass, the electroweak transition is a cross-over and cannot supply us with the necessary strong deviations from thermal equilibrium. Therefore, to explain baryon asymmetry we have to go beyond the Standard Model. There is a wide range of possibilities; **1. GUTs, 2. Leptogenesis** [163] and **3. Affleck-Dine mechanism** [4]. The first one is the idea that baryon number is generically not conserved in Grand Unified Theories such as $SU(5)$. The second approach is that baryon asymmetry can also be generated via leptogenesis. The final baryon number is obtained by $B_f = -\frac{a}{1+a}L_i$ where $a = 28/51$ in the Standard Model. The last one is explaining baryon asymmetry based on supersymmetric theories where ordinary quarks and leptons are accompanied by supersymmetric partners –squarks and sleptons. The corresponding scalar fields carry baryon and lepton number, which can in principle be very large in the case of a scalar condensate [234, 235].

• **Dimensionality problem**

It is described as the fundamental question; why three spatial dimensions we live in ? It must be resolved or answered by only higher dimensional theory than in 4 spacetime dimensions. Superstring theory is such one constructed in 10 dimensional spacetime and hence string theory has the possibility to address to *dimensionality problem*. Superstring theory predicted our world has originally 10 space-time dimensions, although we are only in 3 spatial dimensions. In this point, brane cosmology can allow us to consider a resolution of dimensionality where three-dimensional branes remain as a consequence of its collisions in a nine-dimensional space.

Chapter 3

String theory and Brane-world scenario

Unification of interactions

Among the progress of particle physics, unification of four fundamental interactions, e.g., the strong, week, electromagnetic and gravitational interaction is one of most important subjects. All interactions except for gravity could be unified by grand unified theories. When we discuss about quantization of fields, gravity is again exceptional because it is not *renormalizable*. we have not so far been able to quantize the gravitational interaction. On the other hand, one of most promising approaches is a superstring theory, or M-theory. Such unified theories are usually formulated in higher dimensions than four. In order to unify theories of interactions, one find there exists the *hierarchy problem*, which can be stated that why is the gauge symmetry group of the field theory that is supposed to describe all the phenomena of nature broken not at one, but at two completely different energy levels? For example, in string theory, one would expect it to be broken at the Planck energy $T_{\rm pl} \sim 10^{19}$GeV, but in fact, the symmetry group $SU(2)\times U(1)$ describing the standard electroweak, which is the so-called Weinberg-Saram model [396, 465]) is broken at a much lower energy scale $T_{\rm WS} \sim 100$GeV, which is equal to the mass scale of the gauge bosons for the broken part of the gauge group, i.e., the $W^{\pm}$ and Z bosons. There also exists the difference in the energy levels between the the above energy scales and the energy scale of the Grand Unified Theories (GUTs) $T_{\rm GUTs} \sim 10^{15}$GeV, which are based on gauging a single group such as $SU(5)$ or $SO(10)$ broken to a Standard Model ($SU(3) \times SU(2) \times U(1)$). These differences in energy scales are the root of the hierarchy problem. Superstring/M-theory is higher dimensional theory (10/11-dimensions) more than our known 4 dimensions as seen in this section. These extra dimensions can solve the hierarchy problem because they can lower the value of the Planck mass (see the detail in the section of brane-world). Under the assumption that extra dimensions exist, we must be able to explain why only four dimensions are observed and equivalently, the observational constraint can restrict the extra dimensions. We will the main two constraints from the present experimental data on the ground:

• **Newtonian inverse-square law** [295, 209, 3, 231]

We now see the validity of the Newtons law $F(r) = Gm_1m_2/r^2$ for $r \gtrsim O(0.1\text{mm}) \sim 5 \times 10^{11}\text{GeV}^{-1}$.

• **Accelerator experiment such as hadron collider** [92]

This current energy scale can reach at most $O(\text{TeV}) \sim 10^{-17}$cm, where there no such effect of extra dimensions such as KK modes (seen in the article of Brane-world). The above two limits are used well in the following discussion.

3.1 Superstring theory

In this section, we will explain an concept of superstring theory briefly (see also [366]). We give some important points describing it as follows.

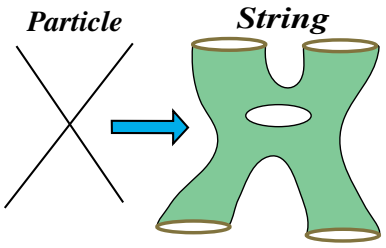

(a)

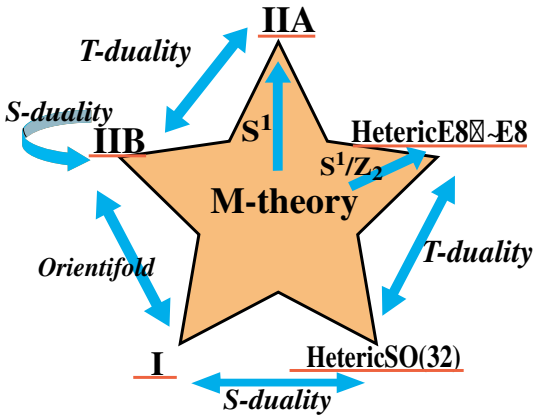

(b)

Figure 3.1: (a): A schematic illustration of string interaction. (b): The relation of M theory and five superstring theories, which the dual symmetries connect each other.

• **String picture:** All particles are made of "String" in the point view of string theory. It is motivated by a quantization of gravity. In order to quantize gravity, one encounter a difficulty of ultraviolet divergence. In the other three forces (weak, electomagnetic and strong), it is usually resolved by a rescaling of the fields and the parameters (*renormalization*) at least at one loop level, however, for the gravitational interaction, the problem appears due to its dimensionful coupling constant as $G_{\rm N} = M_{\rm pl}^{-2}$ and hence is nonrenormalization. This divergence is related to the fact that its interaction occurs at one point in the point view of a Feynman diagram. Therefore, if its diagram is applicable to more one spatial dimensional object (*string*), no pointlike interaction exists and hence it may give a resolution of quantum gravity (see an image in Fig. 3.1(a)). Usually, in the string theory, a dimension of string is called as string's world-sheet. The basic idea is basically described as transition from point particle to one-dimensional object (string).

• **Closed and open strings:** String is classified into two types, that is, closed and open strings. It is determined from their boundary conditions shown in the following. The closed string denotes a graviton, while open string denotes gauge particles and so the string theory has both spin-1 gauge bosons in Standard Model and spin-2 graviton, as expected for an unified theory.

• **Supersymmetry:** Superstring denotes string satisfying symmetry between bosons and fermions (*supersymmetry*). All particle are classified into boson or fermion, depending on their spins and statistical features. Boson has even spin and is related to gauge particle, graviton and Higgs particle, while fermion has odd spin and describes matter fields (quark/lepton). Supersymmetry implies that the two-dimensional field action describing the string theory (3.30), is invariant under a called supersymmetric transformation (3.31), which is generally written by $\delta A = i[\bar{\epsilon}Q, A]$. Here Q is a generator of a Super-Poincare group and satisfies a Super-Poincare algebra in $N = 1$ case $\{Q_\alpha, Q^\dagger_\beta\} = 2P_a(\Gamma^a\Gamma^0)_{\alpha\beta}$ where gamma matrix Γ^a. Super-Poincare group, introduced as an extension of Poincare group, does transform bosons into fermions and visa versa. Supersymmetry is the most general symmetry among all symmetries existing in natural world. It is demanded from resolution of Higgs mass divergence including one loop correction. One loop correction of boson(/fermion) contributes positive(/negative) quantity to calculation of Higgs mass. Moreover supersymmetry makes a unwanted tachyon states, having a negative mass, vanish with the so-called GSO condition as seen around (3.9). Supersymmetry surely breaks in the present time (it is often estimated at $T \sim 1$TeV). But it is thought to be keep in the very early universe. It is perhaps related to the dark energy and dark matter and so very important symmetry (see Sec. 2.4).

• **10 dimensional theory:** (Super)string theory is described in higher dimensional spacetime than our

four dimensional world. This demanding comes from symmetries which string theory has: Poincare invariance, different coordinate invariance and Weyl (conformal) invariance. As a result, Superstring(/bosonic) string has no anomaly in just $D = 10(/26)$ dimensional spacetime. For bosonic string, in order to quantize string, one usually use methods of light-cone gauge or Gupta-Blea quantization or path integral or BRST(Becchi-Rouet-Stora-Tyutin) quantization (which we don't explain in this thesis), however, all quantizations show $D = 26$ to make theory self-consistent. Similarly, superstring is made to be self-consistent in NSR(Neveu-Schwarz-Ramand) formulation or GS(Green-Schwarz) one and both shows $D = 10$. The fundamental theory is described in ten dimensional spacetime, but our world is four. So it is important that know how one can obtain a realistic world from such a higher dimensional theory. Such question how this extra dimensions be is related to the issue of *compactification* discussed as follows.

• **Compactification:** There are many different ways to compactify the six dimensions, and string theory does not say which realization must be found in nature. It only puts some restraints on the allowed types of compact dimensions. They must form a special kind of manifold, called a Cakabi-Yau space. Thus one way of fixing the number of dimensions to four is to compactify six dimensions to a tiny Calabi-Yau space, which is smaller than we can detect with current technology. But there are still millions of different Calabi-Yau spaces to choose among. This compactification is used in the ekpyrotic universe scenario and in KKLT model [225]. Another simple compactification is the Kaluza-Klein compactification [230, 251] such as toroidal one, which is used for introduction of D-branes (see the further article, named T-duality) and in ADD model [16] (see the article, ADD model). Thus the higher dimensional theory has a possibility of explaining the fundamental question why our world is four. It is very interesting topic, the so-called *dimensionality problem* as discussed below.

• **No free parameter:** String theory has basically only one unknown constant parameter as a string length $l_{\rm s}$. This scale is related to string tension T as $l_{\rm s} \propto T^{-1/2}$. No other adjustable constants exists.

• **Uniqueness:** Demanding that the two dimensional world-sheet quantum field theory has supersymmetry, there exists five different types known as consistent superstring theories, i.e., I, IIA, IIB, Heterotic $SO(32)$ and Heterotic $E8 \times E8$. But their types are related to each other in terms of several dualities and hence they are thought to be unified in more one dimensional ($D = 11$) theory (called it M theory). The dual relations among these theories are shown in the Fig. 3.1(b), where S-duality denotes a weak-strong coupling duality $g_s \to 1/g_s$, T-duality is a duality in a toroidally compactified theory with radius R. It denotes invariance to radius-dependent rescaling $R \to \alpha'/R$ as seen in more detail in the following section.

3.1.1 Bosonic string spectrum

Let us try to make a quantum theory of bosonic strings for simplify. When we formulated the action principle for the usual zero dimensional point particle, we use as the relativistic action the length of the particle's world-line. The action of a point particle is obtained by $S = -m\int ds = -m\int d\tau\sqrt{-(\partial_\tau X)^2}$ where m is the rest mass of the particle. Notice that the $L = \int \tau\sqrt{-(\partial_\tau X)^2}$ term denotes the length of the particle's world-line (see Fig. 3.2(a)). If we want to consider a two-dimensional world-sheet $\sigma^a = (\tau, \sigma)$, it is easy to be extended by using the area of the world-sheet of the string A and the action of the string is given as

$$S_{\rm NG} = -T \cdot A = -T \int d\tau\ d\sigma \sqrt{-(\det h_{ab})^2}\,, \quad \text{with} \quad h_{ab} \equiv \partial_a X^\mu \partial_b X_\mu\,, \tag{3.1}$$

where X^μ is the vector-valued function in D-dimensional Minkowski spacetime and T denotes the tension of the string related to the string coupling constant α', which has square of length of the string $l_{\rm s}$ as

$$T = \frac{1}{2\pi\alpha'} = \frac{1}{2\pi l_{\rm s}^2}\,. \tag{3.2}$$

This action is the so-called *Nambu-Goto* action. Introducing an independent world-sheet metric γ_{ab}, the equivalent to it is the so-called *Polyakov* action given by

$$S_{\rm P} = -\frac{T}{2}\int d\tau\ d\sigma\sqrt{-\gamma}\gamma^{ab}h_{ab}\,. \tag{3.3}$$

The equivalence $S_{\rm NG} = S_{\rm P}$ can be seen by varying $S_{\rm P}$ with respect to γ_{ab} and plugging the solution back into the action. The action $S_{\rm p}$ shows several symmetries: **(1)**. D-dimensional Poincare invariance under which X transforming $X \to \Lambda X + a$, γ_{ab} are invariant, where a is a translation vector. **(2)**. Diffeomorphism invariance under which X are invariant, and γ_{ab} transforms like a rank two covariant tensor $\gamma_{ab} \to \frac{\partial\sigma^c}{\partial\sigma'^a}\frac{\partial\sigma^d}{\partial\sigma'^b}\gamma_{cd}$. **(3)**. Two-dimensional Weyl invariance under which X are invariant, and γ are rescaled by an arbitrary function $\omega(\tau,\sigma)$ as $\gamma_{ab} \to \exp(2\omega)\gamma_{ab}$. These total three symmetries on the world-sheet has three independent degrees of freedom related by the fact that the world-sheet metric γ are a 2 by 2 matrix. We can use three gauge symmetries to fix a gauge where the world-sheet metric is diagonal, $\gamma_{ab} = \mathrm{diag}(-1,1)$. This gauge is called conformal gauge. In this case, we vary the Polyakov action with respect to the fields X^μ and obtain the following EOM

$$(\partial_\tau^2 - \partial_\sigma^2)X^\mu = 0\,. \tag{3.4}$$

For the boundary condition, we impose the Neumann conditions [1] at $\sigma = 0,\pi$ where $\sigma \in [0,\pi]$: $\partial_\sigma X^\mu(\tau,\sigma=0) = 0$ and $\partial_\sigma X^\mu(\tau,\sigma=\pi) = 0$, and yields the solution describing the open string:

$$X^\mu(\tau,\sigma) = x^\mu + 2\alpha' p^\mu\tau + i\sqrt{2\alpha'}\sum_{n\neq 0}\frac{1}{n}\alpha_n^\mu e^{-in\tau}\cos(n\sigma)\,. \quad \text{open strings} \tag{3.5}$$

On the other hand, for the second choice of boundary, imposing the condition to $\sigma \in [0,2\pi]$: $X^\mu(\tau,\sigma+2\pi) = X^\mu(\tau,\sigma)$, we also obtain the solution of the closed strings:

$$X^\mu(\tau,\sigma) = x^\mu + \alpha' p^\mu\tau + i\sqrt{\frac{\alpha'}{2}}\sum_{n\neq 0}\frac{1}{n}\big[\tilde{\alpha_n^\mu}e^{-in(\tau+\sigma)} + \alpha_n^\mu e^{-in(\tau-\sigma)}\big]\,. \quad \text{closed stings} \tag{3.6}$$

Here x^μ and p^μ are the average position and total momentum in the center of mass, respectively. The coefficient $\tilde{\alpha}$ and α indicate the oscillation modes and correspond to left and right-moving mode, respectively. The open string has the endpoints on the boundary. These two modes of oscillation in closed strings are related to the rank two tensor indicating gravity $g_{\mu\nu}$. Define light-cone coordinate in spacetime $X^\pm = (X^0 \pm X^1)/\sqrt{2}$ and X^i where $i = 2,\dots D-1$. In this gauge, for the open strings, $X^+ = \alpha' p^+\tau$ and X^+ is not a dynamical variable. To quantize the motion and oscillations of the string, we define the conjugate momentum density by $\Pi \equiv \delta L/\delta(\partial_\tau X)$ and impose the following relations

$$[x^-, p^+] = i\eta^{-+} = -i\,, \quad [X^i(\sigma), \Pi(\sigma)^j] = i\delta^{ij}\delta(\sigma-\sigma')\,. \tag{3.7}$$

Its Fourier components are written in

$$[x^i, p^j] = i\delta^{ij}\,, \quad [\alpha_m^i, \alpha_n^j] = m\delta^{ij}\delta_{m,-n}\,. \tag{3.8}$$

The mass spectrum give by $m^2 = 2p^+H - p^ip^i$ is obtained by

$$m^2 = \frac{1}{\alpha'}\Big(N + \frac{2-D}{24}\Big)\,, \tag{3.9}$$

[1] Notice that for the open strings, we have imposed the Neumann boundary conditions, however, since we can specify boundary conditions separately for each edges of the open string, we indicate these conditions by calling it a NN, ND, DN and DD strings where D denotes the Dirichlet boundary condition defined by a some constant vector b^μ as $X^\mu = b^\mu$ and the first letter indicating the condition at $\sigma = 0$, and the second at $\sigma = \pi$. Of course, in all cases, it can also be solved and quantized. We will only quantize the NN open string, but we will later see the appearance of DD open strings, indicating the existence of physical objects that correspond to the surfaces on which the endpoints of those string are attached.

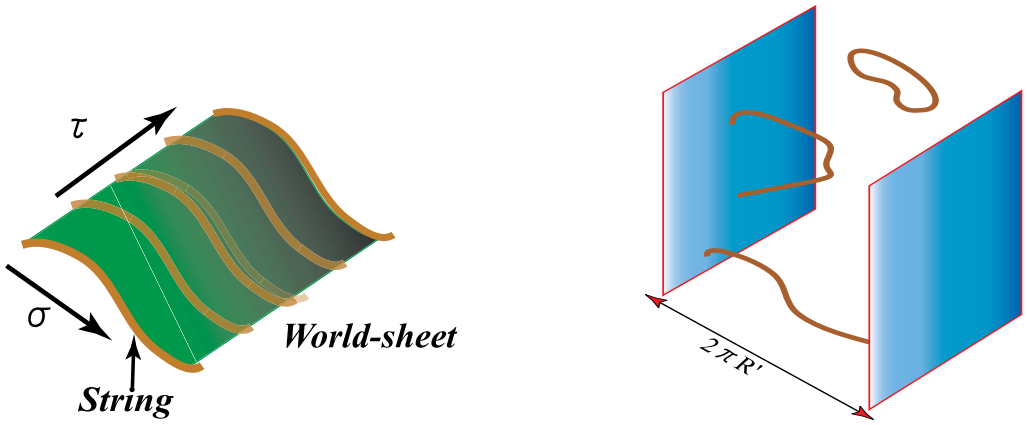

(a) (b)

Figure 3.2: (a): Two dimensional world-sheet of stings (b): T-duality and D-branes, which open string ends on and closed string can travel freely.

where N denotes the level of energy. The lightest ($N = 0$) state $|0; k\rangle$ has the negative mass $m^2 = \frac{2-D}{24\alpha'}$ for $D > 2$. This state is the so-called *tachyon* and indicates an instability in the theory. We will ignore this complication, since the tachyon doesn't appear in the supersymmetric string theory, which is related to the so-called GSO condition. The lowest excited states ($N = 1$) of the string, which defined by a creation operator α^i_{-n}, are obtained by

$$\alpha^i_{-1}|0; k\rangle\,, \quad m^2 = \frac{26 - D}{24\alpha'}\,. \tag{3.10}$$

Lorentz invariance now requires a specific value of D. Imposing it to be massless particles, the number of spacetime dimensions for Lorentz-invariant spectrum is only determined to be

$$m^2 = 0\,, \qquad D = 26\,. \tag{3.11}$$

This is important result of critical dimensions for the boson strings. Similarly, the closed strings also can be canonically quantized in this light-cone gauge. So far we have used the light-cone quantizing method, however, if we try to other quantization (see the above heading named 10 dimensional theory), demanding that the quantized theory should exhibit the symmetries of the classical action (Lorentz, diffeomorphism and Weyl) leads also to the conclusion that $D = 26$. But we will not drive these results in this thesis. Considering the supersymmetry string, the critical dimension can be obtained as $D = 10$ Varying the action with respect to γ_{ab} gives the another EOM for the world-sheet metric $\delta S_{\rm P}/\delta\gamma_{ab} = 0$. This equation does not contributed to by the Einstein-Helbert term in the action since that is a topological term invariant under small variations of the metric in the two dimensional spacetime. Notice the trace of this equation is satisfied irrespective of the values of X and γ, which follows from the Weyl symmetry of the two dimensional field theory, related to the vanishing trace of energy-momentum tensor $T^a_a = 0$. This equation is called Virasoro constraint condition and we impose these conditions on the mass spectrum and obtain the final results for both types of strings as

$$m^2 = \begin{cases} (N-1)/\alpha' & \text{open strings} \\ 2(N + \tilde{N} - 2)/\alpha' & \text{closed strings} \end{cases} \tag{3.12}$$

where N and $\tilde{N}$ correspond to the left- and right-going oscillation modes for the closed strings, respectively and they must have the same value $N = \tilde{N}$, the so-called level-matching condition. Neglecting the tachyon

states having negative squared mass, we see that we get massless (first excited) states $m^2 = 0$ when $N = 1$ for the open string, and when $N+\tilde{N}-2$ for the closed string. Thus we can construct the following massless states:

• **Open string state:** $\alpha^i_{-1}|0;k\rangle$

It represents the open string with no oscillators excited and momentum. This massless state is gauge field A_i like photon.

• **Closed string state:** $\alpha^i_{-1}\alpha^j_{-1}|0,0;k\rangle$

These states have 2-tensor properpty under $SO(D-2)$. It reads that any tensor e^{ij} can be decomposed

$$e^{ij} = G_{ij} + B_{ij} + \phi\,, \quad \text{where } G_{ij} = \frac{1}{2}\Big(e^{ij} + e^{ji} - \frac{2}{D-2}\delta^{ij}e^{kk}\Big)\,, \;\; B_{ij} = \frac{1}{2}(e^{ij} - e^{ji})\,, \;\; \phi = \frac{1}{D-2}\delta^{ij}e^{kk}\,. \tag{3.13}$$

The traceless tensor G_{ij} denotes graviton state, the antisymmetric tensor B_{ij} is called a Kalb-Ramond state and a scalar ϕ is called dilaton state. Since string theory hopes to be a correct quantum theory of gravity, it is good to see that graviton is included in the spectrum.

3.1.2 T-duality and D-brane

We consider a toroidal compactification on radius R by identification as $X^{25} \sim X^{25} + 2\pi Rw$ with integer w. Under this radial compactification, for the closed strings, the field X^{25} in invariant such as $X(\sigma + 2\pi) = X(\sigma) = X(\sigma) + 2\pi Rw$ and can be reduced to

$$X = x + 2P\tau + wR\sigma + \sum\big[e^{-in(\tau+\sigma)}\ldots\big] \tag{3.14}$$

and yields the mass spectrum

$$m^2 = \frac{n^2}{R^2} + \frac{w^2R^2}{\alpha'^2} + \frac{2}{\alpha'}(N + \tilde{N} - 2)\,, \qquad \text{with } N - \tilde{N} = nw\,, \tag{3.15}$$

where n and w are called momentum and winding number, respectively. From the above equation, we see that if we do the transformation $n \Leftrightarrow w$, $R \Leftrightarrow \alpha'/R$, we get the same spectrum of states as before. This is the so-called *T-duality* of the theory. This symmetry can gives the minimum radius, the so-called *"self-dual" radius* close to the string scale,

$$R \Leftrightarrow \alpha'/R \;\Rightarrow\; R \sim \sqrt{\alpha'} \sim l_s\,, \quad (\text{self} - \text{dual radius}) \tag{3.16}$$

and leads to several non-singular universe models, where the so-called *Pre-big bang* [174, 175, 176, 458] , *Ekpyrotic universe* scenarios [246, 432, 247] and *String gas cosmology* [64, 66] etc exist (see in the next section).

The open string don't have a conserved quantum number like the winding number for the closed strings. Notice that instead of Neumann boundary conditions, we now have Dirichlet conditions on X' in the 25 direction,

$$X'^{25}(\tau, \sigma = 0) = x'^{25}\,, \quad X'^{25}(\tau, \sigma = \pi) = x'^{25} + 2\pi\alpha'\frac{n}{R}\,. \tag{3.17}$$

We can give the difference in the X'^{25} for the two ends of the string in terms of the compactification radius of the T-dual coordinate.

$$X'^{25}(\sigma = \pi) - X'^{25}(\sigma = 0) = 2\pi nR'\,. \tag{3.18}$$

Since the radius of the circle in the T-dual theory is R', this says that both ends of the open string end on the same hyperplane, a so-called D24-brane (see Fig. 3.2(b)), since it extends itself in 24 spatial dimensions; the directions we have not T-dualized. The D in the word D-brane, denotes the Dirichlet. The possibility of interaction between different strings implies that all string endpoints end on the same

hyperplane. The open string ends on this hypersurface, on the other hand, the closed string, e.g. graviton, can escape into the T-dualized direction called the bulk. This inspiration leads to a *Brane-world. By compactifying several orthogonal dimensions, we can make D-branes of arbitrary dimensions.* A dualization parallel to the tangent space of a brane reduces its dimension by one, and a dualization orthogonal to the tangent space increase the dimension by the same amount. The D-brane in bosonic string theory is this hypersurface to which the string endpoints are attached. In this case it is a flat, static plane, but a general brane is a dynamical surface moving around in the higher dimensional space. In super-symmetric string theory there is no tachyon, and many brane states are stable. The crucial difference is that the super-symmetric branes carry a conserved charge. The conservation of this charge prohibits the branes from decaying. They are therefore possible candidates for brane universe. The action of $\mathrm{D_p}$-brane, where p indicates spatial dimensions the brane has, is given by

$$S = -T_p \int d^{p+1}\xi e^{-\phi}\sqrt{\det(G_{ab} + B_{ab} + 2\pi\alpha' F_{ab})}\,, \tag{3.19}$$

where T_p is the brane tension, which can be said to be the energy density per volume inherent in the brane. The factor $e^{-\phi}$ describes the brane's coupling to the bulk dilaton field ϕ. $G_{ab} = G_{\mu\nu}\partial_{\xi^a} X^\mu \partial_{\xi^b} X^\nu$ is the pullback of the spacetimes metric from spacetime to the brane volume, and similarly for the antisymmetric B_{ab} Kalb-Ramond bulk two-form field. The action is so-called the Dirac-Born-Infeld action. The action can be derived by finding a solution of string theory on a background containing a $\mathrm{D_p}$-brane, and then demanding that it satisfies conformal invariance. This derivation is out of the scope of this thesis. In the superstring theory, this action (3.19) has to be added by a charge term $\mu_p \int C_{p+1}$. Calculating the one-loop string amplitude, Plochinski (95) [365] showed that the $\mathrm{D_p}$-brane has the so-called RR charge and tension give by

$$\mu_p = (2\pi)^{\frac{7-2p}{2}}(4\pi^2\alpha')^{\frac{3-p}{2}}\,, \qquad T_p = \frac{\sqrt{\pi}}{\kappa}(4\pi^2\alpha')^{\frac{3-p}{2}}\,, \tag{3.20}$$

respectively.

3.1.3 Hagedorn temperature

In the string theory, there exists the maximal value of the temperature, the so-called *Hagedorn temperature* [198, 366] where the thermal partition function of strings diverges. The partition function including a 1-loop correction at high weight h, is approximated by $Z(\tau) \approx \exp(4\pi/l)$ where $l = \tau/i$. On the other hand, using the relation $m^2 = 4(h-1)/\alpha'$, it becomes

$$Z(\tau) = \int_0^\infty dm\, n(m)\exp(-2\pi h l) = \int_0^\infty dm\, n(m)\exp(-\alpha'\pi m^2 l)\,, \tag{3.21}$$

and the equivalence between them implies that the density of string states $n(m)$ grows exponentially as $n(m) \approx \exp(4\pi m\sqrt{\alpha'})$. The thermal partition function is given by

$$\int_0^\infty dm\, \exp(4\pi m\sqrt{\alpha'})\exp(-m/T) = \int_0^\infty dm\, \exp(m(1/T_{\mathrm{H}} - 1/T))\,, \quad \text{where } T_{\mathrm{H}} \equiv \frac{1}{4\pi\sqrt{\alpha'}}\,. \tag{3.22}$$

It is seen that if temperature is greater than the *Hagedorn temperature* $T > T_{\mathrm{H}}$, it diverges since the density of states grows exponentially and it therefore exists the maximum temperature. The Hagedorn temperature will appear in the string gas cosmology as further section.

3.1.4 Supergravity

We will consider the effective action at the low energy limit of string theory (see also review [283]). A closed string is generated by bosonic string, whose massless modes are described by a nonlinear sigma model [84]

$$S_\sigma = -\frac{1}{4\pi\alpha'}\int d^2\sigma\sqrt{-\gamma}\Big(\gamma^{ab}G_{\mu\nu}(X)\partial_a X^\mu \partial_b X^\nu + \epsilon^{ab}B_{\mu\nu}(X)\partial_a X^\mu \partial_b X^\nu + \alpha'\phi(X)R^{(2)}\Big), \tag{3.23}$$

where γ^{ab}, $(2\pi\alpha')$, $G_{\mu\nu}$ and $B_{\mu\nu}$ denote the world-sheet metric, the inverse string tension, the background space-time metric and the background antisymmetric tensor, respectively. The last term represents a topological one where ϕ is a background dilaton, coupled to the world-sheet Ricci scalar $R^{(2)}$. The string coupling is related to the dilaton as $g_s = e^{\phi_0}$. Varying the action (3.23) with respect to the fields X^μ, we obtain equations of motion for stirng in a general space-time

$$\partial_a\Big(\sqrt{\gamma}\gamma^{ab}\partial_b X^\mu\Big) + \Gamma^\mu_{\lambda\nu}\sqrt{\gamma}\gamma^{ab}\partial_a X^\lambda\partial_b X^\nu + \frac{1}{2}H^\mu_{\lambda\nu}\epsilon^{ab}\partial_a X^\lambda\partial_b X^\nu = 0. \tag{3.24}$$

one additionally must satisfy the constraint equations

$$G_{\mu\nu}(X)\Big(\partial_a X^\mu(\sigma,\tau)\partial_b X^\nu(\sigma,\tau) - \frac{1}{2}\gamma_{ab}\gamma^{cd}\partial_c X^\mu\partial_d X^\nu\Big) = 0. \tag{3.25}$$

The background fields, $G_{\mu\nu}, B_{\mu\nu}$, and ϕ, are realized as couplings of the non-linear sigma model and these couplings evolve in accordance with the corresponding beta functions. Thanks to it, the trace of the world-sheet stress tensor given by

$$T^a_a = \beta^G_{\mu\nu}\sqrt{\gamma}\gamma^{ab}\partial_a X^\mu\partial_b X^\nu + \beta^B_{\mu\nu}\epsilon^{ab}\partial_a X^\mu\partial_b X^\nu + \beta^\phi\sqrt{\gamma}R^{(2)}, \tag{3.26}$$

vanishes, where the β functions are found [84]

$$\begin{aligned}
\beta^G_{\mu\nu} &= \Big(R_{\mu\nu} + 2\nabla_\mu\nabla_\nu\phi - \frac{1}{4}H_{\mu\kappa\sigma}H_\nu{}^{\kappa\sigma}\Big) + \mathcal{O}(\alpha'),\\
\beta^B_{\mu\nu} &= \Big(\nabla^\kappa H_{\kappa\mu\nu} - 2\nabla^\kappa\phi H_{\kappa\mu\nu}\Big) + \mathcal{O}(\alpha'),\\
\beta^\phi &= \frac{1}{\alpha'}\Big(\frac{D-26}{48\pi^2}\Big) + \Big(4\nabla_\kappa\phi\nabla^\kappa\phi - 4\nabla_\kappa\nabla^\kappa\phi - R + \frac{1}{12}H_{\kappa\mu\nu}H^{\kappa\mu\nu}\Big) + \mathcal{O}(\alpha'),
\end{aligned} \tag{3.27}$$

with $H = dB$ denoting the field strength of $B_{\mu\nu}$. Therefore the conformal invariance at the quantum level leads

$$T^a_a = 0 \Longleftrightarrow \beta^G_{\mu\nu} = \beta^B_{\mu\nu} = \beta^\phi = 0\,. \tag{3.28}$$

Keeping terms tree level in α', these equations of motion can be derived from an effective action at low energy limit of supergravity in D space-time dimensions

$$S_0 = \frac{1}{2\kappa_D^2}\int d^Dx\sqrt{-G}e^{-2\phi}\Big(R + 4(\nabla\phi)^2 - \frac{1}{12}H^2\Big)\,, \tag{3.29}$$

where D takes the critical dimensions as $D = 26$ ($D = 10$) for the bosonic (super) string. The prefactor takes the form $2\kappa_D^2 = (2\pi\sqrt{\alpha'})^{D-2}g_s^2(2\pi)^{-1} = 16\pi G_D$ where $l_s = \sqrt{\alpha'}$ is the string length and G_D is the D dimensional Newton constant.

Superstring: In the superstring theory, the world-sheet action for a free string is

$$S = \frac{1}{4\pi\alpha'}\int d^2\sigma\eta_{\mu\nu}\left[\eta^{\alpha\beta}\partial_\alpha X^\mu\partial_\beta X^\nu + i\bar\psi^\mu\gamma^\alpha\partial_\alpha\psi^\nu\right]\,. \tag{3.30}$$

The spinors on the world-sheet are denoted by $\psi^\mu = \psi^\mu(\tau,\sigma)$. Eq. (3.30) becomes supersymmetric if it is invariant under the infinitesimal transformation:

$$\delta X^\mu = i\bar\epsilon\psi^\mu, \qquad \delta\psi^\mu = \gamma^\alpha\partial_\alpha X^\mu\epsilon\,. \tag{3.31}$$

Here ϵ represents a constant anti-commuting spinor. The corresponding EOMs are the two dimensional Dirac equations:

$$\left(\frac{\partial}{\partial\sigma} + \frac{\partial}{\partial\tau}\right)\psi^\mu_R = 0\,, \quad \left(\frac{\partial}{\partial\sigma} - \frac{\partial}{\partial\tau}\right)\psi^\mu_L = 0\,. \tag{3.32}$$

We can impose boundary conditions to these equations. Closed strings have either periodic or anti periodic boundary condition for left and right moving ones, i.e., $\psi^{\mu}_{L,R}(\sigma = 2\pi) = \pm\psi^{\mu}_{L,R}(\sigma = 0)$. Here a periodic and anti periodic boundary condition are called the Ramond (R) sector [371] and the Neveu–Schwarz (NS) sector [336, 337], respectively. Thus one has four possibilities. The bosons have the NS–NS and RR sectors, on the other hand the fermions have the NS–R and R–NS sectors. The effective action for the massless superstring can be also derived in [84, 155, 156, 412, 296]. There are different ways of quantizing two-dimensional world-sheet having super-symmetry, leading to the five known consistent string theories (Type I of open and closed strings, Type IIA of IIB of closed strings, $E_8 \times E_8$ or $SO(32)$ Heterotic of closed strings) (see Fig. 3.1(b)). The along with duality relations among these different string theories and the existence of an 11 dimensional theory that reduces to these five different string theories at different weak coupling, the so-called M-theory. Here we write only the effective action for Type IIA superstring.

Type IIA superstring: in which the effective bosonic action referring to $N = 2$, $D = 10$, is given by

$$S_{\rm IIA} = \frac{1}{16\pi\alpha'^4}\left\{\int d^{10}x\sqrt{|g_{10}|}\left[e^{-\phi}\left(R_{10} + (\nabla\Phi)^2 - \frac{1}{12}H_3^2\right) - \frac{1}{4}F_2^2 - \frac{1}{48}(F_4{}')^2\right] + \frac{1}{2}\int B_2 \wedge F_4 \wedge F_4\right\} \tag{3.33}$$

where R_{10} is the Ricci scalar of a metric g_{MN} and $g_{10} \equiv \det g_{MN}$. The antisymmetric tensor field strengths are defined by $H_3 = dB_2$, $F_2 = dA_1$, $F_4 = dA_3$ and $F_4' = F_4 + A_1 \wedge H_3$, where X_p and d denote an antisymmetric p–form potential and the exterior derivative, respectively. The last term in Eq. (3.33) is called a Chern–Simons term.

3.2 Brane-world

String theory predicts a new type of nonlinear structure, called *(D-)brane*, a nomenclature created artificially from "membrane". It is a boundary layer on which edges of open strings stand. This idea suggests a new perspective in cosmology, that is we are living in a brane world, which corresponds to three-dimensional hypersurface in a higher-dimensional spacetime. This new picture of the universe is the so-called *Brane-world*. In this section, we first overview several types of brane-worlds: **(1) Domain wall model**: is first idea of the brane, proposed by Rubakov and Shaposhinkov [387] and independently by Akama [6]. **(2) ADD model** (Arkani-Haned, Dimopoulos and Dvali): proposed by [16], relating to a Kaluza-Klein type compactification [230, 251]. **(3) RS model** (Randall and Sundrum): proposed by [373] **(4) DGP model** (Dvali, Gabadaze and Porrati): proposed by [131], **(5) D$\bar{\rm D}$ -branes inflation model**: proposed by [130, 369], gives us inflaton as a distance between two branes, **(6) Ekpyrotic model**: proposed by [246], which is a colliding branes universe scenario as similar to the D$\bar{\rm D}$-branes inflation model and it is ordinary called the ekpyrotic or cyclic universe scenario, which is main topic of the thesis and will be reviewed in details in the next chapter. **(7) KKLT model** (Kachru, Kallosh, Linde and Trivedi): proposed by [225], which is interesting as model implying a de Sitter vacuum in the string theory.

3.2.1 Domain wall model

Following [387], let us consider a toy model of brane-world and start with a scalar field in five-dimensions given by $\mathcal{L} = -\frac{1}{2}\partial_A\Phi\partial^A\Phi - \frac{\lambda}{4}\Big(\Phi^2 - \eta^2\Big)^2$. We find a kink solution, called domain wall given by,

$$\Phi_{\rm K}(y) = \eta\tanh\Big(\sqrt{\lambda\eta^2/2}\,y\Big) \equiv \eta\tanh\big(m_0 y\big)\,. \tag{3.34}$$

Since transverse to the domain wall is one dimensional, the domain wall is a codimension one object. Its tension is given by $\sigma = \int dy T_{00}(\Phi_{\rm K})$, where T_{00} denotes the (0,0) component of the stress tensor and is determined as follows $\sigma \sim m_0^3/\lambda \sim \sqrt{\lambda}2^{-3/2}v^3$. In the presence of the domain wall, by solving the linear

equation of motion for the field Φ, $\Phi(x^\mu, y) = \Phi_{\rm K}(y) + \delta\Phi(x^\mu, y)$, we find that the four-dimensional part of perturbation $\rho(x^\mu)$ as $\delta\phi(x^\mu, y) = (d\Phi_{\rm K}/dy)\rho(x^\mu)$ satisfies the equation $\partial_\mu^2\rho = 0$, where ρ is the wave function of a massless particle. It means that these particles live just on the brane, that is localization on the brane. Next, let us now introduce five-dimensional fermions given as

$$\mathcal{L}_\Psi = i\bar{\Psi}\Gamma^M\partial_M\Psi - g\Phi\bar{\Psi}\Psi\,. \tag{3.35}$$

It leads to the corresponding EOM, which is obtained by

$$i\Gamma^M\partial_M\Psi - g\Phi_{\rm K}\Psi = 0\,. \tag{3.36}$$

Using massless chiral mode χ_L, it has a normalizable solution as

$$\Psi(x^\mu, y) = \exp\Big[-\int_0^y g\Phi_{\rm K}(z)dz\Big]\chi_L(x^\mu)\,, \text{with}\;\; i\Gamma^\mu\partial_\mu\chi_L = 0\;\; \text{and}\chi_L = (1-\gamma_5)\chi/2\,. \tag{3.37}$$

From this equation, we can also conclude that chiral mode is localized on the domain wall. As you seen, in this simple model, a scalar field and fermions can be localized on the brane. Moreover, in order to build a realistic model building, the model satisfies two properties on a brane: *1. Localization of a gauge fields* and *2. construction of four-dimensional gravity*

3.2.2 ADD model

First, we will explain the Kaluza-Klein theory [230, 251]. In the Kaluza-Klein (KK) approach, they envisioned five-dimensional spacetime to which general relativity was applied. One of the spatial dimension was assumed to be "compactified " to a small circle with a radius L leaving four-dimensional spacetime extended infinitely as we see it. If the extra dimension is compactified on a circle with radius L, it reads $y \to y + 2\pi L$ as $\Phi(x^\mu, y) = \Phi(x^\mu, y + 2\pi L)$. An solution to a five-dimensional Klein-Gordon equation for massless particles, $\Box\Phi(x^\mu, y) = 0$, is given by

$$\Phi(p^\mu, y) = e^{ip^\mu x_\mu}\cdot e^{iny/L}\,, \tag{3.38}$$

where $n = 0, \pm1, \pm2\ldots$. Four-momentum p^μ and n satisfy

$$p^\mu p_\mu + \frac{n^2}{L^2} = 0\,. \tag{3.39}$$

Then the spectrum can be obtained for *zero mode*, $n = 0$ and *Kaluza-Klein(KK) modes*, $n \neq$ with the mass

$$m_n = \frac{|n|}{L}\,. \tag{3.40}$$

It means that the zero mode is only important for low energy ($E \ll 1/L$) while all the KK modes are important for high energy ($E \gg 1/L$). The compactified radius L must be constrained as $L \lesssim 10^{-17}$cm since no KK mode particles have been observed in an energy scale of present accelerator experiments O(TeV) [92]. Based on a brane world picture, a new type of KK cosmology was proposed by Arkani-Hamed, Dimopolos and Dvali (ADD) [16]. They considered simple situation where the brane width is taken to be zero and all extra dimensions have equal size L. We shall discuss a four-dimensional gravity in this scenario. The zero mode has an effective action as

$$\frac{M_{(4+N)}}{2}\int d^4x\int_0^{2\pi L} d^Ny\sqrt{G}\,{}^{(4+N)}R \to \frac{M_{(4+N)}^{2+N}(2\pi L)^N}{2}\int d^4x\sqrt{{}^{(4)}g}\,{}^{(4)}R\,, \tag{3.41}$$

hence, we can obtain the four-dimensional Planck mass,

$$M_{\rm pl}^2 = M_{(4+N)}^{2+N}(2\pi L)^N\,. \tag{3.42}$$

It is seen in this ADD model that the ordinary matter fields are confined on a brane, the extra dimensions are not necessarily required to be so small. This might also be connected with a conjecture that the mass scale $M_{(4+N)}$ in (4+N)-dimensional spacetime at the more fundamental level is as low as $\sim$ TeV, nearly the same as the electroweak mass scale. This removes what is called a *hierarchy problem*. Setting the quantum gravity scale to be $M_{(4+N)} \sim$ TeV, the size of extra dimensions can be obtained as,

$$L \sim 10^{30/N-17}\text{cm}\,. \tag{3.43}$$

For $N = 1$, it leads to $L \sim 10^{13}$cm. Experimental data limiters the validity of the Newtonian inverse-square law for $O(0.1\text{mm}) \lesssim r$ [231, 295]. For $N = 2$, it shows $L \sim 10^{-2}$cm, that is *submillimeter* distances, corresponding to the lowest value which the Newton's law has been tested above. Therefore *it shows a possibility of the unification scale within reach of our near-future experiments*. It implies an important possibility that black hole can be produced in an accelerator such as the CERN Large Hadron Collider [92]. This idea is motivated by the fact that the radius of black holes (called *Shwarzschild radius* $r_{\rm sch}$) in the extra-dimensional scenario, is *10^{32} times larger than that of the usual black holes with the same mass* (see [26, 476]). The Shwarzschild radius is given as $r_{\rm sch} \sim (G_{(4+N)}M)^{1/(N+1)}$ and hence the ratio to the usual radius ${}^{(4)}r_{\rm sch} \sim GM$ is estimated by

$$\frac{{}^{(4+N)}r_{\rm sch}}{{}^{(4)}r_{\rm sch}} \sim \left(\frac{M_{\rm pl}^2}{M_{(4+N)}}\right)\left(\frac{M}{M_{(4+N)}}\right)^{-\frac{N}{N+1}} \sim 10^{32}\left(\frac{M}{M_{(4+N)}}\right)^{-\frac{N}{N+1}}\,, \tag{3.44}$$

where we take $M_{(4+N)}$ TeV scale. This scenario is also ordinarily called *large extra dimension model*.

3.2.3 RS model

New approaches for extra dimensions proposed by Randall and Sundrum are also very important [373]. In their first paper(RSI), they proposed a mechanism to solve the hierarchy problem by a small extra dimension, while in their second paper(RSII), they proposed a single brane model with a positive tension, where 4D Newtonian gravity can be achieved. This mechanism provides us an alternative compactification of extra dimensions and it is called "*warped compactification*". RS brane-world is described by the following action

$$S = \frac{M_5^3}{2}\int d^5x\sqrt{-g}(R - 2\Lambda_5) - \sum_i \int d^4x\sqrt{-q_i}(\sigma_i + L_{\text{matter(i)}})\,, \tag{3.45}$$

where M_5 and Λ_5 are the fundamental scale of gravity and cosmological constant in five-dimension, respectively and σ_i is the tension of the i-th brane.

RSI: considers two branes placed at $y = 0$ and $y = L$ and the Z_2-symmetry is imposed as $y \to -y$ and $y + L \to -y + L$. One is called *visible*-brane, that is our-world at $y = L$, the other is *hidden*-brane at $y = 0$. We assume that the metric ansatz takes the form $ds^2 = a^2(y)\eta_{\mu\nu}dx^\mu dx^\nu + dy^2$. With this ansatz, we find a "warp factor" solution of the Einstein equations as

$$a(y) = e^{-k|y|}\,, \quad \text{with} \quad k = \sqrt{\frac{-\Lambda_5}{6}}\,, \tag{3.46}$$

where $\Lambda_5 = -6k^2$ is negative. It implies that the spacetime between the two 3-branes is a 5-dimensional Anti de Sitter*(AdS)* geometry. We can also see that the branes have equal and opposite tensions $\sigma_1 = -\sigma_2 = 6\Lambda_5^3 k$. $l_{\rm AdS} = 1/k$ is often called *AdS radius*. The effective Planck scale $M_{\rm pl}$ on the negative tension (second) brane is

$$M_{\rm pl}^2 = \frac{M_5^3}{k}[e^{2kL} - 1]\,. \tag{3.47}$$

This result implies that any mass parameter m_0 on visible brane corresponds to a physical mass m on the hidden brane as $m_0 = e^{2kL}m$. If the fundamental mass scale is $m \simeq O(\text{TeV})$ with $ky \sim 35$, our mass

scale m_0 becomes Planck scale. If we take $e^{kL} \sim 10^{15}$ with $L \sim 35 l_{\rm AdS}$, thus RSI solves the hierarchy problem.

RSII: is a positive tension brane at $y = 0$ by taking the limit of $L \to \infty$. In this limit, Eq.(3.47) on opposite brane is

$$M_{\rm pl}^2 = M_5^3/k\,. \tag{3.48}$$

This implies that even in the infinite radius limit, the warped geometry affects its result. Considering gravitational perturbations h around the Minkowski brane as $G_{\mu\nu} = e^{-2k|y|}\eta_{\mu\nu} + h_{\mu\nu}(x^\mu, y)$ in the RSII and expanding $h(x,y) = \hat{\psi}(z)e^{-k|y|/2}e^{ip^\mu x_\mu}$, the linearized basic equation is given by

$$\left[-\frac{1}{2}\partial_z^2 + V(z)\right]\hat{\psi} = m^2\hat{\psi}\,, \quad \text{with} \quad V(z) = \frac{15k^2}{8(k|z|+1)^2} - \frac{3k}{2}\delta(z)\,, \tag{3.49}$$

where we define new coordinate $z \equiv \big(e^{k|y|} - 1\big)/k$. This potential shapes a volcano type. From this potential, we can see that *massless graviton are confined in a brane*. Moreover, the effective gravitational potential can be estimated as [170]

$$V(r) = -G\frac{m_1 m_2}{r}\Big(1 + \frac{2}{3}\frac{l_{\rm AdS}^2}{r^2}\Big)\,. \tag{3.50}$$

The first term is the usual Newtonian potential and the KK modes produce the second term as correction term. As we seen that the lowest distance where four-dimensional Newton law is confirmed is mm scale, thus the AdS radius is reduced to

$$l_{\rm AdS} \lesssim 0.1{\rm mm} \sim 5 \times 10^{11}{\rm GeV}^{-1}\,. \tag{3.51}$$

From this equation and the relation (3.48), we obtain a constraint as

$$M_5 \gtrsim 10^5{\rm TeV}\,. \tag{3.52}$$

We will review cosmology based on the RSII brane model (for reviews of brane-world cosmology, see [309, 275, 71, 462, 310, 352, 164]). Here we will review [418] for showing an equation of motion for brane.

Five-dimensional energy momentum tensor can be taken as the form

$$T_{\mu\nu} = -\Lambda g_{\mu\nu} + S_{\mu\nu}\delta(\chi)\,, \quad \text{with} \quad S_{\mu\nu} = -\lambda q_{\mu\nu} + \tau_{\mu\nu} \tag{3.53}$$

with $\tau_{\mu\nu}n^\mu = 0$. Note that Λ is a negative cosmological constant (AdS). From both the the Gauss equation, which relates to 5D Ricci tensor to 4D Ricci and 5D Einstein equation, with helping of the Israel's junction condition [219], we obtain the gravitational equations on the 3-brane as

$$\bar{G}_{\mu\nu} = -\Lambda_4 q_{\mu\nu} + \frac{1}{M_{\rm pl}^2}\tau_{\mu\nu} + \frac{1}{M_5^6}\pi_{\mu\nu} - E_{\mu\nu}\,, \tag{3.54}$$

$$\text{where} \quad \Lambda_4 = \frac{1}{2M_5^3}\left(\Lambda + \frac{1}{6M_5^3}\lambda^2\right), \quad M_{\rm pl} = \sqrt{\frac{6}{\lambda}}M_5^3\,,$$
$$\pi_{\mu\nu} = -\frac{1}{4}\tau_{\mu\alpha}\tau_\nu^\alpha + \frac{1}{12}\tau\tau_{\mu\nu} + \frac{1}{8}q_{\mu\nu}\tau_{\alpha\beta}\tau^{\alpha\beta} - \frac{1}{24}q_{\mu\nu}\tau^2\,, \quad E_{\mu\nu} \equiv C^\alpha_{\beta\rho\sigma}n_\alpha n^\rho q^\beta_\mu q^\sigma_\nu\,. \tag{3.55}$$

$E_{\mu\nu}$ is related to the 5D Wely tensor. It is an important feature of brane-world that both the bulk and the brane tension contribute to the cosmological constant in the effective four-dimensional theory on the brane. Therefore, 4D positive cosmological constant term, i.e., *explaining dark energy*, arises from the positive tension brane in AdS bulk $\Lambda < 0$. From the Codacci equation and the 5D Einstein equation, we also find the conservation law for matter $D_\nu T_\mu{}^\nu = 0$. Considering our universe is homogeneous and isotropic, this effective equation is reduced to the Friedmann equation given as,

$$H^2 + \frac{K}{a^2} = \frac{1}{3M_{\rm pl}^2}\rho\Big(1 + \frac{\rho}{2\lambda}\Big) + \frac{1}{3}\Lambda + \frac{\mathcal{C}}{a^4}\,. \tag{3.56}$$

Contrasting with the usual Friedmann equation (2.4), the second term in first terms and last term on the right hand side have newly appeared in the brane world cosmology. The ρ^2 term comes from the quadratic term $\pi_{\mu\nu}$, while the last one corresponds to the so-called *"dark " radiation* coming from $E_{00} = \mathcal{C}/a^4$, where $\mathcal{C}$ is the integration constant. Although we will have one unknown parameter $\mathcal{C}$, which we need an information about the bulk spacetime, the system becomes closed.

The cosmological observations impose the lower limit

$$\lambda > (1\mathrm{MeV})^4 \Rightarrow M_5 > 10^4\mathrm{GeV}\,. \tag{3.57}$$

3.2.4 DGP model

If one consider curvature correction terms arisen by a quantum effects, the 4D Einstein-Hilbert term are induced on the brane. This model is the so-called DGP model [131]. The action is given by

$$S = \frac{M_5^3}{2}\int d^5x\sqrt{-g}R + \int d^4x\sqrt{-q}\Big(\frac{M_{\rm pl}^2}{2}\,{}^{(4)}R + L_{\rm matter}\Big)\,. \tag{3.58}$$

Here we do not consider a tension of the brane σ. For the case of the homogeneous and isotropic universe, the effective 4D Friedmann equation is reduced to

$$H^2 + \epsilon\frac{H}{r_c} = \frac{1}{3M_{\rm pl}^2}\rho\,, \tag{3.59}$$

where the critical length is defined as $r_c = M_{\rm pl}^2/(2M_5^3)$. When $r_c \to \infty$ the four-dimensional term dominates and therefore, for $r \ll r_c$, 4D gravitational law on the brane is recovered, while for $r \gg r_c$, 5D law. Especially, when $\epsilon = 1$, this model gives a mechanism to *realize the late-time accelerating expansion of the Universe without introducing additional matter* since form the above equation. We find the universe goes into a de-Sitter phase; $H \to 1/r_c \sim$ const in the limit of vanishing matter energy density $\rho \to 0$ [116]. Such a solution is called the self-acceleration. The other branch $\epsilon = -1$ does not show no cosmic expansion in this limit. This interesting feature is expected to explain the current acceleration and resolve the dark energy problem. However, a remaining problem is that the quantum field theory of gravity(or one-loop correction) needs for the scale where we can estimate $(r_c^2 l_{\rm pl}) \sim 1000$km [301], and it is inconsistent with the range of scales where Newtonian law satisfies.

3.2.5 D$\bar{\rm D}$-branes inflation model

It is an open question as how to derive inflating potentials from string theory. In 1998, Dvali and Tye [130] proposed an interesting idea to derive inflation from D-branes. They argued that two D-branes could generate inflation as follows. If both branes are Bogomolnyi-Prasad-Sommerfeld (BPS) state, meaning that they preserve supersymmetry, and the net force between them vanishes. This calculation can be done explicitly, the interaction amplitude corresponds to the exchange of closed strings between the two branes. One can obtain effective potential as a large distance compared to the string length, which is taken as the form:

$$V \approx 2T + \frac{a}{Y^{d-2}}\left(1 + \sum_{NS} e^{-m_{NS}Y} - 2\sum_{RR} e^{-m_R Y}\right) \tag{3.60}$$

Where T is the tension of branes and Y is the separation between the branes and a a dimension-full constant. If we assume $Y^m \equiv (x_1 - x_2)^m$ where the sub-indices $1, 2$ corresponding to the brane and antibrane respectively, considering two D3 and $\overline{\rm D3}$ -branes and expanding $S_{\rm D} + S_{\bar{\rm D}}$ in powers of $\partial_a Y^m$, we get a potential of the form:

$$V(Y) \;= 2T_3\Big(1 - \frac{A}{Y^4}\Big) \quad \text{where} \quad A = \frac{e^{2\phi}T_3}{2\pi^3 M_s^8}\,. \tag{3.61}$$

This is a string theory derived inflation that has all the properties of successful inflationary models. It has advantage that one can interpret the inflaton field as a geometrical origin, that is the distance of two branes.

3.2.6 Ekpyrotic model

The ekpyrotic universe [246] uses a combination of the two ideas; one is Calabi-Yau compactification and second is that the universe is a brane floating around in the nine spatial dimensions of string theory (see works and reviews of ekpyrotic (cyclic) universe [248, 375, 432, 445, 455]). We start with the eleven dimensions of M-theory. The strong string coupling limit if the heterotic $E_8 \times E_8$ string theory is M-theory on a $\mathbf{R}^{10} \times \mathbf{S}^1/\mathbf{Z}_2$ spacetime [206]. The 10-dimensional $\mathbf{E}_8 \times \mathbf{E}_8$ heterotic string theory is considered to be the most realistic candidate for a successful high-energy generalization of the standard model and quantum gravity. It includes the possibility of chiral couplings, which is an essential ingredient in the standard model of elementary particles. On each boundary of this spacetime we get a Yang-Mills gauge group theory with an $\mathbf{E}_8$ gauge group. We have one copy of such a gauge theory on each boundary, contained in separate M5-branes. Then we compactify six spatial dimensions into $\mathbf{M}^4 \times \mathbf{CY}^6$, where $\mathbf{M}^4$ and $\mathbf{CY}^6$ are 4-dimensional Minkowski spacetime and 6-dimensional Calabi-Yau space, respectively. This leaves us with a five dimensional space. Two of the six compactified dimensions are parallel to the the M5-branes, so in the five dimensional theory, the 5-branes look like 3-branes. This model is the so-called Horava-Witten model [206]. The two 3-branes are on each boundary of the fifth dimension, which is topologically the same as a line element with length R. The boundary 3-branes each have the possibility of having a $\mathbf{E}_8$ Yang-Mills gauge theory on them. We consider the possibility that our universe is stuck on one of them, and that there is a "hidden universe" on the other boundary brane. The construction opens up a possibility where third brane, the bulk brane, can move inside th bulk space between the visible and hidden universe, and collide with the visible universe. This hypothetical event could be an alternative to the standard big bang model, thus avoiding the geometric singularity associated with that phenomenon. This scenario is main topic in the thesis and will be explained in the next chapter.

3.2.7 KKLT model

No-go theorem

In string theory or supergravity, in order to derive a de-Sitter vacua there have been many studies in this direction. Among such approaches, the so-called *No-go theorem* has been found in [180, 314], that is an impossibility for finding de-Sitter solutions in the 10(11) dimensional supergravity action. The no-go theorem is described as follows. We consider a D dimensional gravity theory, with $D > 2$, compactified down to 4 dimensions X_4, by $n = D - 4$ dimensional internal space Y_n. We consider the situation where X_4 is de-Sitter spacetime and Y_n is independent of time, taking the metric form as

$$ds^2(M_{n+4}) = W(y)^{1/2} ds^2(X_4) + ds^2(Y_n)\,. \tag{3.62}$$

We will assume that the D dimensional gravity theory satisfies the following conditions. (1) The gravity action with no higher curvature corrections (2) The non-positive potential $V \leq 0$. (3) The theory contains massless fields with positive kinetic terms. (4) The 4 dimensional effective Newton's constant is finite. They showed that if their assumptions are satisfied, it leads to a positive Ricci curvature of arbitrary timelike vector, i.e., $R^{(4)}_{VV} > 0$. Recalling the Raychaudhuri equation, $3\ddot{a}/a = -R_{VV} - 2\sigma^2 + 2\omega^2$, where σ and ω are shear and rotation, respectively, $R_{VV} > 0$ gives $\ddot{a} < 0$ because the rotation of the universe can be neglected. Therefore this theorem prohibits an accelerated expansion of the universe. However, there exist methods to avoid the no-go theorem. For examples, (1) the internal space is not compact or manifold having its boundary (it is corresponds to RS brane model). (2) The internal space is depend on time such as S-brane solution. (3) Including the higher curvature corrections. (4) Considering a local existing sources such as D_p-brane. This approach is corresponds to the following discussion of *KKLT* model.

KKLT model [225]: showed a possibility of achieving a dS vacua by flux compactifications on a Calabi-Yau manifold in the IIB string theory. Under such compactification, there appear several unfixed fields, the so-called *moduli* fields. The work of Giddings, Kachru and Polchinski (GKP) [185] can fix a axion-dilaton modulus, denoting the shape of Manifold, but assume only a fixed volume modulus. KKLT can fix all the moduli associated with the compactification. The low energy effective action of $N = 1$ supergravity in 4D is given by [24]

$$S = \int d^4x \sqrt{-g} \left[\frac{M_{\rm pl}^2}{2} R + g^{\mu\nu} K_{\alpha\bar{\beta}} \partial_\mu \varphi^\alpha \partial_\nu \bar{\varphi}^\beta - e^{K/M_{\rm pl}^2} \left(K^{\alpha\bar{\beta}} D_\alpha W D_{\bar{\beta}} \bar{W} - \frac{3}{M_{\rm pl}^2} |W|^2 \right) \right], \tag{3.63}$$

where α, β are referring to all moduli φ. Here the superpotential $W(\varphi^\alpha)$ and the Kähler potential $K(\varphi^\alpha, \bar{\varphi}^\beta)$ are given by

$$K_{\alpha\bar{\beta}} \equiv \frac{\partial^2 K}{\partial \varphi^\alpha \partial \bar{\varphi}^\beta}, \quad D_\alpha W \equiv \frac{\partial W}{\partial \varphi^\alpha} + \frac{W}{M_{\rm pl}^2} \frac{\partial K}{\partial \varphi^\alpha}. \tag{3.64}$$

The supersymmetry keeps only when $D_\alpha W = 0$ for all α. They [225] additionally introduce a non-perturbative correction [471] to the superpotential to fix the volume modulus, which is given by

$$W = W_0 + A e^{ia\rho}, \tag{3.65}$$

where W_0 is a tree level term. It can give a anti de-Sitter vacua as

$$V_{\rm AdS} = -3e^K |W|^2 = -\frac{a^2 A^2 e^{-2a\sigma_c}}{6\sigma_c}. \tag{3.66}$$

providing a negative cosmological constant. Therefore they add anti-D3 brane to obtain a positive cosmological constant by using the potential

$$V = \frac{2b_0^4 T_3}{g_s^4} \frac{1}{({\rm Im}\rho)^3} - \frac{a^2 A^2 e^{-2a\sigma_c}}{6\sigma_c}. \tag{3.67}$$

This approach tends to solve a cosmological constant (dark energy) problem due to no end of acceleration. The next work (KKLMMT) is studied in order to cause inflation such as D$\bar{\rm D}$-branes inflation.

KKLMMT model: Kachru, Kallosh, Linde, Maldacena, McAllister and Trivedi (KKLMMT) proposed that Calabi-Yau manifold is considered as similar as KKLT model and D3/$\overline{\rm D3}$-branes are added in this background. Similar to D$\bar{\rm D}$-branes inflation, the distance of two branes Y denotes the inflaton and then collision of branes leads to a end of inflation, taking the effective potential term as

$$V(Y) = 2T_3 \Big(1 - \frac{B}{Y^4} \Big), \tag{3.68}$$

similar to (3.61). For the other models of brane inflation, there exist D3/D7 brane inflation model [210, 265], Racetack inflation [50] and Tacyon inflation model [106].

String landscape

From the viewpoint of constructing de-Sitter vacua in string theory, it is recently known that there are many de-Sitter vacua as more than 10^{100}, that means to resolve cosmological constant problem needs realization of a complicated string landscape [435]. This is called *String landscape problem*.

3.3 Summary

Superstring cosmology

Superstring theory is now the most possible candidate as a unified theory of all interactions [189, 366].

The cosmological implications of string theory is very interesting and it is called *String cosmology*. The goal of superstring cosmology is to examine cosmological questions as the new understanding of string theory. The cosmological problems which string cosmology can be expected to resolve is for example, the following. **(1)***: What are Dark energy and dark matter ?* **(2)***: What is Inflaton? or convincing link with (alternative to) inflation?* **(3)***: Moduli problem* **(4)***: Singularity problem* **(5)***: Dimensionality problem.*

Fundamental object –Brane

String theory has a much richer set of fundamental degree of freedom, consisting—in addition to fundamental strings—of D-branes of various dimensionalities. This fundamental objects, D-branes denote non–perturbative effects of string theory as "soliton" of strings, while string theory has been only described in perturbative form. In order to understand non–perturbative string theory, D-branes are so important. As noted above, these branes can give us several suggestions for solving the above cosmological problems. (1): DGP and RSII give us a new definition of cosmological constant related to higher dimensional theory. It can lead to an interpretation of dark energy. RSII also shows that the same scalar field leads to both inflation and dark energy. For other approach, we can create a positive cosmological constant in the string theory, based on KKLT mechanism. (2): Ekpyrotic, and D$\bar{\text{D}}$-branes inflation can give us a geometrical interpretation for the inflaton field as the distance of two branes. (3): String (brane) gas model can resolve the dimensionality problem (see the details in the next chapter). Other importance of branes is noted as follows. D-branes are **solitons** in string theory. D-brane is a key object, in order to see non– perturbative effects of string theory. They have also been instrumental in the geometrization of gauge interactions and the long-sought correspondence between gauge theories and gravity/string theory as epitomized by the **AdS/CFT correspondence**. The AdS/CFT correspondence was originally proposed [313, 201] and many application and extensions exist [192, 193, 473, 472]. Gauge-theory/gravity correspondence may have far-reaching implications both for the understanding of gauge theory dynamics and the nature of gravity. This gives us a help of calculating of QCD scattering diagram.

As summary, there has been tremendous work on string cosmology, which are roughly categorized for three types, that is, *(1) Flux compactification, (2) Brane-world* and *(3) String gas cosmology.* The first is motivated by the type II B superstring theory, in which the work of KKLT [225] based on flux compactification on a Calabi-Yau manifold. The second is motivated by the D-brane determined as the endpoints of open string, in which Randall and Sundrum [373] proposed the brane-world cosmology. The third approach, string gas cosmology is motivated by the Heterotic superstring theory and it is one of the existing approaches trying to obtain our observed 4D universe starting from a string theory set up, proposed by Brandenberger and Vafa [64](see Sec. 4.2).

Chapter 4

Two scenarios based on colliding branes

In this chapter, we will introduce and review briefly the following two scenarios, which are related to a colliding branes; 1. *Colliding branes universe scenario* and *2. String(brane) gas cosmological scenario*. The first one is called ekpyrotic universe or cyclic universe and can be seen to be alternative to inflation. The latter is one approach to resolve the dimensionality problem. The singularity problem may also be addressed from both scenarios. In both scenarios, a phenomena of colliding two branes is a key process, and which is the main topic of this thesis.

4.1 Colliding branes/Ekpyrotic universe scenario

Not only does the inflationary scenario give some picture of the earlier stage of the universe before the big bang but also it seems to be supported by some recent observational data on CMB. While, it is still unclear what the origin of inflaton is. So far, there is no relation to fundamental unified theories such as string/M-theory. On the other hand, recently a new paradigm on the early universe has been proposed, called the brane world. Such speculation has been inspired by recent developments in string/M-theory, as noted above. One of typical phenomena in brane dynamics is a collision of branes. With this idea and for resolving the key theoretical problems in the big bang theory, a new idea of the early universe has been proposed, colliding branes universe model, the so-called *ekpyrotic* scenario or *cyclic* universe scenario [246, 432, 248], where the word "ekpyrotic" from the Greek-derived word *ekpyrosis* meaning the fire which represents consuming and reconstituting of the world in the Greek philosophy. It is based on a collision of two cold branes. The universe starts with a cold, empty, and nearly BPS (Bogomol'nyi-Prasad-Sommerfield) ground state, which contains two parallel branes at rest. The two branes approach each other and then collide. The energy is dissipated on the brane and the big bang universe starts. Since this scenario is not only motivated by the fundamental unified theory but also may resolve the key theoretical problems, such as the flatness and horizon problems, therefore, it could provide an alternative to an inflationary scenario and would be very attractive. There has been much discussion about density perturbations to see whether this scenario is really a reliable scenario for the early universe, however, it has been shown by many studies that the initial spectrum is not produced as scale invariant, so this point is the problem which this scenario has. We shall review this colliding branes universe (ekpyrotic universe) scenario and explain its trouble.

4.1.1 Idea of ekpyrotic universe

In this section, we shall explain an idea of ekpyrotic universe. In the ekpyrotic universe we have a five dimensional space-time, the fifth dimension being a finite orbifold dimension, and the big bang is realized

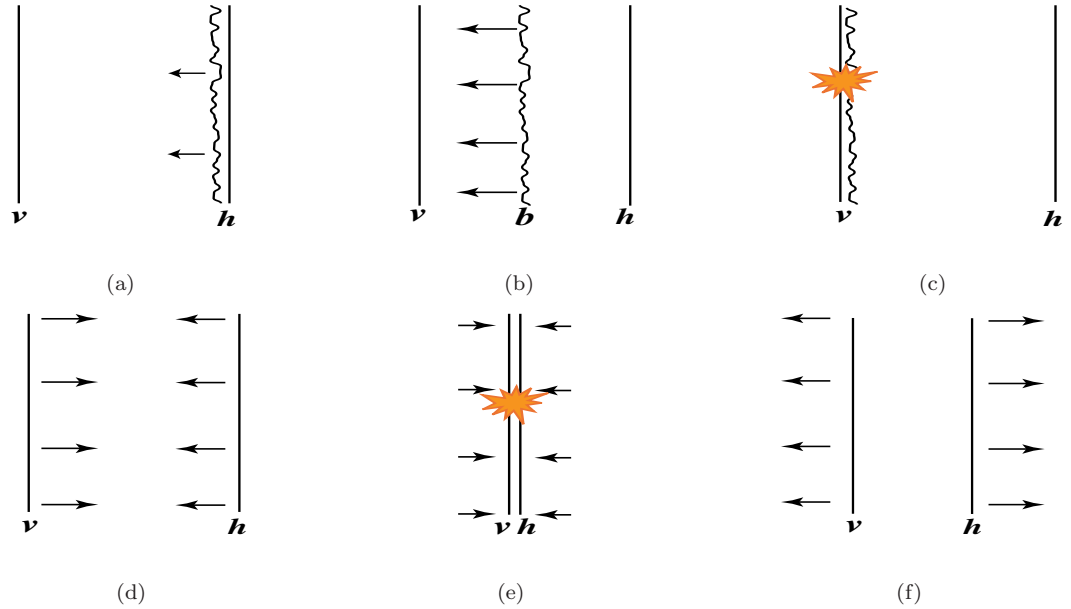

Figure 4.1: Sketches of the ekpyrotic (newer ekpyrotic) universe scenario seen in the upper (lower) figures. The visible, hidden and bulk branes are indicated with letters v, h, b respectively. (a) The initial state of two parallel static branes and the hidden brane spontaneously produces a bulk brane, (b) the bulk brane travels towards the visible brane, acquiring quantum fluctuations, (c) the bulk brane eventually impacts inelastically on the visible brane and is absorbed. (d) The initial state, (e) the fifth dimension starts to contract and two branes then collide, (f) the fifth dimension has bounced at the origin, and is expanding again.

as a collision between a visible brane on which we live now, and another brane, a bulk brane, which interacts with the visible brane through stringy effects, including gravity. There are different versions of this scenario, with different brane configurations.

In the first version, which is original proposed by Khoury, Ovrut, Steinhardt and Turok (2001) [246], there are three branes being $(3+1)$-dimensional surfaces: the visible brane, the hidden brane, and the bulk brane, and they are located at each end of the orbifold dimension, and in the bulk, respectively (See Figure 4.1). The bulk brane is spontaneously produced close to the hidden brane by a mechanism similar to bubble nucleation and is thereafter moving towards the visible brane. The bulk brane is proposed to be light compared to the boundary branes. During the bulk brane movement it is under the influence of a potential created by the exchange of appropriate M-theory fields between the three branes. The subsequent collision of the bulk brane with the visible brane is responsible for depositing enough energy on the visible brane for it to evolve into what we are living in today. The newer ekpyrotic scenario [432] has only two branes, one visible and one hidden (See Figure 4.1). Here, the collision is brought about by a different mechanism: the fifth dimension contracts, vanishes, and grows again. In the new scenario, since the fifth dimension vanishes at the instant of collision, a full description demands a rigorous treatment of this singularity in string theory/M-theory. In this version, we could image the possibility of a cyclic universe, in which the fifth dimension undergoes a cycle of contraction and expansion a number of times, or indefinitely. This is called the *cyclic model*. The ekpyrotic universe is fundamentally different from standard cosmology, and offers radically different explanations for the cosmological problems. In both scenarios the initial state is supported to be in a cold, vacuum, nearly BPS state [298], where branes are flat, parallel and empty. The BPS state is needed to keep a supersymmetry in a 4d effective action. The visible and hidden branes are flat and are described by a Minkowski spacetime, while the bulk is a warped five-dimensional spacetime.

The important points of these scenarios are the followings: **(1)** The Distance between two branes, Y

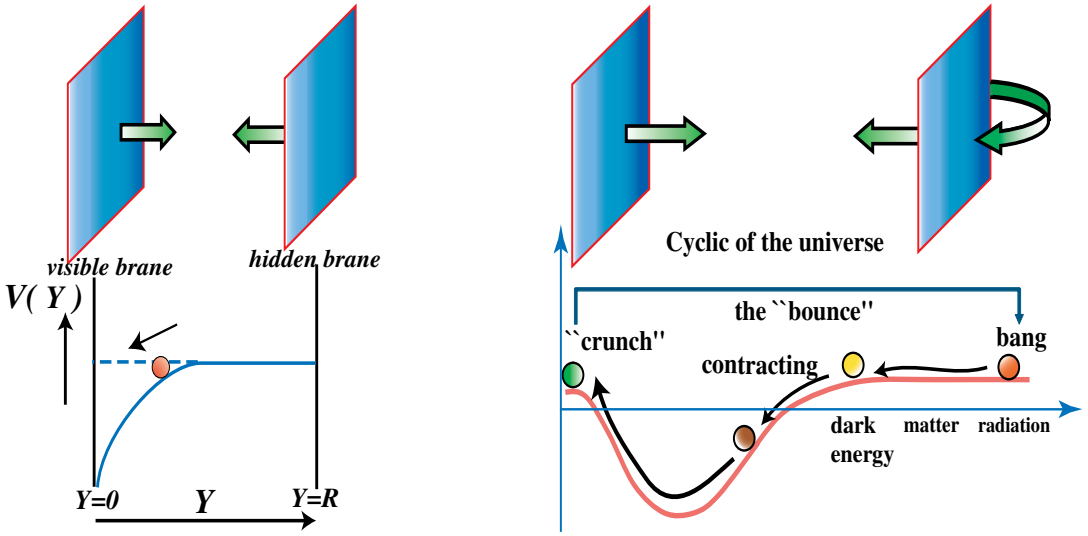

(a) Ekpyrotic universe

(b) Cyclic universe

Figure 4.2: Sketches of the effective potential for ekpyrotic (cyclic) universe scenario. (a): Exponential potential $V(Y) = -V_0 e^{-\alpha Y}$. The bulk brane approaches and collides the visible brane at $Y = 0$. (b): This type of potential adds two new stages of expansion: dark energy and contracting, which is alternative to inflation, and moreover, the universe continues this cycle.

behaves as an effective scalar field with a exponential potential $V(Y) = -V_0 e^{-\alpha Y}$ (see Fig 4.2), which is alternative to Inflaton. **(2)** Our world on the visible brane is seen to contract in the period before the collision, that is, while inflationary scenario has an expansion phase, there is an contracting phase $H < 0$ in this scenario. The recent study of cyclic universe scenario shows that the effective potential leads the universe to additional expansion: dark energy and contracting phase, which is alternative to inflation [144, 433]. It is very attractive to us, however, we will only consider the former simple case, $V(Y) = -V_0 e^{-\alpha Y}$. First, based on the above two features, We will show a resolving of the key theoretical problems which the big bang theory has.

- **Flatness problem**

Spatial flatness of the visible universe follows from the assumption of starting near the BPS state. As we have noted above, the bulk brane becomes flat and parallel as the BPS state. Hence, the geometry of hot big bang universe is originally spatial flat. We address the flatness problem as beginning state of a BPS. Therefore, the flatness problem is not seen to be a problem in the ekpyrotic scenario because of assuming a BPS state as an initial condition.

- **Horizon problem**

In order to resolve this problem, we should compare two scales, that is, one is the particle horizon measured by an observer on the visible brane d_p, while the other is the Hubble radius of our universe at collision $d_H = H^{-1}|_{Y=0}$ whereby we investigate which is larger. If $d_p/d_H > e^{70}$, this problem can be avoided. Compared with inflationary theory, this scenario also leads to two horizon-crossings in which the fluctuations $((k/a)^{-1})$ is stretched out the Hubble radius (see Fig. 4.3). d_p denotes the causally links regions determined from the time taken by the brane traveling toward the visible brane. Here we represent this comoving time as $\tau_{\rm tot}$ and the scale factor of the traveling (bulk/hidden) brane. The effective Friedmann equation is given by $H^2 \sim \frac{1}{2}D^2(Y)\dot{Y}^2 + V(Y)$ and hence the particle horizon at collision times $(Y = 0)$ is obtained as $d_p = D^{1/2}(Y = 0)\tau_{\rm tot}$. Using Friedmann equation, we can obtain

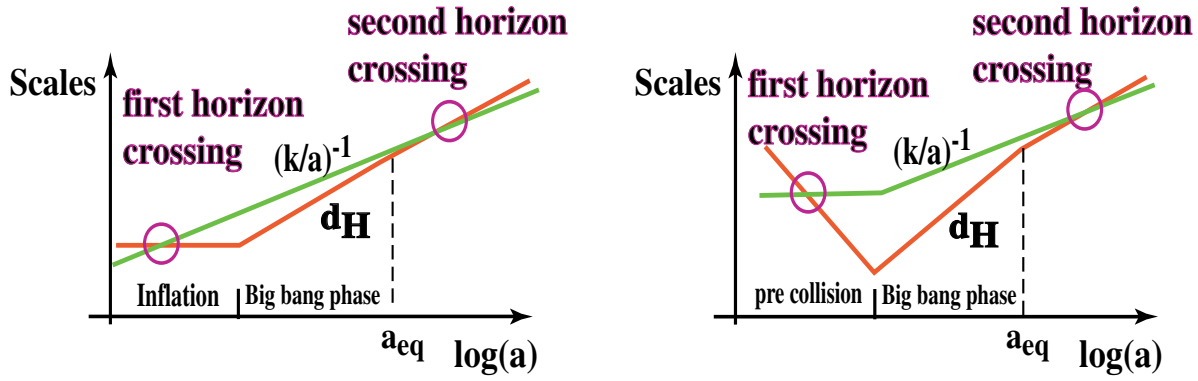

(a) Inflation (b) Ekpyrotic

Figure 4.3: Schematic illustrations of evolution of fluctuations in Inflation (a) and Ekpyrotic universe (b). Note that two horizon-crossings occurs in both scenarios and hence the horizon problem and formation of structure problem are resolved. See the above discussions in Fig. 2.4.

a result omitting the detail as follows,

$$\frac{d_p}{d_H} \sim e^{\alpha R/2} > e^{60} \Longrightarrow \alpha R/2 \gtrsim 60\,, \tag{4.1}$$

where α is parameter shown in the potential term and R denotes the position of the hidden brane as $Y = R$. Therefore, if we impose this condition on these parameters, this problem can be resolved. This condition makes our universe slowly contract, i.e., $a \propto t^p$ with $p \ll 1$ because the potential is $-V(Y)/V_0 = e^{-\sqrt{2/p}Y} \simeq e^{-60Y}$. This feature that the universe contracts very slowly in the ekpyrotic scenario will be also seen as the exact solution describing dynamics in the next subsection.

• Origin of large-scale structure

Though the branes start flat and parallel, they undergo quantum fluctuations during their journey across the fifth dimension. These quantum fluctuations in the traveling brane generate "ripples" during moving towards the visible brane. It results in slightly cooler or hotter regions on brane and it means that time-delay at collision gives inhomogeneity in the temperature and energy density levels on the visible brane [1]. These primordial perturbations then grow to become CMB anisotropies resulting in a seed of large-scale structure. To conform to current experimental observations, this spectrum has to be quite close to scale invariant. The spectral of these fluctuations will be dependent on the form of the brane-brane potential. We will discuss these spectrums in the next subsection. Note that the generated primordial density perturbations in this scenario, cross inside the Horizon late times, as similar to Inflation (see Fig. 4.3).

• Relic density problem

The production of unwanted relics is highly suppressed if the maximal temperature in the ekpyrotic universe lies well below the mass scale at which such relics are produced. In fact, estimating from an effective Friedmann equation and using the equation $T_{\rm R} \sim (3M_{\rm pl}^2 H^2)^{1/4}$, we can obtain the reheating temperature as 10^{11} GeV. While it is known that the mass scale of the monopole $M_{\rm mono}$ is nearly 10^{16} GeV, so this problem can be avoided.

• Initial singularity problem

In contrast to the inflationary scenario, in the ekpyrotic scenario since the big bang is ignited at some finite temperature and there are no curvature singularities, it may be possible that this problem is solved.

[1] This interpretation of time-delay is related to Guth idea as shown in [196, 197].

Since the scenario is based on heterotic M-theory, the singularity theorems of general relativity, which is a low-energy approximation of M-theory, do not necessarily apply. However, the ekpyrotic scenario does not include a description of what happened before the start of brane movement. Any model where time does not extend infinitely far into the past (and that does not contain closed timelike curves) is of course geodesically incomplete and thus singular.

In addition to solving the above cosmological problems, the ekpyrotic scenario also proposes to solve *problems of particle physics*. The BPS property provides us with a $N = 1$ super-symmetric Yang-Mills field theory with E_8 gauge group at low energy on the visible brane. By a brane collision, a so-called small instanton transition can occur. The small instanton may break the gauge group from E_8 to some smaller group, for example $SU(3) \times SU(2) \times U(1)$ or $SU(5)$. It can also set the number of light families to three. The nature of the small instanton transition depends on the type of the vector bundles on the Calabi-Yau manifold dimensions. This interesting feature of course comes from the fact that this scenario has link with a fundamental unified theory, string/M-theory.

As you seen, we have showed an idea of ekpyrotic universe scenario where two branes approach each other and then collide and hot big bang universe starts. The main points of this scenario are that the distance between two branes behaves as a scalar field having the exponential potential, which makes this scenario alternative to inflation, and our universe contracts before collision while the universe expands in the inflationary scenario. It has been shown this contracting universe also resolve the key problems which the big bang theory contains as well as expanding universe, however, for the origin of structure, it has been shown by many studies that its initial spectrum is not produced as scale invariant. Therefore this point is the trouble this scenario has and we shall explain it in more detail in the next section.

4.1.2 Dynamic of the universe and Spectrum of fluctuations

There has been much discussion about the primordial density perturbation in the ekpyrotic universe [10, 246, 227, 304, 65, 151, 460, 247, 318, 453, 188, 334], the main points of discussion are the followings: **(1)** Whether the initial spectrum is scale-invariant in a contracting phase? **(2)** How it will evolve throughout the collision, from contracting phase to expanding phase? This is the so-called "*Matching condition.*" In what follows, we follow briefly the historic flow of these discussions. The spectrum index is defined as exact scale invariance when $n_{\mathcal{R}} - 1 = n_{\rm T} = 0$. The original work [246] claimed the spectrum is nearly scale invariant. In fact, these index was obtained as slightly blue ($n_{\mathcal{R}} - 1 > 0$) for scalar part and strongly blue ($n_{\rm T} \simeq 2$) for tensor part, while inflation shows red spectra $n_{\mathcal{R}} - 1 < 0$ and $n_{\rm T} < 0$. The observational data CMB provides $n_{\mathcal{R}} = 0.93 \pm 0.03$, therefore, the inflationary scenario is favored rather than the ekpyrotic scenario concerning scalar perturbations. From the above results, it may be natural to consider that the observing the gravitational wave spectrum is the key test to distinguish the two scenarios. As well as this work, Kallosh, Kofman and Linde [227] claimed the spectrum is scale-invariant $n_{\mathcal{R}} \sim 1$. These two works approached the called "time delay formalism" proposed by Guth [196] in order to estimate the spectrum. While this formalism ignored back reactions of spacetime, Lyth [304], Brandenberger and Finelli [65, 151], Wands [460] showed $n_{\mathcal{R}} \simeq 3$ (blue) including the effect of back-reaction. This result is inconsistent to the above claim. Against the counterargument, Khoury et al claimed the scale-invariance again [247], in addition to the effect of back-reaction, considering the transition from contracting phase to expanding phase, although there had not been so far studies including the transition. After that, concerning the matching condition, although there are some works [188, 334, 10], nothing supports the above claim of Khoury et al. From now on, we will show these results below. First, we consider whether the initial spectrum is scale-invariant in a contracting phase or not. In this subsection, we show the result, the index for the scalar perturbation $n_{\mathcal{R}} \simeq 3$ shown by Lyth, Brandenberger and Finelli and Wands. In the ekpyrotic scenario a negative exponential potential is usually introduced by

$$V = -V_0 \exp\left(-\sqrt{\frac{2}{p}}\frac{\phi}{M_{\rm pl}}\right). \tag{4.2}$$

It has been known this field has the power-law solution in a flat FRW background, described as follows;

$$a \propto |t|^p\,, \quad H = \frac{p}{t}\,, \quad \phi = M_{\rm pl}\sqrt{2p}\ln\left(\sqrt{\frac{V_0}{p(1-3p)}}\frac{|t|}{M_{\rm pl}}\right). \tag{4.3}$$

Here if we consider $t > 0$ and $p > 1$, this solution denotes a power-law inflation, while if $t < 0$ increasing from $-\infty$ to 0, we can obtain the negative $H < 0$ and comoving horizon $1/(aH)$ decreasing, i.e., the contracting solution. Inspired by string theory, there is a contracting phase as well as the ekpyrotic scenario, the so-called pre-big-bang scenario proposed by Gasperini and Veneziano [458, 174] (see [283, 176] for a review). It is known that the pre-big-bang universe contracts as power-law, $a \propto t^{1/3}$, while the ekpyrotic universe contracts slowly. As mentioned above, in order to resolve the horizon problem, we need slowly contraction $a \propto t^p$ with $p \ll 1$ in the exponential potential. Getting the efficient e-holding and imposing $e^{60} \sim (a_{\rm i}/a_{\rm f})^{(1-p)/p}$ leads to a contraction by factor of a few order $\ln(a_{\rm i}/a_{\rm f}) \sim 3/2$. The solution (4.3) denotes the ekpyrotic universe and pre-big-bang universe for $0 < p \ll 1$ and for $p \simeq \frac{1}{3}$, respectively. We will estimate the spectrum of scalar perturbations in the contracting phase with the potential (4.3). In this case, as noted in the inhomogeneity section, we find the term $z''/z = p(2p-1)/(1-p)^2\tau^{-2}$ in (2.171) and it leads to the index $\nu_{\mathcal{R}}$ as

$$\nu_{\mathcal{R}} \equiv \left|\frac{1-3p}{2(1-p)}\right|, \qquad \nu_{\mathcal{R}} = \begin{cases} \frac{1}{2} & 0 < p \ll 1 \\ 0 & p = \frac{1}{3} \\ \frac{3}{2} & p \gg 1 \end{cases}, \tag{4.4}$$

where in order to comparing, we described the index of inflation, which is approximated $\nu_{\mathcal{R}} \simeq 3/2$, as similar to ekpyrotic and pre-big-bang scenarios. Then by using Eq. (2.193) $\mathcal{P}_{\mathcal{R}_c} \propto k^{3-2\nu_{\mathcal{R}}}$, we obtain the spectral index of curvature perturbations (see also Refs. [304, 65, 453, 452, 10, 151]):

$$n_{\mathcal{R}} = 4 - 2\nu_{\mathcal{R}} = 1 + \frac{2}{1-p}\,, \qquad \begin{cases} n_{\mathcal{R}} \sim 3 & 0 < p \ll 1 \\ n_{\mathcal{R}} \sim 4 & p = \frac{1}{3} \\ n_{\mathcal{R}} \sim 1 & p \gg 1 \end{cases}. \tag{4.5}$$

If we take $p \to \infty$ in an expanding universe or $p = 2/3$ in a collapse phase, the spectra show scale-invariant $n_{\mathcal{R}} = 1$ [10, 429]. The PBB cosmology ($p = 1/3$) shows a high blue spectrum $n_{\mathcal{R}} = 4$. The ekpyrotic scenario yields a slow contraction ($0 < p \ll 1$), hence the index is blue $n_{\mathcal{R}} \simeq 3$. Therefore both these scenarios are disfavored by CMB data from WMAP $0.90 < n_{\mathcal{R}} < 0.97$. The main reason the spectrum is a blue-tilted in a contraction is a generation of curvature perturbation in a kinematic driven not in a slow-roll phase.

On the other hand, let us investigate the tensor part of fluctuations related to the gravitational waves. As well as in the case of a scalar perturbations, the index for the tensor perturbations is found as $\nu_{\rm T} = |1-3p|/(2|1-p|)$. The result of spectrum index is also obtained as

$$n_{\rm T} = \frac{2}{1-p}\,, \qquad \begin{cases} n_{\rm T} \sim 2 & 0 < p \ll 1 \\ n_{\rm T} \sim 3 & p = \frac{1}{3} \\ n_{\rm T} \sim 0 & p \gg 1 \end{cases}, \tag{4.6}$$

and the inflationary scenario also gives the scale-invariant spectrum ($n_{\rm T} = 0$) for the tensor perturbations and the ekpyrotic scenario and the pre-big-bang scenario also give the blue spectrum in this case. Similar to Eq. (2.203), the consistency relation is also realized.

The original work [246] has showed the scale-invariant $n_{\mathcal{R}} \simeq 1$ since assumption of ignoring the effect of the back-reaction of spacetime gives the EOM $v_k'' + (k^2 - 2\tau^{-2})v_k = 0$ for the variable $v = a\delta\phi$ and it leads to the scale-invariant spectrum $\nu_{\mathcal{R}} = 3/2$. The estimation is related to a time delay formalism where we take a spatially flat gauge ($\psi = 0$). However, as shown above, the study involving this effect gives a different results, strong blue spectrum of curvature perturbations $n_{\mathcal{R}} \simeq 3$. There exist mainly two problems about evolution of fluctuations produced in the contracting phase: **(1)** How do we treat the

bounce singularity $a = 0$? and **(2)** How do these fluctuations evolve through the bounce? (1) is related to non-singular bounce model and (2) is corresponds to the matching condition as noted above. Gordon and Turok [188] and Nathalie and Streich [334] use a toy bounce model, which is represented as $a \sim \cosh\tau$ with the potential $V \sim m^2\phi^2$ so that this universe has non singularity (see also [177, 178, 10, 59]). In the work of Allen and Wands [10], by considering a "ghost" field having a negative kinetic term and choosing a good gauge, they can realize a non-singular bounce. They showed that the universe contracts like dust dominated universe, $a \propto (-t)^{2/3}$ and it yields a final scale-invariant spectrum of curvature perturbation $\mathcal{R}_c$.

In order to construct scale-invariant spectrum one takes into account a second scalar field [58, 342, 315]. The authors of ref. [342] used a two-field system: a brane-modulus φ and a dilaton χ. Similar to this work, the recent work [77, 277] propose two scalar field and consider isocurvature perturbations (see same results in [266, 267]). This mode can be made as a scale-invariant and converted to the curvature perturbation as [277]

$$\dot{\mathcal{R}}_c = \frac{H}{\dot{H}}\frac{k^2}{a^2}\psi + \frac{2H}{\dot{\sigma}}\dot{\theta}\delta s\,, \tag{4.7}$$

where σ and s is a adiabatic and entropy perturbation, respectively and θ is determined by a background trajectory. If the trajectory is bend at some time $\dot{\theta} \neq 0$, it implies that the isocurvature perturbation can be converted into curvature perturbation $\mathcal{R}_c$. They show the final result of spectrum index is slightly blue as $0.97 < n_{\mathcal{R}} < 1.02$. Combing this work with a ghost condensation, [77] propose a non-singular bounce model for complete ekpyrotic scenario (see also [107, 108]). For the cyclic universe scenario, evolutions of perturbations are recently described by [144].

4.2 String (brane) gas cosmological scenario

The string cosmology [64, 449, 9, 268] is interesting approach which is motivated by some part of a non-perturbative effect of string theory. Especially here we focus on the symmetry called *T-duality*, leading to a new degrees of freedom called *string winding modes* (see Sec. 3.1.2). Let us consider a toroidal space with a radius of the torus R. The T-duality symmetry is described by

$$R \to \frac{1}{R}\,, \quad (n, m) \to (m, n)\,. \tag{4.8}$$

We choose the background as dilaton gravity. In this background, we consider an ideal gas of fundamental string in all states, including string winding modes, whose setup is the so-called *string gas*. Here the energy density is assumed to be very close to the *Hagedorn temperature* [198], that represents the maximal temperature (see also Sec. 3.1.3). We also assume that the string gas is initially thermalized at this Hagedorn temperature. This approach is the so-called *string gas cosmology*.

String gas cosmology

The first predictions of string gas cosmology (SGC) were proposed by Brandenberger and Vafa [64]. Thanks to the T-duality, SGC will become non-singular since the temperature T obeys the symmetry

$$T(R) = T(1/R) \tag{4.9}$$

and thus the minimal length takes a finite value even if R decreases to zero, that is close to the string length (the "self-dual"radius, see (3.16)). They [64] suggested that string winding modes would prevent more than three spatial dimensions from becoming large. It can give the possibility to explain the emergence of three large and isotropic spatial dimensions, while six remain stabilized near the string scale, the so-called *dimensionality problem*. Brandenberger and Vafa [64] discussed that winding modes can maintain equilibrium in a most three spatial dimensions. It is based on the fact that p dimensional objects can generically intersect in at most $2p + 1$ dimensions. They argued that once the winding modes ($p = 1$) annihilate with anti-winding modes, three spatial dimensions would be free to expand. Thus winding modes can annihilate only in three spatial dimensions and hence it helps to resolve the dimensionality

problem. This mechanism is the so-called *Brandenberger and Vafa (BV) mechanism*.

Brane gas cosmology

This is an interesting scenario, but has several questionable aspects. One is that it critically relies on poorly-understood dynamics at the Planck scale. Another is that it requires a resolution of the moduli problem, and, more importantly, relies on simple toroidal compactification. But the most problematic feature of this solution is that it relies on strings being the sole important objects in string theory, whereas we now know that *branes* also play a critical role. These models of extension to brane gas are the so-called *brane gas cosmology*. Some work has been done on addressing this concern, see in [9, 15, 49, 135, 134, 240, 370, 249, 353, 208, 119]. The authors of [129] suggest another reason that four spacetime dimensions are special. They point out that $4 + 4 < 10$ and that this not true for any larger integer. Their argument was that the worldvolume of 3-branes would not intersect whereas the worldvolume of any larger branes would. Their argument was that larger branes can therefore unwind, whereas 3-branes would survive. They [232] suggest that under some very general and plausible assumptions about brane dynamics in ten dimensions, branes with other numbers of dimensions will be diluted relative to the 3-branes and 7-branes. D3-branes and D7-branes are important for recent ideas about string theory models of inflation, including *KKLT model* [226, 225, 115]. Recent string-theoretic inflation models are based on the presence of 3-branes and 7-branes [226, 225, 115]. This scenario could naturally give rise to this type of inflation.

Their suggestions are very interesting and the key process is annihilation of two branes of various dimensionalities, took place of the annihilation of the winding strings. Thus collision of two branes can resolve the dimensionality problem in brane gas cosmology. In the thesis, for simplify, we will discuss the string gas cosmological scenario in more details.

4.3 Summary

The brane is a fundamental object in the superstring theory. They may be produced more than one and have various dimensionalities. The existence of models with more than one brane suggests that branes may collide. Colliding branes would be a fundamental phenomena in the string cosmology. In this chapter, we have studied two applications of colliding branes to cosmology: ekpyrotic/cyclic universe and brane gas cosmology. The first scenario leads to suppose that the Big bang is associated with the collision and this is alternative to inflationary scenario. The second scenario gives the possibility to resolve the dimensionality problem due to the several dimensions which many branes (gas) have. In addition to resolving these problems, both two scenarios would give a resolution of initial singularity problem. In the remaining of thesis, we will study the collision of two branes in the context of the above scenarios. The ekpyrotic universe scenario is related to the following works in Sec. 5.2, 5.3, 6.1 and 6.2. The last work in Sec 6.3 is related to the string gas universe.

Chapter 5

Colliding branes in Minkowski spacetime

In the above chapter, we have explained the ekpyrotic universe scenario. It has been shown that this scenario not only can resolve the key theoretical problems the big bang theory contains, but also it is motivated by the fundamental unified theories, while inflationary scenario does not have the convincing link with such theories, therefore, it could provide an alternative to an inflationary scenario and would be very attractive. However, it has been seen that there may be so far some serious troubles in density perturbations. But it is necessary to consider the collision process and the reheating process in detail. For the work about the collision of branes, Martin et al have studied collision of branes for using the brane approximated as the delta function [319]. In the analysis using the delta function, the collision process can not be followed in detail. On the other hand, even though there are some works by [97], the reheating mechanism itself in this scenario has not been so far investigated in detail. This may give a reheating mechanism in an ekpyrotic brane scenario.

5.1 Basic idea of colliding branes

• Domain wall

It may be difficult to deal properly with the collision of two branes in basic string theory. Hence, in this work, we adopt a domain wall constructed by some scalar field as a brane, and analyze the collision of two domain walls in a 5-dimensional bulk spacetime. Some other studies have also adopted such a picture [133, 13]. It is worth noting that there is a thick domain wall model for a brane world [145]. In order to analyze particle creation at the brane collision, in this work we consider the simplest situation. We discuss the collision of two domain walls collide in 5D Minkowski spacetime. In Sec. 5.1, we analyze the collision of two domain walls. Then, in Sec. 5.2.2, we investigate particle creation on the wall at the collision. We study a collision of two domain walls in 5-dimensional (5D) Minkowski spacetime. To construct a domain wall structure, we adopt a scalar field Φ with its potential,

$$V(\Phi) = \frac{\lambda}{4}(\Phi^2 - \eta^2)^2 \,, \tag{5.1}$$

where the potential minima are located at $\Phi = \pm\eta$. Since we discuss the collision of two parallel domain walls, the scalar field is assumed to depend only on a time coordinate t and one spatial coordinate z. The remaining three spatial coordinates are denoted by $\vec{x}$. For numerical analysis, we use dimensionless parameters and variables, which are rescaled by η (or its mass scale $m_\eta = \eta^{2/3}$) as

$$\tilde{t} = m_\eta t \,,\ \tilde{z} = m_\eta z \,, \tilde{\Phi} = \frac{\Phi}{\eta} \,,\ \tilde{\lambda} = m_\eta \lambda \,. \tag{5.2}$$

In what follows, we omit the tilde in dimensionless variables for brevity. The equation of motion for Φ in 5D is given by

$$\ddot{\Phi} - \Phi'' + \lambda\,\Phi\,(\Phi^2 - 1) = 0\,, \tag{5.3}$$

where $\dot{}$ and $'$ denote $\partial/\partial t$ and $\partial/\partial z$, respectively. Eq. (5.3) has a static kink solution (K), which is topologically stable. It is called a domain wall, which is described by

$$\Phi_K(z) = \tanh\left[\ \frac{z}{D}\ \right], \tag{5.4}$$

where $D = \sqrt{2/\lambda}$ is the thickness of the wall [469]. We also find another stable solution, that is, the antikink solution ($\bar{K}$), which is obtained from Eq. (5.4) by reflecting the spatial coordinate z as $\Phi_{\bar{K}}(z) = \Phi_K(-z) = -\Phi_K(z)$.

• Lorentz boosting

When a domain wall moves with constant speed v in the z direction, we obtain corresponding solution by boosting Eq. (5.4) as

$$\Phi_v(z,t) = \tanh\left[\ \frac{\gamma}{D}\,(z - vt)\ \right], \tag{5.5}$$

where we assume that the domain wall is initially located at $z = 0$, and $\gamma = 1/\sqrt{1-v^2}$ is the Lorentz factor. In order to discuss the collision of two domain walls, we first have to set up the initial data. Using Eq. (6.12), we can construct such an initial data as follows. Provide a kink solution at $z = -z_0$ and an antikink solution at $z = z_0$, which are separated by a large distance and approaching each other with the same speed v. We then obtain the following explicit profile;

$$\Phi(z,0) = \Phi_v(z + z_0, 0) - \Phi_{-v}(z - z_0, 0) - 1\,. \tag{5.6}$$

The initial value of $\dot{\Phi}$ is also given by its derivative. The spatial separation between two walls is given by $2z_0$, and as long as $z_0 \gg D$, the initial conditions (5.6) and its derivative give a good approximation for two moving domain walls. Using these initial values, we solve the dynamical equation (5.3) numerically, whose results will be shown in the next subsection.

5.2 Reheating mechanism in colliding two branes universe

Even though there are some works by [97], the reheating mechanism itself in this scenario has not been so far investigated in detail. Hence, in this chapter, we study how we can recover the hot big bang universe after the collision of the branes, following our work [436]. It can give a reheating mechanism in an ekpyrotic brane scenario. Here we investigate quantum creation of particles, which are confined to the brane, at the collision of two branes. In order to analyze particle creation at the brane collision, in this work we consider the simplest situation. We discuss the collision of two domain walls collide in 5D Minkowski spacetime. As noted in Sec. 5.1, we analyze the collision of two domain walls. Then, in Sec. 5.2.2, we investigate particle creation on the wall at the collision. Applying the particle production to the energy dissipation of the brane, we discuss the reheating mechanism of a brane universe. We use the unit of $c = \hbar = 1$.

5.2.1 Time evolution of domain walls

We use a numerical approach to solve the equations for the colliding domain walls. The numerical method is shown in Appendix. We have two free parameters in our simulation of the two-wall collision, i.e. a wall thickness $D = \sqrt{2/\lambda}$ and an initial wall velocity v. The collision of two walls has been discussed in 4-dimensional Minkowski space [12]. Although we discuss the domain wall collision in 5-dimensional Minkowski space, our basic equations are exactly the same as the cited case, and we find the same results as there. In particular, the results are very sensitive to the initial velocity v. First let us show the numerical results for two typical initial velocities, i.e. $v = 0.2$ and 0.4, in Figs. 5.1(a), 5.1(b), 5.2(a),

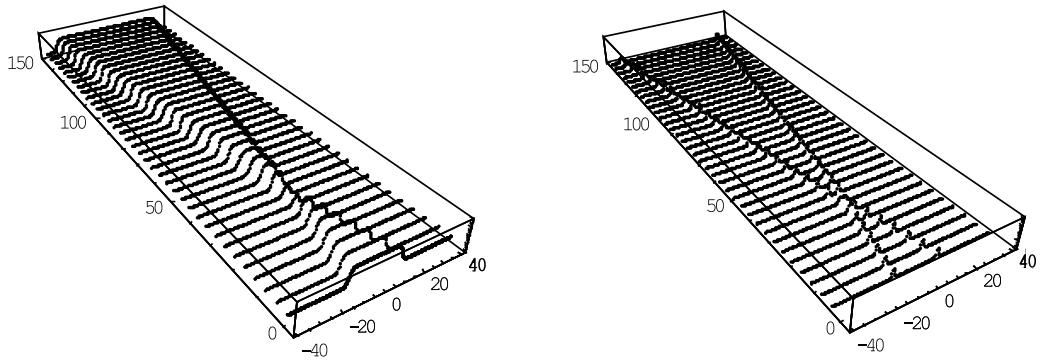

(a) Scalar field (b) Energy density

Figure 5.1: Collision of two domain walls where the initial velocity $v = 0.4$. The time evolutions of the scalar field Φ (a) and energy density ρ_Φ (b) are shown from $t = 0$ to 150. The collision occurs once around $t = 31$. We set $\lambda = 1.0$. (b): The maximum point of ρ_Φ defines the position of a wall ($z = z_{\rm W}(t)$).

and 5.2(b). The evolution of Φ is depicted in Figs. 5.1(a) and 5.2(a), while that of the energy density is shown in Figs. 5.1(b) and 5.2(b). The energy density is given by

$$\rho_\Phi = \frac{1}{2}\left[\dot{\Phi}^2 + \Phi'^2 + \frac{\lambda}{2}(\Phi^2 - 1)^2\right] . \tag{5.7}$$

From Figs. 5.1(b) and 5.2(b), we find some peaks in the energy density, by which we define the positions of moving walls ($z = \pm z_{\rm W}(t)$). If a domain wall is symmetric, its position is defined by $\Phi(z) = 0$. However, in more general case, just as in the present case that the domain wall is oscillating around some moving point, it may be natural to define the position of a domain wall by the maximum point of its energy density. In Figs. 5.1(b) and 5.2(b), we find the behavior of the collision as follows. Where the initial velocity $v = 0.4$, the collision occurs once, while it does twice where $v = 0.2$. To be precise, in the latter case, after two walls collide, they bounce, recede to a finite distance, and then return to collide again. As shown by several authors [12, 85, 423, 39], however, the result highly depends on the incident velocity v. In Appendix, we show our analysis, which confirms the previous work. For a sufficiently large velocity, it is expected that a kink and an antikink will just bounce off once, because there is no time to exchange the energy during the collision process. In fact, it has been shown in [12] that two walls just bounce off once for $v \gtrsim 0.25$. For a lower velocity, we find multiple bounces when they collide. The number of bounces during the collision sensitively depends on the incident velocity. For example, the bounce occurs once for $v = 0.4$, while twice for $v = 0.2$. We also find many bounce solutions for other incident velocities, as shown in Appendix (see also [12]). A set of the values of v which give the same number of bounce forms a fractal structure in the v-space as shown in Fig. 6 of [12]. Depending on an initial velocity, the number of bounces changes drastically.

5.2.2 Particle production on a moving domain wall

Once we find the solution of colliding domain walls, we can evaluate the time evolution of a scalar field on the domain wall. Since we assume that we are living on one domain wall, we are interested in production of a particle confined to the domain wall. We assume that there is some coupling between a 5D scalar field Φ that is responsible for the domain wall and a particle on the domain wall. Because the value of the scalar field changes with time, we expect quantum particle production to occur. This may be important to a reheating mechanism for the colliding domain walls. Hence we have to know the value of the scalar field Φ on the domain wall, i.e. $\Phi_{\rm W}(\tau) = \Phi(t, z_{\rm W}(t))$. Since the wall is moving in a 5D Minkowski space,

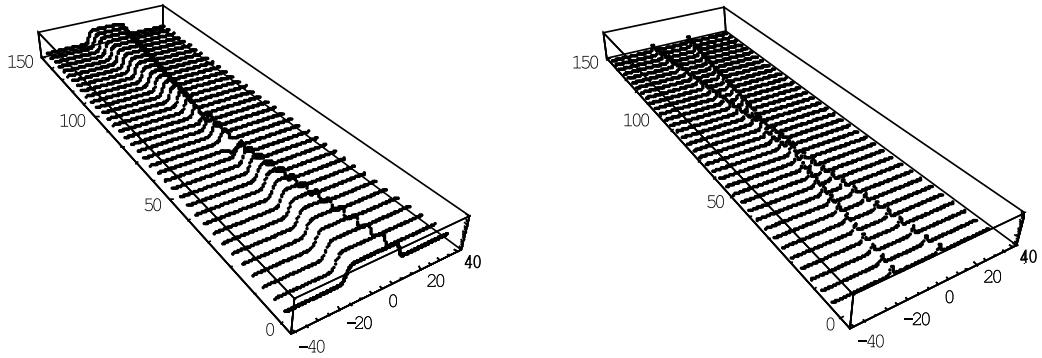

(a) Scalar field (b) Energy density

Figure 5.2: Collision of two domain walls where the initial velocity $v = 0.2$ with $\lambda = 1.0$. We find that collision occurs twice, at $t \approx 58$ and 77. From this figure, we find clearly that collision occurs twice.

we have to use the proper time τ of the wall, which is given by

$$\tau = \int_0^t dt \sqrt{1 - \dot{z}_{\rm W}^2(t)} \,, \tag{5.8}$$

when we estimate the particle production in our 4-dimensional domain wall. Let us consider a particle on the domain wall described by a scalar field ψ. Although the confined scalar field may also be extended in the 5-th direction because the domain wall has a finite width, we assume here that this scalar field is 4-dimensional, which means that it has the value only at the position of the domain wall ($z = z_W(t)$). This ansatz may be justified as follows. Suppose that we have a 5D scalar field Ψ, which is confined on a wall with a width $D_\Psi (\sim D)$. Such a confined scalar field Ψ could be described as

$$\Psi = N \exp\left[-\frac{(z - z_W(\tau))^2}{2D_\Psi^2} \right] \, \psi(x) \,, \tag{5.9}$$

where N is a normalization constant. This assumption may be plausible because a width of the domain wall when two walls collide is the same as the original width D as seen from Fig. 5.3. Assuming an interaction with the scalar field Φ as $1/2\, \bar{g}^2 \Phi^2 \Psi^2$, where $\bar{g}$ is a coupling constant, we find the dynamical equation for Ψ by $-\Box\Psi + \bar{g}^2 \Phi^2 \Psi = 0$. Inserting the ansatz (5.9), we obtain

$$N e^{-\frac{(z - z_W(\tau))^2}{2D_\Psi^2}} \left[\frac{\partial^2 \psi}{\partial \tau^2} + \left(\bar{g}^2 \Phi^2 - \nabla^2 + m_{\rm eff}^2 \right) \psi \right] = 0 \,, \tag{5.10}$$

where

$$m_{\rm eff}^2 = \frac{1 - \dot{z}_W^2}{D_\Psi^2} \left[1 - \frac{(z - z_W(\tau))^2}{D_\Psi^2} \right] + \frac{(z - z_W)}{D_\Psi^2} \ddot{z}_W \,. \tag{5.11}$$

Eq. (5.10) is non-trivial only near the wall ($z \sim z_W(\tau)$) because of the gaussian distribution. Hence Φ in Eq. (5.10) should be evaluated on the wall ($z \sim z_W(\tau)$). The effective mass term is estimated as $m_{\rm eff} \lesssim 1/D_\Psi$ because $|z - z_W(\tau)| \lesssim 1/D$, $\dot{z}_W^2 < 1$, and $|\ddot{z}_W| \lesssim \sigma |\dot{z}_W| < \sigma$, where $\sigma \sim \sqrt{\lambda} \sim 1/D$ is the oscillation frequency of the perturbations discussed given in Appendix. The maximal value of acceleration of a domain wall ($\ddot{z}_W$) can be evaluated in the case of the oscillating field around a static wall. Therefore, if we can ignore the mass term $m_{\rm eff}^2$ ($\lesssim 1/D_\Psi^2 \sim 1/D^2$), the equation for Ψ is approximated by the 4-dimensional equation for ψ as

$$\frac{\partial^2 \psi}{\partial \tau^2} - \nabla^2 \psi + \bar{g}^2 \, \Phi_{\rm W}^2(\tau) \, \psi = 0 \,, \tag{5.12}$$

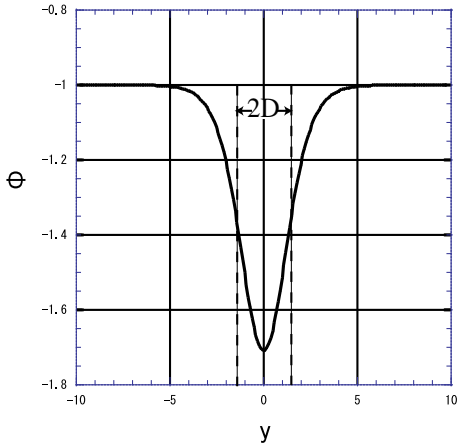

Figure 5.3: The spatial distribution of the scalar field Φ when the domain walls collide. D is the thickness of the wall. The scalar field has a non-vanishing value for the effective width of $2D$ at the collision.

where $\Phi_{\rm W}(\tau) = \Phi(z_W(\tau))$. $\psi(x)$ is the 4-dimensional part of 5D scalar field Ψ. The assumption of dropping the mass term may be a good approximation in the present case because it turns out that the produced particles with the frequencies higher than $1/D$ is much less dominant as we will show later. Once we find the basic equation for a scalar field ψ as Eq. (5.12), it is easy to quantize the scalar field ψ because our background spacetime is 4-dimensional Minkowski space. In a canonical quantization scheme [48], we expand ψ as

$$\psi(\tau, \vec{x}) = \sum_k [a_k\, \psi_k(\tau)\, u_k(\vec{x}) + a_k^\dagger \psi_k^*(\tau) u_k^*(\vec{x})]\,, \tag{5.13}$$

where $u_k(\vec{x}) = (2\pi)^{-\frac{3}{2}} e^{i\vec{k}\cdot\vec{x}}$. The wave equation (5.12) for each mode is now

$$\ddot{\psi_k} + [k^2 + \bar{g}^2 \Phi_{\rm W}^2(\tau)]\psi_k = 0\,, \tag{5.14}$$

where $k = |\vec{k}|$. Since the two domain walls are initially far away from each other, the value of $\Phi_{\rm W}$ is almost zero. We can quantize ψ by a usual quantization scheme. The eigen function with a positive frequency is given by $\psi_k^{(\rm in)} = 1/\sqrt{2\omega_k} e^{-i\omega_k \tau}$, where $\omega_k = \sqrt{k^2 + \bar{g}^2 \Phi_{\rm W}^2(0)} \approx k$. We impose the equal time commutation relation for the operators a_k and $a_k^\dagger$

$$[a_k, a_{k'}] = 0\,, \quad [a_k^\dagger, a_{k'}^\dagger] = 0\,, \quad [a_k, a_{k'}^\dagger] = \delta_{kk'}\,, \tag{5.15}$$

where a_k and $a_k^\dagger$ denote an annihilation and a creation operator, respectively. We then define a vacuum $|0>_{\rm in}$ at $\tau = 0$ by a_k as $a_k|0>_{\rm in} = 0$ for all k. After the collision of domain walls, we expect that the value of $\Phi_{\rm W}$ again approaches zero (see the next subsection for details). We can also define the vacuum state $|0>_{\rm out}$, which is different from the initial vacuum state $|0>_{\rm in}$. The eigen function of ψ_k for $\tau \to \infty$ is then given by a linear combination of $\psi_k^{(\rm in)}$ and $\psi_k^{(\rm in)*}$ as

$$\psi_k^{(\rm out)} = \alpha_k\, \psi_k^{(\rm in)} + \beta_k\, \psi_k^{(\rm in)*}\,, \tag{5.16}$$

and the annihilation and creation operators as

$$\bar{a}_k = \alpha_k a_k + \beta_k^* a_k^\dagger\,, \tag{5.17}$$

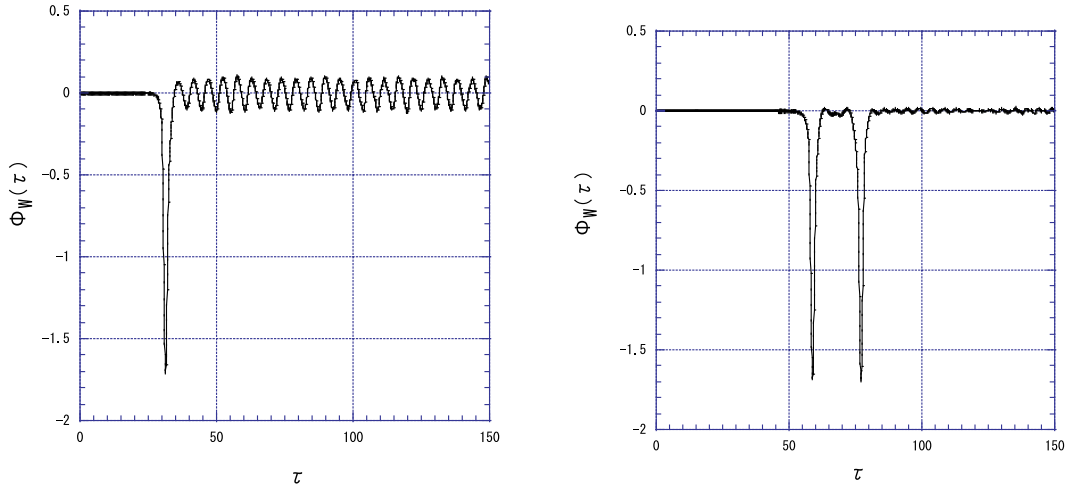

(a) $v = 0.4$ (b) $v = 0.2$

Figure 5.4: Time evolutions of a scalar field on one moving wall for $v = 0.4$ (a) and $v = 0.2$ (b) with fixed $\lambda = 1.0$. The value of the scalar field is given by $\Phi_{\rm W}(\tau) = \Phi(t, z_{\rm W}(t))$, where $z_{\rm W}(t)$ and τ denote the position of the wall and the proper time on the wall, respectively.

where α_k and β_k are the Bogolubov coefficients, which satisfy the normalization condition $|\alpha_k|^2 - |\beta_k|^2 = 1$. The Hamiltonian of this system is given by

$$: H := -\int_{\tau=\text{const}} : T^0{}_0 : \, d^3\vec{x} = \sum_k a_k^\dagger a_k \omega_k \,, \tag{5.18}$$

where : : is the normal ordering operation. The creation of the particles with mode k is evaluated as

$$< 0|_{\rm in} : H_k : |0 >_{\rm in} = |\beta_k|^2 \omega_k \text{ as } \tau \to \infty \,. \tag{5.19}$$

As a result, the number density and energy density of produced particles are obtained by

$$n = \int |\beta_k|^2 d^3\vec{k} \,, \quad \rho = \int |\beta_k|^2 \omega_k d^3\vec{k} \,. \tag{5.20}$$

Now we estimate the particle production by the domain wall collision. In Figs. 5.4(a) and 5.4(b), we depict the time evolution of $\Phi_{\rm W}$ on one moving wall with respect to τ. In Fig. 5.1(b), we found one collision point, which corresponds to a spike in Fig. 5.4(a), and the two-bounce in Fig. 5.2(b) gives two spikes in Fig. 5.4(b). We also show the results for different values of the coupling constant λ in Figs. 5.5(a) and 5.5(b) ($\lambda = 10$). If Fig. 5.5(a) we find that when λ is larger than $\lambda = 10$, the spike of $\Phi_{\rm W}$ becomes sharp. The same thing happens in the case of two bounces (see Fig. 5.5(b)). In Figs. 5.4(a)–5.5(b), we find that $\Phi_{\rm W}$ begins to oscillate after the collision. We also find that the period of these oscillations in Figs. 5.5(a) and 5.5(b) is shorter that those in Figs. 5.4(a) and 5.4(b). One may wonder whether this oscillation is realistic or not. This oscillation, however, turns out not to be a numerical error but a real oscillation of the domain wall. In Appendix, using perturbation analysis we show there is one stable oscillation around the kink solution $\Phi_K(z)$. We expect that the oscillation is excited by the collision. In fact, the amplitude of the oscillation increases as the incident velocity v increases. At a large velocity limit ($v \gtrsim 0.6$), we find $\Phi_\infty^2 \approx 0.18(\gamma - 1)$, where Φ_∞ is the amplitude of the post-oscillation. Since the scalar field on the domain wall oscillates as $\Phi_{\rm W} \approx \Phi_\infty \cos\sigma\tau$ after the collision, our wave equation (5.14) would be rewritten as

$$\ddot{\psi_k} + \left[k^2 + \frac{1}{2}\bar{g}^2\Phi_\infty^2 \left(1 + \cos 2\sigma\tau\right)\right]\psi_k = 0 \,, \tag{5.21}$$

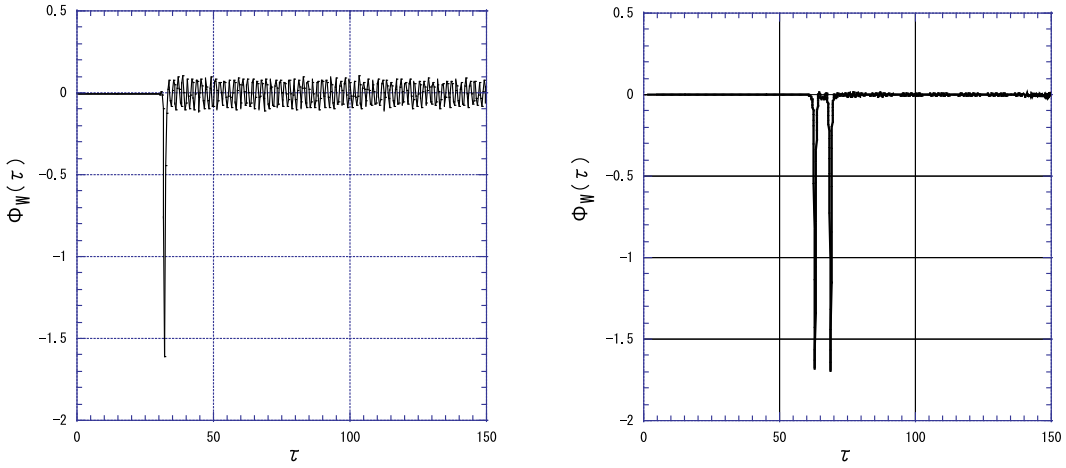

(a) $v = 0.4$ (b) $v = 0.2$

Figure 5.5: Time evolution of a scalar field $\Phi_{\rm W}(\tau)$ on one moving wall for $v = 0.4$ (a) and $v = 0.2$ (b) for $\lambda = 10$.

where $\sigma = \sqrt{3/2}\lambda^{1/2}$ is the eigenvalue of the perturbation eigen function, a so-called Methieu equation. From this equation, we may wonder whether we can ignore this oscillation when we evaluate the particle production rate. In fact, we can discuss a preheating mechanism via a parametric resonance with a similar oscillating behavior [256, 257], in conventional cosmology [289] as well as a brane world cosmology [451]. It is known that for a Methieu equation, there is an exponential instability $\psi_k \propto \exp(\mu_k t)$ within a set of resonance bands, where $\mu_k = \bar{g}\Phi_\infty^2/8$. This instability corresponds to an exponential growth of created particles, which is essential in the preheating mechanism. In order to get successful particle production by this resonance instability, however, we have to require a large value of $\bar{g}^2\Phi_\infty^2$. However, in the present simulation, it is rather small, e.g. $\Phi_\infty \sim 0.1$ where $v = 0.4$. Hence, we may ignore such particle production by parametric resonance in the present calculation. However, if the incident velocity is very fast, such as the speed of light, we may find a large oscillation. Then we could have an instant preheating process when domain walls collide. We also wonder whether or not the standard reheating mechanism due to the decay of an oscillating scalar field is effective. In this case, we have to evaluate the decay rate Γ_ϕ to other particles. Since $\Gamma_\phi \propto \bar{g}^4$, we expect that the reheating temperature is proportional to $\bar{g}^2$, which is small enough to be ignored. Note that there is another factor that reduces the decay rate where the potential is not a spontaneous symmetry breaking type [257]. In what follows, we ignore the creation due to the post-oscillation stage. Hence, we just follow the procedure shown in the previous subsection. Using the evolution of the scalar field $\Phi_{\rm W}$, we calculate the Bogolubov coefficients α_k and β_k. In Table 5.1, we show the results depending on three parameters; v (the incident velocity), λ (the self-coupling constant of the scalar field), and $\bar{g}$ (the coupling constant to a particle ψ).

From Table I, we find the following three features:

(1) The produced energy density ρ depends very much on $\bar{g}$. We study two cases with $\bar{g} = 0.01$ and 0.1. The energy density for $\bar{g} = 0.1$ is 10^4 times larger than that for $\bar{g} = 0.1$, which means that ρ is proportional to $\bar{g}^4$.

(2) The energy density ρ for $v = 0.2$ is twice larger than that for $v = 0.4$. It may be so because the bounce occurs twice for $v = 0.2$, while once for $v = 0.4$.

(3) The energy density is less sensitive to λ.

We also investigate several different initial velocities because the collisional process is very sensitive to its incident velocity. We analyze many cases with two bounces, with three bounces, with four bounces, etc. , in the range $v = 0.2$–0.25, as shown in Appendix. Using those numerical data, we also evaluate

$\bar{g}$	v	λ	D	N_b	n	ρ
0.01	0.4	1.0	1.414	1	3.69×10^{-7}	2.05×10^{-7}
		10	0.447		1.16×10^{-7}	2.05×10^{-7}
	0.2	1.0	1.414	2	7.19×10^{-7}	3.90×10^{-7}
		10	0.447		2.26×10^{-7}	3.91×10^{-7}
0.1	0.4	1.0	1.414	1	3.57×10^{-3}	2.01×10^{-3}
		10	0.447		1.16×10^{-3}	2.05×10^{-3}
	0.2	1.0	1.414	2	6.65×10^{-3}	3.81×10^{-3}
		10	0.447		2.24×10^{-3}	3.88×10^{-3}

Table 5.1: The number and energy densities (n and ρ) of created particles for the typical values of the coupling $\bar{g}$, the incident velocity v and the self-coupling λ. $D = \sqrt{2/\lambda}$ and N_b denote the width of the wall and the number of bounces at the collision, respectively.

the number and energy densities of the particles created at the collision. The results are summarized in Table 5.2. From Table II, we confirm the above three features (1)-(3). In particular, it becomes more clear that the energy density is proportional to the number of bounces N_b. We can summarize our results by the following empirical formula

$$n \approx 25 d \bar{g}^4 N_b \,, \quad \rho \approx 20 \bar{g}^4 N_b \,. \tag{5.22}$$

If the energy of the particles is thermalized by interaction and a thermal equilibrium state is realized, we can estimate the reheating temperature by

$$\rho = \frac{\pi^2}{30} g_{\rm eff} T_{\rm R}^4 \,, \tag{5.23}$$

where $g_{\rm eff}$ is the effective number of degrees of freedom of particles. Hence we find the reheating temperature by the domain wall collision as

$$T_{\rm R} = \left(\frac{\pi^2}{30}\right)^{-1/4} g_{\rm eff}^{-1/4} \rho^{1/4} \approx 0.88 \times \left(\frac{g_{\rm eff}}{100}\right)^{-1/4} \bar{g}\ N_b^{1/4} \,. \tag{5.24}$$

In order to see more details, in Figs. 5.6(a) and 5.6(b), we show a spectrum of the produced particles of number density n, i.e.

$$n = \int_0^\infty dk\ n_k \quad \text{with} \quad n_k = 4\pi |\beta_k|^2 k^2 \,. \tag{5.25}$$

The spectrum n_k is well fitted as a Gaussian distribution as

$$n_k \approx 4\pi A e^{-\frac{k^2}{2k_0^2}} \,, \tag{5.26}$$

where $k_0 = 0.73$ and $A = 3.12\times10^{-8}$ for Fig. 10 and $k_0 = 2.04$ and $A = 3.43\times10^{-9}$ for Fig. 11, although there is small deviation partially. These parameters can be described by physical quantities as $k_0 \approx 1/D$ and $A \approx \Phi_0 D^2 \bar{g}^4$. The reason is well understood. $k_0 \approx 1/D$ means that the typical wave number is given by the width of the scalar field when domain walls collide (see Fig. 5.3). As for β, it corresponds to the " reflection " coefficient of the " potential " given in Figs. 5.4(a)-5.5(b). It will be proportional to the coupling constant $\bar{g}^2$, and the reflection rate ($|\beta|^2$) will be related to the potential depth Φ_0 and the square of the width D^2. This result may support our ansatz that a scalar field ψ is 4-dimensional because the particles with the frequencies higher than $1/D$ are produced very little. The effect of finite

N_b	v	λ	D	n	ρ
2	0.225	1.0	1.414	7.03×10^{-7}	3.72×10^{-7}
		10	0.447	2.21×10^{-7}	3.71×10^{-7}
	0.238	1.0	1.414	7.08×10^{-7}	3.78×10^{-7}
		10	0.447	2.23×10^{-7}	3.78×10^{-7}
3	0.2062	1.0	1.414	1.10×10^{-6}	6.07×10^{-7}
		10	0.447	3.45×10^{-7}	6.06×10^{-7}
	0.2049	1.0	1.414	1.09×10^{-6}	6.01×10^{-7}
		10	0.447	3.43×10^{-7}	6.01×10^{-7}
	0.2298	1.0	1.414	1.10×10^{-6}	6.04×10^{-7}
		10	0.447	3.43×10^{-7}	6.02×10^{-7}
	0.22933	1.0	1.414	1.09×10^{-6}	6.03×10^{-7}
		10	0.447	3.44×10^{-7}	6.01×10^{-7}
4	0.229283	1.0	1.414	1.47×10^{-6}	8.10×10^{-7}
		10	0.447	4.61×10^{-7}	8.09×10^{-7}
	0.2292928	1.0	1.414	1.47×10^{-6}	8.16×10^{-7}
		10	0.447	4.62×10^{-7}	8.17×10^{-7}

Table 5.2: The number and energy densities (n and ρ) of created particles with respect to the number of bounces N_b. v and D are the incident velocity and the width of the wall, respectively. We set $\bar{g} = 0.01$.

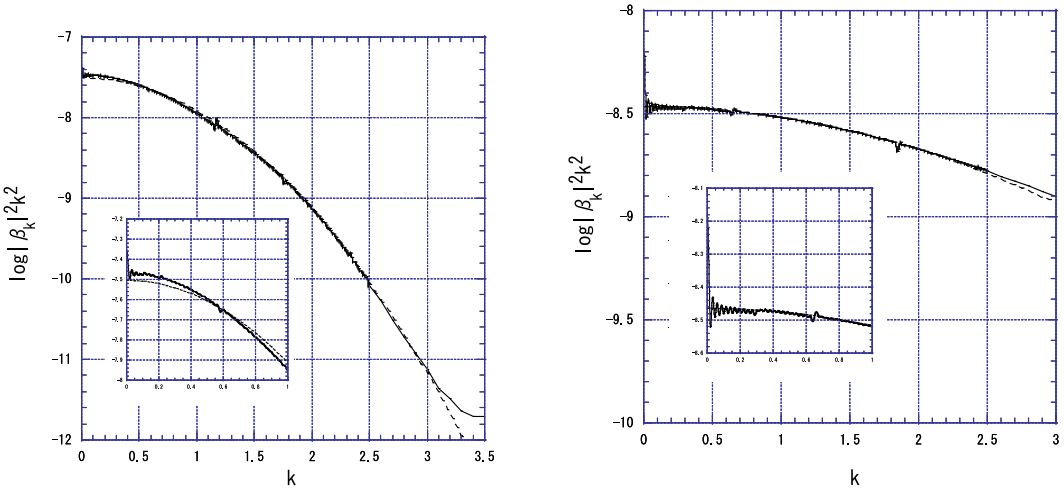

(a) $\lambda = 1.0$ (b) $\lambda = 10$

Figure 5.6: Spectrum of the particles created at the collision. We plot $\log|\beta_k|^2k^2$ with respect to k for (a) $\lambda = 1.0$ and (b) $\lambda = 10$ for the fixed parameters $v = 0.4$ and $\bar{g} = 10^{-2}$. The Gaussian distribution is plotted by a dotted line, which gives a good approximation for $k \leq 3$ (a) and $k \leq 2.5$ (b). In the small box, we enlarge the low frequency region ($k \leq 1$) to see the deviation from the Gaussian distribution.

width of the walls on particle production may not be important. Integrating the fitting spectrum (5.26), we obtain

$$n = \int_0^\infty n_k dk = (2\pi)^{3/2}\Phi_0 D\bar{g}^4 \approx 25 D\bar{g}^4 \,, \tag{5.27}$$

$$\rho = \int_0^\infty n_k \omega_k dk = 4\pi\Phi_0\bar{g}^4 \approx 20\bar{g}^4 \,, \tag{5.28}$$

whose values are exactly the same as those obtained by numerical integration in the case with one bounce (see Eq. (5.22)). We expect that they are enhanced by the factor N_b when we find N_b bounces at the collision. Therefore, although we obtain particle creation numerically, the result is easily understood and summarized by a simple formula.

5.2.3 Summary

We have studied particle production at the collision of two domain walls in 5D Minkowski spacetime. It may give a reheating mechanism in an ekpyrotic (or cyclic) brane scenario. We evaluated the production rate for particles confined to the domain wall. The energy density of created particles was approximated as $\rho \approx 4\pi\Phi_0\bar{g}^4 N_b$ where Φ_0 is the maximum amplitude of $\Phi_{\rm W}$, N_b is the number of bounces at the collision, and $\bar{g}$ is a coupling constant between a particle and a domain wall. If this energy is converted into standard matter fields, we find the reheating temperature as $T_{\rm R} \approx 0.88 \times \bar{g}\ N_b^{1/4}\,(g_{\rm eff}/100)^{-1/4}$. We find that the particle creation is affected more greatly by the coupling constant $\bar{g}$ than the other two parameters v and λ. The initial velocity changes the collision process, that is, the number of bounces at the collision, but this is less sensitive to the temperature. The thickness of a domain wall D (or a self-coupling constant λ) changes the width of potential $\Phi_{\rm w}^2(\tau)$ of a particle field (ψ), and it changes the typical energy scale of created particles, which is estimated as $\omega \sim 1/D$. In order to produce a successful reheating, a reheating temperature must be higher than 10^2 GeV, because we wish to explain the baryon number generation at the electro-weak energy scale [259]. Since Eq. (5.24) is written in the following form;

$$m_\eta \approx 1.1 N_b^{-1/4}\bar{g}^{-1}T_{\rm R} \approx 1.1\times 10^7[{\rm GeV}]\ N_b^{-1/4}\left(\frac{\bar{g}}{10^{-5}}\right)^{-1}\left(\frac{T_{\rm R}}{10^2{\rm GeV}}\right)\ , \tag{5.29}$$

we find a constraint on the fundamental energy scale m_η as $m_\eta \gtrsim 1.1\times 10^7$ GeV for $\bar{g} = 10^{-5}$ and $m_\eta \gtrsim 1.1\times 10^4$ GeV for $\bar{g} = 10^{-2}$, which are slightly larger than TeV scale. Here we assume $g_{\rm eff} = 100$. In the present work, we considered 3-dimensional domain walls in 5-dimensional Minkowski space and showed that particle production at the two-wall collision may provide a successful mechanism for reheating in the ekpyrotic universe. In string/M-theory, however, we expect higher dimensions, e.g. 10 or 11. If we compactify it to the effective 5-dimensional spacetime, our work can be applicable to such a mode. Moreover, if we discuss a collision of p-dimensional walls (branes) in $(p+2)$-dimensional spacetime, our approach can also be extended. In this work, we have not taken account of effects from background spacetime. We are planning to study how such a generalization affects the present results about particle creation at the collision. We shall explain this plan in the next chapter.

5.2.4 Appendix

1. **Numerical method**

   For our numerical analysis of the domain wall collision, we solve the partial differential equation (5.3) on discrete spatial grids with a periodic boundary condition. The scalar field on the grid points is defined by $\Phi_n(t) = \Phi(z_n, t)$, where $z_n = n\triangle y$, for $n = 1, 2, \ldots, N$. We use the fourth-order center difference scheme to approximate the second spatial derivative [207] as

   $$\frac{\partial^2\Phi_n}{\partial z^2} = \frac{1}{12(\triangle z)^2}\left[-\Phi_{n-2} + 16\Phi_{n-1} - 30\Phi_n + 16\Phi_{n+1} - \Phi_{n+2}\right] + O((\triangle z)^4)\ . \tag{5.30}$$

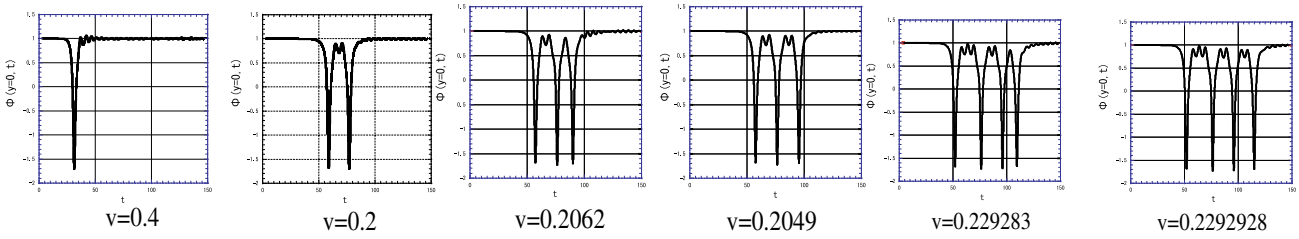

(a) $\upsilon = 0.4$ (b) (c)

Figure 5.7: Time evolution of Φ field at $z = 0$. We set $\lambda = 1.0$. (a): The bounce occurs once for a large velocity, while two bounces are found for the slower velocity. (b): Three bounces are found. (c): $\upsilon = 0.229283$ $\lambda = 1.0$ and (b) $\upsilon = 0.2292928$, $\lambda = 1.0$. Four bounces are found.

This leads to a set of N coupled second-order ordinary differential equations (ODE's) for the Φ_n. The ODE's are solved using a fourth-order Runge-Kutta scheme, and so our numerical algorithm is accurate to the fourth order both in time and in space, with error of $O((\triangle z)^4)$ and $O((\triangle t)^4)$. For the boundaries, we set the left and right grid boundaries at $z_L = -40$ and $z_R = +40$, and impose the condition $\Phi(z = z_L, t) = \Phi(z = z_R, t) = -1$. The grid number is $N = 8000$ with a grid size of $\triangle z = 1.0 \times 10^{-2}$. The initial position of a wall y_0 is set by $z_0 = |z_L + (z_R - z_L + 1)/3| = 13$, equivalently, one-third of the numerical range. For time steps, we set $\triangle t = 0.7 \times \triangle z$. As for the particle production process, we have to solve the second-order ordinary differential equations (5.14) for each wave number k. By using the fourth-order Runge-Kutta scheme, we solve them for the wave number k of $0 < k < 100$ with the width $\triangle k = 1.0 \times 10^{-3}$. We estimate $|\beta_k|^2$ in the equation (5.16). Defining the functions this way:

$$W_1 \equiv \psi_k \dot{\psi}_k^* - \psi_k^* \dot{\psi}_k \,, \quad W_2 \equiv \psi_k \dot{\psi}_k^* + \psi_k^* \dot{\psi}_k \,, \quad W_3 \equiv \psi_k \psi_k^* \,, \tag{5.31}$$

we use the formula

$$|\beta_k|^2 = \frac{(W_3 - W_1/2i\omega)^2 + (W_2/2\omega)^2}{4W_3} \,, \tag{5.32}$$

to evaluate $|\beta_k|$.

2. **Numerical examples of several bounces**

We depict some numerical examples that show several bounces at the collision. First we show two typical examples in Fig. 5.7(a). The figures show the behaviors of the scalar field Φ at $z = 0$ with respect to t. Initially, when two domain walls are located at a large distance, the value of the scalar field at $z = 0$ is 1. Then the two walls approach and collide. At this point the value of $|\Phi - 1|$ increases. After the collision, it again decreases to the initial value. We find some small oscillation around the domain wall structure excited by the collision. From Fig. 5.7(a), we find there is one bounce for $\upsilon = 0.4$, while a bounce occurs twice for $\upsilon = 0.2$. In fact, the results are very much sensitive to the incident velocities as shown in [12]. Here we present several examples to show how the behaviors of the scalar field depend on υ, which confirm the previous studies. In Fig. 5.7(b), we show the case for $\upsilon = 0.2062$ and $\upsilon = 0.2049$, respectively. We find three bounces at the collision. Four-bounce solutions are depicted in Fig. 5.7(c) for $\upsilon = 0.229283$ and $\upsilon = 0.2292928$. These calculation shows that the detail collisional process is very sensitive to the incident velocity.

3. **Perturbations of a domain wall**

We show that the oscillation we have found is a proper oscillation around a static stable domain wall. To show it, we perturb the static domain wall solution (5.4) as $\Phi = \Phi_K(z) + \delta\Phi(t, z)$. In this

appendix, we use the dimensionless variables rescaled by η. Substituting this into Eq. (5.3) and linearizing it, we obtain

$$\delta\ddot{\Phi} - \delta\Phi'' + \lambda(3\Phi_K^2 - 1)\delta\Phi = 0\,. \tag{5.33}$$

Setting $\delta\Phi = e^{-i\sigma t}F(z)$ and introducing new variable $\bar{z} = \tanh(z/D)$, we rewrite Eq. (5.33) as

$$(1-\bar{z}^2)\frac{d^2F}{d\bar{z}^2} - 2\bar{z}\frac{dF}{d\bar{z}} + 2\left[3 - \frac{2-\sigma^2/\lambda}{1-\bar{z}^2}\right]F = 0\,. \tag{5.34}$$

The solution is given by the associated Legendre function. Imposing the boundary condition ($F \to 0$ as $z \to \infty$), we have two regular solutions; $F(\bar{z}) = P_2^2(\bar{z})$ with $\sigma = 0$ and $P_2^1(\bar{z})$ with $\sigma = \sqrt{3/2}\lambda^{1/2}$. The solution of the former mode is just corresponds to a boost of a kink solution in the z direction, because we find $F(z) \approx \Phi_K(z) - \Phi_K(z - dz)$. The solution of the latter is the oscillation mode we find. In fact, taking the average over 10 cycles in the oscillation after the collision in Fig. 5.4(a), we obtain a mean angular frequency of about 1.17, which is very close to $\sigma = \sqrt{3/2} \sim 1.22$. The ratio is about 0.96. We also evaluate the angular frequency for other cases. We find $1.33 = 1.09\sigma$ for Fig. 5.4(b), $3.67 = 0.95\sigma$ for Fig. 5.5(a), and $4.18 = 1.08\sigma$ for Fig. 5.5(b). From the figures, we also find that the amplitude of oscillation gets larger as the incident velocity is faster. This is because the excitation energy of a wall at the collision will be large for a large velocity. We then conclude that the oscillations after the collision of two domain walls are the proper oscillations around a stable domain wall.

5.3 Fermions on Colliding Brane

It has been known since the 70's that topological defects such as domain walls can trap fermions on their world volumes [221]. In the 80's this fact formed an integral part of suggestions that one may regard our universe as a domain wall [6, 388, 459, 181], or more generally a brane in a higher dimensional universe [16, 373, 46, 418]. The idea is that the fermionic chiral matter making up the standard model is composed of such trapped zero modes [179, 25, 374, 127, 241, 384, 262, 324]. A similar mechanism is used in models, such as the Horawa-Witten model [206, 299] of heterotic M-Theory, in which two domain walls are present. Our world is localized on one brane and a shadow world is localized on the other brane. The existence of models with more than one brane suggests that branes may collide, and it is natural to suppose that the Big Bang is associated with the collision [246, 432, 248]. This raises the fascinating questions of what happens to the localized fermions during such collisions? Put more picturesquely, what is the fate of the standard model during brane collision? In this paper we shall embark on what we believe is the first study of this question by solving numerically the Dirac equation for a fermions coupled via Yukawa interaction to a system of two colliding domain walls, i.e. a kink-anti-kink collision in five-dimensional Minkowski spacetime. Each individual domain wall may be described analytically by a static solution and given such a solution one may easily find analytically the fermion zero modes, which from the point of view of the 3+1 dimensional world volume behave like massless chiral fermions. The back reaction of the fermions on the domain wall is here, and throughout this paper, neglected.

Kink-anti-kink collisions, have recently been studied numerically [12, 436, 13]. One solves the scalar field equations with initial data corresponding to a superposition of the boosted profiles of a kink and an anti-kink. It was found [12, 436] that, depending on the initial relative velocity that such domain wall pairs can pass through one another, or bounce, or suffer a number of bounces in a fashion reminiscent of the cyclic universe scenario [432]. One may extend the treatment to include gravity [274, 437, 183, 94, 322] but in this paper we shall, for the sake of our preliminary study, work throughout with gravity switched off. One may now solve the Dirac equation in the time dependent background generated by the kink-anti-kink collision. We use as initial data for the Dirac equation the boosted profiles of the chiral zero modes associated with the individual domain walls.

5.3.1 Fermions on moving branes

We start with a discussion of five-dimensional (5D) four-component fermions in a time-dependent domain wall in 5D Minkowski spacetime. As a domain wall, we adopt a 5D real scalar field Φ with an appropriate potential $V(\Phi)$. The 5D Dirac equation with a Yukawa coupling term $g\Phi\bar{\Psi}\Psi$ is given by

$$(\Gamma^{\hat{A}}\partial_{\hat{A}} + g\Phi)\Psi = 0, \quad (\hat{A} = 0, 1, 2, 3, 5)\,, \tag{5.35}$$

where Ψ is a 5D four-component fermion. $\Gamma^{\hat{A}}$ are the Dirac matrices in 5D Minkowski spacetime satisfying the anticommutation relations as $\{\Gamma^{\hat{A}}, \Gamma^{\hat{B}}\} = 2\eta^{\hat{A}\hat{B}}$, where $\eta^{\hat{A}\hat{B}} = \mathrm{diag}(-1, 1, 1, 1, 1)$ is Minkowski metric[1]. We explicitly use the following Dirac-Pauli representation

$$\Gamma^{\hat{0}} = \begin{pmatrix} -i & 0 \\ 0 & i \end{pmatrix}, \quad \Gamma^{\hat{5}} = \begin{pmatrix} 0 & 1 \\ 1 & 0 \end{pmatrix}, \quad \Gamma^{\hat{k}} = \begin{pmatrix} 0 & -i\sigma^k \\ i\sigma^k & 0 \end{pmatrix}, \quad (k = 1, 2, 3)\,, \tag{5.36}$$

with σ^k being the Pauli 2×2 matrices. Note that Eq. (5.35) implies current conservation law as $\partial_A n^A = 0$, where $n^A \equiv \bar{\Psi}\Gamma^{\hat{A}}\Psi$ is conserved number current. Here we define $\bar{\Psi} \equiv \Psi^\dagger\Gamma_{\hat{0}}$. This gives conserved number density $n \equiv n^0 = \bar{\Psi}\Gamma^{\hat{0}}\Psi = \Psi^\dagger\Psi$. The total number of fermions is defined by $N = \int d^5X n$, which is conserved. Later we shall need the fact that the Dirac equation (5.35) has the following time reversal and reflection symmetries:
(1) If $\Psi(t, \vec{x}, z)$ is a solution of the Dirac equation with scalar field $\Phi(t, \vec{x}, z)$, $\Gamma^{\hat{0}}\Psi(-t, \vec{x}, z)$ is a solution of the Dirac equation with the scalar field $-\Phi(-t, \vec{x}, z)$, where $X^5 = z$ is the coordinate of a fifth dimension. In particular, when there is no interaction ($\Phi = 0$ or $g = 0$), $\Gamma^{\hat{0}}\Psi(-t, \vec{x}, z)$ is time reversal of $\Psi(t, \vec{x}, z)$
(2) If $\Psi(t, \vec{x}, z)$ is a solution of the Dirac equation with scalar field $\Phi(t, \vec{x}, z)$, $\Gamma^{\hat{5}}\Psi(t, \vec{x}, -z)$ is a solution of the Dirac equation with the scalar field $-\Phi(t, \vec{x}, -z)$. In particular, if $\Psi(t, \vec{x}, z)$ is a solution for a kink [an anti-kink], $\Gamma^{\hat{5}}\Psi(t, \vec{x}, z)$ is a solution for an anti-kink [a kink]. It will turn out that the solution with a kink [an anti-kink] is related to positive [negative] chiral fermions, which are defined below (see next subsection).
(3) Combining (1) and (2), we find that $\Gamma^{\hat{5}}\Gamma^{\hat{0}}\Psi(-t, \vec{x}, -z)$ is a solution of the Dirac equation with $\Phi(-t, \vec{x}, -z)$

If we assume some symmetries for a domain wall, we find further properties for fermions as follows.
(i) For the case of a static domain wall, (1) yields that $\Gamma^{\hat{0}}\Psi(t, \vec{x}, z)$ is a solution for an anti-kink [a kink] if $\Psi(t, \vec{x}, z)$ is a solution for a kink [an anti-kink].
(ii) If a domain wall is described by a kink (or an anti-kink), which has symmetry such that $\Phi(t, \vec{x}, -z) = -\Phi(t, \vec{x}, z)$, (2) yields that $\Gamma^{\hat{5}}\Psi(t, \vec{x}, z)$ is a solution for an anti-kink [a kink] if $\Psi(t, \vec{x}, z)$ is a solution for a kink [an anti-kink].
(iii) We may also have time symmetry such that $\Phi(-t, \vec{x}, z) = \Phi(t, \vec{x}, z)$ for collision of two walls. In fact we find from numerical analysis that this ansatz is approximately correct [436]. Assuming z-reflection symmetry as well, we find from (3) that $\Gamma^{\hat{5}}\Gamma^{\hat{0}}\Psi_\pm(-t, \vec{x}, -z)$, which is time reversal and z-reflection of $\Psi_\pm(t, \vec{x}, z)$, is also a solution for the same scalar field $\Phi(t, \vec{x}, z)$.

Before going to analyze concrete examples, we introduce two chiral fermion states

$$\Psi_\pm = \frac{1}{2}\left(1 \pm \Gamma^{\hat{5}}\right)\Psi \tag{5.37}$$

This definition implies

$$\frac{1}{2}\left(1 \pm \Gamma^{\hat{5}}\right)\Psi_\pm = \Psi_\pm, \ \frac{1}{2}\left(1 \mp \Gamma^{\hat{5}}\right)\Psi_\pm = 0\,. \tag{5.38}$$

Using the representation (5.36), we have

$$\Psi_+ = \begin{pmatrix} \psi_+ \\ \psi_+ \end{pmatrix}, \quad \Psi_- = \begin{pmatrix} \psi_- \\ -\psi_- \end{pmatrix}, \tag{5.39}$$

[1]The Capital Latin indices run from 0 to 3 and 5, while the Greek indices from 0 to 3.

where ψ_+ and ψ_- are two-component spinors. The Dirac equation (5.35) is now reduced to

$$(\pm\partial_{\tilde{5}} + g\Phi)\,\psi_\pm + \Gamma^{\hat{\mu}}\partial_{\hat{\mu}}\psi_\mp = 0\,. \tag{5.40}$$

As for a domain wall, now we assume the potential form is given by $V(\Phi) = \frac{\lambda}{4}\left(\Phi^2 - \eta^2\right)^2$. Here we recall the dimension of some variables. Since we discuss five dimensional spacetime, we have the following dimensionality:

$$[\Phi] = [\eta] = L^{-3/2}, [\Psi] = L^{-2}, [g] = L^{1/2}, [\lambda] = L\,, \tag{5.41}$$

where L is a scale length. In what follows, we use units in which $m_\eta(\equiv \eta^{2/3}) = 1$. Then a domain wall solution is given by $\Phi = \epsilon\tanh\left(\frac{z}{D}\right)$, where $\epsilon = \pm$ correspond to a kink and an anti-kink solutions and $D = \sqrt{2/\lambda}$ is the width of a domain wall. Note that $\Phi(z)$ is an odd function of z. As for a fermion, in the case of a static domain wall, separating variables as $\psi_+ = \overset{(4)}{\psi}_+(x^\mu)f_+(z)$ and $\psi_- = \overset{(4)}{\psi}_-(x^\mu)f_-(z)$ and assuming massless chiral fermions on a brane, i.e. $\Gamma^{\hat{\mu}}\partial_\mu \overset{(4)}{\psi}_\pm(x^\mu) = 0$, we find the equations for $f_\pm(z)$ as

$$(\pm\partial_5 + g\Phi(z))\,f_\pm = 0\,. \tag{5.42}$$

We find the solutions are

$$f_\pm \propto \left[\cosh\left(\frac{z}{D}\right)\right]^{\mp\epsilon g D}\,. \tag{5.43}$$

Note that the fermion wave function is an even function of z. Hence the positive-chiral (the negative-chiral) fermion is localized for a kink (an anti-kink) but is not localized for an anti-kink (a kink). To fix numbers of fermions on a wall, $f_\pm$ should be normalized up to an arbitrary phase factor $\phi_{\pm(0)}$, which is set to be zero. Using a number density of fermions given by

$$n \equiv \Psi^\dagger\Psi = 2\left(\psi_+^\dagger\psi_+ + \psi_-^\dagger\psi_-\right)\,, \tag{5.44}$$

we normalize the total number of fermions localized on a static domain wall to be unity, i.e. $N = 1$. More precisely, for a kink (an anti-kink), we impose $\int_{-\infty}^{\infty} n_\pm d\tilde{z} = 1$ which gives

$$f_\pm(z) = \left[\frac{\Gamma(gD+\frac{1}{2})}{2\sqrt{\pi}D\Gamma(gD)}\right]^{1/2}\left[\cosh\left(\frac{z}{D}\right)\right]^{-gD}\,. \tag{5.45}$$

Using this solution, we can describe the wave function of fermion localized on a kink (or an anti-kink) as

$$\Psi^{(\mathrm{K})}(x,z) = \begin{pmatrix} \overset{(4)}{\psi}_+(x)f_+(z) \\ \overset{(4)}{\psi}_+(x)f_+(z) \end{pmatrix}\,,\quad \Psi^{(\mathrm{A})}(x,z) = \begin{pmatrix} \overset{(4)}{\psi}_-(x)f_-(z) \\ -\overset{(4)}{\psi}_-(x)f_-(z) \end{pmatrix}\,. \tag{5.46}$$

To quantize the fermion fields, we define annihilation operators of localized fermions on a kink and on an anti-kink by

$$a_{\mathrm{K}} = \langle\Psi^{(\mathrm{K})},\Psi\rangle \;\text{ and }\; a_{\mathrm{A}} = \langle\Psi^{(\mathrm{A})},\Psi\rangle \tag{5.47}$$

Note that those two states are orthogonal, i.e. $\langle\Psi^{(\mathrm{K})},\Psi^{(\mathrm{A})}\rangle = 0$. To discuss fermions at collision of branes, we first discuss fermions on a domain wall moving with a constant velocity. When a domain wall is moving, however, Φ is time-dependent, and then the above prescription (separation of the fifth coordinate) to find wave functions is no longer valid. Since 3-space is flat, we expand the wave functions by Fourier series as

$$\psi_\pm = \frac{1}{(2\pi)^{3/2}}\int d^3\vec{k}\; e^{i\vec{k}\vec{x}}\psi_\pm(t,z;\vec{k})\,. \tag{5.48}$$

We find the Dirac equations become

$$(\pm\partial_5 + g\Phi)\,\psi_\pm - \Big(i\partial_0 \pm (\vec{k}\cdot\vec{\sigma})\Big)\,\psi_\mp = 0\,. \tag{5.49}$$

In what follows, we shall consider only low energy fermions, that is, we assume that $\vec{k} \approx 0$, that is $|\vec{k}|$ is enough small compared with the mass scale of 5D fermion ($g\Phi$). The equations we have to solve are now

$$i\partial_0\psi_\pm = (\mp\partial_5 + g\Phi)\,\psi_\mp\,. \tag{5.50}$$

Since up- and down-components of $\psi_\pm$ are decoupled, we discuss only up-components here. Note that taking into account $\vec{k}$ mixes the up- and down-components. With this ansatz, we can describe fermion by two single-component chiral wave functions as

$$\Psi = \begin{pmatrix} 1 \\ 0 \\ 1 \\ 0 \end{pmatrix}\psi_+(z,t) + \begin{pmatrix} 1 \\ 0 \\ -1 \\ 0 \end{pmatrix}\psi_-(z,t)\,. \tag{5.51}$$

For a localized fermion on a static kink (or an anti-kink), the wave functions are $\psi_\pm(z,t) = f_\pm(z)$. Next we construct a localized fermion wave function on a moving domain wall with a constant velocity v. In this case, we can find the analytic solution by a Lorentz boost. We find for a kink with velocity v,

$$\psi_+^{(\mathrm{K})}(z,t;v) = \sqrt{\frac{\gamma+1}{2}}\tilde{\psi}^{(\mathrm{K})}\left(\gamma(z-vt)\right)\,,\quad \psi_-^{(\mathrm{K})}(z,t;v) = i\frac{\gamma v}{\gamma+1}\sqrt{\frac{\gamma+1}{2}}\tilde{\psi}^{(\mathrm{K})}\left(\gamma(z-vt)\right) \tag{5.52}$$

and for an anti-kink with velocity v,

$$\psi_-^{(\mathrm{A})}(z,t;v) = \sqrt{\frac{\gamma+1}{2}}\tilde{\psi}^{(\mathrm{A})}\left(\gamma(z-vt)\right)\,,\quad \psi_+^{(\mathrm{A})}(z,t;v) = -i\frac{\gamma v}{\gamma+1}\sqrt{\frac{\gamma+1}{2}}\tilde{\psi}^{(\mathrm{A})}\left(\gamma(z-vt)\right)\,, \tag{5.53}$$

where $\tilde{\psi}^{(\mathrm{K})}(\tilde{z}) = f_+(\tilde{z})$ and $\tilde{\psi}^{(\mathrm{A})}(\tilde{z}) = f_-(\tilde{z})$ are static wave functions of chiral fermions localized on static kink and anti-kink, respectively, and $\gamma = 1/\sqrt{1-v^2}$ is the Lorentz factor. We can check that the total number of fermions is preserved also in the boosted Lorentz frame. From Eqs. (5.52) and (5.53), we find that $n = \gamma\tilde{n}$. Integrating it in the z-direction, we find

$$\int_{t=\mathrm{const}} dz\; n = \int_{t=\mathrm{const}} dz\;\gamma\tilde{n}\left(\gamma(z-vt)\right) = \int d\tilde{z}\;\tilde{n}\left(\tilde{z}\right) = 1\,. \tag{5.54}$$

If a domain wall is given by a kink [an anti-kink], we have only the positive-chiral fermions in a comoving frame [the negative-chiral fermions]. However, from Eqs (5.52) and (5.53), we find that the negative-chiral modes [positive-chiral modes] also appear in this boosted Lorentz frame. For a kink, the ratio of number density of the negative-chiral modes to that of the positive-chiral ones is given by $\gamma^2 v^2/(\gamma+1)^2$. The above wave functions on a moving domain wall with constant velocity can be used for setting the initial data for colliding domain walls.

5.3.2 Initial setup and Outgoing states

We construct our initial data as follows. Provide a kink solution at $z = -z_0$ and an anti-kink solution at $z = z_0$, which are separated by a large distance and approaching each other with the same speed v. We can set up as an initial profile for the scalar field Φ:

$$\Phi(z,t) = \Phi^{(\mathrm{K})}(z,t;v) + \Phi^{(\mathrm{A})}(z,t;-v) - 1\,, \tag{5.55}$$

where

$$\Phi^{(\mathrm{K,A})}(z,t;v) = \pm\tanh(\gamma(z-vt)/D) \tag{5.56}$$

are the Lorentz boosted kink and anti-kink solutions, respectively. Here we have chosen that the initial time is $t = t_{\rm in} \equiv -z_0/v$. The domain walls collide at $t = 0$. For fermions on moving walls, we first expand the wave function as

$$\hat{\Psi} = \Psi_{\rm in}^{(\rm K)}(x, z; v)a_{\rm K} + \Psi_{\rm in}^{(\rm A)}(x, z; -v)a_{\rm A} + \Psi_{\rm in}^{(\rm B)}(x, z)a_{\rm B}\,, \tag{5.57}$$

where $\Psi_{\rm in}^{(\rm K)}(x, z; v)$ and $\Psi_{\rm in}^{(\rm A)}(x, z; -v)$ are the wave function of right-moving localized fermion on a kink and those of left-moving one on an anti-kink, respectively, which are explicitly by Eq. (5.52) and Eq. (5.53). We also denote the bulk fermions symbolically by $\Psi_{\rm in}^{(\rm B)}(x, z)$. We do not give its explicit form because it does not play any important role in the present situation. We have assumed in Eq. (5.57) that $\{\Psi_{\rm in}^{(\rm K)}(x, z; v), \Psi_{\rm in}^{(\rm A)}(x, z; -v)$ and $\Psi_{\rm in}^{(\rm B)}(x, z)\}$ form a complete orthogonal system. Note that $\{\Psi_{\rm in}^{(\rm K)}(x, z; v)$ and $\Psi_{\rm in}^{(\rm A)}(x, z; -v)\}$ are orthogonal.

Now we can set up an initial state for fermion by creation-annihilation operators. We shall call a domain wall associated with fermions a fermion wall, and a domain wall in vacuum a vacuum wall. We shall discuss two cases: one is collision of two fermion walls, and the other is collision of fermion and vacuum walls. For initial state of fermions, we consider two states;

$$|{\rm KA}\rangle \equiv a_{\rm A}^\dagger a_{\rm K}^\dagger |0\rangle \quad |{\rm K0}\rangle \equiv a_{\rm K}^\dagger |0\rangle \tag{5.58}$$

where $|0\rangle$ is a fermion vacuum state. We discuss behaviour of fermions at collision. After collision of two domain walls, each wall will recede to infinity with almost the same velocity as the initial one v. Therefore we expect that positive chiral fermions stay on a left-moving kink and negative ones on a right-moving anti-kink. Those wave functions are given by $\Psi_{\rm out}^{(\rm K)}(x, z; -v)$ and $\Psi_{\rm out}^{(\rm A)}(x, z; v)$. There may be bulk fermions which are left behind after collision, which wave function is symbolically written by $\Psi_{\rm out}^{(\rm B)}(x, z)$. Since the initial wave functions ($\Psi_{\rm in}^{(\rm K)}(x, z; v)$ and $\Psi_{\rm in}^{(\rm A)}(x, z; -v)$) are rewritten as the finial wave functions ($\Psi_{\rm out}^{(\rm K)}(x, z; -v)$, $\Psi_{\rm out}^{(\rm A)}(x, z; v)$, and $\Psi_{\rm out}^{(\rm B)}(x, z)$ at $t = t_{\rm out} \equiv z_0/v$), we find the relations between them by solving the Dirac equation (5.50). Those relations can be written as

$$\begin{aligned}
\Psi_{\rm in}^{(\rm K)}(x, z; v) &\sim \alpha_{\rm K}\Psi_{\rm out}^{(\rm K)}(x, z; -v) + \beta_{\rm K}\Psi_{\rm out}^{(\rm A)}(x, z; v) + \gamma_{\rm K}\Psi_{\rm out}^{(\rm B)}(x, z)\,,\\
\Psi_{\rm in}^{(\rm A)}(x, z; -v) &\sim \alpha_{\rm A}\Psi_{\rm out}^{(\rm A)}(x, z; v) + \beta_{\rm A}\Psi_{\rm out}^{(\rm K)}(x, z; -v) + \gamma_{\rm A}\Psi_{\rm out}^{(\rm B)}(x, z)\,.
\end{aligned} \tag{5.59}$$

In order to define final fermion states, we also describe the wave function as

$$\hat{\Psi} = \Psi_{\rm out}^{(\rm K)}(x, z; -v)b_{\rm K} + \Psi_{\rm out}^{(\rm A)}(x, z; v)b_{\rm A} + \Psi_{\rm out}^{(\rm B)}(x, z)b_{\rm B}\,, \tag{5.60}$$

where $b_{\rm K}$, $b_{\rm A}$ and $b_{\rm B}$ are annihilation operators of those fermion states. From Eqs. (5.57), (**??**), (5.59) and (5.60), we find

$$b_{\rm K} = \alpha_{\rm K}a_{\rm K} + \beta_{\rm A}a_{\rm A}\,, \quad b_{\rm A} = \alpha_{\rm A}a_{\rm A} + \beta_{\rm K}a_{\rm K} \tag{5.61}$$

Using the Bogoliubov coefficients $\alpha_{\rm K}, \beta_{\rm K}$ and $\alpha_{\rm A}, \beta_{\rm A}$, we obtain the expectation values of fermion number on a kink and an anti-kink after collision as

$$\langle N_{\rm K}\rangle \equiv \langle {\rm KA}|b_{\rm K}^\dagger b_{\rm K}|{\rm KA}\rangle = |\alpha_{\rm K}|^2 + |\beta_{\rm A}|^2\,, \quad \langle N_{\rm A}\rangle \equiv \langle {\rm KA}|b_{\rm A}^\dagger b_{\rm A}|{\rm KA}\rangle = |\alpha_{\rm A}|^2 + |\beta_{\rm K}|^2 \tag{5.62}$$

for the case of $|{\rm KA}\rangle$. If the initial state is $|{\rm K0}\rangle$, we find

$$\langle N_{\rm K}\rangle \equiv \langle {\rm K0}|b_{\rm K}^\dagger b_{\rm K}|{\rm K0}\rangle = |\alpha_{\rm K}|^2 \quad \langle N_{\rm A}\rangle \equiv \langle {\rm K0}|b_{\rm A}^\dagger b_{\rm A}|{\rm K0}\rangle = |\beta_{\rm K}|^2\,. \tag{5.63}$$

5.3.3 Time evolution of fermion wave functions

In order to obtain the Bogoliubov coefficients, we have to solve the equations for domain wall Φ [436] and fermion Ψ numerically. For the time evolution of Ψ, we use the Crank-Nicholson method since it is

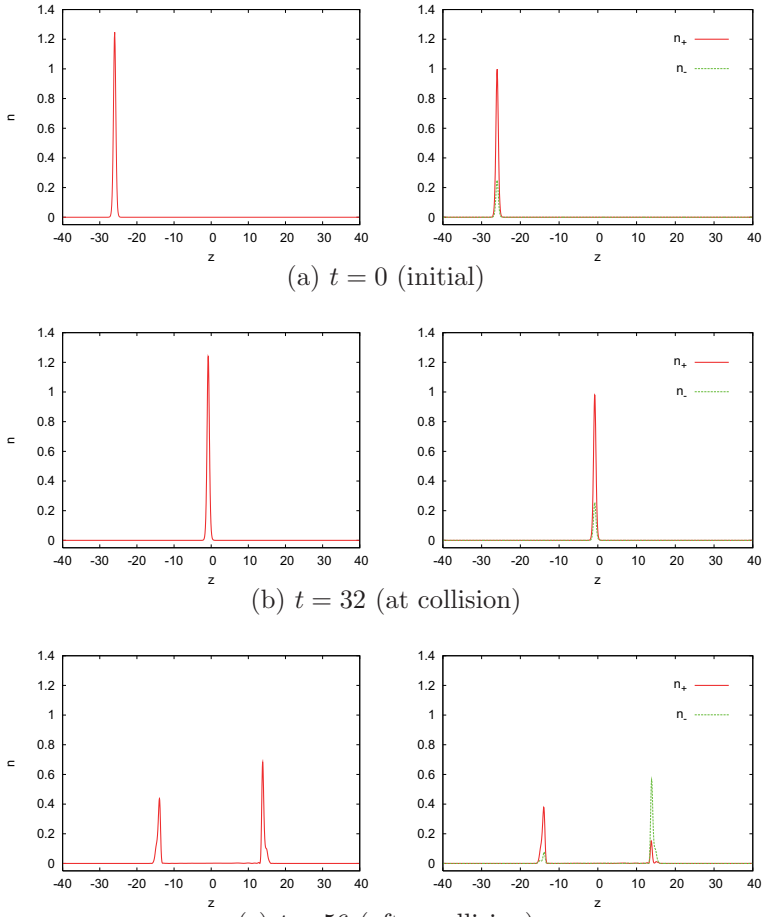

(a) $t = 0$ (initial)

(b) $t = 32$ (at collision)

(c) $t = 56$ (after collision)

Figure 5.8: Snap shots of the number density of the wave function ($n = \Psi^\dagger\Psi$) and those of two chiral states $n_\pm$ for collision of fermion-vacuum walls. We set $D = 1, g = 2$, and $v = 0.8$.

generally shown to be useful for the parabolic type of partial differential equation. In our simulation of two-wall collision, we have three unfixed parameters, i.e. a wall thickness (D) and an initial wall velocity (v) and a coupling between fermions and a domain wall (g). From the solution (5.45), we find the fermions are localized within the domain wall width D if $g \gtrsim 2/D$. When $g < 2/D$, fermions leak out from the domain wall. Hence, in this paper, we analyze for the case of $g \geq 2$. We set $D = 1$, but leave v free. Before showing our results for fermions, we summarize the behaviours of domain walls discussed in [436]. We find a bounce of domain walls, which depends in a complicated way on the initial velocity (There is a fractal structure in the initial velocity space [**?**]). After the collision, two domain walls recede into infinity with almost same velocity $\pm v$. It is similar to collision of solitons. To obtain the Bogoliubov coefficients, we solve the Dirac equation for the collision of fermion-vacuum walls, i.e. fermions are initially localized on one wall, and the other wall is empty ($\Psi^{(\mathrm{K})}_{\mathrm{in}}(x, z; v)$ or $\Psi^{(\mathrm{A})}_{\mathrm{in}}(x, z; -v)$).

We shall give numerical results only for the case that positive chiral fermions are initially localized on a kink ($\Psi^{(\mathrm{K})}_{\mathrm{in}}(x, z; v)$). Because of z-reflection symmetry discussed, we find the same Bogoliubov coefficients for the case that negative chiral fermions are initially localized on an anti-kink ($\Psi^{(\mathrm{A})}_{\mathrm{in}}(x, z; -v)$), i.e. $|\alpha_{\mathrm{K}}|^2 = |\alpha_{\mathrm{A}}|^2$ and $|\beta_{\mathrm{K}}|^2 = |\beta_{\mathrm{A}}|^2$. Setting $g = 2$ and $v = 0.8$, we show the result in Fig. 6.1(a). The other chiral mode appears at collision and the wave function splits into two parts after collision. From the

v	$g=2$			$g=2.5$		
	$\|\alpha_{\rm K}\|^2$	$\|\beta_{\rm K}\|^2$	$\|\gamma_{\rm K}\|^2$	$\|\alpha_{\rm K}\|^2$	$\|\beta_{\rm K}\|^2$	$\|\gamma_{\rm K}\|^2$
0.3	0.94	0.056	0.004	0.47	0.53	0.00
0.4	0.87	0.12	0.01	0.57	0.40	0.03
0.6	0.69	0.30	0.01	0.78	0.17	0.05
0.8	0.42	0.55	0.03	0.88	0.02	0.10

Table 5.3: The Bogoliubov coefficients of fermion wave functions localized on each domain wall after collision ($|\alpha_{\rm K}|^2$ and $|\beta_{\rm K}|^2$) with respect to the initial velocity v. We also show the amount of fermions escaped into bulk space ($|\gamma_{\rm K}|^2 = 1-(|\alpha_{\rm K}|^2+|\beta_{\rm K}|^2)$).

asymptotic behaviour of the wave function as $t\to\infty$, we obtain the Bogoliubov coefficients numerically such that $|\alpha_{\rm K}|^2 = 0.42$ and $|\beta_{\rm K}|^2 = 0.55$. Since a few amount of fermions escapes into bulk space at collision, $|\alpha_{\rm K}|^2+|\beta_{\rm K}|^2$ is not conserved, and the difference between the initial value and the final one ($|\gamma_{\rm K}|^2 = 1-(|\alpha_{\rm K}|^2+|\beta_{\rm K}|^2)$) corresponds to the amount of bulk fermions left behind. The Bogoliubov coefficients depend on the initial wall velocity. In Table 5.3, we summarize our results for different values of velocity. We also show the case of $g=2.5$ in Table 5.3. For the coupling constant $g=2$, $|\alpha_{\rm K}|^2$ and $|\beta_{\rm K}|^2$ are almost equal (0.44 and 0.55), but for $g=2.5$, most fermions remain on the kink ($|\alpha_{\rm K}|^2 = 0.88$ and $|\beta_{\rm K}|^2 = 0.02$). We find that the Bogoliubov coefficients depend sensitively on the coupling constant g as well as the velocity v. In Fig. 5.9, we shows the g-dependence. Since the wave function is changed at collision, when the background scalar field evolves in a complicated way, one might think that the behaviour of wave function would be difficult to describe analytically. However, we may understand the qualitative behaviour in terms of the following naive discussion. Before collision, the wave function is approximated well by $\Psi_{\rm in}^{(\rm K)}(x,z;v)$. In order to evaluate the wave function of fermion after collision, we have to integrate the Dirac equation (5.50). During the collision, the spatial distributions of fermion wave functions are well-described by some symmetric function of the z-coordinate (see Fig. 6.1(a) (b)). So we may approximate them as $\psi_\pm = A_\pm(t)e^{i\phi_\pm(t)}\psi_0(z)$, where $\psi_0(z)$ is a normalized even real function. $A_\pm$ and $\phi_\pm$ are regarded as the amplitudes of positive- (negative-) chiral modes and those phases, respectively. The scalar field Φ evolves as $\Phi: 1\to\Phi_c(\approx -1.5)\to 1$ at the collision point ($z=0$). If we approximate the scalar field as $\Phi=\Phi_c$ at collision for collision time $\Delta t(\sim D/c)$, integration of Eq.(5.50) with respect to z gives the change of amplitudes and phases of wave functions as

$$\frac{1}{\sqrt{1-A_\pm^2}}\partial_0 A_\pm = \pm g\Phi_c\sin(\Delta\phi)\,,\quad \partial_0\phi_\pm = -g\Phi_c\frac{\sqrt{1-A_\pm^2}}{A_\pm}\cos(\Delta\phi)\,, \tag{5.64}$$

where $\Delta\phi\equiv\phi_- - \phi_+$. We have also assumed that total amplitude of wave functions is normalized ($A_+^2+A_-^2=1$). This means that we ignore bulk fermions, which may be justified because $|\gamma_{\rm K}|^2 \ll 1$. If $\Delta\phi=0$ and $A_\pm=1$ initially, then we find $A_+(\Delta t)=1$ (or $A_-(\Delta t)=1$), which guarantees $\Delta\phi=0$ anytime from Eqs. (5.64). We find that $(A_+,\Delta\phi)=(1,0)$ (or $(A_-,\Delta\phi)=(1,0)$) is a fixed point of the system, Eqs. (5.64). However, it turns out that those are unstable. On the other hand, we find that $\Delta\phi=\pi/2$ (or $-\pi/2$) is an attractor (stable fixed points) of the present system. The time scale to approach these attractors is given by $(g|\Phi_c|)^{-1}$ if $\Delta A^2\equiv A_-^2-A_+^2 = O(1)$. Once we assume $\Delta\phi=\pm\pi/2$, then we find that the phases $\phi_\pm$ do not change. Then we can integrate the first equation in (5.64), finding

$$A_\pm^2(\Delta t) = \frac{1}{2}\left[1\pm\sin\left(2\varepsilon g\Phi_c\Delta t + C_0\right)\right]\,, \tag{5.65}$$

where $\varepsilon=\pm1$ and C_0 is an integration constant. This formula may provide a rough evaluation of $|\alpha_{\rm K}|^2, |\beta_{\rm K}|^2$. Comparing the numerical data and the formula (5.65) with $\Phi_c\approx -1.5$, we find the fitting curves in Fig. 5.9 ($\varepsilon=-1$, $\Delta t\approx 1.4$ and $C_0=-1.2$). The above naive analysis explains our results very well. We then conclude that $\Delta\phi=\pm\pi/2$ is generic except for a highly symmetric and fine-tuned initial

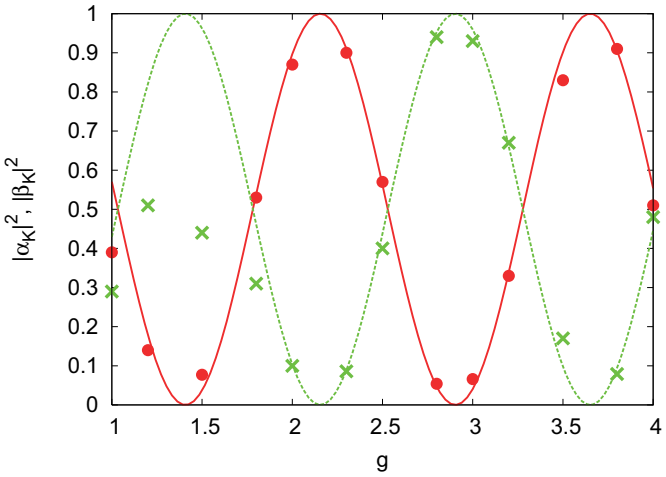

Figure 5.9: The Bogoliubov coefficients $(|\alpha_{\rm K}|^2, |\beta_{\rm K}|^2)$ with $v = 0.4$ in terms of a coupling constant g. The circle and the cross denote $|\alpha_{\rm K}|^2$ and $|\beta_{\rm K}|^2$ respectively. Two sine curves $(|\alpha_{\rm K}|^2, |\beta_{\rm K}|^2 \approx [1 \pm \sin(4.2g - 1.2))]/2$ show the formula (5.65) with the best-fit parameters.

setting ($A_+ = 1$ or $A_- = 1$ and $\Delta\phi = 0$), and the formula (5.65) with $\Delta\phi = \pm\pi/2$ is eventually found after collision. The small difference may be understood by the details of the complicated dynamics of colliding walls.

5.3.4 Fermion numbers on domain walls after collision

We can evaluate the expectation values of fermion numbers after collision as follows. For the initial state of fermions, we consider two cases: case (a) collision of two fermion walls $|{\rm KA}\rangle$ and case (b) collision of fermion and vacuum walls $|{\rm K0}\rangle$.

In the case (a), we find

$$\langle N_{\rm K}\rangle = |\alpha_{\rm K}|^2 + |\beta_{\rm A}|^2 = |\alpha_{\rm K}|^2 + |\beta_{\rm K}|^2 = 1 - |\gamma_{\rm K}|^2 \approx 1 \tag{5.66}$$

$$\langle N_{\rm A}\rangle = |\alpha_{\rm A}|^2 + |\beta_{\rm K}|^2 = |\alpha_{\rm A}|^2 + |\beta_{\rm A}|^2 = 1 - |\gamma_{\rm A}|^2 \approx 1\,. \tag{5.67}$$

We find that most fermions on domain walls remain on both walls even after the collision. A small amount of fermions escapes into the bulk spacetime at collision.

In the case (b), however, we obtain

$$\langle N_{\rm K}\rangle = |\alpha_{\rm K}|^2 \ , \quad \langle N_{\rm A}\rangle = |\beta_{\rm K}|^2\,. \tag{5.68}$$

Since the Bogoliubov coefficients depend sensitively on both the velocity v and the coupling constant g, the amount of fermions on each wall is determined by the fundamental model as well as the details of the collision of the domain walls.

5.3.5 Summary

We have studied the behaviour of five-dimensional fermions localized on domain walls, when two parallel walls collide in five-dimensional Minkowski background spacetime. We have analyzed the dynamical behavior of fermions during collision of fermion-fermion branes (case (a)) and that of fermion-vacuum ones (case (b)). In order to evaluate expectation values of fermion number on a kink and an antikink after collision, we solve the Dirac equation for the wave function in the case (b) and find the Bogoliubov

coefficients, in which $\beta_{\rm K}$ denotes the amount of fermions transferring from a kink to an antikink (a vacuum wall). As a result, in the case (b) some fermions jump up to the vacuum brane at collision. The amount of fermions localized on which brane depends sensitively on the incident velocity and the coupling constants g/λ where g and λ are the Yukawa coupling constant and that of the double-well potential, respectively. It can be intuitively understood that the amount of localized fermions is roughly determined by the duration of collision for which they transfer to another wall or stay on the initial wall, and the localization condition depending on the Yukawa coupling constant between fermions and domain walls. On the other hands, in the case (a), we find that most fermions seem to stay on both branes even after collision. This is because of the relationship $|\beta_{\rm K}| = |\beta_{\rm A}|$, which is guaranteed by a left-right symmetry in the present system. This result means physically that the same state ($k \sim 0$) of fermions are exchanged for each other by the same amount. Therefore, the final amounts of fermions does not depend on parameters.

We conclude with some comments about the subject not mentioned above:

(1) For the case of $g < 2/D$, the localization of fermions is not sufficient. The tail of fermion distribution extends outside the wall. As a result, we find that a considerable amount of fermions escapes into a bulk space at collision. For example, we find $|\alpha_{\rm K}|^2 + |\beta_{\rm K}|^2 = 0.64$ for $g = 1$ and $v = 0.8$. The formula (5.65) is also no longer valid in this case (see Fig. 5.9). This is because localization is not sufficient.

(2) The collision of domain walls is rather complicated. We find a few bounces at collision depending on the incident velocity. The number of bounces is determined in a complicated way (a fractal structure in the initial phase space [12, 436]).

(3) Since we have discussed only the case of zero-momentum fermion on branes ($\vec{k} = 0$), we have only a single state on each brane, which constrains the fermion number to be less than unity. If we take into account degree of freedom of low energy fermions, we can put different states of fermions on each brane. As the result, the final state of fermions after collision is different from the initial state, and it depends sensitively on the coupling constant as well as the initial wall velocity just as the case of collision of fermion-vacuum walls.

(4) In the case of collision of two vacuum branes, nothing happens in the present approximation. The pair production of fermion and antifermion, for which we have to take into account the momentum k, may occur at collision. This pair production process may also be important in the cases of collision of two fermion branes and that of fermion-vacuum branes. The work is in process.

(5) Including self-gravity is important to study. It can drastically changes collision of domain walls [437], resulting in a formation of black hole. It is interesting to see how fermion distribution changes through a singularity.

Chapter 6

Colliding branes in curved spacetime

6.1 Collision of two domain walls in asymptotic Anti de Sitter spacetime

In order to study whether such a reheating process is still efficient in more reliable cosmological models, we have to include the curvature effect. In particular, some brane universe are discussed with a negative cosmological constant [373] Hence, we study here how gravitational effects change our previous results. In order to investigate such an effect, we have not only to investigate the collision of domain walls in a curved spacetime, but also to solve the spacetime by use of the 5D Einstein equations. Inspired by the RS brane model, we include a potential of the scalar field which provides an effective negative cosmological constant in a bulk spacetime. We first set up the initially moving two domain walls, each of which is obtained by boosting an exact static domain wall solution [145]. Although this solution is obtained in the four dimensions, it is easy to extend it to the 5D one. We then solve the 5D Einstein equations and the dynamical equation for a scalar field to analyze collision of thick walls in asymptotically AdS spacetime. We use the unit of $c = \hbar = 1$.

6.1.1 Basic equations and initial settings

We study collision of two domain walls in 5D spacetime. To construct a domain wall structure, we adopt a 5D real scalar field Φ with an appropriate potential $V(\Phi)$, which minimum value is negative. This potential gives an asymptotically anti-de Sitter (AdS) spacetime just as the RS brane model. Since we discuss the collision of two parallel domain walls, the scalar field is assumed to depend only on a time coordinate t and one spatial coordinate z. The remaining three spatial coordinates are denoted by $\vec{x}$. For numerical analysis, we use dimensionless parameters and variables, which are rescaled by the mass scale m_Φ, which is defined by the vacuum expectation value at a local minimum as $\Phi_0 = m_\Phi^{3/2}$, as

$$\tilde{t} = m_\Phi t\,,\ \tilde{z} = m_\Phi z\,, \tilde{\Phi} = \frac{\Phi}{m_\Phi^{3/2}}\,. \tag{6.1}$$

In what follows, we drop the tilde in dimensionless variables for brevity. We can choose a bulk metric as "2D conformal gauge" , i.e.

$$ds^2 = e^{2A(t,z)}(\,-dt^2 + dz^2\,) + e^{2B(t,z)}d\vec{x}^2\,. \tag{6.2}$$

This gauge choice also makes the initial setting easy when we construct moving domain walls by use of the Lorentz boost. In this gauge, the 5D Einstein equations and the dynamical equation for a scalar field

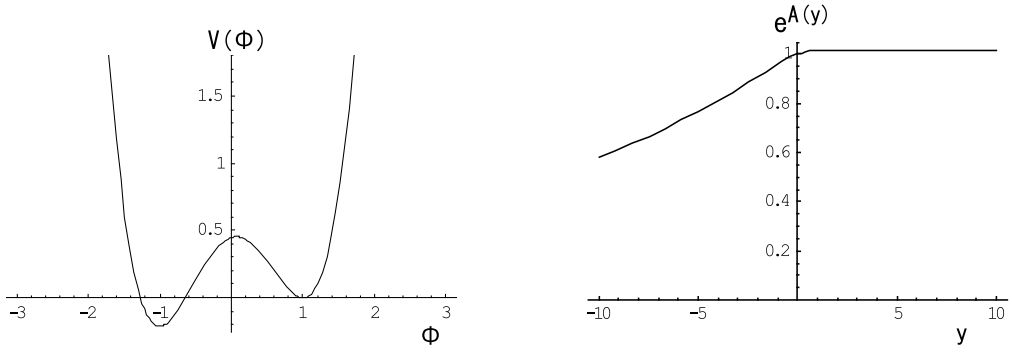

(a) (b)

Figure 6.1: (a): The scalar field potential $V(\Phi)$ is plotted where $D = \sqrt{2}, \kappa_5 = 0.3$. This potential behaves like a double-well potential for $|\Phi| < 5$, except that one of its two minima has a negative value. On the other hand, for $|\Phi| > 5$, this potential behaves differently from a double-well potential, that is $V(\Phi)$ rapidly falls into $-\infty$. (b): The metric component of the exact solution for a static domain wall [145] is plotted where we set $D = \sqrt{2}$ and $\kappa_5 = 0.3$. This spacetime approaches Minkowski space because $A_K \to A_\infty$ (a constant), while it becomes asymptotically AdS because $A_K \to -k|y|$ as $y \to -\infty$, where $k = 8\kappa_5^2/9D$.

are split into three dynamical equations;

$$\begin{aligned}
\ddot{A} =& A'' + 3\dot{B}^2 - 3B'^2 - \kappa_5^2(\dot{\Phi}^2 - \Phi'^2 + \frac{1}{3}e^{2A}V(\Phi))\,, \\
\ddot{B} =& B'' - 3\dot{B}^2 + 3B'^2 + \frac{2}{3}\kappa_5^2 e^{2A}V(\Phi)\,, \\
\ddot{\Phi} =& \Phi'' - 3\dot{B}\dot{\Phi} + 3B'\Phi' - \frac{1}{2}e^{2A}V'(\Phi)\,,
\end{aligned} \tag{6.3}$$

plus two constraint equations;

$$\begin{aligned}
&\dot{B}B' - A'\dot{B} - \dot{A}B' + \dot{B}' = -\frac{2}{3}\kappa_5^2\dot{\Phi}\Phi'\,, \\
&2B'^2 + B'' - A'B' - \dot{A}\dot{B} - \dot{B}^2 = -\frac{1}{3}\kappa_5^2(\dot{\Phi}^2 + \Phi'^2 + e^{2A}V(\Phi))\,,
\end{aligned} \tag{6.4}$$

where a dot ($\dot{}$) and a prime ($'$) denote $\partial/\partial t$ and $\partial/\partial z$, respectively. These are our basic equations. Before solve them numerically, we have to set up our initial data, which satisfies the constraint equations (6.4). For an initial configuration of a domain wall, we use an exact static solution given by [145]. They assume a scalar field Φ with a potential

$$V(\Phi) = \left(\frac{\partial W}{\partial \Phi}\right)^2 - \frac{8}{3}\kappa_5^2 W^2\,, \quad \text{where} \quad W \equiv \frac{1}{D}\left(\Phi - \frac{1}{3}\Phi^3 - \frac{2}{3}\right) \tag{6.5}$$

is a superpotential, and κ_5^2 and D are the five dimensional gravitational constant and the thickness of a domain wall, respectively. The potential minima are located at $\Phi = \pm 1$ in the range of $|\Phi| \lesssim 5$ (see Fig. 6.1(a)). The potential shape is similar to a double-well potential, but it is asymmetric. The minimum value at $\Phi = 1$ vanishes, while that at $\Phi = -1$ is negative. With this potential, we can obtain analytically an exact solution for two colliding domain walls as follows. First, we show a static domain wall solution with this potential. A kink solution of a scalar field (K) is described as

$$\Phi_K(y) = \tanh\left(\frac{y}{D}\right)\,, \tag{6.6}$$

and the metric of 5D spacetime is

$$ds^2 = e^{2A_K(y)}(-dt^2 + d\vec{x}^2) + dy^2\,, \tag{6.7}$$

with

$$A_K(y) = -\frac{4}{9}\kappa_5^2\Big\{\ln\Big[\cosh\Big(\frac{y}{D}\Big)\Big] + \frac{\tanh^2(y/D)}{4} - \frac{y}{D}\Big\}\,. \tag{6.8}$$

Since this exact solution is not given in our gauge, we have used a new coordinate y, which will be associated with z later. This metric approaches that of the AdS spacetime in one asymptotic region ($y \ll -1$), i.e.

$$e^{2A_K} \to e^{-2k|y|} \quad \text{as} \quad y \to -\infty\,, \quad \text{with} \quad k = \frac{8\kappa_5^2}{9d}\,. \tag{6.9}$$

While it becomes a flat Minkowski space in another asymptotic region ($y \gg 1$), i.e.

$$e^{2A_K} \to e^{2A_\infty} \quad \text{as} \quad y \to \infty\,, \quad \text{with} \quad A_\infty = \frac{4}{9}\kappa_5^2\left(\log 2 - \frac{1}{4}\right)\,. \tag{6.10}$$

We depict the behaviour of metric function $\exp[A_K(y)]$ in Fig. 6.1(b). By reflecting the spatial coordinate y, we also find an antikink solution ($\bar{K}$) as $\Phi_{\bar{K}}(y) = \Phi_K(-y) = -\Phi_K(y)$. The corresponding metric of this antikink solution is also obtained by reflection of y-coordinate, i.e. $A_{\bar{K}}(y) = A_K(-y)$. In order to describe this solution under our gauge condition (6.2), that is, in the (t, z) frame, we should transform the present (t, y) coordinates (Eq.(6.7)) into the (t, z) ones (Eq.(6.2)) by defining the coordinate z as

$$z = \int e^{-A_K(y)}dy\,. \tag{6.11}$$

This integration will be performed numerically to find initial data of collision of two domain walls. When a domain wall moves with constant speed v in the fifth direction z, we can obtain the corresponding solution by boosting a static kink solution (K) as

$$\Phi_v(z,t) = \tanh\left[\ \frac{1}{D}\ y^*\left(\gamma(z - vt)\right)\ \right]\,, \tag{6.12}$$

where y^* and z^* are comoving coordinates of a domain wall, and $y^*(z^*)$ is obtained by the inverse transformation of Eq. (6.11). The Lorentz transformation gives $z^* = \gamma(z - vt)$ where $\gamma = 1/\sqrt{1-v^2}$ is the Lorentz factor. We have assumed that the center of a domain wall is initially located at $z = 0$. The corresponding metric is easily obtained by Lorentz boost. Because of the Lorentz invariance in our 2D conformal gauge, i.e., $-dt^{*2} + dz^{*2} = -dt^2 + dz^2$, we find

$$ds^2_{2D} = \exp[2A_K\left(\gamma(z - vt)\right)](-dt^2 + dz^2)\,, \tag{6.13}$$

where $A_K(z^*) = A_K(y^*(z^*))$. The function $A_K(y)$ is given by Eq. (6.8). The center of a domain wall ($z^* = 0$) moves as $z = vt$ in our (t, z)-coordinate frame. Then we regard that the metric describes a spacetime with a domain wall moving with constant speed v in the z direction as well as a scalar field Φ does so. In order to discuss collision of two moving domain walls, we first have to set up its initial data. Using Eqs. (6.12) and (6.13), we can construct an initial data for two moving domain walls as follows. Provide a kink solution at $z = -z_0$ and an antikink solution at $z = z_0$, which are separated by a large distance and approaching each other with the same speed v. We then obtain the following initial data;

$$\Phi(z,0) = \Phi_v(z + z_0, 0) - \Phi_{-v}(z - z_0, 0) - 1\,, \quad A(z,0) = A_v(z + z_0, 0) - A_{-v}(z - z_0, 0) - A_\infty\,, \tag{6.14}$$

where A_∞ is the constant value given by Eq. (6.10). The initial values of $\dot{\Phi}$ and $\dot{A}$ are also given by

$$\dot{\Phi}(z,0) = \dot{\Phi}_v(z + z_0, 0) - \dot{\Phi}_{-v}(z - z_0, 0)\,, \quad \dot{A}(z,0) = \dot{A}_v(z + z_0, 0) - \dot{A}_{-v}(z - z_0, 0)\,. \tag{6.15}$$

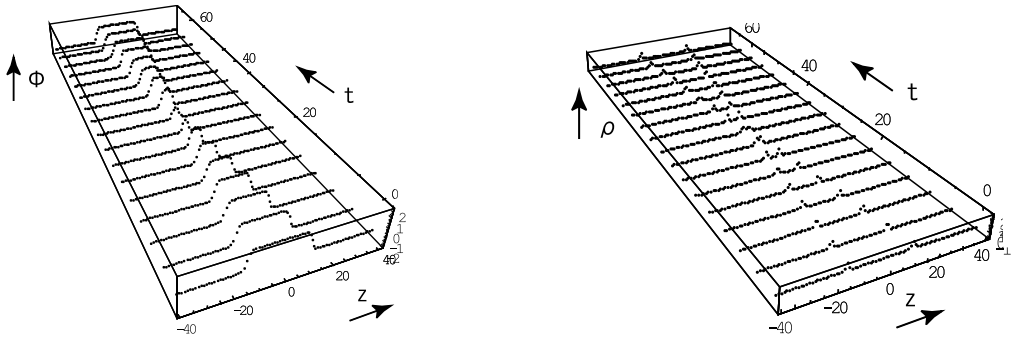

(a) Scalar field (b) Energy density

Figure 6.2: (a): Collision of two domain walls where the initial velocity $v = 0.4$. The time evolutions of the scalar field Φ (a) and the energy density ρ_Φ (b) are shown from $t = 0$ to 70. The maximum point of ρ_Φ defines the position of a wall ($z = z_{\rm W}(t)$). The collision occurs once around $t = 31$. We set $D = \sqrt{2}$, $\kappa_5 = 0.05$. This process is similar to the Minkowski case, $\kappa_5 = 0$.

Obviously, we set $A = B$ and $\dot{A} = \dot{B}$ at initial. Using these initial values, we solve the dynamical equation (6.3) numerically. We adopt a numerical method similar to one used in [436]. The difference is found in a boundary conditions. We impose the Dirichlet boundary condition for the scalar field, which is the same as the paper I, while the Neumann boundary condition is used for the metric as $A'(z) = -k\gamma e^{A(z)}$, which is derived from the asymptotic form of the metric, i.e., $e^{A(z)} \to 1/(k\gamma|z| + 1)$ as $|z| \to \infty$. We have three free parameters in our model, i.e. a wall thickness d, an initial wall velocity v, and a warp factor k (or the gravitational constant κ_5). Two of them $(d, k(\text{or } \kappa_5))$ are fundamental because they appear in the theory. In the paper I, we studied the collision of two domain walls in the fixed Minkowski background [12], where we had two free parameters d and v. So, including the gravitational back reaction, we investigate how κ_5 (or k) changes the previous results. In what follows, fixing the value of d, i.e. $D = \sqrt{2}$, we show our results.

6.1.2 Time evolution of scalar field

First let us set $\kappa_5 = 0$ (or $k = 0$), that is the case of Minkowski background spacetime. Although the scalar field potential is slightly different from that in the paper I, the result is exactly the same. This simulation also gives a check of our numerical code. Next we perform our simulation for $\kappa_5 \neq 0$. For a small value of κ_5, i.e., $\kappa_5 \lesssim 0.05$ (equivalently $k \lesssim 1.57 \times 10^{-3}$ or $m_\Phi \lesssim (0.05)^{2/3} m_5 \approx 0.136 m_5$), the collision process is very similar to the case of the Minkowski background. Setting the initial velocity $v = 0.4$, we show our numerical results for $\kappa_5 = 0.05$ in Figs. 6.2(a) and 6.2(b). The evolution of Φ is depicted in Fig. 6.2(a), while that of the energy density is shown in Fig. 6.2(b). The energy density of the scalar field is given by

$$\rho_\Phi = e^{-2A}\left(\dot{\Phi}^2 + \Phi'^2\right) + V(\Phi)\,. \tag{6.16}$$

We find some peaks in the energy density, by which we define the positions of moving walls ($z = \pm z_{\rm W}(t)$). If a domain wall is symmetric, its position is defined by $\Phi(z) = 0$. However, in more general situation, just as in the present case that the scalar field is oscillating around some moving point, it may be natural to define the position of a domain wall by the maximum point of its energy density. Fig. 6.3(a) denotes the position of brane $z = z_{\rm W}(t)$ with respect to t. The brane moves with constant speed $v = 0.4$ toward the collision point $z = 0$, and collide, then recede to the boundary. We also find small oscillation around a uniform motion after collision. Since we assume that we are living on one domain wall, we are interested in a particle ψ confined on the domain wall. If a particle ψ is coupled with a 5D scalar field Φ, which

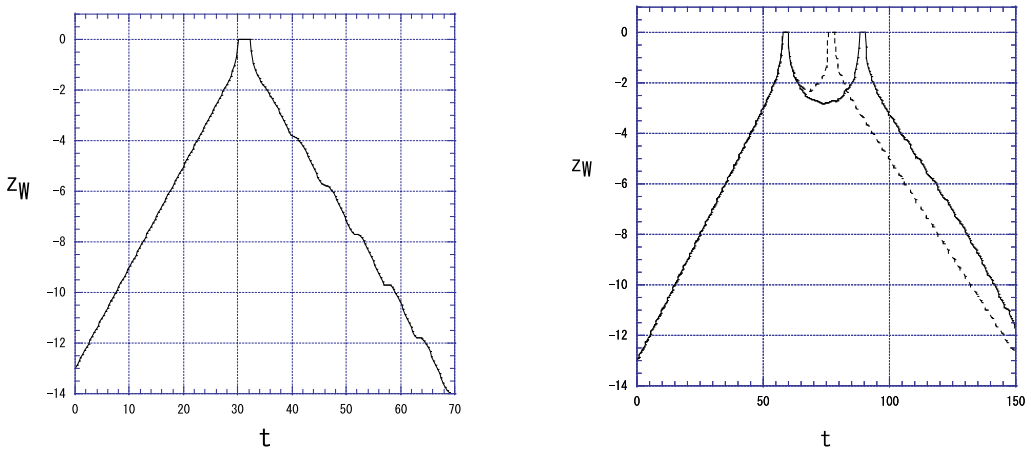

(a) $v = 0.4$ (b) $v = 0.2$

Figure 6.3: Time evolutions of the position of one brane $z = z_{\rm W}$ which starts to move at $z = -13$ with a constant speed $v = 0.4$ (a) and $v = 0.2$ (b), respectively. We set $D = \sqrt{2}$, $\kappa_5 = 0.05$. (b): The dashed line denotes $\kappa_5 = 0.05$ while the dotted line does $\kappa_5 = 0$. The time interval between two bounces is prolonged by an effective negative cosmological constant.

is responsible for the domain wall, we expect quantum production of ψ-particles at collision of domain walls. This is because the value of the scalar field Φ on the domain wall changes with time. This fact may play an important role in a reheating mechanism [436]. Once we find the solution of colliding domain walls, we know the time evolution of a scalar field on the domain wall, and we can evaluate production rate. At the position of a domain wall, the induced metric is given as

$$ds^2 = -d\tau^2 + a^2(\tau) d\vec{x}^2 \,, \tag{6.17}$$

where proper time and the scale factor are determined as

$$\tau = \int e^{A_{\rm W}} dt \,, \quad a(\tau) = e^{B_{\rm W}}(\tau) \,. \tag{6.18}$$

$A_{\rm W}$ and $B_{\rm W}$ are evaluated on the brane, i.e., $A_{\rm W} = A(t, z_{\rm W}(t))$ and $B_{\rm W} = B(t, z_{\rm W}(t))$. The Hubble parameter of the brane universe is defined by

$$H(\tau) \equiv \frac{1}{a}\frac{da}{d\tau}\Big|_{z=z_{\rm W}} = \frac{dB_{\rm W}}{d\tau} = e^{-A_{\rm W}} \dot{B}_{\rm W}(\tau) \,. \tag{6.19}$$

For $v = 0.4$, we depict the time evolution of $\Phi_{\rm W}$ on one moving wall for different values of κ_5 in Figs. 6.4(a) and 6.4(b). The feature of collision is similar, but the behaviour of a scalar field on the moving wall after collision is different for each κ_5. We summarize our numerical results for each value of κ_5 in order.

(i) κ_5=0.01

For a small value of κ_5, e.g., $\kappa_5 = 0.01$ (equivalently $k \sim 6.29 \times 10^{-5}$ or $m_\Phi \sim 0.0464 m_5$), the result is almost the same as the case of the Minkowski background, in which case we find one bounce point, which corresponds to a crossing point in Fig. 6.2(b), and then the oscillations around $\Phi_W = 0$ follow (see the dotted line in Fig. 6.4(a)). This oscillation is explained by using a perturbation analysis in Minkowski spacetime [436]. We have found one stable oscillation mode around the kink solution. This oscillation appears by excitation of the system at collision.

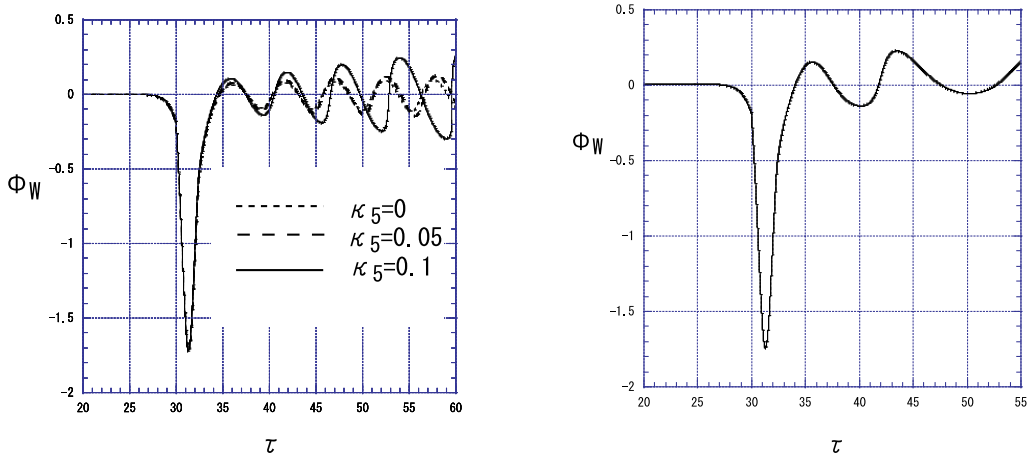

(a) $\kappa_5 \leq 0.1$ (b) $\kappa_5 = 0.15$

Figure 6.4: Time evolution of a scalar field on the moving wall with $v = 0.4$, $D = \sqrt{2}$. We set $\kappa_5 = 0, 0.05, 0.1$ for (a) and $\kappa_5 = 0.15$ for (b). The value of the scalar field on the wall is defined by $\Phi_{\rm W} = \Phi(t, z_{\rm W}(t))$, where $z_{\rm W}(t)$ is the position of the wall. (a): The time of period of oscillation gets slightly longer and the amplitude is a little bit larger as κ_5 increases. (b): $\Phi_{\rm W}$ goes out of oscillation phase 0 at $\tau \sim 55$ and then numerical simulation stops.

(ii) $\kappa_5 = 0.05$

As increasing the value of κ_5 slightly larger, for example $\kappa_5 = 0.05$, (equivalently for $k \sim 1.57 \times 10^{-3}$ or $m_\Phi \sim 0.136 m_5$), the time evolution of $\Phi_{\rm W}$ slightly changes. In Fig. 6.4(a), just as the case of $\kappa_5 = 0$, we find one bounce and successive oscillations. However, the period of oscillation is slightly longer and the amplitude gets a little bit larger as κ_5 increases.

(iii) $\kappa_5 = 0.15$

For $\kappa_5 = 0.15$, (equivalently $k \sim 1.41 \times 10^{-2}$ or $m_\Phi \sim 0.282 m_5$), the behaviour of this oscillation changes drastically. After several oscillations, the scalar field leaves $\Phi_W = 0$ as shown in Fig. 6.4(b). The numerical simulation eventually breaks down because all variables diverge.

(iv) $\kappa_5 > 0.15$

For the larger values of κ_5 than 0.15, the time to appearance of singularity becomes shorter, that is, contrary to the case of $\kappa_5 \lesssim 0.15$, the scalar field after collision does not oscillate but leave $\Phi_{\rm W} = 0$ soon. The time evolution of $\Phi_{\rm W}$ is shown in Fig. 6.5, for $\kappa_5 = 0.2$ ($k = 2.51 \times 10^{-2}$) and $\kappa_5 = 0.25$ ($k = 3.93 \times 10^{-2}$). The metric component A at $z = 0$ also diverges as shown in Fig 6.6. It is not a coordinate singularity, but a curvature singularity. In order to show it, we calculate the so-called Kretschmann invariant scalar, which is the simplest scalar invariant quadratic in the Riemann tensor, and is defined as

$$R^{abcd}R_{abcd} = e^{-4A}\Big[3(\ddot{B} + \dot{B}^2 - \dot{A}\dot{B} - A'B')^2 - 3(A'\dot{B} + \dot{A}B' - \dot{B}' - \dot{B}B')^2 + (\ddot{A} - A'')^2 + 3(B'^2 - \dot{B}^2)^2 + 3(B'' + B'^2 - \dot{A}\dot{B} - A'B')^2\Big]. \tag{6.20}$$

In Fig. 6.6(b), we depict the time evolution of the Kretschmann scalar at the origin $z = 0$, which diverges at $t \simeq 69$. It is caused by the divergence of a quantity $\dot{A}$. We conclude a singularity forms at the origin $z = 0$. This divergence is not a numerical error because a constraints equations (6.4) are always satisfied within 10^{-5} - 10^{-2} % accuracy except at time when the singularity appears. In Appendix

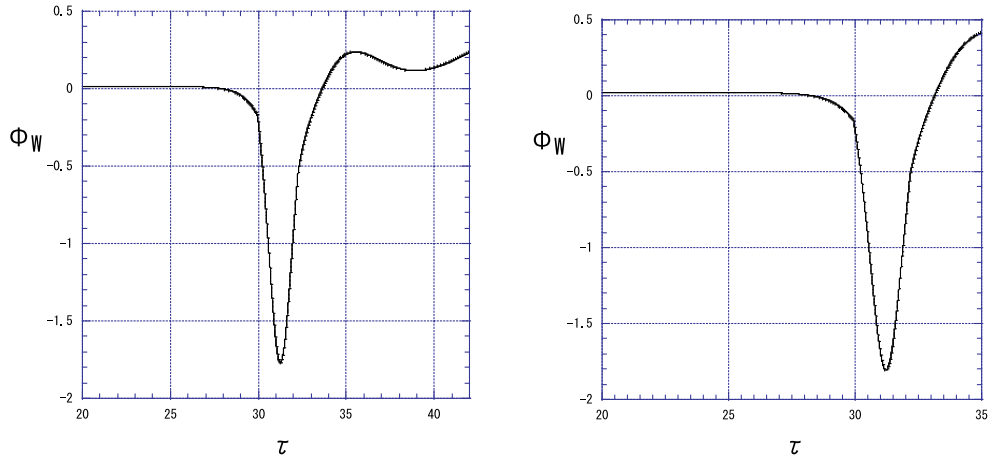

(a) $\kappa_5 = 0.2$ (b) $\kappa_5 = 0.25$

Figure 6.5: Time evolution of the scalar field $\Phi_{\rm W}$ for $v = 0.4$, $D = \sqrt{2}$, setting (a) $\kappa_5 = 0.2$ and (b) $\kappa_5 = 0.25$. The numerical simulation breaks down when (a) $\tau \sim 42$ and (b) $\tau \sim 35$, respectively.

6.1.5, we study the reason why a spacetime is unstable and eventually evolves into a singularity in detail using a perturbation analysis of the Einstein equations and dynamical equation of Φ. We find that a perturbed oscillation mode around an unperturbed kink solution becomes overstable for $\kappa_5 = 0.1$. From our analysis, we conclude that gravitational back reaction makes a kink solution unstable contrary to the Minkowski case. Next, we show the result for the case of the initial velocity $v = 0.2$. In the Minkowski case, this incident velocity shows two-bounce at collision process (see Fig. 6.7 (a)). After two walls collide, they bounce, recede to some finite distance, turn back and then collide again. For small values of κ_5, e.g., $\kappa_5 \leq 0.05$, the collision process is very similar to the case of $\kappa_5 = 0$ (see Fig. 6.7(b)). As κ_5 increases, the time interval between first and second bounces becomes longer as shown in Fig. 6.3(b). This can be understood from the fact that the above mentioned oscillation after collision will radiate the energy. So a kink-antikink pair is loosely bounded and it takes longer time to collide again. For the case of $\kappa_5 \gtrsim 0.1$, this feature of collision is drastically changed. Two-bounce collision never occurs, that is, two walls collide only once. This is because a lot of energy of a kink-antikink pair is radiated away via the unstable oscillation after collision and it has not enough energy to form a trapped state. After the first bounce, the domain walls never collide again but recede each other. For larger value of κ_5, we find only one-bounce collision. Namely, a "negative cosmological constant" outside a kink-antikink pair keeps away two walls toward the boundary, so it plays as an effective attractive force.

6.1.3 Time evolution of metric

We evaluate the time evolutions of the metric $A_{\rm W}, B_{\rm W}$ on the brane and plot them in Figs. 6.8. Both of two quantities decrease with time except that $B_{\rm W}$ increases slightly through the bounce. From those two quantities, using Eqs. (6.18) and (6.19), we evaluate a scale factor of our universe $a(\tau) = e^{B_{\rm W}}(\tau)$ and the Hubble expansion parameter $H \equiv \frac{da}{d\tau}/a$, where τ is the proper time of domain wall defined by Eq. (6.18), and show them in Figs. 6.9 setting $v = 0.4$. From this figure, we find that our universe expands slightly before bounce then eventually contracts. For each κ_5, the scale factor a and the Hubble parameter H are also plotted in Figs. 6.9(a) and 6.9(b). From these figures, we see that our universe contracts faster as κ_5 gets larger, i.e. a negative cosmological constant increases. Next we investigate the scale factor a and the Hubble parameter H for the case of $v = 0.2$. Setting $\kappa_5 = 0.05$, that is the case of two-bounce collision. We find two contracting phases, which correspond to each bounce at collision as we expected. For $\kappa_5 \gtrsim 0.1$,

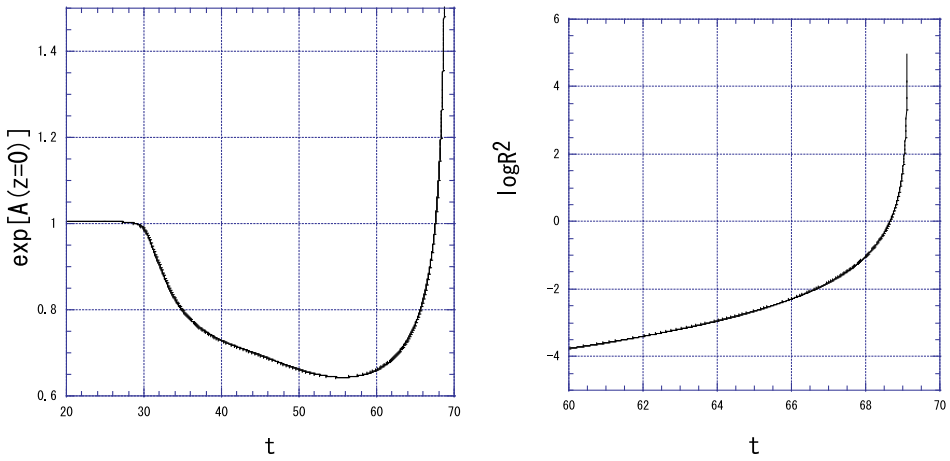

(a) (b)

Figure 6.6: (a): Time evolution of the metric component A at $z = 0$ for $\upsilon = 0.4,\ d = \sqrt{2},\ \kappa_5 = 0.15$. It diverges at $t \sim 70$. (b): In this case, Kretschmann scalar invariant ($R^{abcd}R_{abcd}$) at the origin $z = 0$. We find that the Kretschmann scalar diverges at $t \simeq 69$. This means that it is not a coordinate singularity, but a curvature singularity.

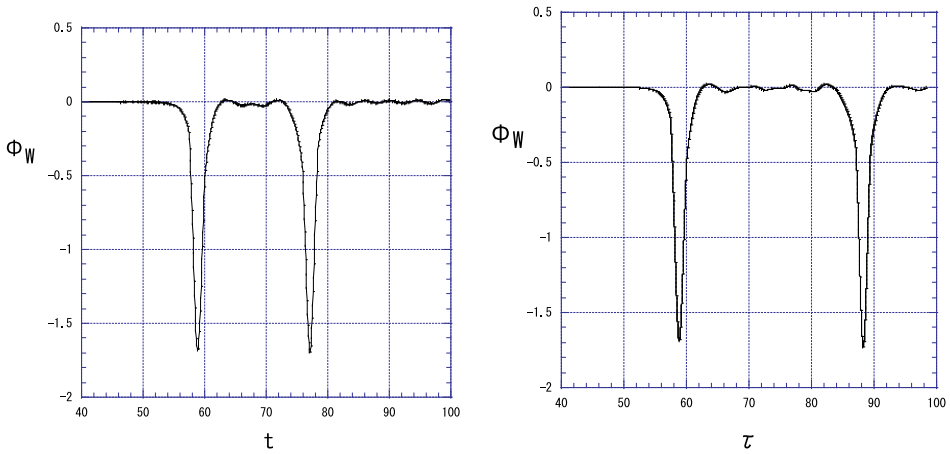

(a) $\kappa_5 = 0$ (Minkowski) (b) $\kappa_5 = 0.05$

Figure 6.7: Time evolution of a scalar field $\Phi_{\rm W}$ for $\upsilon = 0.2,\ D = \sqrt{2}$. For (a) $\kappa_5 = 0$ and (b) $\kappa_5 = 0.05$, we find two peaks which correspond to twice bounces at collision. Moreover, it is seen that an effective negative cosmological constant prolongs the time interval between two bounces.

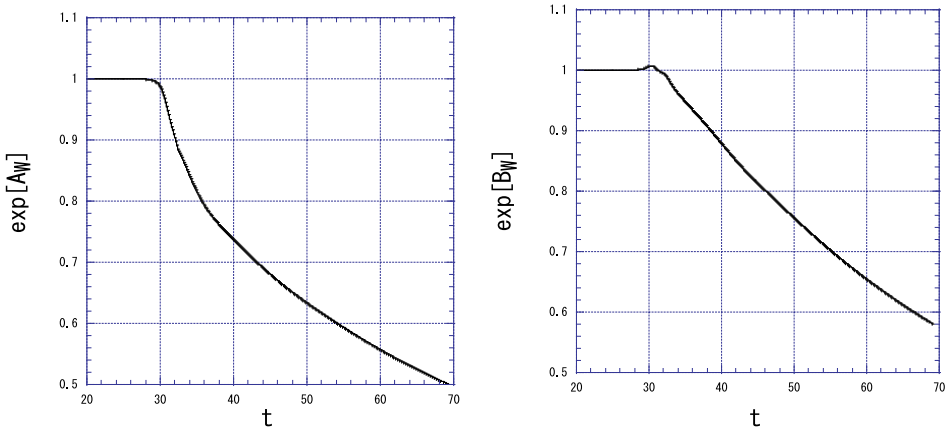

$A_{\rm W}$ $B_{\rm W}$

Figure 6.8: Time evolution of the metric A and B on the moving wall for $\upsilon = 0.4,\ D = \sqrt{2},\ \kappa_5 = 0.15$. The value of the metric is given by $A_{\rm W} = A(t, z_{\rm W}(t))$, where $z_{\rm W}(t)$ is the position of the wall. Both of two quantities decreases with time.

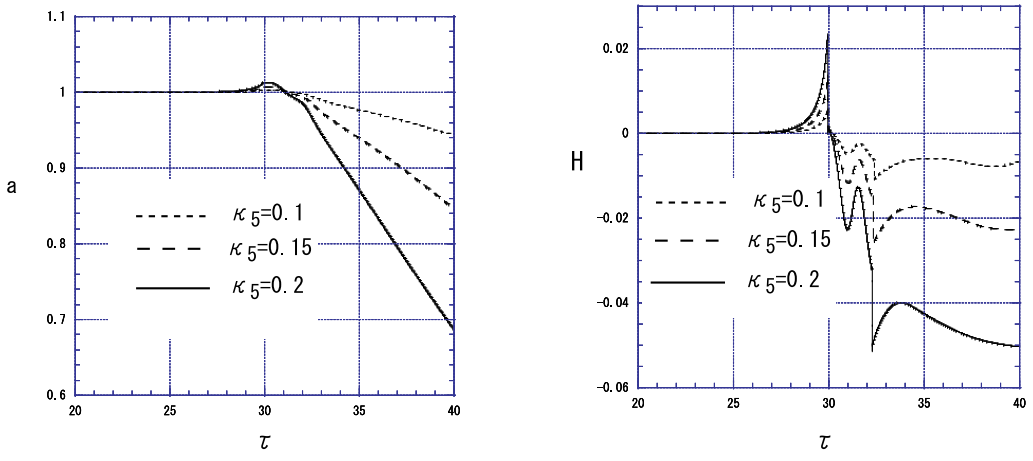

(a) (b)

Figure 6.9: Time evolutions of the scale factor $a = e^{B_{\rm W}}$ (a) and the Hubble parameter $H \equiv \dot{a}(\tau)/a$ (b) for $\upsilon = 0.4,\ D = \sqrt{2}$. We set $\kappa_5 = 0.1, 0.15$ and 0.2. (a): As κ_5 gets larger, the speed of contraction becomes larger. (b): As κ_5 gets larger, the typical time scales of expansion and contraction become larger.

the bounce occurs once only because of a large negative cosmological constant and we find the universe contracts slower than the case $v = 0.4$. Our universe contracts faster as v gets larger. Finally, we find in Fig. 6.9(b) that there are two discontinuous stages in the evolution of the Hubble parameter at $t \sim 30$ and ~ 32. As we will see, we can conclude that these discontinuities appear just because of ambiguity of the definition of a wall-position, $z = z_{\rm W}$. The Hubble parameter mainly depends on the derivative of the metric with respect to t, $\dot{B}$. In this paper, we define the position of wall by one where the energy density of scalar field gets maximum. However, this position does not move continuously through a bounce. Actually, we show $\dot{z}_{\rm W}$ has also two discontinuous stages, where the speed of a wall apparently exceeds the speed of light. Namely near the bounce, the definition of wall-position is not well-defined. This is because there is no wall configuration during the collision. Hence these discontinuities of the Hubble parameter seem to be apparent. We should look at the global time evolution.

6.1.4 Summary

We have investigated collision of two domain walls in 5D asymptotically AdS spacetime. We evaluate the values of both a scalar field corresponding to a domain wall and metric on the moving wall for different value of the warp factor k which is related to a gravitational effect κ_5. We analyze two typical incident velocities, i.e. $v = 0.4$, and $v = 0.2$, which correspond to one-bounce and two-bounce solutions in the Minkowski spacetime, respectively. For the case of $v = 0.4$, the global feature of collision is same for different values of κ_5, but the behaviour of oscillation after the collision is different for each κ_5. For small value of $\kappa_5 \lesssim 0.01$, the oscillation is the same as Minkowski case, but for $\kappa_5 \gtrsim 0.05$, it becomes an overstable oscillation. So its period and amplitude get larger as κ_5 increases. In the cause of this unstable oscillation, the singularity appears after collision. This singularity is very similar to that found in Khan and Penrose [242], in which they discuss collision of plane waves and formation of a singularity. Hence the appearance of singularity in the present model could be understandable because we take into account a gravitational effect in collision of two domain walls. In the time evolution of our universe, we find that the universe first expands a little just before collision and then contracts just after collision. This result is consistent with [274]. We cannot explain our hot big bang universe as it is. It is also found that the speed of expansion and contraction gets faster as κ_5 increases. For the second case, i.e., $v = 0.2$, we show the bounce does not occur twice for larger value of κ_5 ($\kappa_5 \gtrsim 0.1$) corresponding to the unstable oscillation. We shall discuss about the value of a warp factor k. We consider a curvature length $l = 1/k$ written in the following form

$$l = 1.97 \times 10^{-17} \Big(\frac{10^{-2}}{k} \Big) \Big(\frac{\rm TeV}{m_\Phi} \Big) \ [\rm m] \,, \tag{6.21}$$

where m_Φ is a mass scale of a domain wall. Here we set a value of a warp factor k in the region $0.01 \lesssim k \lesssim 0.25$. On the other hand, we also know from the experimental data of testing a gravitational inverse-square law that the curvature length must be smaller than 0.1 mm [3, 209, 295]. From this constraint equation, we obtain

$$k > 1.97 \times 10^{-15} \Big(\frac{\rm TeV}{m_\Phi} \Big) \,. \tag{6.22}$$

So the values of k used in our simulation satisfy this constraint.

6.1.5 Appendix

In Fig. 6.4(a), we find oscillations after collision and those amplitudes and periods increase as κ_5 gets larger. To understand this feature, we analyze perturbations around a static domain wall solution. We use the coordinate y, by which a static domain wall solution is given by analytically $(\Phi_K(y), A_K(y))$, which are given by Eqs. (6.6) and (6.8). We perturb the basic equations (6.3) and (6.4) by setting $A = A_K(y) + a(t, y)$, $B = A_K(y) + b(t, y)$, and $\Phi = \Phi_K(y) + \phi(t, y)$. We find two sets of perturbation equations:

(1) dynamical equations

$$e^{-2A_K}\ddot{a} = \frac{\partial^2 a}{\partial y^2} + \frac{dA_K}{dy}\frac{\partial a}{\partial y} - 6\frac{dA_K}{dy}\frac{\partial b}{\partial y} + \kappa_5^2\left(2\frac{d\Phi_K}{dy}\frac{\partial \phi}{\partial y} - \frac{2}{3}V\big|_K a - \frac{1}{3}\frac{dV}{d\Phi}\Big|_K \phi\right), \tag{6.23}$$

$$e^{-2A_K}\ddot{b} = \frac{\partial^2 b}{\partial y^2} + 7\frac{dA_K}{dy}\frac{\partial b}{\partial y} + \frac{2}{3}\kappa_5^2\left(2V\big|_K a + \frac{dV}{d\Phi}\Big|_K \phi\right), \tag{6.24}$$

$$e^{-2A_K}\ddot{\phi} = \frac{\partial^2 \phi}{\partial y^2} + 4\frac{dA_K}{dy}\frac{\partial \phi}{\partial y} + 3\frac{d\Phi_K}{dy}\frac{\partial b}{\partial y} - \frac{1}{2}\left(2\frac{dV}{d\Phi}\Big|_K a + \frac{d^2V}{d\Phi^2}\Big|_K \phi\right), \tag{6.25}$$

(2) constraint equations

$$\frac{\partial \dot{b}}{\partial y} - \frac{dA_K}{dy}\dot{a} = -\frac{2}{3}\kappa_5^2\frac{d\Phi_K}{dy}\dot{\phi}, \tag{6.26}$$

$$\frac{\partial^2 b}{\partial y^2} + 4\frac{dA_K}{dy}\frac{\partial b}{\partial y} - \frac{dA_K}{dy}\frac{\partial a}{\partial y} + \frac{2}{3}\kappa_5^2\left(V\big|_K a + \frac{1}{2}\frac{dV}{d\Phi}\Big|_K \phi + \frac{d\Phi_K}{dy}\frac{d\phi}{dy}\right) = 0 \tag{6.27}$$

In order to find the eigenvalue and eigen functions, we set $a = \tilde{a}(y)e^{i\omega t}$, $b = \tilde{b}(y)e^{i\omega t}$, and $\phi = \tilde{\phi}(y)e^{i\omega t}$. Then the constraint equation (6.26) is reduced to be

$$\frac{d\tilde{b}}{dy} - \frac{dA_K}{dy}\tilde{a} = -\frac{2}{3}\kappa_5^2\frac{d\Phi_K}{dy}\tilde{\phi} \tag{6.28}$$

Inserting Eq. (6.28) into another constraint (6.27) and using the equations for a background solution, we find that the constraint equation (6.27) turns out to be trivial. So we have only one constraint equation (6.28). Eliminating $d\tilde{b}/dy$ in (6.23) and (6.25) by use of Eq. (6.28), we obtain two coupled perturbation equations in terms of $\tilde{a}, \tilde{\phi}$ as

$$\begin{aligned}
\frac{d^2\tilde{a}}{dy^2} &= \left[6\left(\frac{dA_K}{dy}\right)^2 + \frac{2}{3}\kappa_5^2 V\big|_K - e^{-2A_K}\omega^2\right]\tilde{a} - \frac{dA_K}{dy}\frac{d\tilde{a}}{dy} - \kappa_5^2\left(4\frac{dA_K}{dy}\frac{d\Phi_K}{dy} - \frac{1}{3}\frac{dV}{d\Phi}\Big|_K\right)\tilde{\phi} - 2\kappa_5^2\frac{d\Phi_K}{dy}\frac{d\tilde{\phi}}{dy}, \\
\frac{d^2\tilde{\phi}}{dy^2} &= \left(\frac{dV}{d\Phi}\Big|_K - 3\frac{d\Phi_K}{dy}\frac{dA_K}{dy}\right)\tilde{a} - 4\frac{dA_K}{dy}\frac{d\tilde{\phi}}{dy} + \left[2\kappa_5^2\left(\frac{d\Phi_K}{dy}\right)^2 + \frac{1}{2}\frac{d^2V}{d\Phi^2}\Big|_K - e^{-2A_K}\omega^2\right]\tilde{\phi}.
\end{aligned} \tag{6.29}$$

Eq. (6.24) is guaranteed by the other two dynamical equations and constraint equations. Eqs. (6.29) have the asymptotic forms as $y \to \infty$ as

$$\tilde{a} = e^{\pm\sqrt{A_1}y}, \quad \tilde{\phi} = e^{\pm\sqrt{A_2}y}, \tag{6.30}$$

where

$$A_1 = -e^{-2A_\infty}\omega^2, \quad A_2 = \frac{1}{2}\frac{d^2V}{d\Phi^2}\Big|_{\Phi=1} - e^{-2A_\infty}\omega^2. \tag{6.31}$$

Here we choose both negative signs in Eqs. (6.30) because negative signs correspond to out-going wave modes. We solve numerically these equations (6.29) connecting the above asymptotic solutions and find the complex eigen frequency ω. For $\kappa_5 = 0.1$, we obtain a stable mode as $\omega_s = 1.23 + 1.07 \times 10^{-3}i$ and unstable mode as $\omega_u = 0.644 - 2.90 \times 10^{-2}i$. Compared this unstable mode with the value obtained from the oscillations after collision found in Fig. 6.4(a) (Notice that we use a proper time τ in Fig. 6.4(a). Then it should be evaluated in the physical time t). We obtain $0.772 \approx 1.2 \times \Re[\omega_u]$ for the real part of the frequency and $-0.029 \approx 1.0 \times \Im[\omega_u]$ for the imaginary part. So we may conclude that the overstable oscillations after the collision of two domain walls found in Fig. 6.4(a) are explained by the unstable mode around a static domain wall solution.

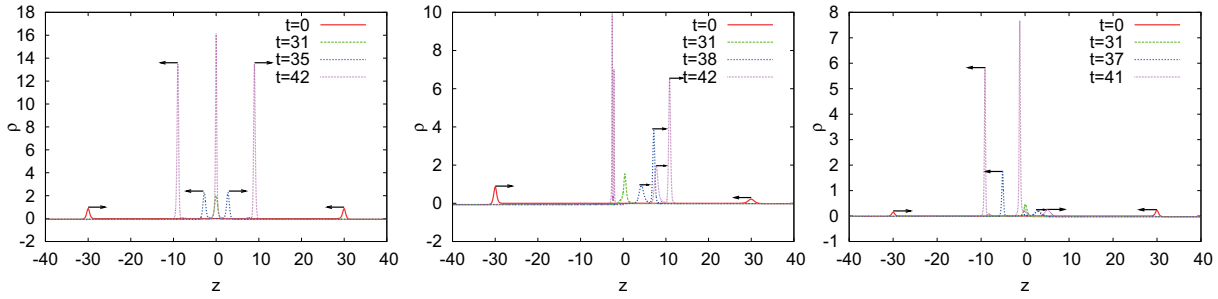

(a) $D_K = D_A = 1,\ L_K = L_A = 0.18$ (b) $D_K = 1$ and $D_A = 2$ (c) $L_K = 0.18$ and $L_A = 0.22$

Figure 6.10: Energy density ρ on $t =$ const. surfaces: (a) collision of two identical walls at the center, (b) collision of two walls with different thickness, and (c) two walls with different amplitude. The sharp peaks represent the domain walls, and the arrows show the directions of a wall's velocity. For (b) and (c), all the unspecified parameters are the same as those in (a).

6.2 Dynamics of colliding branes and black brane production

It is known that primordial black holes and domain walls may have been produced in the early universe through the physical process of the collapse of cosmological density perturbations and the series of phase transitions during the cooling phase of universe. On the other hand, black holes and domain walls (also known as branes) also play an important role in string theory as fundamental constituents. In addition, according to M-theory, branes are of particular relevance to cosmology: branes are free to move in a bulk space, and they may approach and collide, causing the big bang/crunch or an inflation on branes [246, 248, 432].

In view of the phenomenological relevance, understanding how the domain walls/branes interact dynamically is an important problem, and more knowledge in this area could help in clarifying many issues regarding the early universe. In the past few years much attention have been paid to understanding the dynamics of domain walls (e.g., [13, 152, 161, 320, 327, 417, 437]). In particular, the interaction between black holes and domain walls has been the subject of study. Nevertheless, even more fundamental processes like collision, recoil, and reconnection of branes are less understood. The collision and recoil of domain walls in the cosmological context described above was studied in [437], where a reheating mechanism via particle productions was discussed within a toy model. In this paper, we consider the problem from a different perspective. The collision of domain walls/branes is a violent phenomenon, and, as partially observed in our previous study, a spacetime singularity might appear through a collision. If this is the case, a low-energy description of colliding branes breaks down at some point, implying a complete loss of predictability, without the complete theory of quantum gravity. We investigate the process of collision using a BPS domain wall in five-dimensional supergravity, and our main goal is to determine the final outcome of the kink-anti-kink collisions including self-gravity. As we will see, singularity formation is a generic consequence of collisions. However, the singularity is spacelike and hidden inside the horizon. The horizon extends in a spatially flat direction along the brane so that a black brane is produced through the collision. To clarify and to provide further examples of black brane production, we will also study collisions using another model of domain walls.

6.2.1 Model I

The system we intend to study consists of two domain walls that are initially located far away from each other. The initial data for such a configuration is constructed by superposing domain wall solutions in an appropriate manner. As a model of a domain wall, we consider a gravitationally interacting scalar field

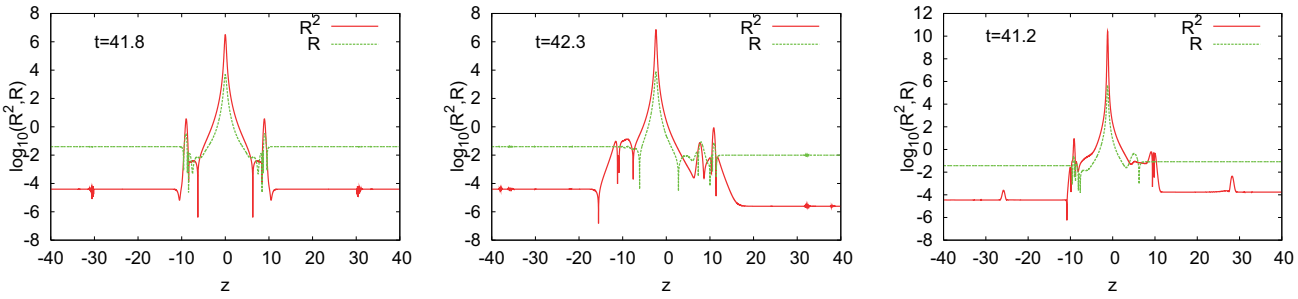

Figure 6.11: R and $R^{abcd}R_{abcd}$ at t =const. surface, corresponding to the simulations in Fig. 6.10.

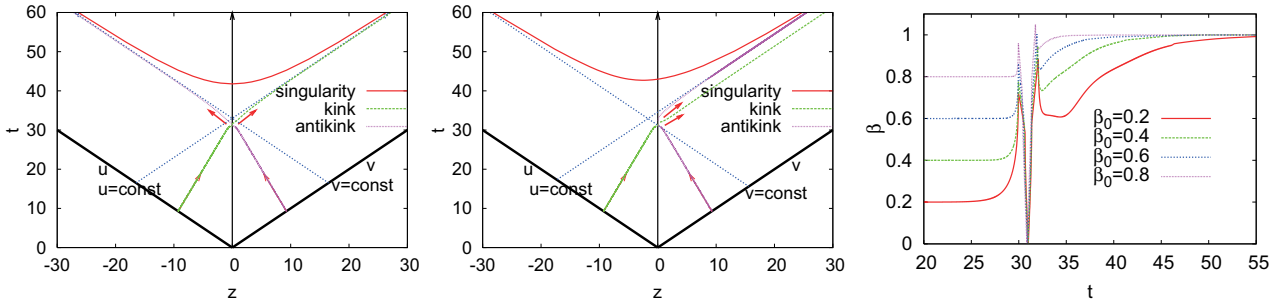

(a) (b) (c)

Figure 6.12: (a) and (b) show the numerical results in the null coordinates, corresponding to Fig. 6.10(a) and 6.10(b), respectively. Dotted lines with arrows describe the orbit of walls. Thick lines are u, v-axes, and dotted straight lines show u, v =const., to which the spacelike singularity asymptotes. The position of a wall is defined by its maximum energy density. (c) Time variation of the (kink) wall's speed. Irrespective of the initial speed, the final speed after the collision goes to unity.

of the Lagrangian $\mathcal{L} = \frac{R}{2\kappa^2} - \frac{1}{2}\nabla^a\phi\nabla_a\phi - V$. The following solution of 5D Einstein equations represent a single domain wall (*Model I*), which has a spatially flat direction in three dimensions $d\vec{x}_3^2$.

$$ds^2 = e^{2U}(-dt^2 + d\vec{x}_3^2) + dr^2\,, \quad U = -\frac{L^2}{3}\left[\log\left[\cosh\left(\frac{2(r-r_0)}{D}\right)\right] + \frac{2a(r-r_0)}{D}\right], \tag{6.32}$$
$$\phi = \frac{2L}{\kappa}\left\{\tan^{-1}\left[\tanh\left(\frac{r-r_0}{D}\right)\right] - \frac{\pi}{4}\right\}, \quad V(\phi) = \frac{2L^2}{3\kappa^2 D^2}\left[\omega_0 + \omega_1\cos\left(\frac{\kappa\phi}{L}\right) + \omega_2\cos^2\left(\frac{\kappa\phi}{L}\right)\right],$$

where $\omega_0 = 3 - 4a^2L^2$, $\omega_1 = -8aL^2$, $\omega_2 = -3 - 4L^2$. There are three unfixed parameters, i.e., wall thickness δ, amplitude L of scalar field, and the position r_0 of the kink's core. We will hereafter take $\kappa^2 = 1$. We will call this domain wall solution the *kink* solution (for $a < 0$). The *anti-kink* solution is defined by the reflecting r-coordinate in the above solution. In the limit of $r \to \pm\infty$, the scalar field asymptotes constants, and the scalar potential plays the role of the cosmological constant $\Lambda = \kappa^2 V$ in the limit

$$\Lambda = -\frac{8L^4}{3D^2}\Big[1 + a\ \mathrm{sign}(r)\Big]^2_{r\to\pm\infty}. \tag{6.33}$$

The domain wall for $|a| < 1$ gives a warp factor decreasing for both infinities of an extra dimension, and the cases of $|a| = 1$ become the wall solutions interpolating between AdS and flat Minkowski vacua. For $|a| > 1$, the warp factor decreases in one direction, and increases in the other. This domain wall can be

embedded into the five-dimensional supergravity coupled with hypermultiplets as an exact BPS domain wall [14]. After integrating out irrelevant fields with canonical normalization, the above solution is found to be identical to the exact BPS solution in [14]. We shall restrict our analysis to collisions along a r-direction, preserving the symmetry along the homogeneous $\vec{x}_3$-directions. Even with this simplification, such a setup is of relevance in a number of physical situations. The initial data for such a collision can be obtained as follows. First of all, we introduce a new coordinate z by $z = \int dr e^{-U}$ and work on the conformal gauge,

$$ds^2 = e^{2A(t,z)}(-dt^2 + dz^2) + e^{2B(t,z)}d\vec{x}^2. \tag{6.34}$$

Then the above single static wall is boosted along the fifth direction z, and we obtain a wall moving with constant velocity β [437]. To discuss collisions of two moving domain walls, we set a kink solution at $z = -z_0$ and an anti-kink solution at $z = z_0$, which are separated by a large distance and approaching each other with the same (or different) speed β. Such superposition and matching of the metric and scalar field at the center is possible for $|a| = 1$, and sufficiently smooth initial data that satisfies the constraint equations at the initial time can be obtained, as long as the spatial separation between the two walls is much larger than the thickness of walls. Therefore, we take $|a| = 1$ throughout this paper. Obviously, we set $A = B$ and velocity $\dot{A} = \dot{B}$ at the outset, and the initial values of $\dot{\phi}$ and $\dot{A}$ are given by the above construction. During the evolutions, the Neumann boundary conditions are imposed at the outer boundaries. The asymptotics of the scalar field is $\phi \propto (\gamma|z|/\sqrt{6/|\Lambda|} + 1)^{-3/2L^2}$, and the metric behaves $e^A \propto (\gamma|z|/\sqrt{6/|\Lambda|} + 1)^{-1}$ as $|z| \to \infty$, where $\gamma = 1/\sqrt{1-\beta^2}$ is the Lorentz factor. The kink and anti-kink solutions are characterized by their own width and amplitude, (D_K, L_K) and (D_A, L_A), respectively. Therefore, we have three types of unfixed parameters for the initial setup; D, L and β. Using a fourth-order accurate finite difference code, we have solved the system numerically and evaluated the constraints at each time step for various families of initial data. The overall picture does not depend on a specific choice of the parameters. Some examples of numerical results are reported in Fig. 6.10, in which the time evolutions of energy density $\rho = \frac{e^{-2A}}{2}\left[(\partial_t\phi)^2 + (\partial_z\phi)^2\right] + V$ in $\{t, z\}$-flame are shown. In all these cases, the two walls with initial velocity $\beta_0 = 0.4$ collide at $z = 0$ and $t \approx 31$. Fig. 6.10(a) describes the symmetric collision of two identical walls. In this case, the walls *pass through* one another so that the initial kink solution at $z < 0$ goes to $z > 0$. (The kink and anti-kink solutions are distinguished by their relative field values at the center and infinity $z = \pm\infty$.) The energy density of wall, i.e. the wall's tension, increases during this process. This would be caused by the fact that the induced universe on the walls are contracting during the process, with $\dot{B} < 0$. After the collision, a sharp peak of density appears at the collision point $z = 0$, and it implies an emergence of singularity. In fact, the curvature diverges rapidly at the point, whereas the curvature on the wall remains finite and small at the moment (Fig. 6.11). Here our criterion of curvature singularity is that the Kretschmann scalar exceeds $R^{abcd}R_{abcd} > 10^6$. At the time $t \approx 42$ of singularity formation, the energy density localized at $z = 0$ is 1.2 times bigger than those on the walls, and a portion of energy is stored in this small region, which will be inside an event horizon, as we see below.

This basic picture of collision holds for other cases. For the asymmetric collisions, such as two walls with different width, amplitude, and/or speeds, the emergence of singularity is still a generic feature. Figs. 6.10(b) and 6.10(c) show examples of collisions in which different thickness or amplitude of scalar field are taken for the two walls, without changing other parameters. Among these cases, Fig. 6.10(b) shows that one of the walls recoils at the collision, due to the larger momentum of one of the walls: the initial kink solution at $z = -30$ in Fig. 6.10(b) goes to $z > 0$ after the collision, while the anti-kink at $z = +30$ bounds back. Interestingly, in these asymmetric collisions, the curvature singularities appear off the collision point. For Figs. 6.10(b) and 6.10(c), they are at $z = -2.4$ and $z = -1.2$, respectively. For the wide range of initial parameters, the emergence of singularity is the generic consequence. However, as expected and discussed below, the singularity does not appear for $L \ll 1$ and/or $\beta_0 \ll 1$ for fixed D. In such "non-relativistic" cases, the two walls just pass through, and the final configurations of fields are well described by the boosted walls, as we applied for the initial configurations.

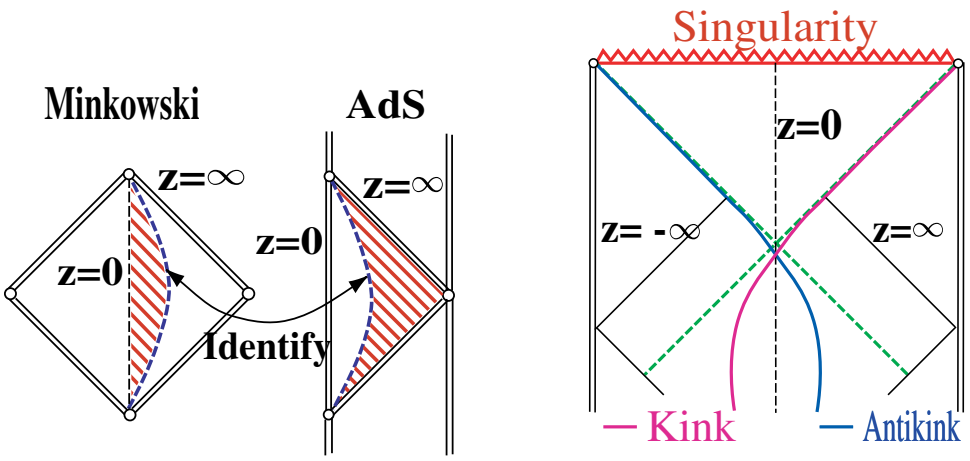

Figure 6.13: Schematic conformal diagrams for a single domain wall that asymptotes to AdS (Minkowski) as $z \to \infty$ ($z \to 0$) *(Left)* and for colliding walls, producing a black brane *(Right)*.

6.2.2 Horizon formation

The next task at hand is to confirm the nature of singularity. In numerical investigations of singularity formation and global structure of the spacetime, null coordinates are useful to prevent the singularity from corrupting the rest of the spacetime. In these coordinates, horizons are not particularly special and we can follow the collision all the way to the singularity even when a horizon appears through a collision. We evolve the colliding walls in the double-null coordinates (e.g., [162, 199]),

$$ds^2 = -2e^{2A}dudv + e^{2B}d\bar{x}^2\,, \tag{6.35}$$

where $\sqrt{2}u = (t - z)$, $\sqrt{2}v = (t + z)$. In this gauge, the Einstein equations and the dynamical equation for a scalar field are split into three dynamical and two constraint equations. Let us first focus on the symmetric collision in Fig. 6.10(a). The corresponding evolution in the null coordinates is described in Fig. 6.12. It shows that the curvature singularity is spacelike, approaching u or v = const. lines at late times, which corresponds to the event horizon. This result is very generic, and we have observed similar results for the wide range of initial data (velocity, etc.). This system has homogeneous 3-spatial directions, and so the horizon also extends in these directions. This means that a black brane is produced by the collision of walls, so that this collision provides the dynamical mechanism of generating black branes in higher dimensions.

Another interesting feature is that after the collision the walls are trapped around the surface of the horizon. The final speeds of walls asymptote to the speed of light [Fig. 6.12(c)], irrespective of the initial velocity. The bulk outside the two walls is not exactly AdS, but asymptotes to it. Because of this behavior, the walls are pulled outside, accelerating in the directions. A schematic picture of a conformal diagram is given in Fig. 6.13 Another example corresponding to to the asymmetric collision in Fig. 6.10(b) is shown in Fig. 6.12(b). Even in this asymmetric collision, the event horizon forms from the point where the spacelike singularity appears. An interesting difference is that the kink wall escapes from the horizon, and only the antikink wall is trapped nearby.

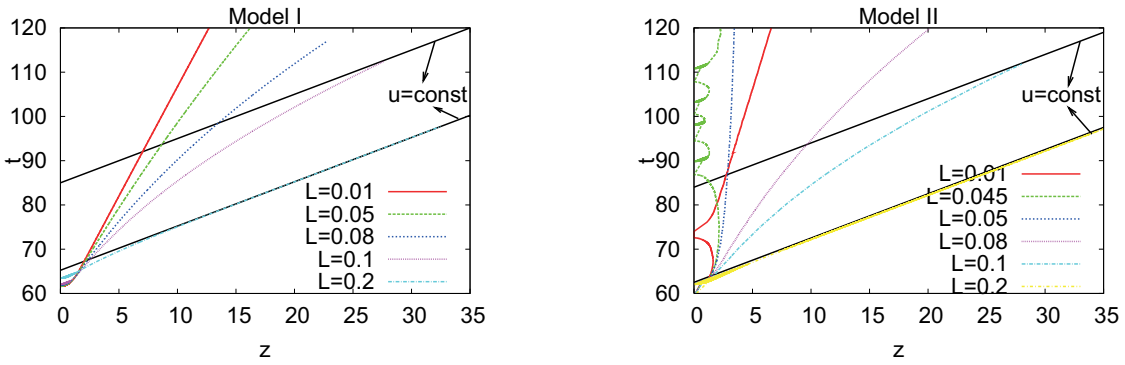

Figure 6.14: The orbits of a wall after the symmetric collisions at $t \approx 60$ ($\beta_0 = 0.2$ and $D = 1$) are described for the two models (Model I, II), to show the dependence on L. Solid straight (black) lines represent u =const. lines along the spacelike singularities for $L = 0.1, 0.2$.

6.2.3 Model II

The initial data discussed so far is based on the single BPS domain wall. There is another simple model in which collisions of walls can be tested. It is the model used in the previous work [437],

$$U = -\frac{2L^2}{3}\left(\log[\cosh(r/D)] + \frac{\tanh^2(r/D)}{4} - \frac{r}{D}\right), \tag{6.36}$$
$$\phi = \frac{\sqrt{3}\,L}{\kappa}\tanh\left(\frac{r}{D}\right), \quad V = \frac{9L^4}{4D^2\kappa^4}\left[2\left(\frac{\partial W}{\partial\phi}\right)^2 - \frac{8\kappa^2}{3}W^2\right],$$

where $W = -\frac{1}{9\sqrt{3}}\left(\frac{\kappa}{L}\phi\right)^3 + \frac{\kappa}{\sqrt{3}L}\phi - \frac{2}{3}$. The basic property of the wall is quite similar to the wall in the previous sections; the bulk in $r > 0$ asymptotes to the Minkowski spacetimes, while the spacetime in $r < 0$ asymptotes to the AdS, recovering (6.33). This single domain wall solution is found simply by extending the four-dimensional solution in [145]. It is interesting to study various aspects of the wall collisions in this model and compare them with the previous model. We have performed many simulations and confirmed that all phenomena observed in the previous sections, such as the singularity and horizon formation hold with qualitatively similar behaviors. A basic exception is that in this model the walls *bounce back* after the collision, contrary to the case in Model I. Thus the causal structures of such a collision look like Fig. 6.12(a), but kink and anti-kink profiles are exchanged after a collision. This difference comes from the nonlinear interaction through the dynamics of collision.

Such details of model dependence become more significant for weak field cases in which no singularity appears. In Fig. 6.14, we compare the difference of the two models by showing the orbits of a wall after the symmetric collisions for various values of L. For Model I, the spacelike singularity appears for $L \gtrsim 0.1$, and the walls asymptote to the null lines, as discussed above. On the other hand, for $L \lesssim 0.1$, the velocity of the wall becomes timelike with constant speed after the collisions, and no singularity appears. In fact, the final configurations of scalar fields are well approximated by superposing boosted walls, so that the two walls just pass through one another in these cases. Note that if the initial velocity is increased the horizon appears even for smaller L. For Model II, multiple collisions take place for $L \ll 1$ (Fig. 6.14). For $L = 0.01$, the collision takes place two times, and then the wall bounces back with constant velocity. This behavior is compatible with and typical in the non-gravitating system of the previous study [437]. As L increases, the two walls gravitate toward one another and multiple bounces take place (e.g., $L = 0.045$). The marginal value of L is $L = 0.05$ in Fig. 6.14, in which the gravitational attractive force and the repulsive force due to outer AdS region are in balance. Therefore, a quasi-static configuration of two walls is realized after the collision.

6.2.4 Summary

We have considered a system of colliding domain walls, whose initial data is set up based on a single BPS domain wall, and found that the role of gravity at the collision is significant in that it can drastically change the picture of "silent" collisions without self-gravity. The main result of our study is that horizon formation is a generic phenomena in the collision of walls. In the non-relativistic cases, such as $L \ll 1$ and/or $\beta \ll 1$, "silent" collisions without singularity and horizon are realized, but such cases are very limited and unlikely in an early universe of brane-worlds.

The local interaction and dynamics at the collision depends on which model we are looking at. For Model I, the domain walls can pass through one another, while in Model II they bounce at the collision and go back. However, the basic feature of horizon formation does not change in these models, and we have concluded that the horizon formation (and singularity behind it) is a generic consequence of kink-anti-kink collisions. The horizon has three homogeneous spatial directions, so that a black three-brane is produced by such a collision. The bulk outside the two walls is approximated by the AdS, and then we look at the created black hole as it sits on the AdS. In the pure AdS, a possible black hole is a topological black hole, which has a flat 3-dimensional hypersurface with vanishing curvature. The end state of the present scenario would be this type of black hole (Fig. 6.13), although the field fills the bulk outside the horizon. Here, a further interesting possibility comes from the fact that a spatially homogeneous horizon suffers from Gregory-Laflamme instability in general. The end state of this instability has not been clearly understood so far, and the horizon may break up, resulting in multiple black holes that are stuck on the walls [269]. Furthermore, during this process, a good deal of energy will be radiated away by gravitational waves, and they remain as primordial gravitational wave backgrounds. Thus this possibility provides a new way of producing primordial black holes and gravitational waves in an early universe with higher dimensional bulk filled by walls/branes.

There are several interesting directions, which may be pursued on the basis of these results and/or by relaxing several conditions. One of such issue is a study of the effects and roles of other fields in supergravity, a subject sets aside in our analysis. Other fields contained in the hypermultiplets will be excited (or thermalized) during the collisions, and analyzing them should provide many cosmological insights into brane-world cosmologies [184]. Furthermore, there is one most important question left to answer: To what extent is the production of black holes/branes generic in a class of more generic theory and context, such as collisions of different types of walls with an arbitrary incident angle. We foresee no major obstacle in anticipating that horizon formation would be suppressed.

6.3 Dimensionality problem

From cosmological aspects, an ultimate goal of string theory is to resolve three interesting problems: the cosmological constant, the initial singularity problem, and the origin of the three spatial dimensions and time. For the initial singularity problems, the tachyon condensation of winding strings may play a role when the radius of universe shrinks smaller than the string scale, according to a recent proposal [323]. Here, we focus on the dimensionality problem in the context of the Brandenberger-Vafa (BV) scenario [64] (see [129, 232]). In the original BV scenario [64], it is assumed that all nine spatial dimensions start from the toroidally compactified radii near the string length and the universe is filled with an ideal gas of fundamental matter, so-called string gas. It is also assumed that the string gas is initially thermalized at the critical temperature T_H, called the Hagedorn temperature [198]. In order to resolve the dimensionality problem, the string winding modes play a particularly important role. The winding strings prevent the dimensions which they wrap from expanding, as shown in [449, 450]. The annihilation of winding and anti-winding strings determines how many dimensions expand and how many dimensions stay at the string length. A simple counting argument suggests that this annihilation occurs mostly in the space-time dimensions of $D = 4$, so the three spatial dimensions become large. Some studies have already examined various aspects of the BV scenario and it has been extended in a variety of ways [449, 450, 395, 136, 9, 35, 113, 44, 87, 68, 54, 69]. (See also recent reviews [66, 67, 38]). The interaction

(annihilation) rate Γ of the string winding modes, with the string coupling e^{ϕ}, is roughly

$$\Gamma \simeq 100 \ln E\, e^{4\phi}\,. \tag{6.37}$$

(See [113] and Sec. 6.3.4 for more detailed discussion). Assuming that this interaction works efficiently at an early stage of the universe, decompactification proceeds. However, there are three main assumptions on this scenario: adiabatic evolution, weak coupling and thermal equilibrium. A critical point of this scenario is the last assumption about thermal equilibrium [113] (see also [136] for another assessment). The thermal equilibrium condition is given by

$$\Gamma > H, \tag{6.38}$$

where H is the Hubble expansion rate. Let us briefly estimate this condition based on a typical cosmological evolution at the Hagedorn temperature with "string matter". The radius of the universe asymptotes to a constant value, whose order is the string scale or several times of it. This means that all dimensions will be still small, which is inconsistent with our large four dimensions. However, if the radii (of three dimensions) asymptote to a sufficiently large value, then the universe could be matched to a radiation dominated phase. This type of evolution is only allowed when the initial dilaton satisfies a certain condition. From the condition indicated with Eq. (6.37), the interaction rate is found to be bounded from above as

$$\Gamma \lesssim \left(O(10^{-1})H_0^3\right)H_0\,, \tag{6.39}$$

where the subscript 0 denotes the value at an initial time (Sec. 6.3.4). This shows that the thermal equilibrium condition is not satisfied at the initial phase of the universe, under the adiabatic condition $H \lesssim 1$. Therefore, no consistent treatment with well-defined thermodynamic functions can be carried out [118], and all analysis based on such an approach cannot be trusted. This non-equilibrium aspect of string gas is related to cosmological expansion at the Hagedorn phase. Some features are necessary for resolving this difficulty, for instance:

- The universe does not evolve toward a constant radius at late times.
- Initial evolution of the universe is modified.

In the latter case, the universe may or may not evolve toward a constant radius, and the initial constraint for the dilation may be replaced by a weaker condition. There are several possibilities for achieving the above two evolutions. In the straightforward derivation of the interaction rate (6.39), we have assumed a simple dilaton-gravity system without taking into account any nontrivial coupling between the dilaton and "string matter" (gas) fields. Any nontrivial coupling modifies the dynamics of dilaton and cosmological expansion, and it may weaken the difficult requirement for the initial condition. For example, incorporating the NS-NS and R-R fields into the action [87, 68], or the effects of higher curvature corrections [54] will alter the evolution of the universe at an early stage. With these ideas in mind, we wish to pursue the possibility of resolving the thermal equilibrium issue. We adopt a simple modification of the scenario by taking into account the dilaton potential. This simple alternative will allow us to study the system rather extensively and give insight into other possibilities and approaches. We will see that the above two features are realized in the simple models in the present paper. In the next section, general aspects of dilaton-gravity and string gas in the extreme Hagedorn regime of high-energy densities are briefly reviewed. We will take the dilaton potential to be of two types. The first case is discussed in Sec. III, the second in Sec IV. For both cases, we analyze the dynamics of the Hagedorn regime with a single scale factor (Hubble radius) and with large and small radii. In Sec. V we discuss the thermal equilibrium of string gas for the two models. The final section is devoted to summary and discussion. We adopt the string scale $\alpha' = 1$.

6.3.1 String gas in 10D dilaton gravity

Dilaton-gravity comes from the low-energy effective action of string theory. Ignoring contributions from the antisymmetric two-form and including a potential $V(\phi)$ for the dilaton, [1] the action of this system is described as

$$S = \int d^{10}x\sqrt{|g|}\left[e^{-2\phi}\left(R + 4(\nabla\phi)^2 + V\right) + \mathcal{L}_M\right], \tag{6.40}$$

where g denotes a determinant of metric $g_{\mu\nu}$ and $\mathcal{L}_M$ denotes a Lagrangian of some matter. Assuming a spatially-homogeneous universe,

$$ds^2 = -dt^2 + \sum_{i=1}^{9} e^{2\lambda_i(t)}dx_i^2, \quad \phi = \phi(t)\,, \tag{6.41}$$

we can reduce the action to

$$S = \int dt\sqrt{-g_{00}}(-g^{00})\left[e^{-\psi}(\sum_{i=1}^{9}\dot{\lambda}_i^2 - \dot{\psi}^2 + V(\phi)) - F(\lambda_i, \beta\sqrt{-g_{00}})\right], \tag{6.42}$$

where we have introduced a shifted dilaton $\psi \equiv 2\phi - \sum_{i=1}^{9}\lambda_i$ to simplify the obtained equation of motion. In the reduced action, we have introduced the (one loop) free energy F of a closed string as the Lagrangian of matter. This is only possible in an early universe in which the string gas is in thermal equilibrium at the temperature β^{-1}. Variation with respect to g_{00}, λ_i, ψ yields the following equations of motion:

$$\begin{aligned}
&-\sum_{i=1}^{9}\dot{\lambda}_i^2 + \dot{\psi}^2 = e^{\psi}E - V(\phi)\,,\\
&\ddot{\lambda}_i - \dot{\psi}\dot{\lambda}_i = \frac{1}{2}e^{\psi}P_i + \frac{1}{4}V'(\phi)\,,\\
&\ddot{\psi} - \frac{1}{2}\sum_{i=1}^{9}\dot{\lambda}_i^2 - \frac{1}{2}\dot{\psi}^2 = \frac{1}{2}V(\phi) - \frac{1}{4}V'(\phi)\,,
\end{aligned} \tag{6.43}$$

where $E = \rho e^{\sum\lambda_i}$ and $P_i = p_i e^{\sum\lambda_i}$ are the total energy and total pressure in i-th direction, respectively. These quantities are related to the free energy F by the basic thermodynamic relation:

$$E = F + \beta\frac{\partial F}{\partial\beta}\,, \quad P_i = -\frac{\partial F}{\partial\lambda_i}\,.$$

Employing Eqs. (6.43), the conservation of the total energy is

$$\dot{E} + \sum_{i}^{9}\dot{\lambda}_i P_i = 0\,. \tag{6.44}$$

The basic equations become simple forms in terms of the shifted dilaton. In some cases, however, the equations written by the original dilaton are convenient. Here, if we separate the spatial dimensions into spatial large d-dimensions and small $(9-d)$-dimensions, which are denoted as

$$R = e^{\mu}, \quad r = e^{\nu}\,, \tag{6.45}$$

respectively,

[1] We give the dilaton potential in string frame, while corresponding potential in Einstein frame is given in Appendix 6.3.6. Note that the initial data in Einstein frame also differ from ones in string frame.

6.3.2 Hagedorn regime

The original BV scenario [64] assumed that all nine spatial dimensions are compactified with radii $R \sim 1$ and the universe is filled with string gas in thermal equilibrium around the Hagedorn temperature T_H [198]. The partition function has poles depending on the radii of the universe, and accordingly the equation of state changes. For small radii, the leading order expression for the temperature and the pressure which come from the density of states Ω is derived in [35]. For large enough E, as a result, the temperature remains close to the Hagedorn temperature T_H, and the pressure is vanishingly small,

$$T \sim T_H\,, \quad P_d \sim 0\,, \quad P_{\,9-d} \sim 0\,. \tag{6.46}$$

Therefore, the string gas in the universe with small radii at the Hagedorn temperature can be treated as a pressureless fluid, as expected by T-duality. As the universe grows with larger radii, the above mentioned poles move on the β plane. This causes the density of states Ω to change and yields a different temperature and pressure from those of the former "small radius" regime [119]. There will exist a critical radius $\bar{R}$. When the radius is below the critical radius, the universe is still described by a pressureless state at the Hagedorn temperature, while above the value, the temperature and the equation of state are

$$\frac{1}{T} = \frac{\beta_H E - 9}{E}\,, \quad P \propto \Big(\frac{E}{\beta_H E - 9}\Big) dR^d(E)\,, \tag{6.47}$$

where d denotes the expanding spatial dimensions. Note that these quantities depend on the total energy E and that it is necessary to solve the equation of motions for E as a function of time numerically. It was shown that the radius rapidly expands like an acceleration expansion while the dilaton continues its monotonic decrease [113].

The above small and large radius phases are the basic states of string gas near the Hagedorn temperature, and the BV mechanism explains how the particular spatial dimensions enter into the second phase. These discussions are, of course, based on the assumption of the thermal equilibrium of string gas and that is the point of our discussion in this paper. When the energy density decreases and the temperature falls much below the Hagedorn temperature, the string gas will behave as radiation, with $P = \frac{1}{d}E$ yielding the radiation dominated evolution, $R \propto t^{2/(d+1)}$ in [35, 113]. In what follows, we discuss the evolution of spacetime and dilaton and, based on the analysis, we study the thermal equilibrium of string gas at the initial Hagedorn regime, where the string gas behaves as pressureless dust.

6.3.3 Time evolution of universe and dilaton

We will take the potential of the dilaton to be of two types, each with a different nature. The first example is a simple exponential potential (Model I), while the second is a double-well potential (Model II). In order to describe the typical behavior of the system, we analyze the simple situation, in which all radii are the same, $\mu = \nu$. The more generic situation in which small spatial dimensions ($r = e^{\nu}$) and large spatial dimensions ($R = e^{\mu}$) are separated will be also discussed in. However, as a result, both radii evolve in the same manner since the potential acts on each radius in the same way.

Exponential potential (Model I)

As a toy model, we discuss a dilaton field with a runaway potential. (See [45] for early works in other context),

$$V(\phi) = b\, e^{2a\phi}\,, \tag{6.48}$$

where a and b are constant parameters. For simplicity, we assume $\phi \lesssim 0$ with $a > 0$ hereafter to achieve the weak coupling regime $e^{\phi} < 1$. Additionally, we take $|b| = 1$ since the basic behavior does not change according to the magnitude of b. The effective potential in the Einstein frame will allow us to intuitively understand the behavior of the dilaton. As discussed in Appendix 6.3.6, the effective potential of the dilaton in the Einstein frame $W(\phi)$ is described as

$$W = -e^{\frac{\phi}{2}} V\,, \tag{6.49}$$

and hence the case with $b < 0$ is the usual exponential potential in the Einstein frame. We will also analyze this case. For the following two limits, analytic asymptotic solutions can be found. Let us begin with discussing these solutions before we present numerical solutions.

$V \to 0$ **limit**

This case is reduced to the standard analysis without the potential term. The equations (6.43) with zero pressure give

$$\begin{aligned} \ddot{\mu} &= (2\dot{\phi} - 9\dot{\mu})\dot{\mu} + \frac{1}{4}V', \\ \ddot{\phi} &= \dot{\phi}^2 - 18\dot{\mu}^2 + \frac{1}{4}V + V', \\ E &= e^{9\mu - 2\phi}(72\dot{\mu}^2 - 36\dot{\mu}\dot{\phi} + 4\dot{\phi}^2 + V), \end{aligned} \tag{6.50}$$

and then the $V \to 0$ approximation yields

$$\frac{d}{dt}\ln\dot{\mu} = \dot{\psi}, \quad \ddot{\psi} = \frac{9}{2}\dot{\mu}^2 + \frac{1}{2}\dot{\psi}^2, \quad \frac{d^2}{dt^2}(e^{-\psi}) = \frac{E}{2}. \tag{6.51}$$

Since the total energy is constant, $E = E_0 = \text{const}$, obtained from Eq. (6.44), the analytic solutions for $\psi(= 2\phi - 9\mu)$ and μ are easily obtained from Eq. (6.51) as

$$\begin{aligned} e^{-\psi} &= \frac{E_0}{4}(t - t_*)^2 + B(t - t_*) + \frac{B^2 - 9A^2}{E_0}, \\ \mu &= \mu_* + \frac{1}{3}\ln\left|\frac{(E_0(t - t_*) + 2B - 6A)(B + 3A)}{(E_0(t - t_*) + 2B + 6A)(B - 3A)}\right|, \end{aligned} \tag{6.52}$$

where t_* is the time when the condition $V(\phi) \simeq 0$ is satisfied. The integration constants are given by $A = \dot{\mu}_* e^{-\psi_*}$, $B = -\dot{\psi}_* e^{-\psi_*}$, where μ_* and ψ_* are the field values at the time $t = t_*$. The solutions behave asymptotically in three ways (see Fig. 6.15(a)). The first type (i) is that in which the radius grows as $\lim_{t\to 0}\ln|1/t|$ and diverges ($\mu \to \infty$) at $E_0(t - t_*) = 2|B + 3A|$. At the same time, the dilaton also grows and diverges [2]. These behaviors appear if the conditions $B + 3A < 0$ and $|B + 3A| < |B - 3A|$ are satisfied, yielding $0 < 6\dot{\mu}_* < \dot{\phi}_*$. The second type of evolution (ii) is that in which the radius contracts as $\lim_{t\to 0}\ln|t|$ and $|\mu|$ diverges at $E_0(t - t_*) = 2|B - 3A|$. Similarly, the dilaton contracts. These behaviors appear if the conditions $B - 3A < 0$ and $|B - 3A| < |B + 3A|$ are satisfied, yielding $3\dot{\mu}_* < \dot{\phi}_*$ with $\dot{\mu}_* < 0$. The last type (iii) is that in which the radius converges to a constant value, which is achieved for $0 < B + 3A, B - 3A$.

The first two types of evolution will be seen in the double-well potential case. In the present model, only the last behaviors are important and we comment on its asymptotic radius. The asymptotic evolution at $t \to \infty$ of the spacetime is

$$R_\infty = e^{\mu_\infty} = e^{\mu_*}\left|\frac{B + 3A}{B - 3A}\right|^{1/3}, \tag{6.53}$$

and it converges to a constant radius [449], while the (shifted) dilaton rolls monotonically to the weak coupling. Without fine-tuning ($B \simeq 3A$), the asymptotic value R_∞ is not very large, and the radius remains small. We call this solution *the convergent solution*.

$V, V' \gg \dot{\phi}\dot{\mu},\ \dot{\phi}^2,\ \dot{\mu}^2$ **limit**

In the potential dominated case, the equations (6.50) are reduced to

$$\ddot{\mu} = \frac{1}{4}V'(\phi) = b\frac{a}{2}e^{2a\phi}, \quad \ddot{\phi} = \frac{1}{4}V(\phi) + V'(\phi) = b\frac{8a + 1}{4}e^{2a\phi}. \tag{6.54}$$

[2] At the strong-coupling regime after the growth of the dilaton, we cannot predict what will happen. A possibility of a static universe in the strong-coupling regime is recently discussed in [69].

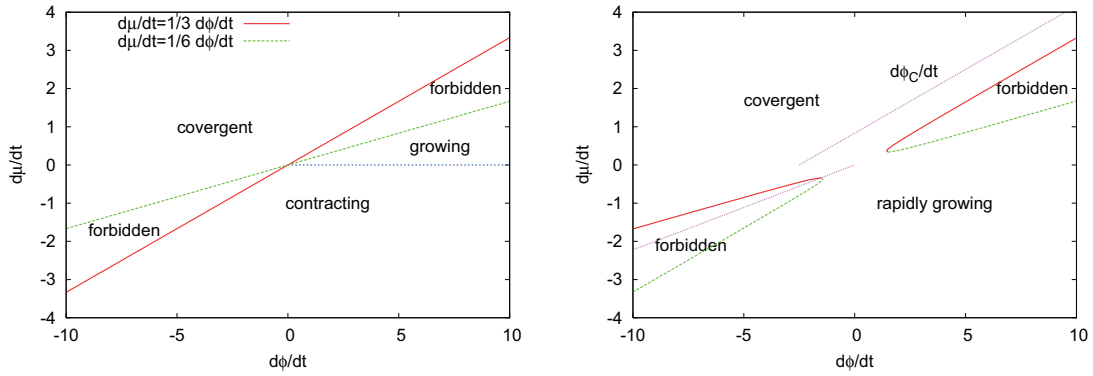

(a) (b)

Figure 6.15: Evolution of asymptotic solutions (6.52) with respect to the initial data $(\dot{\mu}_*, \dot{\phi}_*)$. Other initial data are fixed, as $\mu_* = \phi_* = 0$ with $t_* = 0$. Fig. 6.15(a) shows the asymptotic solutions with $V = 0$. The forbidden region $E \lesssim 0$ is equivalent to $3|\dot{\mu}| \lesssim |\dot{\phi}| \lesssim 6|\dot{\mu}|$. The growing and contracting solutions correspond to $0 < \dot{\mu}_* \lesssim \dot{\phi}_*/6$ and $\dot{\mu}_* \lesssim \dot{\phi}_*/3$ with $\dot{\mu}_* < 0$, respectively. For the other choice of initial data $(\dot{\mu}_*, \dot{\phi}_*)$, the radius converges to a constant value μ_∞ of Eq. (6.53). Fig. 6.15(b) shows the asymptotic solutions for the exponential potential $V = be^{2a\phi}$ with $a = 2$ and $b = 1$. The forbidden region $E \lesssim 0$ is equivalent to $(9\dot{\mu} - \sqrt{9\dot{\mu}^2 - 1})/2 \lesssim \dot{\phi} \lesssim (9\dot{\mu} + \sqrt{9\dot{\mu}^2 - 1})/2$. The rapidly growing and convergent solutions correspond to $\dot{\phi}_C < \dot{\phi}_*$ and $\dot{\phi}_* < \dot{\phi}_C$, respectively. The critical velocity $\dot{\phi}_C$ is approximated by straight lines of Eq. (6.81) $(\dot{\mu}_* \simeq \dot{\phi}_*/3 + 5/6)$ with $\dot{\mu}_* > 0$ and Eq. (6.83) $(\dot{\mu}_* \simeq 2/9\dot{\phi}_*)$ with $\dot{\mu}_* < 0$ (Appendix B).

As for $b = 1$, if the initial condition satisfies

$$\frac{8a+1}{4a} e^{2a\phi_*} > \dot{\phi}_*^2 , \tag{6.55}$$

the analytic solutions for these equations are given by

$$\begin{aligned} \phi &= -\frac{1}{a} \ln\left\{ \frac{1}{2C_1} \sqrt{8 + \frac{1}{a}} \sin\left[aC_1 (t - t_* + C_2) \right] \right\} , \\ \mu &= \frac{2a}{8a+1} \phi + D_1 (t - t_*) + D_2 . \end{aligned} \tag{6.56}$$

Here C_1, C_2, D_1 and D_2 are the integration constants given by

$$C_1 = \sqrt{\frac{8a+1}{4a} e^{2a\phi_*} - \dot{\phi}_*^2} , \quad C_2 = \frac{1}{aC_1} \cot^{-1} \left| \frac{\dot{\phi}_*}{C_1} \right| , \quad D_1 = \dot{\mu}_* - \frac{2a}{8a+1} \dot{\phi}_* , \quad D_2 = \mu_* - \frac{2a}{8a+1} \phi_* . \tag{6.57}$$

μ_* and ϕ_* are the field values at the time $t = t_*$ when the condition $V, V' \gg \dot{\phi}\dot{\mu}, \dot{\phi}^2, \dot{\mu}^2$ becomes a good approximation. Both the dilaton and radius diverge at

$$(t - t_*) \sim \frac{\pi}{aC_1} - C_2 . \tag{6.58}$$

We call the solution (6.56) *the rapidly growing solution*. For the exponential potential case, these features of the system are understood clearly by employing phase-space analysis in Appendix 6.3.6.

Double-well potential (Model II)

Model	Parameter		Type of solution
$V = be^{2a\phi}$	$b > 0$	$a > 1$	convergent solution ($\dot{\phi}_0 < \dot{\phi}_C$)
			rapidly growing solution ($\dot{\phi}_0 > \dot{\phi}_C$)
		$a \leq 1$	rapidly growing solution
	$b < 0$	$a > 1$	convergent solution ($\dot{\phi}_0 < \dot{\phi}_C$)
			contracting solution ($\dot{\phi}_0 > \dot{\phi}_C$)
			convergent solution ($H_0 > 0$ and $\dot{\phi}_0 \lesssim 0$)
$V = \frac{\lambda}{4}\left[\left(\frac{\phi}{\eta}\right)^2 - 1\right]^2$	$\lambda > 0$	$\eta \gg 1$	rapidly growing solution ($\dot{\phi}_0 \lesssim 0$)
	$\lambda < 0$		stabilized dilaton with $\phi \to -\eta$. ($H_0 > 0$ and $\dot{\phi}_0 \lesssim 0$)

Table 6.1: Summary of basic behaviors

As a second model, we consider the double-well potential,

$$V(\phi) = \frac{\lambda}{4}\left[\left(\frac{\phi}{\eta}\right)^2 - 1\right]^2 , \tag{6.59}$$

where λ and η are a coupling constant and a vacuum expectation value (VEV) of ϕ, respectively. Similar to the previous model, λ is taken to be positive or negative. The later case corresponds to an ordinary concave effective potential picture $W \sim -V$ (Appendix 6.3.6). For simplicity, we assume until S**??** that all radii are the same, $\mu = \nu$.

For $\lambda < 0$
the dilaton stays at the minimum (VEV) of the double-well potential $\phi_V = \pm\eta$. Expanding ϕ around the VEV,

$$V \approx O(\delta\phi^2) , \quad V' \approx \frac{2\lambda}{\eta^2}\delta\phi + O(\delta\phi^2) , \tag{6.60}$$

we find that Eqs. (6.50) are approximated as

$$\ddot{\mu} + 9\dot{\mu}^2 \approx 0 , \quad \delta\ddot{\phi} - \frac{2\lambda}{\eta^2}\delta\phi + 9\dot{\mu}\delta\dot{\phi} + \frac{E}{4}e^{-9\mu+2\phi_V} \approx 0 . \tag{6.61}$$

These equations have the following solutions:

$$\delta\phi \sim C_1 J_0(z) + C_2 N_0(z) , \quad \mu \sim D_2 + \frac{1}{9}\ln\left|t - t_* - \frac{D_1}{9}\right| , \quad z = \frac{\sqrt{2|\lambda|}}{\eta}\left(t - t_* - \frac{D_1}{9}\right) , \tag{6.62}$$

where $J_\nu(z), N_\nu(z)$ are the Bessel functions with the amplitude C_1 and C_2. D_1 and D_2 are given by

$$D_1 = -\frac{1}{\dot{\mu}_*} , \quad D_2 = \mu_* + \frac{1}{9}\ln 9|\dot{\mu}_*| . \tag{6.63}$$

Note that when we derive the above solutions, we have used the fact that the last term in (6.61) decays as $e^{-9\mu+2\phi_V} \propto 1/t$, so that it can be omitted at late times. The amplitude of $\delta\phi$ becomes $\propto 1/\sqrt{t}$ for $\lambda < 0$, which is equivalent to a decaying solution. We will call this solution *the stabilized dilaton solution.*

6.3.4 Thermal equilibrium of string gas

We will take the potential of the dilaton to be of two types, each with a different nature. The first example is a simple exponential potential (Model I), while the second is a double-well potential, discussed in the

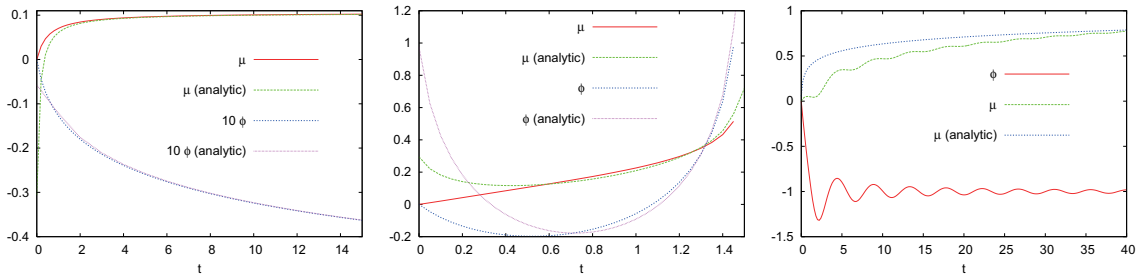

(a) Convergent solution (b) Rapidly growing solution (c) Stabilized dilaton solution

Figure 6.16: (a): Plot of typical convergent solutions of the dilaton ϕ (blue line) and radius $R = e^{\mu}$ (red line) for $\mu_0 = \phi_0 = 0, \dot{\mu}_0 = 0.2, \dot{\phi}_0 = -3$ and $a = 2, b = 1$. The analytic solutions (green and pink lines) of Eq. (6.52) are also plotted as a reference. Here the integration constants, $\mu_*, \phi_*, \dot{\mu}_*, \dot{\phi}_*$, are chosen appropriately. The asymptotic evolutions are well approximated by the analytic solutions. The same results can be obtained for the case $\dot{\phi}_0 > 0$ with $\dot{\mu}_0 \gtrsim O(1)$. (b): Plot of typical rapidly growing solutions for the same initial conditions in Fig. 6.16(a) except for $\dot{\phi}_0 = -1$. (c): Typical evolutions of the stabilizing solutions with the same initial conditions as in Fig. 6.16(b) except for $\lambda = -1, \eta = 1$. The analytic solutions (6.62) are also plotted as a reference. The dilaton goes to the VEV ($\phi_V = -\eta$) as oscillating. The radius expands monotonically.

next section (Model II). First, we shall discuss the exponential potential case. In order to describe the typical behavior of the system, we analyze the simple situation, in which all radii are the same, $\mu = \nu$. The more generic situation in which small spatial dimensions ($r = e^{\nu}$) and large spatial dimensions ($R = e^{\mu}$) are separated will be discussed later in this section. In order to resolve the dimensionality problem, the annihilation of winding strings play a critical role in the context of the BV scenario. The interaction rate Γ of annihilation, equivalently, the process where any winding/anti-winding string pair annihilates to the momentum string pair with the coupling given by e^{ϕ}, is roughly [113]

$$\Gamma \simeq 100 \ln E\, e^{4\phi}, \tag{6.64}$$

where 100 is a numerical factor of sum over both spins and momentum states and E is the total energy of string gas. The thermal equilibrium condition is given by

$$\Gamma > H, \tag{6.65}$$

where H is the Hubble expansion rate. The assumption of the thermal equilibrium of string gas is necessary for the BV scenario to work. However, a typical cosmological evolution around the Hagedorn temperature is that the radii of the universe asymptote to a constant value R_∞ as described by Eq. (6.53). As discussed, R_∞ does not become large without fine-tuning. It means that all dimensions are still small and it is inconsistent with our large four dimensions. Nevertheless, if the radii (of three dimensions) asymptote to a sufficiently large value, the universe could be matched to a radiation dominated phase, and only such a case is a viable scenario. Therefore, we require that the asymptotic radius will be larger than a critical radius $\bar{R}$, i.e., $R_\infty > \bar{R}$. Here $\bar{R}$ is a characteristic scale which divides a "small" radius from a "large" one (Sec. 6.3.2). Then, from (6.43) and (6.53), we obtain a constraint equation on the initial value of dilaton as

$$e^{\psi_0} < \frac{9\dot{\mu}_0^2}{E_0}\left[\left(\frac{(\bar{R}e^{-\mu_0})^3 + 1}{(\bar{R}e^{-\mu_0})^3 - 1}\right)^2 - 1\right], \tag{6.66}$$

where the subscript 0 implies the value at an initial time. Substituting this initial constraint into (6.64), the interaction rate at an initial state is roughly estimated as

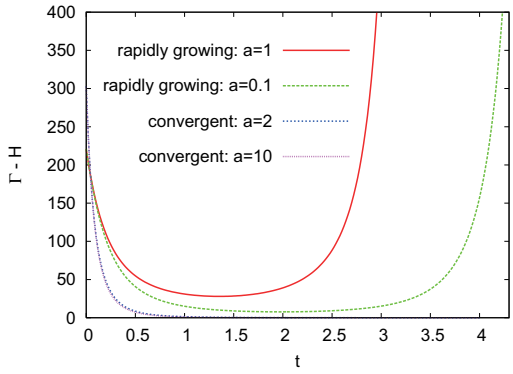

(a) Exponential potential

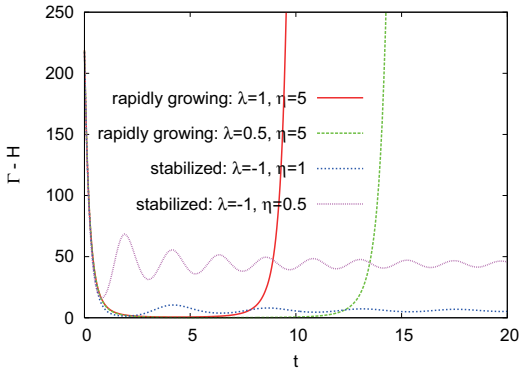

(b) Double-well potential

Figure 6.17: Plot of $\Gamma - H$ for the model of (a) exponential potential ($b = 1$) and (b) double-well potential, respectively. The initial conditions are $\mu_0 = 0, \phi_0 = -0.1, \dot{\mu}_0 = 0.3$ and $\dot{\phi}_0 = -1$ (the rapidly growing solutions as red and green lines), or $\dot{\phi}_0 = -3$ (the convergent solutions as blue and pink lines). $\Gamma - H > 0$ means thermal equilibrium. (a): For the rapidly growing solutions, the weak coupling condition ($e^{\phi} < 1$) breaks down at $t \gtrsim 3$ for $a = 1$ and $t \gtrsim 4$ for $a = 0.1$. (b): For the rapidly growing solutions, the weak coupling condition breaks down at $t \gtrsim 10$ for $\lambda = 1$ and $t \gtrsim 15$ for $\lambda = 0.5$.

$$\Gamma \lesssim 100 \ln E \Big(\frac{9\dot{H}_0^2}{E_0}\Big)^2 O(10^{-1}) \lesssim \Big(O(10^{-1}) H_0^3\Big) H_0 \,, \tag{6.67}$$

where we have taken $\bar{R} \sim 3$, $\mu_0 \sim 0$ and sufficiently high energy, $E \sim 100$. This shows that the thermal equilibrium condition is not satisfied at an initial condition as long as the adiabatic condition $H_0 \lesssim 1$ holds. In what follows, we test the thermal equilibrium condition (6.65) for our models.

Exponential potential case

(i) $b > 0$ case

The exponential potential with $b > 0$ and $a > 1$ allows two types of trajectory for its solutions, i.e., the rapidly growing and convergent ones, described by the analytic solutions (6.52) and (6.56), respectively. Firstly, the convergent solution makes the radius grow toward the asymptotic value of Eq. (6.53), yielding the constraint of Eq. (6.66). However, once the potential term is included, the constraint (6.66) does not directly restrict the initial value of dilaton at $t = t_0$, but it provides a constraint at a late time, $t = t_*$. Therefore, it could relax the constraint on the initial dilaton value, resulting in better realization of the thermal equilibrium. Figure 6.17(a) plots the thermal equilibrium condition with time: $\Gamma - H > 0$ is equivalent to the thermal equilibrium condition. From this figure, we find the thermal equilibrium is realized until $t \sim 1$, which is equivalent to the time scale on which the potential term works, $t \lesssim t_*$. This duration does not depend sensitively on a. The final scale of the radius is, however, not so large, and it may be insufficient to continue the decompactification process. Nevertheless, a noteworthy point is that the thermal equilibrium is realized at the initial phase, contrary to the naive scenario.

Secondly, the rapidly growing solution is the solution in which the radius grows unboundedly, and thus the initial constraint cannot be applied in this case. Contrary to the convergent case, the dilaton grows toward the strong coupling, and the weak coupling condition breaks down. We see that the thermal equilibrium is also realized as seen in Fig. 6.17(a). So the thermal equilibrium is at least realized until the time of the violating, even though the time of the breaking becomes longer as a decreases. The duration of thermal equilibrium becomes large at most by a factor of two. For $a \leq 1$, all solutions are the rapidly

growing type, and, for example, the duration is about $t \sim 5$ for $a = 0.01$.

(ii) $b < 0$ case

In this case, all solutions with $a > 1$ that satisfy the weak coupling condition become convergent solutions. Thermal equilibrium is the same as the convergent solutions in $b > 0$, and hence the initial equilibrium continues until $t \sim O(1)$.

Double-well potential case

(i) $\lambda > 0$ case

All solutions with $\eta \gg 1$ that satisfy the weak coupling condition become rapidly growing solutions. In Fig. 6.17(b) we plot the thermal equilibrium condition. The basic behavior of thermal equilibrium is the same as in the growing solution for the exponential potential with $b > 0$, except for the time scale: the initial equilibrium is realized until $t \sim O(10)$ where the weak coupling condition violates. The thermal equilibrium is only marginally satisfied at almost all times until the violating.

(i) $\lambda < 0$ case

In this case, all solutions which satisfy the weak coupling condition become the stabilized dilaton solutions. If we take η to be small, e.g., $\eta \lesssim O(1)$, the thermal equilibrium continues unboundedly (Fig. 6.17(b)). This is because the solution stabilizes the dilaton at the VEV ($\phi = -\eta$) and then the interaction rate $\Gamma \propto e^{4\phi}$ asymptotes to $e^{-4\eta} \sim O(0.1)$. At the same time, the Hubble expansion rate asymptotes to zero, $H \propto 1/t \to 0$, and then we have $(\Gamma - H)|_{t\to\infty} > 0$. As Fig. 6.17(b) shows, the thermal equilibrium continues unboundedly as long as $\eta \lesssim 1$. This result is the best situation for the BV scenario in our models. As for $\eta > 1$, the thermal equilibrium is only marginally satisfied at late times, $\Gamma - H \approx 0$.

6.3.5 Summary

We have studied the thermal equilibrium of string gas in the Hagedorn regime where the universe is in high energy. Thermal equilibrium is the one of the important assumptions for the BV scenario in order to induce the dynamical decompactification of three large spatial dimensions. However, the initial thermal equilibrium condition of string gas is not realized in the original scenario based on dilaton-gravity. To resolve this difficulty, we have explored possibilities for avoiding the issue. As a first step to tackle this problem, we have studied a minimal modification of the original model, by introducing a potential term of the dilaton. This simple setup allows us to study the system rather extensively. However, this does not mean that stabilization of the dilaton or the effects of the potential term is a necessary ingredient. We wish to emphasize that effects of matter (e.g., flux or any kind of corrections, etc.) would not be negligible, and taking into account such effects, we could avoid the issue of thermal equilibrium in the early universe. We expect our simple setup will provide implications for such effects. We have taken the dilaton potential to comprise two simple potentials, i.e., the exponential potential and the double-well potential, and have analyzed both the dynamics of the system and the thermal equilibrium condition at the initial stage of the universe. Even though we have mainly studied the evolution of the scale factor with same radii, there is no significant difference in the typical evolutions of different radii. Based on the solutions, we have examined whether they satisfy three basic assumptions, i.e., the adiabatic condition $H_0 \lesssim O(1)$, the weak coupling condition and the thermal equilibrium condition $\Gamma > H$. As a result, we find the following cases.

Exponential potential : $V = b\, e^{2a\phi}$

(i) $b > 0$: the convergent and rapidly growing solution

The convergent and the rapidly growing solutions for $a > 1$ are acceptable cases. The former case is that the radius converges to a constant value and the dilaton rolls monotonically to the weak coupling regime. In the latter case, both radius and dilaton asymptotically grow in short time. These different evolution is determined by whether the initial velocity of dilaton $\dot{\phi}_0$ is smaller or larger than the critical velocity $\dot{\phi}_C$. On the other hand, for $a \leq 1$, all numerical solutions are asymptotically the rapidly growing solutions. Both of two solutions satisfy the thermal equilibrium condition during some initial time.

(ii) $b < 0$: the convergent solution

In this case, the convergent solutions are sensible solutions since the others are contracting evolutions. For any value of a, all numerical solutions satisfy the thermal equilibrium condition during the initial time.

Double-well potential : $V = \frac{\lambda}{4}((\frac{\phi}{\eta})^2 - 1)^2$

(i) $\lambda > 0$ *: the rapidly growing solution*

For $\eta \gg 1$, all numerical solutions are rapidly growing solutions, and they satisfy the thermal equilibrium condition during some initial time which is relatively longer than the above cases.

(ii) $\lambda < 0$ *: the stabilized dilaton*

In this case, the dilaton is stabilized and it does hold the weak coupling condition. For any value of η, all numerical solutions are reduced to the stabilized dilaton solutions. If we choose $\eta \lesssim O(1)$, the thermal equilibrium continues unboundedly.

From these results, we conclude that it is possible to realize the thermal equilibrium of string gas at the initial Hagedorn regime. At the end of the paper, we would like to ask if the evolutions can be matched to a late-time universe. For the convergent solutions, the universe will not enter into the large-radius phase $R > \bar{R}$, because $\bar{R}$ does not become large without fine-tuning, as discussed above. Besides, the time scale of the thermal equilibrium will too short for the BV mechanism to work, compared with Hubble time. Similarly, for the rapidly growing solutions, the short time scale will be a problem for the exponential potential. However, for the double-well potential, the duration becomes relatively longer and the situation is better. Nevertheless, it remains as a problem that the dilaton asymptotes to the strong coupling, where we cannot predict what will happen.

On the other hand, the stabilized dilaton solutions can make the radius grow as $R \propto t$, and it would be possible to match it to a late-time universe. Moreover, the thermal equilibrium continues unboundedly. This solution is the best case among all examples presented in our paper. It implies that the (quasi-) stabilized dilaton at an early stage of the universe improves the situation. Besides, this example implies an interesting possibility for constructing a model that resolves the stabilization and dimensionality problem at the same time. It remains an interesting question whether we can build a model which can be embedded in string theory resolving all problems described above.

6.3.6 Appendix

1. **Effective potential**

In this Appendix we will show the effective potential of the dilaton in the Einstein frame derived by conformal transformation. We will use a conformal factor as Ω^2 that is a function of the D dimensional spacetime coordinates x^μ. The conformally transformed metric is $\tilde{g}_{\mu\nu} = \Omega^2 g_{\mu\nu}$, and the determinant of the metric scales as $\sqrt{-\tilde{g}} = \Omega^D \sqrt{-g}$ .. Consider the dilaton-gravity action in D dimensions,

$$S = \int d^D x \sqrt{|g|} e^{-2\phi} \Big[R + 4(\nabla\phi)^2 + V \Big] . \tag{6.68}$$

Under the conformal transformation, the action becomes [283]

$$S = \int d^D x \sqrt{|\tilde{g}|} e^{-2\phi} \Omega^{2-D} \Big[\tilde{R} + 4(\tilde{\nabla}\phi)^2 + (D-2)(D-1)\Omega^{-2}(\tilde{\nabla}\Omega)^2 + \Omega^{-2}V + 4(D-1)\Omega^{-1}(\tilde{\nabla}\Omega)(\tilde{\nabla}\phi) \Big] \tag{6.69}$$

The last term comes from integrations by parts. If we set the conformal factor as $\Omega^{2-D} = e^{2\phi}$, the action in the Einstein frame is

$$S = \int d^D x \sqrt{|\tilde{g}|} \left[\tilde{R} + 4\Big(1 - \frac{D-1}{D-2}\Big)(\tilde{\nabla}\phi)^2 + e^{\frac{4\phi}{D-2}} V \right] . \tag{6.70}$$

In the case $D = 10$ the Lagrangian of the dilaton which is minimally coupled to the metric in this frame, is reduced to

$$L_\phi = -\frac{1}{2}(\tilde{\nabla}\phi)^2 - W(\phi) , \tag{6.71}$$

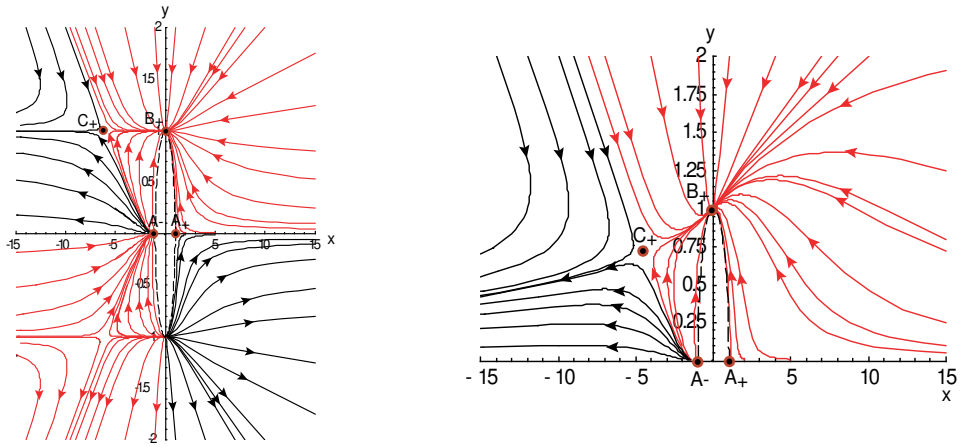

(a) $a = 2$ (b) $a = 3$

Figure 6.18: (a): The phase trajectories for $a = 2$ in (x, y) and (x, z) planes. There are four fixed points in the upper half-planes. B_+ is the attractor point for the rapidly growing solution. C_+ divides the convergent solution from the rapidly growing one. The red lines show the trajectories approaching the rapidly growing solutions, and the black lines show the trajectories approaching the convergent solutions. The arrows represent the direction of time evolution. The color of the lines indicates the end state of these solutions. (b): The phase trajectories for $a = 3$ in (x, y) and (x, z) planes. The four fixed points are the same as in Fig. 6.18(a).

with the canonically normalized potential

$$W(\phi) = -e^{\frac{\phi}{2}} V(\phi)\,. \tag{6.72}$$

2. Autonomous phase plane

In this Appendix, we describe the asymptotic behavior of the system with the exponential potential. We define the dimensionless phase-space variables [103, 10]

$$x \equiv \frac{2\dot{\phi} - 9H}{3H}, \quad y \equiv \frac{\sqrt{|V|}}{3H}, \quad z \equiv \frac{\sqrt{\rho} e^{\phi}}{3H}\,. \tag{6.73}$$

The Eqs. (6.50) are reduced to a so-called plane autonomous system, which consists of three evolution equations and a constraint equation,

$$\begin{aligned} x' &= \frac{3}{2}\left[1 - x^2 + (1-a)y^2 - 3axy^2\right], \quad y' = -\frac{3}{2} y\left[(2-a)x + 3ay^2 - 3a\right], \\ z' &= -\frac{3}{2} z(x + 3ay^2)\,, \qquad\qquad 1 = x^2 + y^2 - z^2\,. \end{aligned} \tag{6.74}$$

Here a prime denotes a derivative with respect to the number of e-foldings, $\ln(R) = \mu$. Since the system is invariant under changing as $y \to -y$ and $z \to -z$, we mainly consider only the upper half-planes, $y \geq 0$ and $z \geq 0$, in the following discussion [3]. We solve this system numerically to find the phase-trajectories. In Figs. 6.18(a) - 6.19(b), we show phase trajectories on the y-x and z-x planes for $a = 1/2,\ 1,\ 2,\ 3$. In this system, there are three types of fixed point (critical point), defined by $x' = 0, y' = 0, z' = 0$:

$$A_\pm \quad : \quad x = \pm 1, \quad y = 0, \quad z = 0\,,$$

[3] $y < 0$ corresponds to the contracting evolution ($\dot{\mu} < 0$), and the lines of phase-trajectory are the same as $y \geq 0$, except the direction of the arrow (Fig. 6.18(a)).

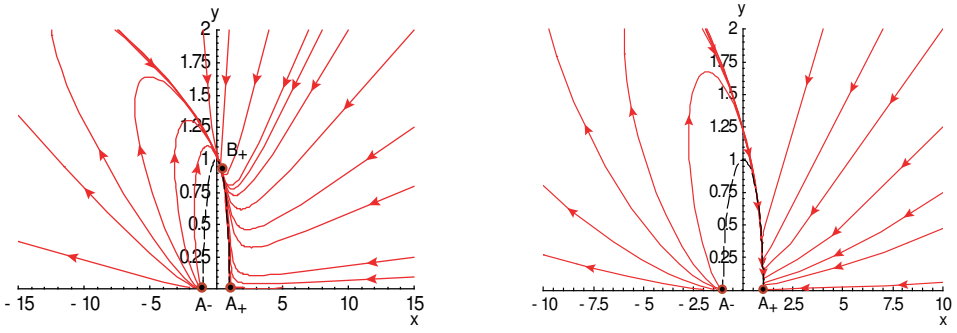

(a) $a = 1$ (b) $a = 0.5$

Figure 6.19: (a): The phase trajectories for $a = 1$ in (x, y) and (x, z) planes. A_+, A_- and B_+ are the fixed points. C_+ does not exist, contrary to the other cases, and hence there is no trajectory approaching convergent solutions. All trajectories approach B_+, and all these solutions are asymptotically rapidly growing solutions. (b): The phase trajectories for $a = 1/2$ in (x, y) and (x, z) planes. A_+, A_- are the fixed points. A_+ is an attractor point replaced by B_+ corresponding to the rapidly growing solutions. All trajectories approach A_+, and these solutions are asymptotically the rapidly growing solutions.

$$\begin{aligned} B_\pm \quad &: \quad x = \frac{2-a}{3a}, \quad y = \pm\frac{2\sqrt{2a^2+a-1}}{3a}, \quad z = 0\,, \\ C_\pm \quad &: \quad x = -\frac{3a}{a-1}, \quad y = \pm\frac{1}{\sqrt{a-1}}, \quad z = \pm\frac{\sqrt{8a^2+3a-2}}{a-1}\,. \end{aligned} \tag{6.75}$$

$C_\pm$ is vanishing for $0 < a \leq 1$, and $B_\pm$ is also vanishing for $0 < a \leq 1/2$. For $a \leq 1$, there are four fixed points A_+, A_-, B_+ and C_+ in the regime $y \geq 0$ and $z \geq 0$. For $1/2 < a \leq 1$, there are three fixed points, A_+, A_- and B_+. For $0 < a \leq 1/2$, A_+ and A_- are the fixed points. It can be understood from the global behaviors on the phase-space that $A_\pm$ may correspond to an unstable node (or saddle node). In the following we show that the critical point B_+ describes the rapidly growing solution of Eq. (6.56) and C_+ divides the convergent solution (6.52) from the rapidly growing one. In order to see the behavior of these solutions on the phase-space, we rewrite these solutions in terms of the phase-space variables (x, y, z). From Eqs. (6.56), the rapidly growing solution with $b = \pm 1$ at late times ($\dot{\mu} \to \infty$) gives

$$x = \frac{2\dot{\phi} - 9\dot{\mu}}{3\dot{\mu}} \propto \frac{1}{3}\,, \quad y = \frac{e^{a\phi}}{3\dot{\mu}} \propto 1/\cos\Big[aC_1(t - t_* + C_2)\Big]\,, \quad z = \frac{\sqrt{\rho}e^{\phi}}{3\dot{\mu}} = \frac{\sin\Big[aC_1(t - t_* + C_2)\Big]^{1-1/a}}{\cos\Big[aC_1(t - t_* + C_2)\Big]} \tag{6.76}$$

Therefore, for $a > 1$, x and y asymptote to finite values, while z goes to zero at the divergent point $aC_1(t - t_* + C_2) \sim \pi$, as seen in Eq. (6.58). The trajectories approach the attractor point B_+, which are plotted by the red lines in Figs. 6.18(a)-6.18(b). Similarly, all trajectories for $1/2 < a \leq 1$ approach the attractor point B_+ (Fig. 6.19(a)), while for $0 < a \leq 1/2$ the critical point A_+ plays a role of B_+ corresponding to the rapidly growing solution (Fig. 6.19(b)). On the other hand, the behavior of the convergent solution at late times, when the (shifted) dilaton decreases to the negative infinity, $\psi(= 2\phi - 9\mu) \to -\infty$, follows from Eq. (6.52):

$$x = \frac{\dot{\psi}}{3\dot{\mu}} \propto -\frac{E_0}{2}(t - t_*) - B\,, \quad y = \frac{e^{a\phi}}{3\dot{\mu}} \propto e^{(\frac{a}{2}-1)\psi}\,, \quad z = \frac{\sqrt{\rho}e^{\phi}}{3\dot{\mu}} = e^{-\frac{\psi}{2}}\,. \tag{6.77}$$

Therefore, $x \to -\infty$ and $z \to \infty$ for $a \geq 2$, while y goes to a finite value at late times. In Figs. 6.18(a)-6.18(b), the trajectories that approach asymptotically the convergent solution are plotted by the black

lines. From these figures for $a > 1$, we see two types of asymptotic trajectory: the trajectory approaching B_+ which represents the rapidly growing solution and the one approaching the convergent solution ($|x|, |z| \to \infty$). These two types of trajectory are clearly divided by flows around the fixed point C_+. For $0 < a \leq 1$, all trajectories approach the rapidly growing solution because the fixed point C_+ disappear as shown in Figs. 6.19(a) and 6.19(b). From these figures, for $a > 1$, we can estimate the critical line which divides the rapidly growing solution from the convergent one in the phase-plane (x, y). The critical line is approximated by the straight line passing through A_- and C_+

$$y \simeq -\frac{\sqrt{a-1}}{2a+1}(x+1)\,. \quad (y \geq 0)\,. \tag{6.78}$$

Therefore, the trajectories that asymptote to the convergent solution are given by

$$y \lesssim -\frac{\sqrt{a-1}}{2a+1}(x+1), \tag{6.79}$$

while the trajectories that asymptote to the rapidly growing solution are characterized by the opposite inequality sign. This condition can be rewritten in terms of the initial dilaton and spacetime variables. Assuming $\phi_0 \simeq 0$, the condition for the convergent solution is

$$\dot{\phi}_0 \lesssim 3\dot{\mu}_0 - \frac{2a+1}{2\sqrt{a-1}}, \tag{6.80}$$

which is applicable for the expanding case $\dot{\mu}_0 > 0$ ($y > 0$). In our numerical analysis, we vary the initial velocity of the dilaton, fixing other initial conditions. From the above equation, the critical velocity for the initially expanding case that divides the late-time evolutions is approximately given by

$$\dot{\varphi}_C \sim 3\dot{\mu}_0 - \frac{2a+1}{2\sqrt{a-1}}\,. \tag{6.81}$$

Any velocity lower than the critical velocity yields the convergent solution, while any velocity beyond the critical one yields the rapidly growing one. The analytic estimation (6.81) is in good agreement with the critical velocity $\dot{\phi}_C$ obtained from the numerical analysis. For example, we find $\dot{\phi}_C/\dot{\varphi}_C \sim 0.88$ for $\dot{\mu}_0 = 0.2$ and $\dot{\phi}_C/\dot{\varphi}_C \sim 1.3$ for $\dot{\mu}_0 = 0.5$, based on our numerical simulation for $a = 2$. For the contracting case $y < 0$, the trajectories asymptoting to the convergent solutions are obtained from Fig. 6.18(a):

$$x \gtrsim 0. \quad (y < 0)\,. \tag{6.82}$$

The condition required for the convergent solution is $2\dot{\phi}_0 \lesssim 9\dot{\mu}_0$, and then the critical velocity $\dot{\varphi}_C$ for $\dot{\mu}_0 < 0$ is

$$\dot{\varphi}_C \sim 9/2\dot{\mu}_0. \tag{6.83}$$

Chapter 7

Conclusions

We will conclude this thesis. It is known from the modern accurate observations, surprising us greatly, that the current universe is mainly about 90 percents fulfilled with the unknown dark components: dark energy and dark matter. The recent WMAP observational data tells us the universe is made of dark energy (74%), dark matter (22%), and ordinary matter (4%) such as baryon. The modern universe not only needs the dark components but also inflation leading to early accelerating expansion. These unknown components of the universe may be not independent of the unified theory of all forces existing in nature. For the recent studies of the unified theory, one of most promising approaches is a superstring theory, or M-theory, considered as a quantization of fields including gravitational interaction. The cosmological implications of string theory are recent paid more attention to, that is the so-called *string cosmology*. It has been partly based on by the basic idea of string theory and corresponding brane-world. The goal of string cosmology is to give a new answer to the cosmological unresolved questions such as what are the origin of dark energy and dark matter? String theory has a much richer set of fundamental degree of freedom, consisting of D-branes. This fundamental objects, D-branes denote non–perturbative effects of string theory as "soliton" of strings, while string theory has been only described in perturbative form. Inspired by such speculation, recently a new paradigm on the early universe has been proposed, the so-called brane-world. The existence of models with more than one brane suggests that branes may collide. Colliding branes would be a fundamental phenomena in the string cosmology. *We have studied several applications of colliding branes to string cosmology.*

First, we have estimated a reheating temperature by collision, which is relate to the ekpyrotic universe scenario (Sec. 5.2). We introduced scalar field coupled with domain walls denoting branes and this work would provide a new reheating mechanism. For simplify, in the case of Minkowski spacetime, we have calculated a quantum particle creation and estimated the reheating temperature as $T_{\rm R} \approx 0.88\ \bar{g}\ N_b^{1/4}$, where g and N_b denote the coupling constant and the number of bounces. It can provide an efficient value of reheating temperature to have the baryogenesis at the electro-weak energy scale. Moreover we have considered a standard particles (fermions) which is confined on such domain walls (Sec. 5.3). We have studied the behaviour of five-dimensional fermions localized on branes, when two parallel branes collide in a five-dimensional Minkowski background spacetime. We found that most fermions are localized on both branes as a whole even after collision. However, how much fermions are localized on which brane depends sensitively on the incident velocity and the coupling constants unless the fermions exist on both branes. This work is a first step. Since we have discussed only the case of zero-momentum fermion on branes ($\vec{k} = 0$), we have only a single state on each brane, which constrains the fermion number to be less than unity. If we take into account degree of freedom of low energy fermions, we can put different states of fermions on each brane. This is future work and we expect it to resolve baryon and anti-baryon antisymmetry, $\Delta n_{\rm b}/s \sim 10^{-10}$. In the case of collision of two vacuum branes, nothing happens in the present approximation, however, the pair production of fermion and antifermion, for which we have to take into account the momentum k, may also occur at collision. This pair production process may also be important future work. Based on Sec. 6.1, including self-gravity, we studied collision of two domain

walls in 5-dimensional asymptotically Anti de Sitter spacetime. We have evaluated a dynamics of 5D scalar field as the domain wall with self-gravity and investigated how a negative cosmological constant in the bulk changes the result shown in Minkowski background. As a result, for small value of gravitational effect, the collision process is the same as Minkowski case, but for large case, it becomes an unstable oscillation and then the singularity appears after collision. Hence the appearance of singularity in the present model could be understandable because we take into account a gravitational effect in collision of two domain walls. In the time evolution of our universe, we find that the universe first expands a little just before collision and then contracts just after collision. We cannot explain our hot big bang universe as it is. However, we have found a possibility to formation of higher dimensional black holes by colliding branes (Sec. 6.2). Finally, for the topic of dimensionality problem, based on Sec. 6.3, we have studied a thermal equilibrium of string gas at Hagedorn temperature. In this work, we found a solution, which implies that the (quasi-) stabilized dilaton at an early stage of the universe improves the situation. Besides, this example has implied an interesting possibility for constructing a model that resolves the stabilization and dimensionality problem at the same time.

Acknowledgments

I would like to be grateful to my supervisor, Kei-ichi Maeda for useful suggestions, discussions and great collaborations. He gave me an expert guidance throughout my master and PhD course. It is my pleasure to thank Gary W. Gibbons and Hideaki Kudoh for fruitful collaborations and great helpfulness. I also would like to thank my examiners Ichiro Ohba, Tsuneaki Daishido and Shoichi Yamada for their helpful comments.

Also, Takahiko Matsubara, Yasushi Sudo and Naoshi Sugiyama, encouraged me in study of cosmology, by giving their short term lectures, valuable lecture notes and books, which I have used as references in the thesis. I am also grateful to Antonio De Felice, Minoru Eto, Antonino Flachi, Gary T. Horowitz, Tsutomu Kobayashi, Lev Kofman, Johannes Martin, Shuntaro Mizuno, Shinji Mukohyama, Masato Nozawa, Marco Peloso, Valery Rubakov, Shun Saito, Tetsuya Shiromizu, Makoto Tanabe, Takashi Torii, David Wands and Jun'ichi Yokoyama for useful discussions, comments and advices.

Thanks to Satoshi Kitagawa and Yuko Urakawa for valuable discussions in a seminar of studying cosmology (Mukhanov's text book). Also thanks to the colleagues at Waseda University, especially to Kenta Kiuchi, Hidefumi Nomura, Masato Nozawa, Makoto Tanabe and Yuko Urakawa, as well as the members at Maeda and Yamada laboratory, whose combined help and friendship give me an enjoyable place to study my work through enjoyable conversations and lots of drinks. My endless thanks are extended to my family and friends for their continued love, support and encouragement.

This work was supported by JSPS (17-53192) and Grants-in-Aid for the 21st Century COE Program at Waseda University, which are also gratefully acknowledged. With their support, I could visit many countries for discussions and presentations. Especially, I thank Kazuya Koyama and David Wands during my visit at the Institute of Cosmology and Gravitation (ICG), Antonio De Felice for the hospitality at University of Sussex, Hideaki Kudoh and Gary T. Horowitz for the hospitality at the department of Physics at University of California, Santa Barbara, as well as the members at there, especially, Jim Cresswell, Elisabetta Majerotto and Mehri Torki in ICG.

I deeply grateful to my parents, grandparents, my friends and a pleasant environment, *Ikebukuro* and *Kaname-cho!* Finally, after I have done this thesis, I took an enjoyable trip in Kanazawa and Noto, in which many thanks to many people and nice places to give me lots of treasures.

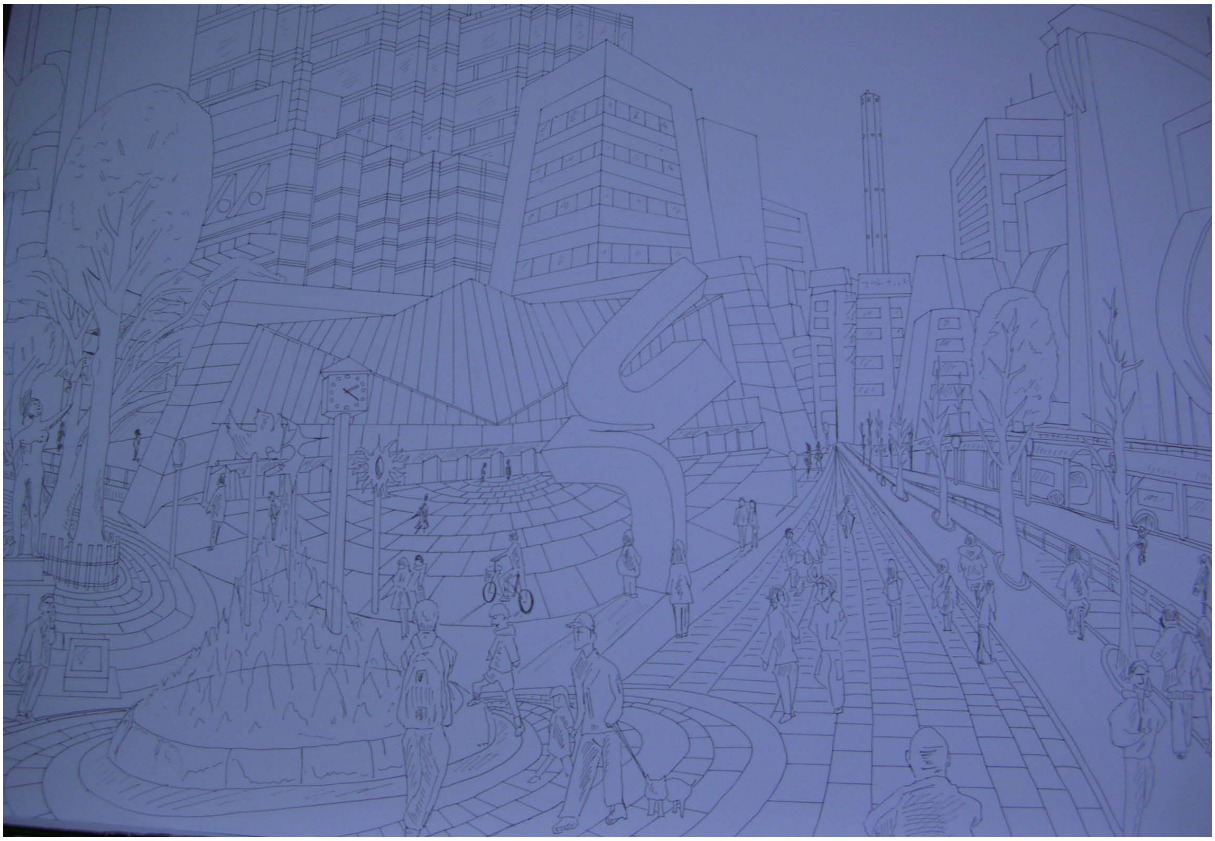

Figure 7.1: *My illustration of Ikebukuro West Gate Park in April, 2007.*

I know for sure that life is beautiful around the world.
Many thanks to everyone, everything and environment around me.
Want anything, and then he gives me a chance I could get!
Yu-ichi

Bibliography

[1] L. F. Abbott, E. Fahri and M. Wise Phys. Lett. B **117**, 29 (1982).

[2] V. Acquaviva, N. Bartolo, S. Matarrese and A. Riotto, Nucl. Phys. B **667**, 119 (2003).

[3] E. G. Adelberger, B. R. Heckel and A. E. Nelson, Ann. Rev. Nucl. Part. Sci. **53** 77 (2003) [hep-ph/0307284].

[4] I. Affleck and M. Dine, Nucl. Phys. B **249**, 361 (1985).

[5] Y. Aghababaie, C. P. Burgess, S. L. Parameswaran and F. Quevedo, Nucl. Phys. B **680**, 389 (2004).

[6] K. Akama, Lect. Notes Phys. **176**, 267 (1982) [hep-th/0001113].

[7] A. Albrecht and P. J. Steinhardt, Phys. Rev. Lett. **48**, 1220 (1982).

[8] G. Aldering [SNAP Collaboration], "Future Research Direction and Visions for Astronomy", Alan M. Dressler, editor, Proceedings of the SPIE, Volume 4835, pp. 146-157 [astro-ph/0209550].

[9] S. Alexander, R. H. Brandenberger and D. Easson, Phys. Rev. D **62**, 103509 (2000) [hep-th/0005212].

[10] L. E. Allen and D. Wands, Phys. Rev. D **70**, 063515 (2004) [astro-ph/0404441].

[11] R. A. Alpher, H. Bethe and G. Gamow, Phys. Rev. **73**, 803 (1948).

[12] P. Anninos, S. Oliveira and R. A. Matzner, Phys. Rev. D **44**, 1147 (1991).

[13] N. D. Antunes, E. J. Copeland, M. Hindmarsh and A. Lukas, Phys. Rev. D **68**, 066005 (2003) [hep-th/0208219];
N. D. Antunes, E. J. Copeland, M. Hindmarsh and A. Lukas, *ibid.* D **69**, 065016 (2004) [hep-th/0310103].

[14] M. Arai, S. Fujita, M. Naganuma, and N. Sakai, Phys. Lett. B **556**, 192 (2003) `[hep-th/0212175]`.

[15] S. Arapoglu, and A. Kaya, 2004, Phys. Lett. B **603**, 107.

[16] N. Arkani-Hamed, S. Dimopoulos and G. R. Dvali, Phys. Lett. B **429**, 263 (1998) [hep-ph/9803315];
N. Arkani-Hamed, S. Dimopoulos and G. R. Dvali, Phys. Rev. D **59**, 086004 (1999) [hep-ph/9807344].

[17] N. Arkani-Hamed, S. Dimopoulos, N. Kaloper, and R. Sundrum, Phys. Lett. B **480**, 193 (2000).

[18] N. Arkani-Hamed, P. Creminelli, S. Mukohyama and M. Zaldarriaga, JCAP **0404**, 001 (2004).

[19] C. Armendariz-Picon, T. Damour and V. Mukhanov, Phys. Lett. B **458**, 209 (1999).

[20] C. Armendáriz-Picón, V. Mukhanov, and P. J. Steinhardt, Phys. Rev. Lett. **85**, 4438 (2000).

[21] C. Armendáriz-Picón, V. Mukhanov, and P. J. Steinhardt, Phys. Rev. D **63**, 103510 (2001).

[22] J. Baacke, K. Heitmann and C. Patzold, Phys. Rev. D **56**, 6556 (1997).

[23] N. A. Bahcall, J. P. Ostriker, S. Perlmutter and P. J. Steinhardt, Science **284**, 1481 (1999).

[24] D. Bailin and A. A. Love, *Supersymmetric Gauge field theory and String theory*, Institute of Physics Publisghing, Boston and New York (1994).

[25] B. Bajc and G. Gabadadze, Phys. Lett. B **474** (2000) 282 [hep-th/9912232].

[26] T. Banks and W. Fischler, arXiv:hep-th/9906038.

[27] J. M. Bardeen, Phys. Rev. D **22**, 1882 (1980).

[28] J. M. Bardeen, P. J. Steinhardt and M. S. Turner, Phys. Rev. D **28**, 679 (1983).

[29] J. M. Bardeen, J. R. Bond, N. Kaiser, and A. S. Szalay, Astrophys. J. **304**, 15 (1986).

[30] J. M. Bardeen, *Lectures given at 2nd Guo Shou-jing Summer School on Particle Physics and Cosmology, Nanjing, China, Jul 1988.*

[31] V. Barger, H. S. Lee and D. Marfatia, Phys. Lett. B **565**, 33 (2003) [hep-ph/0302150].

[32] J. D. Barrow and F. J. Tipler, *The Anthropic Cosmological Principle* (Clarendon Press, Oxford, 1986).

[33] J. D. Barrow and R. Maartens, Phys. Lett. B **532**, 153 (2002) [gr-qc/0108073].

[34] N. Bartolo, E. Komatsu, S. Matarrese and A. Riotto, Phys. Rept. **402**, 103 (2004).

[35] B. A. Bassett, M. Borunda, M. Serone and S. Tsujikawa, Phys. Rev. D **67**, 123506 (2003) [hep-th/0301180].

[36] B. A. Bassett, S. Tsujikawa and D. Wands, Rev. Mod. Phys. **78**, 537 (2006) [astro-ph/0507632].

[37] T. J. Battefeld and G. Geshnizjani, Phys. Rev. D **73**, 064013 (2006) [hep-th/0503160];
T. J. Battefeld, S. P. Patil and R. H. Brandenberger, Phys. Rev. D **73**, 086002 (2006) [hep-th/0509043].

[38] T. J. Battefeld and S. Watson, Rev. Mod. Phys. **78**, 435 (2006) [hep-th/0510022].

[39] T. I. Belova and A. E. Kudryavtsev, Physica D **32**, 18 (1988).

[40] C. L. Bennett *et al.*, Astrophys. J. **464**, L1 (1996) [astro-ph/9601067].

[41] C. L. Bennett *et al.* [WMAP Collaboration], Astrophys. J. Suppl. **148**, 1 (2003) [astro-ph/0302207].

[42] M. C. Bento and O. Bertolami, Phys. Lett. B **228**, 348 (1989).

[43] E. A. Bergshoeff et al., JHEP **0005**, 009 (2000).

[44] A. J. Berndsen and J. M. Cline, Int. J. Mod. Phys. A **19**, 5311 (2004) [hep-th/0408185].

[45] A. Berndsen, T. Biswas and J. M. Cline, JCAP **0508**, 012 (2005) [hep-th/0505151].

[46] P. Binétruy, C. Deffayet, and Langlois, Nucl. Phys.**565**, 269 (2000) [hep-th/9905012].

[47] P. Binétruy, C. Deffayet, U. Ellwanger and D. Langlois, Phys. Lett. B **477**, 285 (2000) [hep-th/9910219].

[48] N. D. Birrell and P. C. W. Davies, *Quantum Fields In Curved Space* (Cambridge University Press, Cambridge, England, 1982).

[49] T. Biswas, 2004, JHEP **02**, 039.

[50] J. J. Blanco-Pillado *et al.*, JHEP **0609**, 002 (2006) [hep-th/0603129].

[51] S. Blau and A. Guth, *inflationary Cosmology*, in '300 Years of Gravitation' ed. by S. Hawking and W. Israel (Cambridge Univ. Press, Cambridge, 1987).

[52] E. B. Bogomol'nyi, Sov. J. Nucl. Phys. **24**, 449 (1976); M. K. Prasad and C. M. Sommerfield, Phys. Rev. Lett. **35**, 760 (1975).

[53] BOOMERanG, home page: http://cmb.phys.cwru.edu/boomerang/

[54] M. Borunda and L. Boubekeur, JCAP **0610**, 002 (2006) [hep-th/0604085].

[55] R. Bousso and J. Polchinski, JHEP **0006**, 006 (2000).

[56] D. Boyanovsky, H. J. de Vega, R. Holman and J. F. J. Salgado, Phys. Rev. D **54**, 7570 (1996).

[57] D. Boyanovsky, D. Cormier, H. J. de Vega, R. Holman, A. Singh and M. Srednicki, Phys. Rev. D **56**, 1939 (1997).

[58] V. Bozza, M. Gasperini, M. Giovannini and G. Veneziano, Phys. Rev. D **67**, 063514 (2003).

[59] V. Bozza and G. Veneziano, JCAP **0509**, 007 (2005) [gr-qc/0506040].

[60] R. H. Brandenberger, R. Kahn and W. H. Press, Phys. Rev. D **28**, 1809 (1983).

[61] R. H. Brandenberger, Nucl. Phys. B **245**, 328 (1984).

[62] R. H. Brandenberger, Rev. Mod. Phys. **57**, 1 (1985).

[63] R. H. Brandenberger and C. T. Hill, Phys. Lett. B **179**, 30 (1986).

[64] R. H. Brandenberger and C. Vafa, Nucl. Phys. B **316**, 391 (1989).

[65] R. H. Brandenberger and F. Finelli, JHEP **0111**, 056 (2001) [hep-th/0109004].

[66] R. H. Brandenberger, arXiv:hep-th/0509099.

[67] R. H. Brandenberger, Prog. Theor. Phys. Suppl. **163**, 358 (2006) [hep-th/0509159].

[68] R. H. Brandenberger, Y. K. Cheung and S. Watson, JHEP **0605**, 025 (2006) [hep-th/0501032].

[69] R. H. Brandenberger *et al.*, JCAP **0611**, 009 (2006) [hep-th/0608186].

[70] J. D. Bratt, A. C. Gault, R. J. Scherrer and T. P. Walker, Phys. Lett. B **546**, 19 (2002) [astro-ph/0208133].

[71] P. Brax and C. van de Bruck, Class. Quant. Grav. **20**, R201 (2003) [hep-th/0303095];
P. Brax, C. van de Bruck and A. C. Davis, [hep-th/0404011].

[72] J. D. Brown and C. Teitelboim, Phys. Lett. B **195** (1987) 177;
J. D. Brown and C. Teitelboim, Nucl. Phys. B **297**, 787 (1988).

[73] R. Brustein and P. J. Steinhardt, Phys. Lett. B **302**, 196 (1993) [hep-th/9212049].

[74] R. Brustein, M. Gasperini, M. Giovannini, V. F. Mukhanov and G. Veneziano, Phys. Rev. D **51**, 6744 (1995).

[75] R. Brustein and R. Madden, Phys. Rev. D **57**, 712 (1998).

[76] R. Brustein and M. Hadad, Phys. Rev. Lett. **82**, 3016 (1999) [hep-ph/9810526].

[77] E. I. Buchbinder, J. Khoury and B. A. Ovrut, arXiv:hep-th/0702154.

[78] E. F. Bunn, A. R. Liddle and M. J. White, Phys. Rev. D **54**, 5917 (1996).

[79] C. P. Burgess, P. Martineau, F. Quevedo, G. Rajesh and R. J. Zhang, JHEP **0203**, 052 (2002) [hep-th/0111025].

[80] C. P. Burgess, R. Kallosh and F. Quevedo, JHEP **0310**, 056 (2003).

[81] G. Calcagni, JCAP **0311**, 009 (2003) [hep-ph/0310304].

[82] G. Calcagni, S. Tsujikawa and M. Sami, Class. Quant. Grav. **22**, 3977 (2005) [hep-th/0505193].

[83] R. R. Caldwell, R. Dave and P. J. Steinhardt, Phys. Rev. Lett. **80**, 1582 (1998).

[84] J. Callan, G. Curtis, E. J. Martinec, M. J. Perry, and D. Friedan, 1985, Nucl. Phys. B **262**, 593.

[85] D. K. Campbell, J. F. Schonfeld and C. A. Wingate, Physica **9D**, 1 (1983).

[86] A. Campos and C. F. Sopuerta, D **63**, 104012 (2001) [hep-th/0101060];
A. Campos and C. F. Sopuerta, Phys. Rev. D **64**, 104011 (2001) [hep-th/0105100].

[87] A. Campos, Phys. Rev. D **71**, 083510 (2005) [hep-th/0501092].

[88] A. Capolupo, S. Capozziello and G. Vitiello, arXiv:0705.0319 [hep-th].

[89] C. Cartier, E. J. Copeland and R. Madden, JHEP **0001**, 035 (2000).

[90] C. Cartier, J. c. Hwang and E. J. Copeland, Phys. Rev. D **64**, 103504 (2001).

[91] C. Cartier, R. Durrer and E. J. Copeland, Phys. Rev. D **67**, 103517 (2003).

[92] CERN, website: http://public.web.cern.ch/Public/Welcome.html

[93] CFHTLS, home page: http://www.cfht.hawaii.edu/

[94] W. Chen, Z.-W. Chong, G.W. Gibbons, H. Lu, C.N. Pope, Nucl. Phys. B **732**, 118 (2006) [hep-th/0502077].

[95] T. Chiba, T. Okabe and M. Yamaguchi, Phys. Rev. D **62**, 023511 (2000).

[96] T. R. Choudhury and T. Padmanabhan, Astron. Astrophys. **429**, 807 (2005).

[97] J.M. Cline, H. Firouzjahi and P. Martineau, JHEP **0211**, 041 (2002); N. Barnaby and J. M. Cline, Phys. Rev. D **70**, 023506 (2004) [hep-th/0403223].

[98] S. R. Coleman, Nucl. Phys. B **310**, 643 (1988).

[99] P. Coles and F. Lucchin, *Cosmology, The origin and evolution of cosmic structure*, Wiley.

[100] M. Colless et al. [The 2DFGRS Collaboration], Mon. Not. Roy. Astron. Soc. **328**, 1039 (2001) [arXiv:astro-ph/0106498] and see the website: http://magnum.anu.edu.au/ TDFgg/

[101] A. Conley et al. [Supernova Cosmology Collaboration], Astrophys. J. **644**, 1 (2006) [astro-ph/0602411].

[102] E. J. Copeland, A. R. Liddle, D. H. Lyth, E. D. Stewart and D. Wands, Phys. Rev. D **49**, 6410 (1994) [astro-ph/9401011].

[103] E. J. Copeland, A. R. Liddle and D. Wands, Phys. Rev. D **57**, 4686 (1998) [gr-qc/9711068].

[104] E. J. Copeland, A. R. Liddle and J. E. Lidsey, Phys. Rev. D **64**, 023509 (2001) [astro-ph/0006421].

[105] E. J. Copeland, M. Sami and S. Tsujikawa, Int. J. Mod. Phys. D **15**, 1753 (2006) [hep-th/0603057].

[106] D. Cremades, F. Quevedo and A. Sinha, JHEP **0510**, 106 (2005) [hep-th/0505252].

[107] P. Creminelli, A. Nicolis and M. Zaldarriaga, Phys. Rev. D **71**, 063505 (2005) [hep-th/0411270].

[108] P. Creminelli and L. Senatore, [hep-th/0702165].

[109] R. G. Crittenden and N. Turok, Phys. Rev. Lett. **76**, 575 (1996).

[110] C. Csaki, M. Graesser, C. Kolda and J. Terning Phys. Lett. B **462**, 34 (1999).

[111] R. A. Daly and E. J. Guerra, Astron. J. **124**, 1831 (2002).

[112] R. A. Daly and S. G. Djorgovski, Astrophys. J. **597**, 9 (2003).

[113] R. Danos, A. R. Frey and A. Mazumdar, Phys. Rev. D **70**, 106010 (2004) [hep-th/0409162].

[114] K. Dasgupta, G. Rajesh and S. Sethi, JHEP **0008**, 023 (1999).

[115] K. Dasgupta, C. Herdeiro, S. Hirano, and R. Kallosh, Phys. Rev. D **65**, 126002 (2002) [hep-th/0203019].

[116] C. Deffayet, G. R. Dvali and G. Gabadadze, Phys. Rev. D **65**, 044023 (2002) [astro-ph/0105068].

[117] N. Deo, S. Jain and C. I. Tan, Phys. Lett. B **220**, 125 (1989).

[118] N. Deo, S. Jain and C. I. Tan, Phys. Rev. D **40**, 2626 (1989).

[119] N. Deo, S. Jain, and C.-I. Tan, Phys. Rev. D **45**, 3641 (1992).

[120] N. Deruelle and V. F. Mukhanov, Phys. Rev. D **52**, 5549 (1995).

[121] M. Dine, Phys. Lett. B **482**, 213 (2000) [hep-th/0002047].

[122] S. Dodelson, W. H. Kinney and E. W. Kolb, Phys. Rev. D **56**, 3207 (1997) [astro-ph/9702166].

[123] S. Dodelson, *Modern cosmology*, Academic Press (2003).

[124] A. D. Dolgov, *The very early universe*, eds. by G. W. Gibbons and S. T. Siklos (Cambridge, UK, 1982).

[125] A. D. Dolgov and A. D. Linde, Phys. Lett. B **116**, 329 (1982).

[126] A. D. Dolgov and D. P. Kirilova, Sov. J. Nucl. Phys., **51**, 172 (1990).

[127] S. L. Dubovsky, V. A. Rubakov, and P. G. Tinyakov, Phys. Rev. D **62** (2000) 105011 [hep-th/0006046].

[128] R. Durrer, Fund. Cosmic Phys. **15**, 209 (1994) [astro-ph/9311041].

[129] R. Durrer, M. Kunz and M. Sakellariadou, Phys. Lett. B **614**, 125 (2005) [hep-th/0501163].

[130] G. Dvali and S.-H.H. Tye, Phys. Lett. B **450** (1999) 72 [hep-ph/9812483].

[131] G. R. Dvali, G. Gabadadze and M. Porrati, Phys. Lett. B **485**, 208 (2000).

[132] G. Dvali, Q. Shafi and S.Solganik, arXiv:hep-th/0105203.

[133] G. Dvali and A. Vilenkin, Phys. Rev. D **67**, 046002 (2003).

[134] D. A. Easson, Int. J. Mod. Phys. A **18**, 4295 (2003) [hep-th/0110225].

[135] R. Easther, B. R. Greene and M. G. Jackson, Phys. Rev. D **66**, 023502 (2002) [hep-th/0204099];
R. Easther, B. R. Greene, M. G. Jackson and D. Kabat, Phys. Rev. D **67**, 123501 (2003) [hep-th/0211124];
R. Easther, B. R. Greene, M. G. Jackson and D. Kabat, JCAP **0401**, 006 (2004) [hep-th/0307233].

[136] R. Easther, B. R. Greene, M. G. Jackson and D. Kabat, JCAP **0502**, 009 (2005) [hep-th/0409121].

[137] G. Efstathiou, W. J. Sutherland and S. J. Maddox, Nature **348**, 705 (1990).

[138] D. J. Eisenstein *et al.* [SDSS Collaboration], Astrophys. J. **633**, 560 (2005) [astro-ph/0501171].

[139] O. Elgaroy, et al., Phys. Rev. Lett. **90**, 021802 [hep-ph/0204152].

[140] J. R. Ellis, J. S. Hagelin, D. V. Nanopoulos, K A. Olive and M. Srednicki, Nucl. Phys. B **238** 453 (1984).

[141] G. F. R. Ellis and M. Bruni, Phys. Rev. D **40**, 1804 (1989);
G. F. R. Ellis, J. Hwang and M. Bruni, Phys. Rev. D **40** 1819 (1989).

[142] J. R. Ellis, N. Kaloper, K. A. Olive and J. Yokoyama, Phys. Rev. D **59**, 103503 (1999).

[143] J. R. Ellis, Prog. Theor. Phys. Suppl. **152**, 108 (2004) [astro-ph/0304183].

[144] J. K. Erickson, S. Gratton, P. J. Steinhardt and N. Turok, [hep-th/0607164].

[145] M. Eto and N. Sakai, Phys. Rev. D **68**, 125001 (2003) [hep-th/0307276];
M. Eto, S. Fujita, M. Naganuma and N. Sakai, Phys. Rev. D **69**, 025007 (2004).

[146] M. Fairbairn and M. H. G. Tytgat, Phys. Lett. B **546**, 1 (2002).

[147] A. Feinstein, Phys. Rev. D **66**, 063511 (2002).

[148] G. N. Felder, L. Kofman and A. D. Linde, Phys. Rev. D **59**, 123523 (1999) [hep-ph/9812289].

[149] G. N. Felder, L. Kofman and A. D. Linde, Phys. Rev. D **60**, 103505 (1999) [hep-ph/9903350].

[150] J. L. Feng, J. March-Russell, S. Sethi and F. Wilczek, Nucl. Phys. B **602**, 307 (2001).

[151] F. Finelli and R. Brandenberger, Phys. Rev. D **65**, 103522 (2002) [hep-th/0112249].

[152] A. Flachi, O. Pujolas, M. Sasaki and T. Tanaka, Phys. Rev. D **74**, 045013 (2006) [hep-th/0604139];
A. Flachi and T. Tanaka, Phys. Rev. Lett. **95**, 161302 (2005) [hep-th/0506145].

[153] S. Foffa, M. Maggiore and R. Sturani, Nucl. Phys. B **552**, 395 (1999).

[154] L. H. Ford, Phys. Rev. D **35**, 2955 (1987).

[155] E. S. Fradkin and A. A. Tseytlin, Phys. Lett. B **158**, 316 (1985).

[156] E. S. Fradkin and A. A. Tseytlin, Nucl. Phys. **261**, 1 (1985).

[157] P. Fre, M. Trigiante and A. Van Proeyen, Class. Quant. Grav. **19**, 4167 (2002).

[158] W. L. Freedman *et al.*, Astrophys. J. **553**, 47 (2001) [astro-ph/0012376].

[159] K. Freese, J. A. Frieman and A. V. Olinto, Phys. Rev. Lett. **65**, 3233 (1990).

[160] A. V. Frolov and L. Kofman, arXiv:hep-th/0209133.

[161] V. P. Frolov, M. Snajdr and D. Stojkovic, Phys. Rev. D **68**, 044002 (2003) [gr-qc/0304083].
A. V. Frolov and U.-L. Pen, Phys. Rev. D **68**, 124024 (2003) [gr-qc/0307081].

[162] A. V. Frolov, Phys. Rev. D **70**, 104023 (2004) [hep-th/0409117].

[163] M. Fukugita and T. Yanagida, Phys. Lett. B **174**, 45 (1986).

[164] G. Gabadadze, arXiv:hep-ph/0308112.

[165] G. Gamow, Phys. Rev. **70**, 572 (1946).

[166] G. Gamow, Phys. Rev. **71**, 273 (1947).

[167] J. Garcia-Bellido, A. D. Linde and D. Wands, Phys. Rev. D **54**, 6040 (1996).

[168] M. R. Garousi, Nucl. Phys. B **584**, 284 (2000); Nucl. Phys. B **647**, 117 (2002); JHEP **0305**, 058 (2003).

[169] J. Garriga and A. Vilenkin, Phys. Rev. D **61**, 083502 (2000).

[170] J. Garriga and T. Tanaka, Phys. Rev. Lett. **84**, 2778 (2000) [hep-th/9911055].

[171] J. Garriga, M. Livio and A. Vilenkin, Phys. Rev. D **61**, 023503 (2000).

[172] J. Garriga and A. Vilenkin, Phys. Rev. D **67**, 043503 (2003).

[173] J. Garriga, A. Linde and A. Vilenkin, Phys. Rev. D **69**, 063521 (2004).

[174] M. Gasperini and G. Veneziano, Astropart. Phys. **1**, 317 (1993) [hep-th/9211021].

[175] M. Gasperini, M. Maggiore and G. Veneziano, Nucl. Phys. B **494**, 315 (1997).

[176] M. Gasperini and G. Veneziano, Phys. Rept. **373** [hep-th/0207130].

[177] M. Gasperini, M. Giovannini and G. Veneziano, Phys. Lett. B **569**, 113 (2003).

[178] M. Gasperini, M. Giovannini and G. Veneziano, Nucl. Phys. B **694**, 206 (2004).

[179] T. Gherghetta and A. Pomarol, Nucl. Phys. B **586** (2000) 141 [hep-ph/0003129].

[180] G.W. Gibbons, *Aspects of Supergravity Theories*, in *Supersymmetry, Supergravity, and Related Topics*, eds. F. del Aguila, J.A. de Azcárraga and L.E. Ibañez (World Scientific 1985) pp. 346-351.

[181] G.W. Gibbons, D.L. Wiltshire, Nucl. Phys. B **287**, 717 (1987) [hep-th/0109093].

[182] G.W. Gibbons, Phys. Lett. B **537**, 1 (2002).

[183] G.W. Gibbons, H. Lu, C.N. Pope, Phys. Rev. Lett. **94**, 131602 (2005) [hep-th/0501117].

[184] G.W. Gibbons, K. Maeda and Y. Takamizu, Phys. Lett. B **647**, 1 (2007) [hep-th/0610286].

[185] S. Giddings, S. Kachru and J. Polchinski, Phys. Rev. D **66**, 106006 (2002).

[186] Y. G. Gong, Class. Quant. Grav. **22**, 2121 (2005).

[187] C. Gordon and R. Maartens, D **63**, 044022 (2001) [hep-th/0009010].

[188] C. Gordon and N. Turok, Phys. Rev. D **67**, 123508 (2003) [hep-th/0206138].

[189] M. B. Green, J. H. Schwarz, and E. Witten, *Superstring Theory*, in 2 vols., (Cambridge University Press, Cambridge, 1987).

[190] J. B. Griffiths, *Colliding Plane Waves in General Relativity* (Oxford University Press, Oxford, 1991).

[191] L. P. Grishchuk, Sov. Phys. JETP **40**, 409 (1975).

[192] S. S. Gubser, I. R. Klebanov and A. M. Polyakov, Phys. Lett. B **428**, 105 (1998) [hep-th/9802109].

[193] S. S. Gubser, I. R. Klebanov and A. M. Polyakov, Nucl. Phys. B **636**, 99 (2002) [hep-th/0204051].

[194] V. G. Gurzadyan and S. S. Xue, Mod. Phys. Lett. A **18**, 561 (2003).

[195] A. H. Guth, Phys. Rev. D **23**, 347 (1981).

[196] A. H. Guth and S. Y. Pi, Phys. Rev. Lett. **49**, 1110 (1982).

[197] A. H. Guth and B. Jain, Phys. Rev. D **45**, 426 (1992).

[198] R. Hagedorn, Nuovo Cim. Suppl. **3**, 147 (1965).

[199] R. S. Hamade and J. M. Stewart, Class. Quant. Grav. **13**, 497 (1996) [gr-qc/9506044].

[200] S. W. Hawking, I. G. Moss and J. M. Stewart, Phys. Rev. D **26**, 2681 (1982).

[201] S. Hawking, J. M. Maldacena and A. Strominger, JHEP **0105**, 001 (2001) [hep-th/0002145].

[202] S. W. Hawking, T. Hertog and H. S. Reall, Phys. Rev. D **63**, 083504 (2001).

[203] C. Hayashi, Prog. Theor. Phys. **5**, 224 (1950).

[204] H. Hoekstra, arXiv:astro-ph/0510546.

[205] D. Hooper and S. Dodelson, Astropart. Phys. **27**, 113 (2007) [astro-ph/0512232].

[206] P. Horava and E. Witten, Nucl. Phys. B **460**, 506 (1996) [hep-th/9510209];
P. Horava and E. Witten, Nucl. Phys. B **475**, 94 (1996) [hep-th/9603142].

[207] R. W. Hornbeck, *Numerical Methods* (Prentice-Hall, Englewood Cliffs, NJ, 1975).

[208] K., Hotta, K. Kikkawa, and H. Kunitomo, 1997, Prog. Theor. Phys. **98**, 687.

[209] C. D. Hoyle, et al., Phys. Rev. Lett. **86** 1418 (2001) [hep-ph/0011014].

[210] J. P. Hsu, R. Kallosh and S. Prokushkin, JCAP **0312**, 009 (2003) [hep-th/0311077].

[211] E. Hubble, Proceedings of the National Academy of Sciences **15**, 224 (1929).

[212] E. Hubble, "The Realm of the Nebulae" *Yale University Press*, (1936).

[213] G. Huey and J. E. Lidsey, Phys. Lett. B **514**, 217 (2001) [astro-ph/0104006].

[214] G. Huey and J. E. Lidsey, Phys. Rev. D **66**, 043514 (2002) [astro-ph/0205236].

[215] D. Huterer and A. Cooray, Phys. Rev. D **71**, 023506 (2005).

[216] J. C. Hwang and E. T. Vishniac, Astrophys. J. **353**, 1 (1990).

[217] J. C. Hwang and H. Noh, Phys. Rev. D **54**, 1460 (1996).

[218] K. Ichiki, M. Yahiro, T. Kajino, M. Orito and G. J. Mathews, Phys. Rev. D **66**, 043521 (2002) [astro-ph/0203272].

[219] W. Israel, Nuovo Cim. B **44S10**, 1 (1966) [Erratum-ibid. B **48**, 463 (1967 NUCIA,B44,1.1966)].

[220] Y. I. Izotov and T. X. Thuan, arXiv:0704.3842 [astro-ph].

[221] R. Jackiw and C. Rebbi, Phys. Rev. D, **13** (1976) 3398.

[222] J. Jungman, M. Kamionkowski and K. Griest, Phys. Rep. **267**, 195 (1996).

[223] S. Kachru, M. Schulz, and E. Silverstein, Phys. Rev. D **62**, 045021 (2000).

[224] S. Kachru, J. Pearson and H. Verlinde, JHEP **0206**, 021 (2002).

[225] S. Kachru, R. Kallosh, A. Linde, and S. P. Trivedi, Phys. Rev. D **68**, 046005 (2003) [hep-th/0301240].

[226] S. Kachru et al., JCAP **0310**, 013 (2003) [hep-th/0308055].

[227] R. Kallosh, L. Kofman and A. D. Linde, Phys. Rev. D **64**, 123523 (2001) [hep-th/0104073].

[228] R. Kallosh and A. Linde, Phys. Rev. D **67**, 023510 (2003).

[229] N. Kaloper, Phys. Rev. D **60**, 123506 (1999).

[230] Th. Kaluza, Sitzungsber. Preuss. Akad. Wiss. Phys. Math. Klasse 996 (1921); Reprinted with the English translation in *Modern Kaluza-Klein Theories*, T. Appelquist, A. Chodos, P.G.O. Freund (Addison-Wesley, Menlo Park, 1987).

[231] D. J. Kapner et al., Phys. Rev. Lett. **98**, 021101 (2007) [hep-ph/0611184].

[232] A. Karch and L. Randall, Phys. Rev. Lett. **95**, 161601 (2005) [hep-th/0506053].

[233] M. Kasai, H. Asada and T. Futamase, Prog. Theor. Phys. **115**, 827 (2006) [astro-ph/0602506].

[234] S. Kasuya and M. Kawasaki, Phys. Rev. D **62**, 023512 (2000) [hep-ph/0002285].

[235] S. Kasuya, M. Kawasaki and F. Takahashi, Phys. Rev. D **68**, 023501 (2003) [hep-ph/0302154].

[236] M. Kawasaki and T. Moroi, Prog. Theor. Phys. **93**, 879 (1995).

[237] M. Kawasaki, K. Kohri and N. Sugiyama, Phys. Rev. D **62**, 023506 (2000) [astro-ph/0002127].

[238] M. Kawasaki, K. Kohri and T. Moroi, Phys. Lett. B **625**, 7 (2005) [astro-ph/0402490].

[239] M. Kawasaki, K. Kohri and T. Moroi, Phys. Rev. D **71**, 083502 (2005) [astro-ph/0408426].

[240] A. Kaya, and T. Rador, 2003, Phys. Lett. B **565**, 19; Kaya, A., 2003, Class. Quant. Grav. **20**, 4533; Kaya, A., 2004, JCAP **0408**, 014; Kaya, A., 2005a, Phys. Rev. D **72**, 066006; Kaya, A., 2005b, JHEP **03**, 003.

[241] A. Kehagias and K. Tamvakis, Phys. Lett. B **504** (2001) 38 [hep-th/0010112].

[242] K. A. Khan and R. Penrose, Nature **229**, 185 (1971).

[243] S. Y. Khlebnikov and I. I. Tkachev, Phys. Rev. Lett. **77**, 219 (1996).

[244] S. Y. Khlebnikov and I. I. Tkachev, Phys. Lett. B **390**, 80 (1997).

[245] S. Y. Khlebnikov and I. I. Tkachev, Phys. Rev. Lett. **79**, 1607 (1997).

[246] J. Khoury, B. A. Ovrut, P. J. Steinhardt and N. Turok, Phys. Rev. D **64**, 123522 (2001) [hep-th/0103239].

[247] J. Khoury, B. A. Ovrut, N. Seiberg, P. J. Steinhardt and N. Turok, Phys. Rev. D **65**, 086007 (2002) [hep-th/0108187];
J. Khoury, B. A. Ovrut, P. J. Steinhardt and N. Turok, Phys. Rev. D **66**, 046005 (2002) [hep-th/0109050].

[248] J. Khoury, P. J. Steinhardt and N. Turok, Phys. Rev. Lett. **92**, 031302 (2004).

[249] J. Y. Kim, 2004, Phys. Rev. D **70**, 104024.

[250] W. H. Kinney, E. W. Kolb, A. Melchiorri and A. Riotto, Phys. Rev. D **69**, 103516 (2004) [hep-ph/0305130].

[251] O. Klein, Z. F .Physik, **37**, 895 (1926); Reprinted with the English translation in *Modern Kaluza-Klein Theories*, T. Appelquist, A. Chodos, P.G.O. Freund (Addison-Wesley, Menlo Park, 1987).

[252] R. A. Knop *et al.* [The Supernova Cosmology Project Collaboration], Astrophys. J. **598**, 102 (2003).

[253] L. Knox, A. Albrecht and Y. S. Song, arXiv:astro-ph/0408141.

[254] M. Kobayashi and T. Maskawa, Prog. Theor. Phys. **49**, 652 (1973).

[255] H. Kodama and M. Sasaki, *Prog. Theor. Phys. Suppl.* No. 78, 1 (1984).

[256] L. Kofman, A. D. Linde and A. A. Starobinsky, Phys. Rev. Lett. **73**, 3195 (1994) [hep-th/9405187].

[257] L. Kofman, A. D. Linde and A. A. Starobinsky, Phys. Rev. D **56**, 3258 (1997) [hep-ph/9704452].

[258] L. Kofman and A. Linde, JHEP **0207**, 004 (2002).

[259] E. W. Kolb and M. S. Turner, *The Early Universe* (Westview Press, Chicago, United States of America, 1990).

[260] E. Kolb, Phys. Rev. Lett. **81**, 4048 (1998).

[261] E. W. Kolb, S. Matarrese and A. Riotto, New J. Phys. **8**, 322 (2006) [astro-ph/0506534].

[262] R. Koley and S. Kar, Class. Quantum Grav. **22** (2005) 753 [hep-th/0407158].

[263] E. Komatsu and D. N. Spergel, Phys. Rev. D **63**, 063002 (2001).

[264] E. Komatsu *et al.*, Astrophys. J. Suppl. **148**, 119 (2003).

[265] F. Koyama, Y. Tachikawa and T. Watari, Phys. Rev. D **69**, 106001 (2004) [Erratum-ibid. D **70**, 129907 (2004)] [hep-th/0311191].

[266] K. Koyama and D. Wands, JCAP **0704**, 008 (2007) [hep-th/0703040].

[267] K. Koyama, S. Mizuno and D. Wands, arXiv:0704.1152 [hep-th].

[268] J. Kripfganz and H. Perlt, Class. Quant. Grav. **5**, 453 (1988).

[269] H. Kudoh, T. Tanaka and T. Nakamura, Phys. Rev. D **68**, 024035 (2003);
H. Kudoh, Phys. Rev. D **69**, 104019 (2004).

[270] B.-S. Kyae and Q. Shafi, Phys. Lett. B **526** (2002) 379 [hep-ph/0111101].

[271] N. W. Mac Lachlan, Theory and Applications of Mathieu Functions (Dover, New York, 1961).

[272] D. Langlois, R. Maartens and D. Wands, Phys. Lett. B **489**, 259 (2000) [hep-th/0006007].

[273] D. Langlois, R. Maartens, M. Sasaki and D. Wands, Phys. Rev. D **63**, 084009 (2001) [hep-th/0012044].

[274] D. Langlois, K. Maeda, D. Wands, Phys. Rev. Lett.**88**, 181301 (2002) [gr-qc/0111013].

[275] D. Langlois, arXiv:gr-qc/0207047; D. Langlois, Prog. Theor. Phys. Suppl. **148**, 181 (2003) [hep-th/0209261].

[276] S. M. Leach and A. R. Liddle, Phys. Rev. D **68**, 123508 (2003) [astro-ph/0306305].

[277] J. L. Lehners, P. McFadden, N. Turok and P. J. Steinhardt, arXiv:hep-th/0702153.

[278] A. R. Liddle, P. Parsons and J. D. Barrow, Phys. Rev. D **50**, 7222 (1994) [astro-ph/9408015].

[279] A. R. Liddle, arXiv:astro-ph/9901124.

[280] A. R. Liddle, amd D. Lyth, *Cosmological Inflation and Large-Scale Structure* (Cambridge, 2000).

[281] A. R. Liddle and L. A. Urena-Lopez, Phys. Rev. Lett. **97**, 161301 (2006) [astro-ph/0605205].

[282] J. E. Lidsey et al., Rev. Mod. Phys. **69**, 373 (1997) [astro-ph/9508078].

[283] J. E. Lidsey, D. Wands and E. J. Copeland, Phys. Rept. **337**, 343 (2000) [hep-th/9909061].

[284] J. E. Lidsey, Lect. Notes Phys. **646**, 357 (2004) Lect. Notes Phys. **646**, 357 (2004) [astro-ph/0305528].

[285] E. Lifshitz, *Zh. Eksp. Teor. Fiz.* **16**, 587 (1946);
E. Lifshitz and I. Khalatnikov, *Adv. Phys.* **12**, 185 (1968).

[286] A. D. Linde, Phys. Lett. B **108**, 389 (1982).

[287] A. D. Linde, Phys. Lett. B **129**, 177 (1983).

[288] A. D. Linde, Rept. Prog. Phys. **47**, 925 (1984).

[289] A. D. Linde, *Particle Physics and Inflationary Cosmology* (Harwood, 1990).

[290] A. D. Linde, Phys. Lett. B **259**, 38 (1991).

[291] A. D. Linde, Phys. Rev. D **49**, 748 (1994) [astro-ph/9307002].

[292] A. D. Linde and A. Riotto, Phys. Rev. D **56**, 1841 (1997).

[293] E. V. Linder and A. Jenkins, Mon. Not. Roy. Astron. Soc. **346**, 573 (2003).

[294] LISA, home page: http://lisa.nasa.gov/

[295] J. C. Long, H. W. Chan and J. C. Price, Nucl. Phys. B **539** 23 (1999) [hep-ph/9805217].

[296] C. Lovelace, Nucl. Phys. B **273**, 416 (1986).

[297] F. Lucchin and S. Matarrese, D **32**, 1316 (1985).

[298] A. Lukas, B. A. Ovrut and D. Waldram, Nucl. Phys. B **532**, 43 (1998) [hep-th/9710208];
A. Lukas, B. A. Ovrut and D. Waldram, Phys. Rev. D **57**, 7529 (1998) [hep-th/9711197].

[299] A. Lukas, B.A. Ovrut, K.S. Stelle, D. Waldram Phys. Rev. D bf 59, 086001 (1999) [hep-th/9803235];
A. Lukas, B. A. Ovrut, and D. Waldram, Phys. Rev. D **60** 086001 (1999) [hep-th/9806022].

[300] V. N. Lukash, Sov. Phys. JETP **52**, 807 (1980).

[301] M. A. Luty, M. Porrati and R. Rattazzi, JHEP **0309**, 029 (2003) [hep-th/0303116].

[302] D. H. Lyth, Phys. Rev. D **31**, 1792 (1985).

[303] D. H. Lyth and A. Riotto, Phys. Rept. **314**, 1 (1999) [hep-ph/9807278].

[304] D. H. Lyth, Phys. Lett. B **524**, 1 (2002) [hep-ph/0106153].

[305] D. H. Lyth and D. Wands, Phys. Rev. D **68**, 103515 (2003).

[306] D. H. Lyth, K. A. Malik and M. Sasaki, JCAP **0505**, 004 (2005).

[307] R. Maartens, D. Wands, B. A. Bassett and I. Heard, D **62**, 041301 (2000) [hep-ph/9912464].

[308] R. Maartens, D **62**, 084023 (2000) [hep-th/0004166].

[309] R. Maartens, arXiv:gr-qc/0101059; R. Maartens, Prog. Theor. Phys. Suppl. **148**, 213 (2003); [gr-qc/0304089]; R. Maartens, Living Rev. Rel. **7**, 7 (2004) [gr-qc/0312059].

[310] K. Maeda, Prog. Theor. Phys. Suppl. **148**, 59 (2003); K. Maeda, Lect. Notes Phys. **646**, 323 (2004).

[311] K. Maeda and N. Ohta, Phys. Lett. B **597**, 400 (2004).

[312] A. S. Majumdar, Phys. Rev. D **64**, 083503 (2001).

[313] J. M. Maldacena, Adv. Theor. Math. Phys. **2**, 231 (1998) [Int. J. Theor. Phys. **38**, 1113 (1999)] [hep-th/9711200].

[314] J. Maldacena and C. Nuñez, Int. J. Mod. Phys. **A16** 822 (2001).

[315] F. Di Marco, F. Finelli and R. Brandenberger, Phys. Rev. D **67**, 063512 (2003).

[316] H. Martel, P. R. Shapiro and S. Weinberg, Astrophys. J. **492**, 29 (1998).

[317] J. Martin and D. J. Schwarz, Phys. Rev. D **57**, 3302 (1998).

[318] J. Martin, P. Peter, N. Pinto Neto and D. J. Schwarz, Phys. Rev. D **65**, 123513 (2002); J. Martin, P. Peter, N. Pinto-Neto and D. J. Schwarz, *ibid.* D **67**, 028301 (2003).

[319] J. Martin, G. N. Felder, A. V. Frolov, M. Peloso and L. Kofman, Phys. Rev. D **69**, 084017 (2004); J. Martin, G. N. Felder, A. V. Frolov, L. Kofman and M. Peloso, [hep-ph/0404141].

[320] J. Martin, G. N. Felder, A. V. Frolov, L. Kofman and M. Peloso, Comput. Phys. Commun. **171**, 69 (2005) [hep-ph/0404141].

[321] A. Mazumdar, S. Panda and A. Perez-Lorenzana, Nucl. Phys. B **614**, 101 (2001).

[322] P.L. McFadden, N. Turok, P.J. Steinhardt, arXiv:hep-th/0512123.

[323] J. McGreevy and E. Silverstein, JHEP **0508**, 090 (2005) [hep-th/0506130].

[324] A. Melfo, N. Pantoja, and J.D. Tempo, Phys. Rev. D **73** (2006) 044033 [hep-th/0601161].

[325] M. Milgrom, Astrophys. J. **270**, 365; **270**, 371; **270**, 384 (1983).

[326] H. Minakata and H. Sugiyama, Phys. Lett. B **567**, 305 (2003) [hep-ph/0212240].

[327] Y. Morisawa, D. Ida, A. Ishibashi and K. Nakao, Phys. Rev. D **67**, 025017 (2003) [gr-qc/0209070].

[328] T. Moroi, Nucl. Phys. B **448**, 220 (1995) [hep-ph/9503210].

[329] V. F. Mukhanov, Sov. Phys. JETP **67**, 1297 (1988) [Zh. Eksp. Teor. Fiz. **94N7**, 1 (1988)].

[330] V. F. Mukhanov, H. A. Feldman and R. H. Brandenberger, Phys. Rept. **215**, 203 (1992).

[331] V. F. Mukhanov, Int. J. Theor. Phys. **43**, 669 (2004) [astro-ph/0303073].

[332] V. F. Mukhanov, "*Physical foundations of cosmology*," *Cambridge, UK: Univ. Pr. (2005) 421 p.*

[333] Y. Nambu and M. Tanimoto, arXiv:gr-qc/0507057.

[334] D. Nathalie and A. Streich, Phys. Rev. D **70**, 103504 (2004) [gr-qc/0405003].

[335] S. Nesseris and L. Perivolaropoulos, Phys. Rev. D **70**, 043531 (2004).

[336] A. Neveu and J. Schwarz, Nucl. Phys. B **31**, 86 (1971).

[337] A. Neveu and J. Schwarz, Phys. Rev. D **4**, 1109 (1971).

[338] T. Nihei, Phys. Lett. B **465**, 81 (1999).

[339] S. Nojiri, S. D. Odintsov and S. Zerbini, Phys. Rev. D **62**, 064006 (2000).

[340] S. Nojiri and S. D. Odintsov, Phys. Lett. B **484**, 119 (2000).

[341] S. Nojiri and S. D. Odintsov, Phys. Rev. D **68**, 123512 (2003).

[342] A. Notari and A. Riotto, Nucl. Phys. B **644**, 371 (2002).

[343] M. Oguri and K. Takahashi, Phys. Rev. D **73**, 123002 (2006) [astro-ph/0604476].

[344] K. A. Olive, Phys. Rept. **190**, 307 (1990).

[345] B. Paczynski, Astrophys. J. **304**, 1 (1986).

[346] T. Padmanabhan, Phys. Rev. D **66**, 021301 (2002).

[347] T. Padmanabhan and T. R. Choudhury, Mon. Not. Roy. Astron. Soc. **344**, 823 (2003).

[348] T. Padmanabhan, Phys. Rept. **380**, 235 (2003); T. Padmanabhan, Current Science, **88**, 1057 (2005) [astro-ph/0510492].

[349] T. Padmanabhan, Class. Quan. Grav., **22**, L107 (2005).

[350] L. Page *et al.*, Astrophys. J. Suppl. **148**, 233 (2003).

[351] S. Panda, M. Sami and S. Tsujikawa, Phys. Rev. D **73**, 023515 (2006) [hep-th/0510112].

[352] E. Papantonopoulos, Lect. Notes Phys. **592**, 458 (2002) [hep-th/0202044].

[353] C. Park, S.-J. Sin, and S. Lee, 2000, Phys. Rev. D **61**, 083514.

[354] R. D. Peccei and H. R. Quinn, Phys. Rev. Lett. **38**, 1440 (1977).

[355] P. J. E. Peebles, *Principle of Physical Cosmology*, Princeton (1993).

[356] P. J. E. Peebles and A. Vilenkin, Phys. Rev. D **59**, 063505 (1999).

[357] M. Peimbert, V. Luridiana, A. Peimbert and L. Carigi, arXiv:astro-ph/0701313.

[358] M. Peimbert, V. Luridiana and A. Peimbert, arXiv:astro-ph/0701580.

[359] H. V. Peiris *et al.*, Astrophys. J. Suppl. **148**, 213 (2003) [astro-ph/0302225].

[360] S. Perlmutter *et al.*, Astrophys. J. **517**, 565 (1999).

[361] M. Persic, P. Salucci and F. Stel, Mon. Not. Roy. Astron. Soc. **281**, 27 (1996) [astro-ph/9506004].

[362] S. Podariu, R. A. Daly, M. P. Mory and B. Ratra, Astrophys. J. **584**, 577 (2003).

[363] D. Polarski and A. A. Starobinsky, Nucl. Phys. B **385**, 623 (1992).

[364] D. Polarski and A. A. Starobinsky, Class. Quant. Grav. **13**, 377 (1996) [gr-qc/9504030].

[365] J. Polchinski, Phys. Rev. Lett. **75**, 4724 (1995).

[366] J. Polchinski, *String Theory I* & *II* (Cambridge Univ. Press, Cambridge, 1998).

[367] A.C. Pope, et al, Astrophys. J. **607**, 655 (2004) [astro-ph/0401249].

[368] T. Prokopec and T. G. Roos, Phys. Rev. D **55**, 3768 (1997).

[369] F. Quevedo, Class. Quant. Grav. **19**, 5721 (2002) [hep-th/0210292].

[370] T. Rador, 2005a, Phys. Lett. B **621**, 176; T. Rador, 2005, [hep-th/0504047]; T. Rador, 2005, JHEP **06**, 001.

[371] P. Ramond, Phys. Rev. D **3**, 2415 (1971).

[372] L. Randall, M. Soljacic and A. H. Guth, Nucl. Phys. B **472**, 377 (1996).

[373] L. Randall and R. Sundrum, Phys. Rev. Lett. **83**, 3370 (1999) [hep-ph/9905221]; L. Randall and R. Sundrum, Phys. Rev. Lett. **83**, 4690 (1999) [hep-th/9906064].

[374] S. Randjbar-Daemi and M. Shaposhnikov, Phys. Lett. B **492** (2000) 361 [hep-th/0008079].

[375] S. Rasanen, arXiv:astro-ph/0208282.

[376] B. Ratra and J. Peebles, Phys. Rev D **37**, 321 (1988).

[377] H. S. Reall, Phys. Rev. D **59**, 103506 (1999).

[378] M. J. Rees and D. W. Sciama, Nature **217**, 511 (1968).

[379] A. Refregier, Ann. Rev. Astron. Astrophys. **41**, 645 (2003) [astro-ph/0307212].

[380] S. J. Rey, Phys. Rev. Lett. **77**, 1929 (1996).

[381] A. G. Riess *et al.*, Astron. J. **116**, 1009 (1998); Astron. J. **117**, 707 (1999).

[382] A. G. Riess *et al.* [Supernova Search Team Collaboration], Astrophys. J. **607**, 665 (2004).

[383] G. I. Rigopoulos and E. P. S. Shellard, Phys. Rev. D **68**, 123518 (2003).

[384] C. Ringeval, P. Peter, and J.-P. Uzan, Phys. Rev. D **65** (2002) 044016 [hep-th/0109194].

[385] L. Roszkowski, arXiv:hep-ph/9903467.

[386] D. P. Roy, arXiv:physics/0007025.

[387] V. A. Rubakov and M. E. Shaposhnikov, Phys. Lett. B **125**, 136 (1983).

[388] V. A. Rubakov and M. E. Shaposhnikov, Phys. Lett. B **152**, 136 (1983).

[389] R. K. Sachs and A. M. Wolfe, Astrophys. J. **147**, 73 (1967).

[390] V. Sahni, PhD thesis, Moscow State University, Moscow, 1984.

[391] V. Sahni and P. Coles, Phys. Rept., **262**, 1 (1995).

[392] V. Sahni and A. A. Starobinsky, Int. J. Mod. Phys. D **9**, 373 (2000); V. Sahni, Lect. Notes Phys. **653**, 141 (2004) [astro-ph/0403324].

[393] V. Sahni, M. Sami and T. Souradeep, Phys. Rev. D **65** 023518 (2002).

[394] V. Sahni, Lect. Notes Phys. **653**, 141 (2004) [astro-ph/0403324].

[395] M. Sakellariadou, Nucl. Phys. B **468**, 319 (1996) [hep-th/9511075].

[396] A. Salam, *Originally printed in *Svartholm: Elementary Particle Theory, Proceedings Of The Nobel Symposium Held 1968 At Lerum, Sweden*, Stockholm 1968, 367-377.*

[397] D. S. Salopek and J. R. Bond, Phys. Rev. D **42**, 3936 (1990).

[398] D. S. Salopek and J. M. Stewart, Phys. Rev. D **51**, 517 (1995) [astro-ph/9409055].

[399] M. Sami, P. Chingangbam and T. Qureshi, Phys. Rev. D **66**, 043530 (2002).

[400] M. Sami, Mod. Phys. Lett. A **18**, 691 (2003).

[401] M. Sami, N. Dadhich and T. Shiromizu, Phys. Lett. B **568** 118 (2003) [hep-th/0304187].

[402] M. Sami and V. Sahni, Phys. Rev. D **70**, 083513 (2004) [hep-th/0402086].

[403] R.H. Sanders and S.S McGaugh, Ann. Rev. Astron. Astrophys. **40**, 263 (2002) [astro-ph/0204521].

[404] S. Sarkar, Rept. Prog. Phys. **59**, 1493 (1996) [hep-ph/9602260].

[405] M. Sasaki, Prog. Theor. Phys. **76**, 1036 (1986).

[406] M. Sasaki and E. D. Stewart, Prog. Theor. Phys. **95**, 71 (1996).

[407] M. Sasaki and T. Tanaka, Prog. Theor. Phys. **99**, 763 (1998).

[408] K. Sato, Mon. Not. Ray. Astron. Soc. **195**, 467 (1981); K. Sato, Phys. Lett. B **99**, 66 (1981).

[409] B. Schaefer, Based on talk given at AAS, Washington, Jan 2006 and explained at `http://cosmicvariance.com/2006/01/11/evolving-dark-energy/`.

[410] D. Seery and A. Taylor, Phys. Rev. D **71**, 063508 (2005) [astro-ph/0309512].

[411] U. Seljak *et al.*, Phys. Rev. D **71**, 103515 (2005).

[412] A. Sen, Phys. Rev. Lett. **55**, 1846 (1985).

[413] A. Sen, JHEP **9910**, 008 (1999).

[414] A. Sen, JHEP **0204**, 048 (2002); JHEP **0207**, 065 (2002).

[415] H. J. Seo and D. J. Eisenstein, Astrophys. J. **598**, 720 (2003) [astro-ph/0307460].

[416] N. Seto, S. Kawamura and T. Nakamura, Phys. Rev. Lett. **87**, 221103 (2001) [astro-ph/0108011].

[417] H. Shinkai and K. Maeda, Phys. Rev. D **48**, 3910 (1993) [gr-qc/9305014].

[418] T. Shiromizu, K. Maeda and M. Sasaki, Phys. Rev. D **62**, 024012 (2000) [gr-qc/9910076].

[419] G. Shiu and S.-H. H. Tye, Phys. Lett. B **516** (2001) 421 [hep-th/0106274].

[420] Y. Shtanov, J. H. Traschen and R. H. Brandenberger, Phys. Rev. D **51**, 5438 (1995) [hep-ph/9407247].

[421] J. L. Sievers *et al.*, Astrophys. J. **591**, 599 (2003).

[422] J. Silk, Astrophys. J. **151** (1968) 459.

[423] V. Silveira, Phys. Rev. D **38**, 3823 (1988).

[424] E. Silverstein, arXiv:hep-th/0106209.

[425] Y. Sofue and V. Rubin, Ann. Rev. Astron. Astrophys. **39**, 137 (2001) [astro-ph/0010594].

[426] D. T. Son, Phys. Rev. D **54**, 3745 (1996).

[427] D. N. Spergel *et al.* [WMAP Collaboration], arXiv:astro-ph/0603449; D. N. Spergel *et al.* [WMAP Collaboration], Astrophys. J. Suppl. **148**, 175 (2003). See also the website: http://wmap.gsfc.nasa.gov/

[428] B. Spokoiny, Phys. Lett. B **315**, 40 (1993) [gr-qc/9306008].

[429] A. A. Starobinsky, JETP Lett. **30** (1979) 682 [Pisma Zh. Eksp. Teor. Fiz. **30** (1979) 719].

[430] A. A. Starobinsky, Phys. Lett. B **91** (1980) 99.

[431] A. A. Starobinsky and V. Sahni, in *Modern Theoretical and Experimental Problems of General relativity* MGPI Press, Moscow, 1984, p. 77.

[432] P. J. Steinhardt and N. Turok, Phys. Rev. D **65**, 126003 (2002).

[433] P. J. Steinhardt and N. Turok, Science **296**, 1436 (2002).

[434] E. D. Stewart and D. H. Lyth, Phys. Lett. B **302**, 171 (1993).

[435] L. Susskind, arXiv:hep-th/0302219.

[436] Y. Takamizu and K. Maeda, Phys. Rev. D **70**, 123514 (2004) [hep-th/0406235].

[437] Y. Takamizu and K. Maeda, Phys. Rev. D **73** 103508 (2006) [hep-th/0603076].

[438] Y. Takamizu and H. Kudoh, Phys. Rev. D **74**, 103511 (2006) [hep-th/0607231].

[439] Y. Takamizu, H. Kudoh and K. Maeda, Phys. Rev. D **75**, 061304 (2007) [gr-qc/0702138].

[440] M. Tegmark *et al.* [SDSS Collaboration], Phys. Rev. D **69**, 103501 (2004) and see the website: http://www.sdss.org/

[441] S. Thomas and J. Ward, Phys. Rev. D **72**, 083519 (2005).

[442] G. 't Hooft, arXiv:gr-qc/9310026.

[443] A. J. Tolley and N. Turok, Phys. Rev. D **66**, 106005 (2002).

[444] A. J. Tolley, N. Turok and P. J. Steinhardt, Phys. Rev. D **69**, 106005 (2004).

[445] A. J. Tolley, Phys. Rev. D **73**, 123522 (2006) [hep-th/0505158].

[446] J. L. Tonry *et al.* [Supernova Search Team Collaboration], Astrophys. J. **594**, 1 (2003).

[447] P. Townsend, Phys. Lett. B **350**, 184 (1995) [hep-th/9501068].

[448] J. H. Traschen and R. H. Brandenberger, Phys. Rev. D **42**, 2491 (1990).

[449] A. A. Tseytlin and C. Vafa, Nucl. Phys. B **372**, 443 (1992) [hep-th/9109048].

[450] A. A. Tseytlin, Class. Quant. Grav. **9**, 979 (1992) [hep-th/9112004].

[451] S. Tsujikawa, K. Maeda and S. Mizuno, Phys. Rev. D **63**, 123511 (2001).

[452] S. Tsujikawa, R. Brandenberger and F. Finelli, Phys. Rev. D **66**, 083513 (2002).

[453] S. Tsujikawa, Phys. Lett. B **526**, 179 (2002).

[454] S. Tsujikawa, D. Parkinson and B. A. Bassett, Phys. Rev. D **67**, 083516 (2003).

[455] N. Turok and P. J. Seinhardt, Phys. Scripta **T117**, 76 (2005) [hep-th/0403020].

[456] S.-H. Tye and I. Wasserman, Phys. Rev. Lett. **86**, 1682 (2001); H. T. Cho, C. L. Ho and K. W. Ng, Phys. Lett. B **643**, 71 (2006) [hep-ph/0508018].

[457] Van der Bij, J. J. H. Van Dam and Y. J. Ng, Physica **116 A**, 307 (1982); W. Buchmuller and N. Dragon, Phys. Lett. B **207** (1988) 292.

[458] G. Veneziano, Phys. Lett. B **265**, 287 (1991).

[459] M. Visser, Phys. Lett. B **159**, 22 (1985) [hep-th/9910093].

[460] D. Wands, Phys. Rev. D **60**, 023507 (1999) [gr-qc/9809062].

[461] D. Wands, K. A. Malik, D. H. Lyth and A. R. Liddle, D **62**, 043527 (2000) [astro-ph/0003278].

[462] D. Wands, Class. Quant. Grav. **19**, 3403 (2002) [hep-th/0203107].

[463] L. M. Wang, V. F. Mukhanov and P. J. Steinhardt, Phys. Lett. B **414**, 18 (1997) [astro-ph/9709032].

[464] Y. Wang and P. Mukherjee, Astrophys. J. **606**, 654 (2004).

[465] S. Weinberg, Phys. Rev. Lett. **19**, 1264 (1967).

[466] S. Weinberg, *Gravitation and Cosmology*, J. Wiley, New York (1972).

[467] S. Weinberg, Phys. Rev. Lett. **59**, 2607 (1987).

[468] S. Weinberg, Rev. Mod. Phys. **61**, 1 (1989).

[469] L. Windrow, Phys. Rev. D **40**, 1002 (1989).

[470] E. Witten, Nucl. Phys. B **443**, 85 (1995) [hep-th/9503124].

[471] E. Witten, Nucl. Phys. B **474**, 343 (1996).

[472] E. Witten, JHEP **9812**, 012 (1998) [hep-th/9812012].

[473] E. Witten, arXiv:hep-th/0106109.

[474] J. Yokoyama, Phys. Rev. Lett. **88**, 151302 (2002).

[475] M. Yoshimura, Prog. Theor. Phys. **94**, 873 (1995).

[476] H. Yoshino and Y. Nambu, Phys. Rev. D **67**, 024009 (2003) [gr-qc/0209003].

[477] F. Zwicky, Helv. Phys. Acta., **6**, 110 (1933).